EFFICIENT SMOOTHED PARTICLE HYDRODYNAMICS MODELLING OF TUNED LIQUID DAMPERS

EFFICIENT SMOOTHED PARTICLE HYDRODYNAMICS MODELLING OF TUNED LIQUID DAMPERS

By
KEVIN P. MCNAMARA, B.A.Sc.

A Thesis Submitted to the School of Graduate Studies in Partial Fulfilment of the Requirements for the Degree Doctor of Philosophy

McMaster University

McMaster University

DOCTOR OF PHILOSOPHY (2021)

(Civil Engineering)

Hamilton, Ontario, Canada

TITLE: Efficient Smoothed Particle Hydrodynamics Modelling of Tuned Liquid Dampers

AUTHOR: Kevin P. McNamara, B.A.Sc. (University of Waterloo)

SUPERVISOR: Dr. Michael J. Tait

NUMBER OF PAGES: xxiii, 248

Lay Abstract

Tall buildings are often susceptible to swaying in the wind. Though this is not a cause for concern over the safety of the structure, perceptible motion can alarm occupants. Many tall buildings use systems to reduce the sway, such as installing a large tank of liquid at the top of the building known as a tuned liquid damper (TLD). The liquid in the tank sloshes and opposes the sway of the structure. Engineers often use models to calculate the response of a TLD. The goal of this thesis is to create an efficient model based on a technique which represents the sloshing liquid in a TLD using small moving particles. The model is validated using experimental testing data. The model can represent complicated phenomena that is difficult or impossible to capture with existing models and can be used to extend knowledge about the behavior of TLDs.

Abstract

The tuned liquid damper (TLD) is used to reduce the motion of many tall structures around the world. A TLD consists of a partially filled tank of liquid located near the location of maximum structural response. Due to the nonlinear behavior of sloshing liquids, a suitable nonlinear model must be employed for proper TLD design. Existing models typically have limitations on liquid depth, excitation amplitude, and are often unable to directly capture complicated phenomena such as sloshing impact with the TLD ceiling.

The goal of this study is to create a TLD model without such limitations. A smoothed particle hydrodynamics (SPH) model is developed for a TLD. SPH has seen application to TLDs in the past, however the computational requirements often make it infeasible for use outside of an academic setting. An efficient method for representing TLD damping elements is proposed in this study. This method significantly reduces the computational time by allowing for a much larger particle resolution. This enables the simulation of multiple hours of time, which has not been previously achieved using SPH.

The model is validated with experimental data. The TLD model is coupled to a structure to represent a structure-TLD system under large amplitude excitations. Modifications to the SPH solid boundary conditions for long-duration simulations are investigated to mitigate the loss of fluid particles. The influence of limiting TLD freeboard on structure-TLD system response is investigated. The model is used to simulate the response of a series-type pendulum tuned mass damper (TMD)-TLD system considering both horizontal and vertical excitation. The model is demonstrated to capture the response of TLDs across a range of complex scenarios.

Acknowledgements

I would like to express my gratitude to my supervisor, Dr. Mike Tait, for his constant encouragement and advice throughout this study. His supervisory approach enabled me to work independently and grow as a researcher and engineer, and his flexibility when life got in the way was appreciated. Thank you to Dr. Shayne Love for his willingness to answer my (many) questions throughout this study and his advice and ideas which kept this research interesting and applicable to industry. I would like to thank Dr. Wael El-Dakhakhni for his guidance and helpful suggestions, and Dr. Tracy Becker and Dr. Jon Galsworthy for their time on my supervisory committee.

I would like to express my appreciation to my colleagues at RWDI and Motioneering for their mentorship and their encouragement to embark on this study. Thank you also to RWDI and Motioneering for the opportunity to work on various experimental projects, most of which are not mentioned in this thesis. My many hours working in the Applied Dynamics Lab would not have been possible without the assistance and technical advice of Kent Wheeler and Paul Heerema, which was greatly appreciated.

Thank you to the friends and colleagues I met throughout my time at McMaster. Thank you to Bishoy Awad for the helpful discussions about SPH, and for working through many bugs in the code with me. I would like to thank Matt East, Paul Steneker, Bryanna Noade, Richard Darlington and Alexander Sciascetti for their friendship, support, and all the good memories.

The support of my family has been greatly appreciated throughout this study.

There are no words to express my gratitude to my best friend and partner, Leila, for her constant support throughout this study and everything else that has happened in the last five years. Without her, this work would not have been possible.

This thesis is dedicated to the memory of my mother, Janice. Her encouragement and support made me the person that I am today.

Table of Contents

List of Figures

List of Tables

List of All Abbreviations and Symbols

A	Area
A_{sc}, A_{DE}	Fluid acceleration at screen or damping element
b	TLD tank breadth
c	Damping constant
C_s	Structure generalized damping
C_D	Drag coefficient
C_l	Loss coefficient
C_m	Added mass coefficient
$\frac{D}{Dt}$	Lagrangian derivative
dp	Fluid particle spacing
$dt, \Delta t$	Simulation timestep
E_d	Energy dissipated per cycle
f	Frequency
$\boldsymbol{f_b}$	Body force vector
$\boldsymbol{F_{ext}}$	External applied force
F_0	Applied transient force amplitude
$\boldsymbol{F_{screen}}, \boldsymbol{F_{DE}}$	TLD screen or damping element force
F_{sw}	TLD sloshing force
F_w, F_{TLD}	TLD liquid force
$\boldsymbol{g}$	Gravity, body force vector
G	TLD freeboard
H	TLD tank height
h	TLD fluid height
h_{ker}	SPH kernel function support radius
$H(\omega)$	Complex frequency response function
$\lvert H_s(f) \rvert$	Structure mechanical admittance function
K_s	Structure generalized stiffness

L	TLD tank length, Lagrangian variable
L_c	Pendulum TMD cable length
m	Mass
m_w	Mass of fluid
M_s	Structure generalized mass
P	Fluid pressure
Q	Non-conservative force
q_{max}	SPH kernel function support radius
$\boldsymbol{r}$	Fluid particle location vector
S	Solidity ratio
S_0	Spectral amplitude
$S_{FF}(f)$	Spectrum of applied force
$S_{XX}(f)$	Spectrum of structure displacement
$S_{\eta\eta}(f)$	Spectrum of wave height
T	Kinetic energy
t	Time variable
$\boldsymbol{u}$	Fluid particle velocity vector
U_{sc}, U_{DE}	Fluid velocity at screen or damping element
V	Volume, potential energy
W_{ij}	SPH kernel function
X	Structure displacement
X_0	Excitation amplitude
x_{screen}, x_{DE}	TLD screen or damping element coordinate
α	Pressure blending factor
β	Frequency ratio
Γ	Modal participation factor
ζ	Damping ratio
ζ_{eff}	Effective damping

η	Free surface height
θ	Pendulum TMD response angle
μ	Mass ratio
ν	Fluid viscosity
ρ	Fluid density
σ	RMS response
σ_F	RMS of applied force
Ψ_{FB}	Freeboard efficiency factor
Ω	Tuning ratio
ω	Angular frequency
ω_n	Natural angular frequency
ω_e	Excitation angular frequency
∞	Unlimited TLD freeboard

Common Subscripts

eff	Effective
eq	Equivalent mechanical property
FB	Freeboard
s	Structure property
TLD	TLD property
TMD	TMD property

Common Superscripts

(opt)	Optimal value
*	Intermediate value
'	Normalized value
$\dot{x}$	Time derivative of x
$\hat{x}$	Peak value of x

Common Initialisms

DVA	Dynamic vibration absorber
PPE	Pressure Poisson equation
RMS	Root mean square
SPH	Smoothed particle hydrodynamics
TLD	Tuned liquid damper
TMD	Tuned mass damper

Co-Authorship

This thesis has been prepared according to the "sandwich" thesis format set out by the Faculty of Graduate Studies at McMaster University. The thesis has been co-authored as follows:

Chapter 2: Incompressible smoothed particle hydrodynamics model of a rectangular tuned liquid damper containing screens

Authors: K.P. McNamara, B.N. Awad, M.J. Tait, J.S. Love

The SPH model code was developed by K.P. McNamara under the supervision of Dr. M.J. Tait. B.N. Awad assisted with model development and debugging. Experimental data was provided by Dr. M.J. Tait and Dr. J.S. Love. Numerical simulations were completed by K.P. McNamara. The manuscript was written by K.P. McNamara. B.N. Awad assisted with writing the introduction and model description. The manuscript was modified under the supervision of Dr. M.J. Tait and Dr. J.S. Love. Chapter 2 has been published in the Journal of Fluids and Structures.

Chapter 3: Modelling the response of structure-tuned liquid damper systems under large amplitude excitation using SPH

Authors: K.P. McNamara and M.J. Tait

The SPH model code and numerical modelling was completed by K.P. McNamara under the supervision of Dr. M.J. Tait. The manuscript was written by K.P. McNamara and modifications were completed under the supervision of Dr. M.J. Tait. Chapter 3 has been published in the ASME Journal of Vibration and Acoustics.

Chapter 4: Mitigating fluid particle loss for multiple-hour duration SPH sloshing simulation

Authors: K.P. McNamara and M.J. Tait

The SPH model code and numerical modelling was completed by K.P. McNamara under the supervision of Dr. M.J. Tait. The manuscript was written by K.P. McNamara and modifications were completed under the supervision of Dr. M.J. Tait. Chapter 4 has been submitted for possible publication in Computational Particle Mechanics.

Chapter 5: Numerical investigation of the response of structures equipped with a limited freeboard tuned liquid damper

Authors: K.P. McNamara, J.S. Love, M.J. Tait

The SPH model and numerical modelling was completed by K.P. McNamara under the supervision of Dr. J.S. Love and Dr. M.J. Tait. The manuscript was written by K.P. McNamara and modifications were completed under the supervision of Dr. J.S. Love and Dr. M.J. Tait. Chapter 5 has been submitted for possible publication in the Journal of Fluids and Structures.

Chapter 6: Nonlinear modelling of series-type pendulum tuned mass damper-tuned liquid damper

Authors: K.P. McNamara, J.S. Love, M.J. Tait

The SPH model code, numerical modelling, and experimental testing was completed by K.P. McNamara under the supervision of Dr. J.S. Love and Dr. M.J. Tait. The manuscript was written by K.P. McNamara and modifications were completed under the supervision of Dr. J.S. Love and Dr. M.J. Tait. Chapter 6 has been submitted for possible publication in the ASME Journal of Vibration and Acoustics.

Chapter 1: Overview of Study

1.1 Background

The trajectory of modern structural design has led to buildings that push the envelope of height and slenderness. According to the Council on Tall Buildings and Urban Habitat, there are over 100 buildings with height exceeding 300 metres currently under construction worldwide [1]. With the introduction of lightweight materials, structures have become more flexible and sensitive to dynamic loading from the environment. Wind loading is particularly important for tall structures with long natural periods. Structures are being designed not only to resist wind forces, but also to reduce wind loads through shape optimization, twisting, false floors, and other architectural openings [2]. In addition to considering ultimate limit state structural design, engineers must combat wind-induced vibration at the serviceability level. It is common for buildings to sway in the wind; however, the sway becomes increasingly prominent in slender and flexible structures. Many modern structures have governing accelerations occurring at low return periods, such as the 1-year or 1-month event [3]. If the motion of the structure exceeds certain thresholds, occupants begin to perceive the movement, causing alarm and discomfort [4, 5]. It has become imperative for engineers to develop methods and systems to reduce wind-induced structural motion.

One method to reduce the dynamic behavior of a tall structure is to modify its mass and stiffness, shifting the natural frequency away from the regions of large wind-induced motion [6]. However, this can add significant material cost, and may be impossible depending on the stage of the project. The other structural parameter which must be considered is damping, which is a measure of the ability to dissipate energy. Unlike mass and stiffness, damping is difficult to directly quantify for a structure, though is known to be very small for tall flexible structures subject to wind loading [7]. Different structural systems provide varying levels of inherent damping [8, 9]. Damping can be significantly increased by introducing a supplementary damping system. Historically, only landmark structures would be likely to include a supplementary damping system. However, modern structures have increasingly taken advantage of these systems. As of 2018, 18% of

buildings with height greater than 250 metres are equipped with some type of supplementary damping system [10].

Many types of supplementary damping systems exist to reduce the dynamic response of structures. These systems are typically grouped into two general categories: distributed systems and mass systems. In distributed systems many devices are installed in various locations across a structure. Most distributed systems operate by dissipating energy when the ends of the device move relative to one another. Examples of distributed systems are viscous fluid, viscoelastic, metallic, and friction dampers [7]. These systems are particularly effective for resisting seismic motion but can also help to improve wind-induced responses. Mass systems, often also known as dynamic vibration absorbers (DVA), consist of placing a large mass near the location of maximum structural response. The DVA mass is typically in the range of 1-5% of the generalized mass of the primary structure. The natural frequency of the DVA is tuned to be close to that of the primary structure using optimal formulae which minimize the response [11]. The response of a properly tuned DVA will oppose the motion of the primary structure. Due to the coupling between the structure and DVA motions, the frequency response function of the structure will be modified by the presence of the DVA, as illustrated in Figure 1.1. This can result in significant motion reductions.

There are two fundamental categories of passive DVAs consisting of mass systems and liquid systems, as shown in Figure 1.2. Tuned mass dampers (TMD) utilize a large solid mass, often configured as a pendulum or spring-mass-dashpot system [12]. The large mass absorbs energy from the primary structure, which is typically dissipated using viscous fluid dampers, though innovative energy dissipation solutions such as an eddy current system have been implemented [13]. The other fundamental DVA category is liquid based systems, where the solid mass is replaced with a liquid. Examples are the tuned liquid column damper (TLCD) and the tuned liquid damper (TLD), which is also known as the tuned sloshing damper (TSD). TLCDs consist of a U-shaped tank partially filled with liquid that sloshes when the structure sways. Energy is dissipated with turbulence using orifice plates and screens [14]. TLDs consist of a partially filled tank of liquid that sloshes in

response to structural vibration. Both TLDs and TLCDs are often used as fire suppression storage tanks, which allows them to serve a dual purpose. One downside to a TLD compared to a TMD is that only a portion of the liquid participates in sloshing, which results in an effective TLD mass that is less than the total mass of liquid [15].

1.2 Tuned Liquid Dampers

TLDs have been implemented in many structures around the world. The TLD has the benefit of simple construction and minimal components, which makes it attractive and economical compared to the TMD. Early TLD designs often consisted of many small tanks which achieved the required liquid mass in ensemble [16]. More recent applications typically utilize one or multiple large tanks [17]. Sloshing liquids in containers like TLDs are typically classified based on the ratio of liquid depth to tank length [18], as illustrated in Figure 1.3. Shallow TLDs have small depth to length ratios, which has the benefit of providing low natural frequencies and a high percentage of liquid mass participation [15]. Energy is dissipated in shallow TLDs through wave breaking and wave impact with the tank walls [19]. Shallow TLDs often have chaotic and highly nonlinear sloshing responses, which can be unpredictable and complicated to model numerically, often requiring some form of empirical parameter [20, 21]. Additionally, due to the shallow depth, multiple TLD tanks may be required to achieve the necessary liquid mass. Intermediate and deep TLDs have more liquid mass, however a smaller percentage of the liquid participates in sloshing, and there is low inherent damping, primarily due to viscous interaction at the tank boundaries [22].

Flow obstructing devices are commonly used in TLDs to increase the damping beyond what the liquid alone provides. The flow obstructions induce turbulence in the sloshing liquid, leading to energy dissipation. Additionally, the obstructions help to regularize the flow, which reduces nonlinearities and can simplify numerical modelling. Examples of flow obstructing devices implemented in TLDs are nets [23], screens [24], baffles [25], and paddles [26]. Unlike a TMD, the TLD does not need to overcome friction to activate, meaning that it can operate at very low responses [27]. However, the damping force provided by the flow obstructions is proportional to liquid velocity squared, which means

that TLD performance is amplitude dependent. Each TLD will have a response at which the damping approaches the optimal value for a DVA [15]. Below this response level, the damping will be smaller than optimal. Above this response level the TLD will be more than optimally damped, potentially reducing its performance. However, TLDs have been demonstrated to have robust and efficient performance across a variety of scenarios [28].

It is possible to decouple the response of a 2D rectangular TLD into independent directions [24]. This allows a TLD to be tuned to work in both primary directions, targeting motion reduction in multiple modes of the primary structure. In the simplest form, TLDs are often rectangular [29] or circular in shape [30]. Various modified shapes have been investigated, such as annular [31, 32], spherical [33], conical [34], and sloped bottom [35] tanks. These different shapes can achieve a wide range of sloshing frequencies and can also increase the percentage of liquid mass participation. TLDs can be designed to fit within unique spaces or around building components, either through irregular tank shapes [36], or the introduction of core penetrations within the tank [37].

1.2.1 Numerical TLD Models

Numerical models for TLDs are integral to the design process, allowing engineers to efficiently calculate the response of structure-TLD systems. Various numerical models have been developed for TLDs. Using potential flow theory, the TLD response can be represented as an infinite summation of sloshing modes [38]. Linear equivalent mechanical models have been developed to capture the fundamental TLD sloshing mode response [15]. These models are computationally efficient, and the response can be easily solved in the frequency domain. Linear equivalent mechanical models can be coupled to a structure and have been demonstrated to predict the structure response well, though they do not capture the nonlinear TLD wave heights [15]. To obtain an improved estimate of the nonlinear sloshing response, multi-modal models which consider nonlinear coupling among the different sloshing modes have been applied to TLDs [39, 40, 41] and structure-TLD systems [36]. The nonlinear model response is often determined using time integration techniques, which increases the computational requirements compared to frequency

domain methods. Frequency domain methods to predict peak nonlinear TLD wave heights have also been proposed [42].

The Navier-Stokes (NS) equations describe the motion of fluids through conservation of mass and conservation of momentum. Exact solutions to the NS equations exist only under certain conditions, and thus various methods have been developed to solve the equations numerically. Shallow water wave theory (SWWT), which uses a depth-averaged version of the NS equations, has been applied to shallow TLDs [20, 19], as well as TLDs with flow obstructions such as nets [23] and screens [43]. In SWWT, the domain can be discretized in one or two dimensions, representing the liquid surface. Solutions to the SWWT equations for TLDs have been found using the random choice [19], finite difference [43], and Lagrangian particle path methods [44].

Models based on potential flow and SWWT often have limitations in terms of liquid depth and response amplitude. This can lead to certain assumptions becoming invalid, for example the assumed ordering of modal contributions in the multi-modal method [18]. Additionally, at large amplitudes convergence issues may arise. More robust computational fluid dynamics (CFD) methods which solve the full NS equations can overcome these limitations, however these methods often require significant computational resources. TLDs have been modelled using the mesh based finite difference method [45] and finite volume method [31, 46]. Capturing the free surface can be complicated with mesh-based methods, often requiring complicated tracking algorithms [47] and domain re-meshing at large amplitudes [48]. In contrast, meshless methods can inherently capture the free surface. Examples of meshless CFD methods include smoothed particle hydrodynamics (SPH), element-free Galerkin, and moving particle semi-implicit (MPS) [48]. SPH was selected for this research due to its ability to capture large free surface motions and sloshing wave impact with the tank ceiling. Additionally, of the meshless methods, SPH has seen the most research and development in recent years, which provides a significant number of resources to be used in developing an in-house code.

1.2.1.1 Smoothed Particle Hydrodynamics

SPH was first introduced in the 1970s for astrophysics applications [49, 50]. The fluid is represented by a series of discrete particles which are used as integration points in a Lagrangian framework. Properties of the fluid at each particle such as velocity, density, and pressure are calculated from weighted contributions of the neighbouring particles [51]. This allows the NS equations to be discretized as a series of summations which can be efficiently calculated numerically. The original astrophysics implementation of SPH focused on compressible flows without solid boundary conditions. SPH was extended to applications involving a free surface and incompressible fluids by introducing solid boundary treatments and a stiff equation of state to relate fluid pressure and density. Incompressible fluids are represented as weakly compressible by limiting fluctuations in density to sufficiently small values [52]. This implementation is commonly referred to as weakly compressible SPH (WCSPH) and has been used for various free surface applications [53]. One major limitation to WCSPH is the calculation of pressure fields, which can result in noisy and unphysical pressure values [54]. Significant research has been done to improve WCSPH pressures, such as the introduction of numerical dissipation terms [55] or regularization of the fluid density after a certain number of timesteps [56]. While effective, these methods can increase the computational burden of WCSPH.

An alternative is the incompressible SPH (ISPH) method [57]. In this method, rather than relating pressure and density through an equation of state, a pressure Poisson equation (PPE) is solved directly based on enforcing the incompressible fluid conditions of a divergence free velocity field [57], an invariant fluid density [58], or a blended combination of the two [59, 60]. Solving the PPE is computationally expensive compared to the equation of state in WCSPH, however the increased accuracy of ISPH can allow for larger timesteps [61]. The PPE solution can be found using implicit methods which require inversion of a sparse matrix [62], or explicit methods which can be solved directly by employing a sufficiently small timestep [63, 64, 65]. ISPH calculates smooth pressure fields without additional numerical dissipation, which is particularly attractive for sloshing liquid problems.

SPH has been applied to TLDs and sloshing liquids in tanks in various studies. Bulian et al. [66], Marsh et al. [67], and Green et al. [68, 69, 70] have studied the response of shallow depth sloshing liquids in tanks without internal flow obstructions. Kashani et al. [71] and Halabian et al. [72] investigated the response of TLDs with damping screens using ISPH and WCSPH. Other studies have investigated the response of sloshing liquids with baffles [73] and porous elements like screens and breakwaters [74, 75, 76]. Due to the computational demands of SPH compared to other models, the method has not seen significant application to TLDs.

1.3 Impetus for Research

Numerical models are an important tool used in the design of TLDs. Many TLD numerical models have been developed. These methods often have limits on excitation amplitude, liquid depth, and are unable to capture complicated phenomena such as impact with the tank ceiling. The limitations of existing numerical models place constraints on the ability of TLD designers to simulate complex TLD phenomena, often leading to the need for experimental testing.

The SPH method can model a TLD without these limitations and has seen recent application to sloshing liquids in tanks and TLDs. However, TLDs are often used as an application for demonstrating the power of the SPH method, rather than focusing on developing an SPH model that is tailored to modelling TLDs and applicable to scenarios that expand the knowledge of TLD behavior. In particular, the computational requirements of SPH limit the duration of simulations despite the availability of powerful computational infrastructure. This limits the feasibility of using SPH to study actual TLDs, where it is often necessary to simulate the response over multiple hours.

Development of an efficient SPH model for TLD applications capable of simulating long durations would greatly expand the ability of researchers and TLD designers to numerically model TLDs. Numerically modelling the behavior of TLDs with shallow liquid depths, large amplitude sloshing, and tank modifications such as limited freeboard would allow for improved understanding of TLD behavior, and advancements to TLD design.

1.4 Research Objectives

The primary objectives of this research are:

- Develop an efficient SPH model code for TLDs equipped with damping screens.
- Investigate the feasibility of using SPH for long duration simulations (i.e. random wind loading).
- Couple the SPH model to a structure to investigate the structure-TLD system response under large amplitude excitations.
- Validate the SPH model using experimental data for a variety of TLD and structure-TLD system cases.
- Numerically investigate the response of limited freeboard TLDs to determine the impact on performance of designing for sloshing impact with the tank ceiling.

1.5 Organization of Thesis

This thesis was prepared using a "sandwich" thesis format consisting of a series of published articles and articles submitted for potential publication. As a result, there is some repetition between the chapters, particularly in the introduction and numerical modelling sections. Each chapter has its own literature review and reference list.

Chapter 2 introduces the explicit incompressible SPH numerical model created for this study. The SPH model is validated using hydrostatic and dam break simulation cases. A novel SPH formulation for TLD damping screens is presented and validated with experimental data covering a range of TLD tank sizes, liquid depths, screen arrangements, and excitation amplitudes.

Chapter 3 couples the SPH model developed in Chapter 2 to a structure to calculate the response of a structure-TLD system. The structure is subject to large amplitude excitation consisting of long duration random and short duration transient excitations. The results are compared to experimental data for the system. The performance of the SPH model for keeping fluid particles contained within the tank boundaries is discussed.

Chapter 4 uses the structure-TLD model presented in Chapter 3 to investigate the loss of SPH fluid particles through solid boundaries over the course of long duration simulations of a structure-TLD system. When the excitation is large and splashing occurs in the TLD, fluid particle penetration of the tank boundaries can occur, which was observed in Chapter 3. Four methods to mitigate the boundary penetration are investigated in terms of containing the fluid particles and accurately capturing the structure-TLD response. The boundary condition modifications show improved agreement with experimental data compared to the results of Chapter 3.

Chapter 5 uses the structure-TLD model presented in Chapter 3 to numerically study the impact of limiting TLD freeboard on the response of a structure-TLD system. The structure-TLD system response is determined for a range of excitation amplitudes and freeboard levels, and the performance of the limited freeboard TLD at controlling structural motion is assessed. A linearized mechanical model is introduced for the structure-limited freeboard TLD system to account for added energy dissipation from ceiling impact.

Chapter 6 investigates the nonlinear response of a series-type pendulum TMD-TLD system. An experimental shake table testing program was completed for the system. The fully nonlinear pendulum equation of motion is coupled to a TLD represented by the SPH model presented in Chapter 2. The nonlinear model results are compared to the experimental shake table testing data for the system as well as a simplified linear mechanical model.

Chapter 7 reviews the conclusions and contributions from the research and presents potential future work.

1.6 References

[1] Council on Tall Buildings and Urban Habitat, "100 Tallest Under Construction Buildings in the World," 2021. [Online]. Available: https://www.skyscrapercenter.com/buildings?list=tallest100-construction. [Accessed 01 07 2021].

[2] A. R. Tamboli, Ed., Tall and Supertall Buildings: Planning and Design, New York: McGraw Hill Education, 2014.

[3] T. Haskett and A. Smith, "Feeling at Home in the Clouds," *Structure Magazine*, December 2017.

[4] A. Kareem, T. Kijewski and Y. Tamura, "Mitigation of motions of tall buildings with specific examples of recent applications," *Wind and Structures*, vol. 2, no. 3, pp. 201-251, 1999.

[5] W. H. Melbourne, "Comfort Criteria for Wind-Induced Motion in Structures," *Structural Engineering International*, vol. 8, no. 1, pp. 40-44, 1998.

[6] B. J. Vickery, N. Isyumov and A. G. Davenport, "The Role of Damping, Mass and Stiffness in the Reduction of Wind Effects on Structures," *Journal of Wind Engineering and Industrial Aerodynamics*, vol. 11, no. 1-3, pp. 285-294, 1983.

[7] A. Lago, D. Trabucco and A. Wood, Eds., Damping Technologies for Tall Buildings, Butterworth-Heinemann, 2018.

[8] A. G. Davenport and P. Hill-Carrol, "Damping in tall buildings: its variability and treatment in design," in *Building Motion in Wind*, New York, 1986.

[9] S. Campbell, K. C. Kwok, P. A. Hitchcock, K. T. Tse and H. Y. Leung, "Field measurements of natural periods of vibration and structural damping of wind-excited tall residential buildings," *Wind and Structures*, vol. 10, no. 5, pp. 401-420, 2007.

[10] A. Lago, H. Faridani and D. Trabucco, "Structural Engineering: Damping Technologies for Tall Buildings," *CTBUH Journal*, vol. 3, pp. 42-47, 2018.

[11] G. B. Warburton, "Optimum absorber parameters for various combinations of response and excitation parameters," *Earthquake Engineering and Structural Dynamics*, vol. 10, pp. 381-401, 1982.

[12] J. Connor and S. Laflamme, Structural Motion Engineering, Switzerland: Springer International Publishing, 2014.

[13] C. S. Lee, D. Li, T. C. Haskett, A. W. Smith and D. Kelly, "Case study of performance of a tuned mass damper with an eddy current damping system for building motion control in wind," in *CSCE Annual Conference*, Laval, 2019.

[14] S. Yalla and A. Kareem, "Optimum Absorber Parameters for Tuned Liquid Column Dampers," *Journal of Structural Engineering*, vol. 126, no. 8, pp. 906-915, 2000.

[15] M. J. Tait, "Modelling and preliminary design of a structure-TLD system," *Engineering Structures*, vol. 30, no. 10, pp. 2644-2655, 2008.

[16] Y. Tamura, R. Kohsaka, O. Nakamura, K. Miyashita and V. J. Modi, "Wind-induced responses of an airport tower - efficiency of tuned liquid damper," *Journal of Wind Engineering and Industrial Aerodynamics*, vol. 65, pp. 121-131, 1996.

[17] J. S. Love, B. Morava, J. K. Robinson and T. C. Haskett, "Tuned Sloshing Dampers in Tall Buildings: A Practical Performance-Based Design Approach," *Practice Periodical on Structural Design and Construction*, vol. 26, no. 3, p. 04021016, 2021.

[18] O. M. Faltinsen and A. N. Timokha, Sloshing, New York: Cambridge University Press, 2009.

[19] D. Reed, J. Yu, H. Yeh and S. Gardarsson, "Investigation of Tuned Liquid Dampers Under Large Amplitude Excitation," *Journal of Engineering Mechanics*, vol. 124, no. 4, pp. 405-413, 1998.

[20] L. M. Sun, Y. Fujino, B. M. Pacheco and P. Chaiseri, "Modelling of tuned liquid damper (TLD)," *Journal of Wind Engineering and Industrial Aerodynamics*, vol. 43, no. 1-3, pp. 1883-1894, 1992.

[21] A. Kareem, S. Yalla and M. McCullough, *Sloshing-slamming dynamics - S2 - Analogy for tuned liquid dampers*, vol. 44, R. A. Ibrahim, V. I. Babitsky and M. Okuma, Eds., Berlin, Heildelberg: Springer, 2009, pp. 123-133.

[22] J. W. Miles, "Surface-Wave Damping in Closed Basins," *Proc. R. Soc. Lond. Ser. A Math. Phys. Eng. Sci.*, vol. 297, pp. 459-475, 1967.

[23] S. Kaneko and M. Ishikawa, "Modeling of tuned liquid dampers with submerged nets," *Journal of Pressure Vessel Technology*, vol. 121, no. 3, pp. 334-344, 1999.

[24] M. J. Tait, A. A. El Damatty and N. Isyumov, "An investigation of tuned liquid dampers equipped with damping screens under 2D excitation," *Earthquake Engineering and Structural Dynamics*, vol. 34, no. 7, pp. 719-735, 2005.

[25] C. Shang and J. Zhao, "Periods and energy dissipations of a novel TLD rectangular tank with angle-adjustable baffles," *Journal of Shanghai Jiaotong University (Science)*, vol. 13, pp. 139-144, 2008.

[26] J. S. Love and T. C. Haskett, "Nonlinear modelling of tuned sloshing dampers with large internal obstructions: Damping and frequency effects," *Journal of Fluids and Structures*, vol. 79, pp. 1-13, 2018.

[27] J. S. Love and B. Morava, "Practical Experience with Full-scale Performance Verification of Dynamic Vibration Absorbers Installed in Tall Buildings," *International Journal of High-Rise Buildings*, vol. 10, no. 2, pp. 85-92, 2021.

[28] M. J. Tait, N. Isyumov and A. A. El Damatty, "Performance of Tuned Liquid Dampers," *Journal of Engineering Mechanics,* vol. 134, no. 5, pp. 417-427, 2008.

[29] M. J. Tait, *The Performance of 1-D and 2-D Tuned Liquid Dampers,* Ph.D. Thesis. University of Western Ontario, 2004.

[30] S. Kaneko and Y. Mizota, "Dynamical Modeling of Deepwater-Type Cylindrical Tuned Liquid Damper With a Submerged Net," *ASME Journal of Pressure Vessel Technology,* vol. 122, no. 1, pp. 96-104, 2000.

[31] A. Ghaemmaghami, R. Kianoush and X. X. Yuan, "Numerical Modeling of Dynamic Behavior of Annular Tuned Liquid Dampers for Applications in Wind Towers," *Computer-Aided Civil and Infrastructure Engineering,* vol. 28, pp. 38-51, 2013.

[32] K. P. McNamara, J. S. Love, M. J. Tait and T. C. Haskett, "Response of an Annular Tuned Liquid Damper Equipped with Damping Screens," *ASME Journal of Vibration and Acoustics,* vol. 143, no. 1, p. 011011, 2021.

[33] J. Chen and C. T. Georgakis, "Spherical tuned liquid damper for vibration control in wind turbines," *Journal of Vibration and Control,* vol. 21, no. 10, pp. 1875-1885, 2015.

[34] X. Deng and M. J. Tait, "Equivalent mechanical models of tuned liquid dampers with different tank geometries," *Canadian Journal of Civil Engineering,* vol. 35, no. 10, pp. 1088-1101, 2008.

[35] S. Gardarsson, H. Yeh and D. A. Reed, "Behavior of Sloped-Bottom Tuned Liquid Dampers," *Journal of Engineering Mechanics,* vol. 127, no. 3, pp. 266-271, 2001.

[36] J. S. Love and M. J. Tait, "The response of structures equipped with tuned liquid dampers of complex geometry," *JVC/Journal of Vibration and Control,* vol. 21, no. 6, pp. 1171-1187, 2015.

[37] J. S. Love, K. P. McNamara, M. J. Tait and T. C. Haskett, "Tuned sloshing dampers with large rectangular core penetrations," *Journal of Vibration and Acoustics,* vol. 142, p. 061003, 2020.

[38] R. Ibrahim, Liquid Sloshing Dynamics, Cambridge: Cambridge University Press, 2005.

[39] O. M. Faltinsen, O. F. Rognebakke, I. A. Lukovsky and A. N. Timokha, "Multidimensional modal analysis of nonlinear sloshing in a rectangular tank with finite water depth," *Journal of Fluid Mechanics,* vol. 407, pp. 201-234, 2000.

[40] J. S. Love and M. J. Tait, "Nonlinear simulation of a tuned liquid damper with damping screens using a modal expansion technique," *Journal of Fluids and Structures,* vol. 26, no. 7-8, pp. 1058-1077, 2010.

[41] J. S. Love and M. J. Tait, "Non-linear multimodal model for tuned liquid dampers of arbitrary tank geometry," *International Journal of Non-Linear Mechanics,* vol. 46, no. 8, pp. 1065-1075, 2011.

[42] J. S. Love and M. J. Tait, "Frequency domain prediction of peak nonlinear wave heights of structure-TLD systems," *Engineering Structures,* vol. 194, pp. 1-10, 2019.

[43] M. J. Tait, A. A. El Damatty, N. Isyumov and M. R. Siddique, "Numerical flow models to simulate tuned liquid dampers (TLD) with slat screens," *Journal of Fluids and Structures,* vol. 20, no. 8, pp. 1007-1023, 2005.

[44] H. Alemi Ardakani and T. J. Bridges, "Dynamic coupling between shallow-water sloshing and horizontal vehicle motion," *European Journal of Applied Mathematics,* vol. 21, no. 6, pp. 479-517, 2010.

[45] M. Marivani and M. S. Hamed, "Numerical simulation of structure response outfitted with a tuned liquid damper," *Computers and Structures,* vol. 87, no. 17-18, pp. 1154-1165, 2009.

[46] A. Ashasi-Sorkhabi, H. Malekghasemi, A. Ghaemmaghami and O. Mercan, "Experimental investigations of tuned liquid damper-structure interactions in resonance considering multiple parameters," *Journal of Sound and Vibration,* vol. 388, pp. 141-153, 2017.

[47] A. Jafari and N. Ashgriz, "Numerical Techniques for Free Surface Flows: Interface Capturing and Interface Tracking," *Encyclopedia of Microfluidics and Nanofluidics,* 2014.

[48] T. Belytschko, Y. Krongauz, D. Organ, M. Fleming and P. Krysl, "Meshless Methods: An Overview and Recent Developments," *Computer Method in Applied Mechanics and Engineering,* vol. 139, no. 1-4, pp. 3-47, 1996.

[49] R. A. Gingold and J. J. Monaghan, "Smoothed particle hydrodynamics: theory and application to non-spherical stars," *Monthly Notices of the Royal Astronomical Society,* vol. 181, pp. 375-389, 1977.

[50] L. Lucy, "A numerical approach to the testing of the fission hypothesis," *The Astronomical Journal,* vol. 82, no. 12, pp. 1013-1024, 1977.

[51] J. J. Monaghan, "Smoothed Particle Hydrodynamics," *Annual Review of Astronomy and Astrophysics,* vol. 30, pp. 543-74, 1992.

[52] J. J. Monaghan, "Simulating free surface flows with SPH," *Journal of Computational Physics,* vol. 110, no. 2, pp. 399-406, 1994.

[53] D. Violeau and B. D. Rogers, "Smoothed particle hydrodynamics (SPH) for free-surface flows: Past, present and future," *Journal of Hydraulic Research,* vol. 54, no. 1, pp. 1-26, 2016.

[54] D. Molteni and A. Colagrossi, "A simple procedure to improve the pressure evaluation in hydrodynamic context using the SPH," *Computer Physics Communications,* vol. 180, no. 6, pp. 861-872, 2009.

[55] M. Antuono, A. Colagrossi and S. Marrone, "Numerical diffusive terms in weakly-compressible SPH schemes," *Computer Physics Communications,* vol. 183, no. 12, pp. 2570-2580, 2012.

[56] A. Colagrossi and M. Landrini, "Numerical simulation of interfacial flows by smoothed particle hydrodynamics," *Journal of Computational Physics,* vol. 191, pp. 448-475, 2003.

[57] S. J. Cummins and M. Rudman, "An SPH Projection Method," *Journal of Computational Physics,* vol. 152, pp. 584-607, 1999.

[58] S. Shao and E. Y. Lo, "Incompressible SPH method for simulating Newtonian and non-Newtonian flows with a free surface," *Advances in Water Resources,* vol. 26, pp. 787-800, 2003.

[59] R. Xu, P. Stansby and D. Laurence, "Accuracy and stability in incompressible SPH (ISPH) based on the projection method and a new approach," *Journal of Computational Physics,* vol. 228, no. 18, pp. 6703-6725, 2009.

[60] H. Jiang, Y. You, Z. Hu, X. Zheng and A. Ma, "Comparative study on violent sloshing withwater jet flows by using the ISPH method," *Water (Switzerland),* vol. 11, p. 2590, 2019.

[61] D. Violeau and A. Leroy, "Optimal time step for incompressible SPH," *Journal of Computational Physics,* vol. 288, pp. 119-130, 2015.

[62] A. D. Chow, B. D. Rogers, S. J. Lind and P. K. Stansby, "Incompressible SPH (ISPH) with fast Poisson solver on a GPU," *Computer Physics Communications,* vol. 226, pp. 83-103, 2018.

[63] S. M. Hosseini, M. T. Manzari and S. K. Hannani, "A fully explicit three-step SPH algorithm for simulation of non-Newtonian fluid flow," *International Journal of Numerical Methods for Heat & Fluid Flow,* vol. 17, no. 7, pp. 715-735, 2007.

[64] S. Yeylaghi, B. Moa, P. Oshkai, B. Buckham and C. Crawford, "ISPH modelling of an oscillating wave surge converter using an OpenMP-based parallel approach," *Journal of Ocean Engineering and Marine Energy,* vol. 2, pp. 301-312, 2016.

[65] Nomeritae, E. Daly, S. Grimaldi and H. H. Bui, "Explicit incompressible SPH algorithm for free-surface flow modelling: A comparison with weakly compressible schemes," *Advances in Water Resources,* vol. 97, pp. 156-167, 2016.

[66] G. Bulian, A. Souto-Iglesias, L. Delorme and E. Botia-Vera, "Smoothed particle hydrodynamics (SPH) simulation of a tuned liquid damper (TLD) with angular motion," *Journal of Hydraulic Research,* vol. 48, no. sup1, pp. 28-39, 2009.

[67] A. Marsh, M. Prakash, E. Semercigil and O. F. Turan, "A study of sloshing absorber geometry for structural control with SPH," *Journal of Fluids and Structures,* vol. 27, no. 8, pp. 1165-1181, 2011.

[68] M. D. Green, *Sloshing simulations with the smoothed particle hydrodynamics (SPH) method,* PhD Thesis, Imperial College London, 2017.

[69] M. D. Green and J. Peiro, "Long duration SPH simulations of sloshing in tanks with a low fill ratio and high stretching," *Computers and Fluids,* vol. 174, pp. 179-199, 2018.

[70] M. D. Green, Y. Zhou, J. M. Dominguez, M. G. Gesteira and J. Peiro, "Smooth particle hydrodynamics simulations of long-duration violent three-dimensional sloshing in tanks," *Ocean Engineering,* vol. 229, p. 108925, 2021.

[71] A. H. Kashani, A. M. Halabian and K. Asghari, "A numerical study of tuned liquid damper based on incompressible SPH method combined with TMD analogy," *Journal of Fluids and Structures,* vol. 82, pp. 394-411, 2018.

[72] A. M. Halabian, A. Karamnasab and M. R. Chamani, "A New Hybrid SPH-FEM Model to Evaluate Seismic Response of TSD Equipped-Structures," *Journal of Earthquake and Tsunami,* vol. 13, no. 2, pp. 1-27, 2019.

[73] X. Y. Cao, F. R. Ming and A. M. Zhang, "Sloshing in a rectangular tank based on SPH simulation," *Applied Ocean Research,* vol. 47, pp. 241-254, 2014.

[74] F. Aristodemo, D. D. Meringolo and P. Veltri, "A multi-node approach to simulate thin coastal structures in the SPH context," *Coastal Engineering Proceedings,* vol. 1, no. 35, 2016.

[75] D. D. Meringolo, F. Aristodemo and P. Veltri, "SPH numerical modeling of wave-perforated breakwater interaction," *Coastal Engineering,* vol. 101, pp. 48-68, 2015.

[76] A. Valizadeh and M. Rudman, "A numerical approach for simulating flow through thin porous media," *European Journal of Mechanics, B/Fluids,* vol. 65, pp. 31-44, 2017.

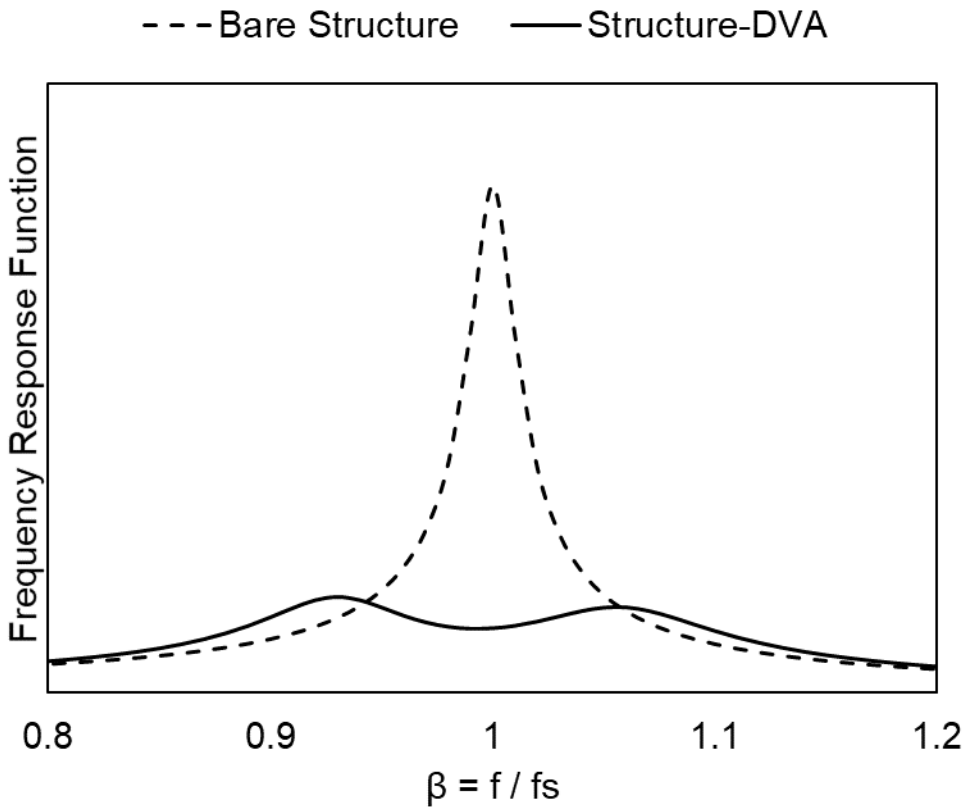

Figure 1.1: Frequency Response Function for structure and structure-DVA system

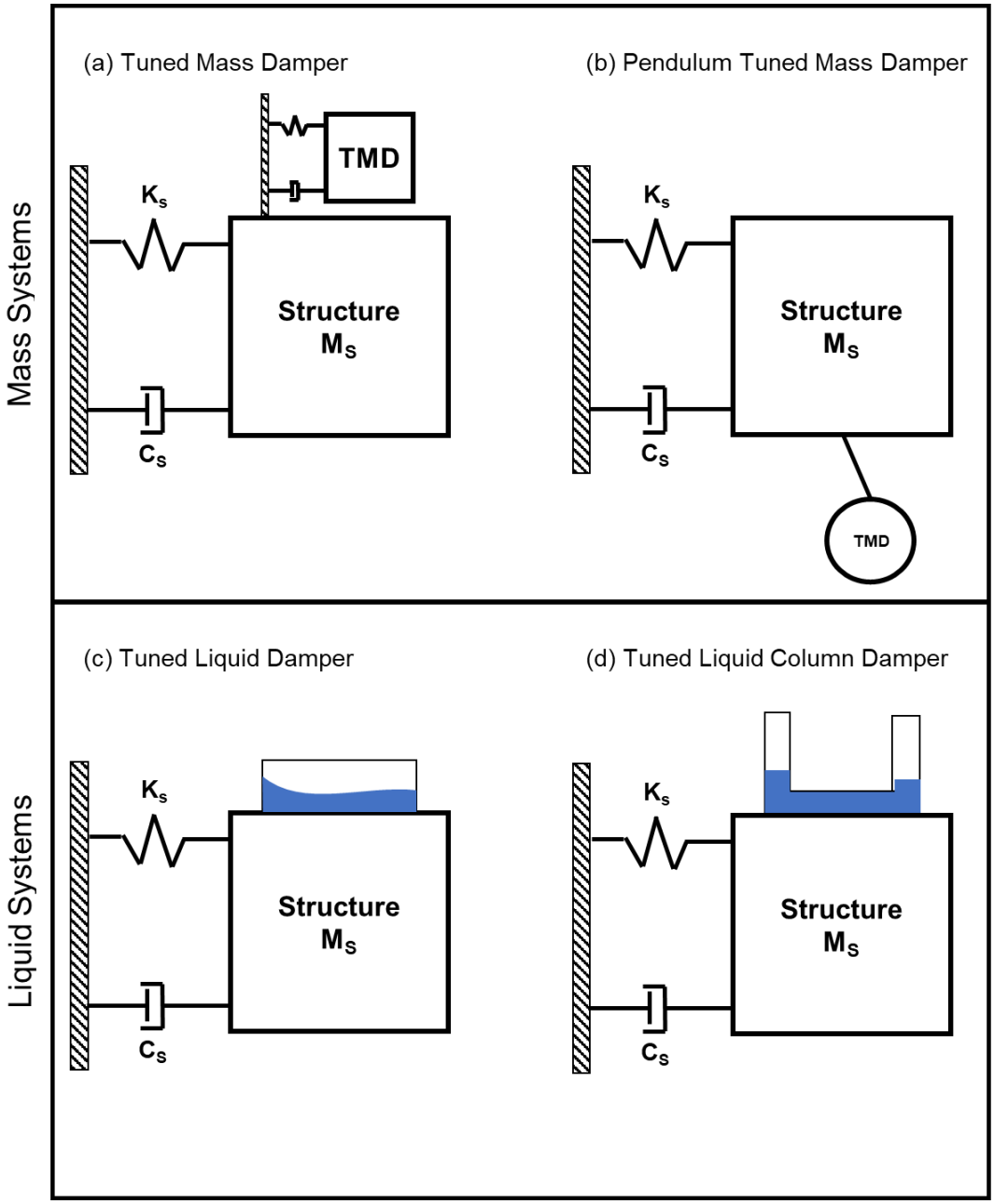

Figure 1.2: Schematics of structure-DVA systems

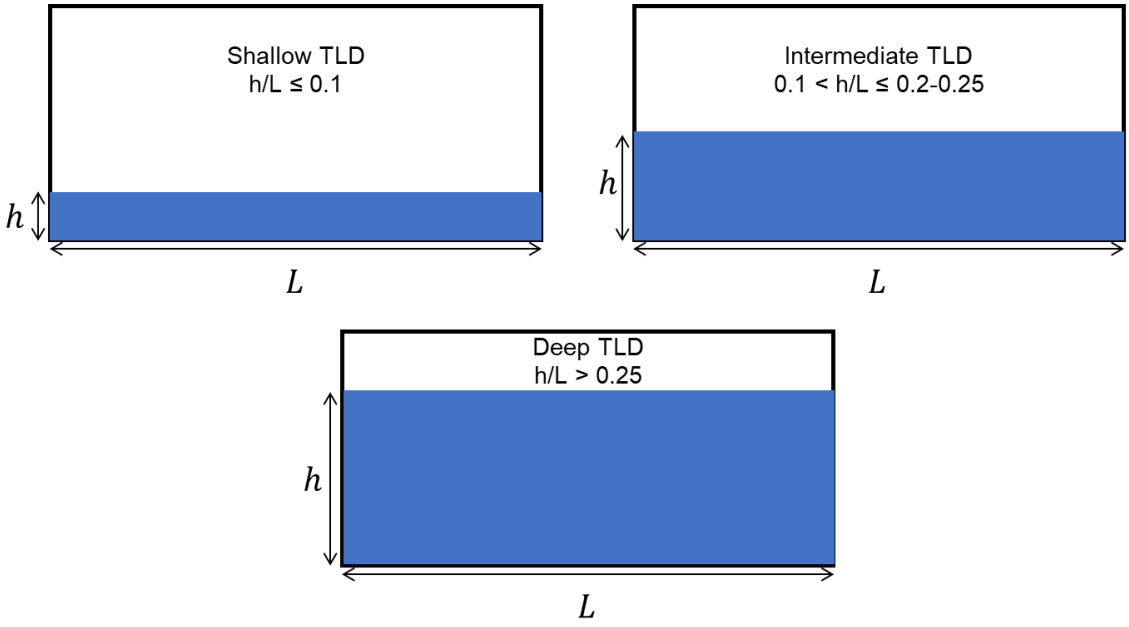

Figure 1.3: Classification of TLD based on ratio of liquid depth to tank length

Chapter 2: Incompressible smoothed particle hydrodynamics model of a rectangular tuned liquid damper containing screens

Reproduced with permission from Elsevier.

McNamara K.P., Awad B.N., Tait M.J, Love J.S., "Incompressible smoothed particle hydrodynamics model of a rectangular tuned liquid damper containing screens." Journal of Fluids and Structures 103 (2021): 103295, DOI: 10.1016/j.jfluidstructs.2021.103295

Abstract

Damping screens are often installed within a tuned liquid damper (TLD) to increase the energy dissipation beyond what the sloshing liquid alone can provide. Many numerical models exist to study the response of a TLD; however, there are often associated limitations on fluid depth or excitation amplitude. The smoothed particle hydrodynamics (SPH) method can capture the fully nonlinear TLD response without limitation by solving the Navier-Stokes equations throughout the fluid domain. A two-dimensional explicit incompressible SPH model is presented and validated against a hydrostatic and dam break flow scenario. The damping screens are modelled in SPH on a macroscopic level using Morison's equation for force on an object submerged in fluid flow. This implementation is computationally efficient compared to explicitly modelling the damping screens using solid particles as it allows for a much larger initial particle spacing. The SPH model results for screen forces, wave heights, and TLD sloshing water forces are validated against experimental time and frequency response data. The SPH model is found to be in excellent agreement with the experimental data for a range of TLD tank dimensions (L = 0.966 and 1.524 m), fluid depths (h/L = 0.05 to 0.25), excitation amplitudes (X_0/L = 0.0025 to 0.031), and excitation frequencies (β = 0.7 to 1.3). The presented SPH model for a TLD with damping screens can be used to study the nonlinear response of a rectangular TLD.

KEYWORDS: tuned liquid damper (TLD), damping screen, smoothed particle hydrodynamics (SPH).

2.1 Introduction

The tuned liquid damper (TLD), also known as the tuned sloshing damper (TSD) is a type of dynamic vibration absorber (DVA) often employed to suppress unwanted vibration in structures. The TLD consists of a partially filled tank of liquid (generally water) that is installed near the location of the maximum vibration of a targeted structural mode. The sloshing frequency of the TLD is tuned to be near the targeted structural modal frequency by adjusting the tank dimensions and liquid depth. When the structure vibrates, the liquid in the TLD sloshes, applying a force to the structure and reducing its vibration. The TLD is an attractive technology compared to other DVAs, such as the tuned mass damper (TMD), due to its low cost and simple construction. Numerical models of a TLD are an integral part of the design process which allow the study of both the TLD and structure-TLD system response to external loadings such as wind or earthquakes.

The nonlinearity of the sloshing in a TLD leads to significant challenges when attempting to model the TLD across the full range of geometries, liquid depths, and excitation amplitudes that may be necessary for a real-world TLD application. Many different TLD numerical models have been studied in the literature. Equivalent linear mechanical models, wherein the TLD is represented as an equivalent TMD with mass, stiffness, and damping parameters have been investigated as a simplified tool for preliminary TLD studies (Tait, 2008); however, they are limited to capturing only one or a few modes of sloshing. Other models have been based on potential flow theory for deeper tanks where the response is inherently less nonlinear (Kaneko & Yoshida, 1999). For shallow depth TLDs, nonlinear models based on shallow water wave theory have been presented (Tait, El Damatty, Isyumov, & Siddique, 2005); however, these models typically have limits of applicability based on fluid depth and convergence at large amplitudes. The geometry of a TLD is often dictated by the structure into which it will be installed. Various tank geometries have been studied (Deng & Tait, 2008), extending to a TLD of arbitrary geometry where the sloshing modes are determined by the finite element method (Love & Tait, 2011).

Computational fluid dynamics (CFD) models are an attractive option for capturing the fully nonlinear response of a TLD by solving the Navier-Stokes (NS) equations throughout the entire fluid domain. Previous studies investigated fluid-structure interaction (FSI) with a sloshing tank using the finite element method (FEM) (Cho & Lee, 2004), Finite Difference Method (FDM) (Chen & Nokes, 2005), and Boundary Element Method (BEM) (Huang, Duan, & Zhu, 2010). These methods are based on a pre-defined mesh that is unable to capture large deformations of the free surface and wave breaking without improvements, such as free surface capturing and tracking techniques, which are complex and require large computational overhead (Gao, 2011).

Lagrangian mesh-free methods have evolved recently to deal with large-amplitude free surface flows. The Smoothed Particle Hydrodynamics (SPH) method discretizes the fluid domain into individual particles rather than cells (Monaghan, 1992). SPH is capable of capturing wave breaking and large fluid responses without expensive tracking algorithms (Monaghan, 1994). SPH has been applied to many different applications of sloshing motion and FSI. Two main approaches are used across SPH simulations involving a free surface, namely weakly compressible SPH (WCSPH) and incompressible SPH (ISPH). WCSPH was proposed by Monaghan (1994) and solves the NS equations through an explicit scheme that relates density and pressure using an equation of state. The equation of state is selected such that fluctuations in density are limited; however, this can lead to oscillations in pressure if not handled correctly (Violeau & Rogers, 2016). ISPH was first implemented by Cummins and Rudman (1999). ISPH enforces incompressibility of the fluid by solving a pressure Poisson equation (PPE) and ensuring either a divergence free (Cummins & Rudman, 1999) or density invariant (Shao & Lo, 2003) condition, or some combination of both (Jiang, You, Hu, Zheng, & Ma, 2019). ISPH is generally grouped into implicit and explicit schemes depending on how the PPE is solved.

Sloshing in tanks and TLDs has been investigated using SPH in various studies. Bulian et al. (2009) investigated the response of a TLD undergoing angular motion coupled to a simplified structure using WCSPH, finding good agreement with experimental data for

both the TLD and structure response. Marsh et al. (2011) studied the performance of a series of different tank shapes, including rectangular, cylindrical, and trapezoidal using WCSPH. Cao et al. (2014) used a WCSPH scheme to investigate the wave heights and sloshing induced pressures in a rectangular tank in both 2D and 3D and found that a baffle at the mid-tank significantly reduced the fluid response. Green and Peiro (2018) completed long duration SPH studies on rectangular TLDs and found good agreement with experimental data for wave heights and sloshing water forces. Halabian et al. (2019) studied a rectangular TLD coupled to a structure undergoing earthquake excitation. Jiang et al. (2019) studied violent sloshing using an ISPH model and found good agreement with experimental data for free surface profiles and impact pressures in a rectangular tank.

The sloshing motion in a TLD typically does not achieve the required energy dissipation to control the vibration of a structure effectively. Flow damping devices, such as nets (Kaneko & Ishikawa, 1999), baffles (Chu, Wu, Wu, & Wang, 2018), paddles (Love & Haskett, 2018), or screens (Tait, El Damatty, Isyumov, & Siddique, 2005) are often installed to increase the TLD damping. These damping devices can be implemented on a microscopic level, where the devices are explicitly modelled and the flow around them is fully captured, or a macroscopic level, where the overall impact of the devices is included in the model, but the localized flow is not necessarily captured.

This study will focus on slat type damping screens as implemented by Tait et al. (2005). Kashani et al. (2018) studied the TLD equipped with slat screens using ISPH where the slats were modelled on a microscopic scale and compared to experimental results from Tait et al. (2005). Other SPH studies have considered explicitly modelling thin perforated walls comparable to the slat screens using boundary particles (Aristodemo, Meringolo, & Veltri, 2016). The major drawback to explicitly modelling the slat screens on a microscopic scale in SPH is that the particle spacing must be very fine to capture the screen geometry effectively, leading to high computational cost. Valizadeh and Rudman (2017) presented a macroscopic porous screen implementation in SPH that included a force term derived from the pressure drop through a screen for channels undergoing steady flow.

This paper presents a computationally efficient macroscopic damping screen implementation for studying a rectangular TLD using SPH. A two-dimensional explicit ISPH model for free surface flows that was developed in-house is presented. The model is validated against hydrostatic and dam break cases. The damping screen implementation based on Morison's equation for force on a submerged object under oscillating flow is presented and adapted for SPH. The SPH damping screen implementation is validated using a broad set of existing experimental shake table testing results, considering multiple TLD tank geometries (L = 0.966 m and 1.524 m), damping screens, fluid depths (h/L = 0.05 to 0.25), and excitation amplitudes (X_0/L = 0.0025 to 0.031). The SPH model is found to show excellent agreement with experimental results.

2.2 Smoothed Particle Hydrodynamics Model

A schematic of a rectangular TLD containing damping screens is shown in Figure 2.1. The origin is placed at the bottom left corner of the tank. The dimensions of the TLD tank define the solid domain boundaries, with length *L* and height *H*. The fluid in the tank is water that is filled to a constant height *h* across the entire tank length. Damping screens with openings are placed at different locations in the tank x_{screen}. For this study, the screens are assumed to be vertical. This section outlines the explicit incompressible SPH model developed to model a TLD equipped with damping screens.

2.2.1 Governing Equations and Domain Discretization

The governing equations solved by the SPH model are the Lagrangian form of the Navier-Stokes (NS) equations for incompressible flow:

$$\frac{D\rho}{Dt} + \rho\nabla\mathbf{u} = 0 \tag{2.1}$$

$$\frac{\mathrm{D}\mathbf{u}}{Dt} = -\frac{1}{\rho}\nabla P + v\nabla^2\mathbf{u} + \mathbf{g} \tag{2.2}$$

where ρ is the density of the fluid (assumed to be 1000 kg/m^3 for water), **u** is the fluid velocity vector, P is the fluid pressure, v is the kinematic viscosity (10^{-6} m^2/s for water), and **g** is the body force vector, which includes gravity and external forces. In this notation, **bold** symbols denote a vector quantity.

In the SPH method, the fluid domain is represented by a series of discrete particles that each have associated properties, such as position, velocity, pressure, and density. The particles are evenly spaced at an initial distance *dp*. For a specific particle *j*, the volume is equal to $V_j = dp^{nd}$, where *nd* is the number of spatial dimensions. For a 2D simulation, the particle spacing is *dp* by *dp*, with a unit dimension in the perpendicular direction, so the volume and mass of each particle are $V_j = 1 \cdot dp^2$ and $m_j = \rho V = \rho dp^2$. The flow properties are interpolated using a kernel function approximation (Monaghan, 1992):

$$\mathrm{A}(r_i) \approx \int_{\Omega} A(r_j)\ W(r_i - r_j, h_{ker})\ dr \tag{2.3}$$

where *A(r)* is an arbitrary function of interest (i.e. velocity, density), Ω is the particle neighbourhood, *W* is the kernel function, and h_{ker} is the smoothing length. This concept is illustrated in Figure 2.2.

The approximation of equation **(2.3)** is calculated by the summation of neighbour particles:

$$A_i = \sum_{j=1}^{N} A_j \frac{m_j}{\rho_j} W(r_i - r_j, h_{ker}) \tag{2.4}$$

where *j* indicates all particles within the neighbourhood of particle *i* (*j*=1, 2, …N), and m_j and ρ_j are the mass and density of the particle. Controlling the size of the kernel domain is based on the smoothing length h_{ker}, which is a key parameter for the accuracy of the results. In this study the fifth order Wendland kernel function is used (Wendland, 1995):

$$W(q) = W_c \begin{cases} (1+2q)\left(1-\frac{q}{2}\right)^4 & 0 \le q \le 2 \\ 0 & q > 2 \end{cases} \tag{2.5}$$

where $q = \frac{|r_i - r_j|}{h_{ker}}$ and for 2D simulations $W_c = \frac{7}{\pi h_{ker}^2}$.

The first-order derivative adopted in this paper is the symmetrized form which conserves both linear and angular momentum (Monaghan, 1992):

$$(\nabla A)_i = \rho_i \sum_{j=1}^{N} m_j \left(\frac{A_j}{\rho_j^2} + \frac{A_i}{\rho_i^2}\right) \nabla_j W_{ij} \tag{2.6}$$

The Laplacian operator is defined as (Cummins & Rudman, 1999):

$$\nabla.\left(\frac{1}{\rho}\nabla A\right)_i = \sum_{j=1}^{N} \left(\frac{8m_j}{(\rho_i + \rho_j)^2} \frac{A_{ij}\boldsymbol{r_{ij}}.\boldsymbol{\nabla_i} W_{ij}}{r_{ij}^2 + \eta^2}\right) \tag{2.7}$$

where $A_{ij} = A_i - A_j$, $\boldsymbol{r_{ij}} = \boldsymbol{r_i} - \boldsymbol{r_j}$, $\eta = 0.001 h_{ker}$ and $\boldsymbol{\nabla_j} W_{ij} = \frac{W_c}{h_{ker}} \left(-5q\left(1 - \frac{q}{3}\right)^3\right) \frac{\boldsymbol{r_i} - \boldsymbol{r_j}}{||\boldsymbol{r_i} - \boldsymbol{r_j}||}$.

2.2.2 Time Integration

In the present study, the ISPH algorithm follows the widely used projection method to solve the NS equations (Cummins & Rudman, 1999). The predictive step calculates an intermediate velocity $\boldsymbol{u^*}$ considering only viscous and body forces (Shao & Lo, 2003), and then uses this velocity to calculate the intermediate position $\boldsymbol{r^*}$:

$$\boldsymbol{u}^* = \mathbf{u}(t) + (v\nabla^2\mathbf{u} + \mathbf{g} + \mathbf{F}_{\boldsymbol{ext}} + \mathbf{F}_{\boldsymbol{screen}})\Delta t \tag{2.8}$$

$$\boldsymbol{r}^* = \mathbf{r}(t) + \boldsymbol{u}^* \Delta t \tag{2.9}$$

where $v\nabla^2\mathbf{u}$ is the viscous force, $\mathbf{g}$ is the gravitational acceleration, $\mathbf{F_{ext}}$ is the external force applied to the fluid (i.e. base acceleration or excitation force acting on the TLD), and $\mathbf{F_{screen}}$ is the force from the damping screens which is introduced in Section 2.2.4.

An intermediate density ρ^* is calculated based on the intermediate velocity and position of the fluid particles (Nomeritae, Daly, Grimaldi, & Bui, 2016). The fluid pressure is then calculated by solving the pressure Poisson equation (PPE):

$$\boldsymbol{\nabla}.\left(\frac{\boldsymbol{\nabla} P}{\rho}\right) = \left(\frac{\boldsymbol{\nabla}.\boldsymbol{u}^*}{\Delta t}\right) \tag{2.10}$$

Based on Jiang et al. (2019), a pressure stabilizing source term is added to the PPE to combine both the divergence-free and density-invariant incompressible SPH conditions:

$$\boldsymbol{\nabla}.\left(\frac{\boldsymbol{\nabla}P}{\rho}\right) = \alpha\frac{\rho_0 - \rho^*}{\rho_0 \Delta \mathrm{t}^2} + (1-\alpha)\frac{\boldsymbol{\nabla}.\boldsymbol{u}^*}{\Delta t} \tag{2.11}$$

where the first term represents the density-invariant effect and the second term represents the divergence-free effect, and α is equal to 0.01. The PPE is discretized by the following expression (Yeylaghi, Moa, Oshkai, Buckham, & Crawford, 2016):

$$\sum_{j=1}^{N} A_{ij}P_{ij} = (1-\alpha)\left(\frac{-1}{\Delta t}\right)\sum_{j=1}^{N} B_{ij} + \alpha\frac{\rho_0 - \rho^*}{\Delta \mathrm{t}^2}$$
$$A_{ij} = \frac{8m_j}{\left(\rho_i + \rho_j\right)^2}\frac{\boldsymbol{r_{ij}}.\boldsymbol{\nabla_i}W_{ij}}{r_{ij}^2 + \eta^2}, B_{ij} = \frac{m_j}{\rho_j}(\boldsymbol{u_j^*} - \boldsymbol{u_i^*})\boldsymbol{\nabla_j}W_{ij} \tag{2.12}$$

This equation is solved using an explicit approach, where the timestep is assumed to be sufficiently small such that the pressure of each particle at time $t+\Delta t$ can be calculated from the pressure of the neighbour particles at time t. Thus, equation **(2.12)** can be re-arranged:

$$P_i(t+\Delta t) = \frac{\sum_{j=1}^{N} A_{ij}P_j(t) + (1-\alpha)\left(\frac{-1}{\Delta t}\right)\sum_{j=1}^{N} B_{ij} + \alpha\frac{\rho_0 - \rho^*}{\Delta \mathrm{t}^2}}{\sum_{j=1}^{N} A_{ij}} \tag{2.13}$$

If a particle pressure is calculated to be negative, it is set to zero as negative pressures should not occur in the simulations considered (Nomeritae, Daly, Grimaldi, & Bui, 2016).

Incompressibility is imposed at the end of the timestep by correcting the velocity of the fluid particles considering the pressure term:

$$\mathbf{u}(\mathrm{t}+\Delta \mathrm{t}) = \mathbf{u}^* + \left(-\frac{1}{\rho}\boldsymbol{\nabla}\mathrm{P}\right)\Delta \mathrm{t} \tag{2.14}$$

Then the positions are updated:

$$\mathbf{r}(\mathrm{t}+\Delta \mathrm{t}) = \mathbf{r}(\mathrm{t}) + \left(\frac{\mathbf{u}(\mathrm{t}+\Delta \mathrm{t}) + \mathbf{u}(\mathrm{t})}{2}\right)\Delta \mathrm{t} \tag{2.15}$$

2.2.3 Boundary Conditions

Multiple layers of fixed dummy particles are used to model the solid boundaries of the SPH domain following the method outlined by Adami et al. (2012). The boundary particles have the same spacing, density, and mass as the fluid particles, and do not change position

throughout the simulation. The pressure of each boundary particle (subscript *w*) is determined from the surrounding fluid particles (subscript *i*) by the expression:

$$P_w = \frac{\sum_{i=1}^{N} P_i W_{wi} + \mathrm{g}\left(\sum_{i=1}^{N} \rho_i r_{wi} W_{wi}\right)}{\sum_{i=1}^{N} W_{wi}} \tag{2.16}$$

The velocity of the boundary particles is calculated to enforce either a free-slip or no-slip condition, as illustrated in Figure 2.3. A no-slip condition is implemented by reflecting the perpendicular fluid velocity and enforcing the parallel velocity to be zero. A free-slip condition is implemented by reflecting the perpendicular fluid velocity and enforcing the parallel velocity at the solid-fluid interface to be the same as the fluid velocity. A free-slip condition is implemented in this study.

In addition to the solid boundaries, for the incompressible SPH scheme it is necessary to enforce the Dirichlet boundary condition of zero pressure on the free surface (Shao & Lo, 2003). A false density is calculated for each fluid particle (Yeylaghi, Moa, Oshkai, Buckham, & Crawford, 2016):

$$\rho_{fi} = \sum_{j=1}^{N} m_j W_{ij} \tag{2.17}$$

The kernel function is truncated near the free surface, and thus a free surface particle can be identified by false density values $\rho_f < 0.90\rho_0$, where ρ_0 is the initial fluid density. The pressure of free surface particles is set to zero at each timestep.

2.2.4 Damping Screen Implementation

Damping screens placed in a TLD act to increase the energy dissipation of the TLD, which improves its performance as the TLD damping will be closer to its optimal value. The damping screens considered in this study consist of solid horizontal sharp-edged slats of height h_{slat} with openings between them of height h_{gap} distributed over the total height of the screen H_{screen} (typically the height of the TLD tank) as depicted in Figure 2.4. The screens are placed perpendicular to the direction of TLD excitation, and they are assumed to have a very small thickness relative to the length of the tank.

SPH has the capability of modelling the damping screen geometry explicitly using solid particles to represent the individual screen sections (Kashani, Halabian, & Asghari, 2018). This implementation is ideal when the behaviour of the screens is unknown and allows for testing of different screen geometries and slat distributions without the need for experimental study. However, the SPH model requires a very small particle size to capture the geometry of the screen and the surrounding flow accurately. For the model used in this study, explicitly modelling the screens would require around 50 times the number of particles, increasing the CPU time by a factor of approximately 700.

Since the screens have a very small thickness relative to the length of the tank, the influence of the screens on the flow in the tank is concentrated near the screens. For cases where the energy dissipation behaviour of the screens is known (i.e. damping and added mass effects are determined theoretically or experimentally), the screens can be modelled on a macroscopic scale. The overall influence of the screens on the TLD response is captured; however, the fine detail of the localized flow at the screens is not. This allows for a much larger particle spacing, and significantly reduced SPH simulation runtime. This concept is appropriate for a TLD, where the main quantities of interest are the overall fluid base shear forces and wave height near the tank walls, and has been applied to previous TLD models (Tait, El Damatty, Isyumov, & Siddique, 2005; Love & Tait, 2010).

When an object is submerged in a moving fluid it experiences forces due to the flow. Consequently, the fluid also experiences an equal and opposite force. The Morison equation is commonly used to represent wave-induced force on a submerged object (Morison, O'Brien, Johnson, & Schaaf, 1950). For oscillating flow, the equation is of the form:

$$F = \frac{1}{2} C_D \rho A |u| u + C_m \rho V_m \frac{du}{dt} \qquad \textbf{(2.18)}$$

where C_D is the drag coefficient, A is the projected area of the object, u is the flow velocity perpendicular to the screen, C_m is the added mass coefficient, and V_m is the volume of the displaced fluid. The values of C_D and C_m must be determined theoretically or empirically. The terms in the equation are typically separated into the drag force (first term) and inertial

force (second term). The drag force contributes to the energy dissipation from the screens in a TLD, whereas the inertia force contributes to the kinetic energy of the fluid but does not dissipate energy (Tait, 2008).

The force applied over a small height of the screen (assuming a tank width of unity in a 2D simulation) is given by the following expression (Love & Tait, 2010):

$$dF = \frac{1}{2} C_D \rho |u| u dy + C_m \rho t_{screen} \frac{du}{dt} dy \tag{2.19}$$

where t_{screen} is the thickness of the screen. To account for the fact that the screens are not completely solid, the solidity ratio, S, which is the ratio of the solid screen area to the total screen area (including openings) is introduced. The screen loss coefficient, $C_l = SC_D$, can then be defined. The total force exerted on the slat screen over the height of the fluid can be calculated by the expression:

$$F = \frac{1}{2} C_l \rho \int_0^{\eta} |u| u dy + C_m \rho t_{screen} S \int_0^{\eta} \frac{du}{dt} dy \tag{2.20}$$

where η is the wave height at the location of the screen. To implement the screens in SPH, the screen is discretized across the height of the tank using dummy particles with the same initial spacing as the fluid particles (dp), as illustrated in Figure 2.5. This allows the integral in equation **(2.20)** to be evaluated numerically as a summation of the force acting on each screen particle:

$$F_{screen} = \sum_j F_{screen-j} = \frac{1}{2} C_l \rho \sum_j |U_{sc,j}| U_{sc,j} dp + C_m \rho t_{screen} S \sum_j a_{sc,j} dp \tag{2.21}$$

where j is summed over the screen particles, dp is the initial particle spacing (equivalent to the projected area of the screen particle in two dimensions), $U_{sc,j}$ and $a_{sc,j}$ are the velocity and acceleration of the fluid at the location of screen particle j, calculated by:

$$U_{sc,j} = \sum_f \frac{m_f}{\rho_f} u_f W_{jf}\,, a_{sc,j} = \sum_f \frac{m_f}{\rho_f} a_f W_{jf} = \sum_f \frac{m_f}{\rho_f} \frac{u_f(t) - u_f(t - \Delta t)}{\Delta t} W_{jf} \tag{2.22}$$

where f is summed over the neighbouring fluid particles, and W_{jf} is the kernel function, which can have a different smoothing length (h_{screen}) and kernel function than the fluid

particles. In this study the value of h_{screen} was set equal to $3h_{ker}$. Only the fluid velocity perpendicular to the screen is considered.

During the prediction step, the force acting on each screen particle *j* is calculated using equation **(2.21)**. This total screen particle force can be considered as the summation of the contributions from the neighbouring fluid particles. The contribution of each neighbouring fluid particle on the screen force is assumed to be proportional to the kernel function value. Thus, the force acting on the neighbouring fluid particles due to the screens is calculated as:

$$F_{screen-f} = -\sum_{j} F_{screen-j} \frac{W_{jf}}{\sum_f W_{jf}} \tag{2.23}$$

This force is implemented during the prediction step calculation and applied to the fluid particles in equation **(2.8)**. This force is the only interaction between the screen particles and the fluid particles, and other quantities such as the velocity and pressure are not solved for the screen particles. This means that when the fluid particles move through the screens, they are influenced by the screen force, but are not obstructed from their motion (i.e. having to flow around individual slats).

2.3 Validation of Base SPH Model

The base SPH model without TLD damping screens is validated against common scenarios: a hydrostatic tank of water and a dam break flow. The pressure profile in a hydrostatic tank is compared to the theoretical value for various SPH input parameters. The dam break flow is compared to experimental data from Martin and Moyce (1952).

2.3.1 Hydrostatic Tank

The case of a hydrostatic tank of water is commonly used for SPH model validation. The water is initialized with a hydrostatic pressure profile and allowed to sit without external excitation. Since the water is initially in equilibrium, there should be no change to the position or pressure of each fluid particle. However, due to the SPH approximations, minimal changes in position and pressure occur, though the overall pressure profile should remain hydrostatic. The simulation was run for a total of ten seconds. The tank dimensions

were length L = 0.2 m and height H = 0.4 m, with initial water depth h = 0.2 m. The base simulation had initial particle spacing dp = 0.01 m, with a smoothing length h_{ker} = 1.2dp, and a timestep $dt = 10^{-4}$ seconds. To study the effect of these parameters, three additional simulations were run changing only one parameter with (1) h_{ker} = 1.4dp, (2) $dt = 5\text{x}10^{-4}$ seconds, and (3) dp = 0.005 m. Figure 2.6 plots the pressure of each SPH fluid particle versus height at the end of the 10 second simulation. The pressure is normalized by the maximum theoretical hydrostatic pressure, ρgh, and the height is normalized by the fluid depth, h. The SPH results show agreement with the theoretical values at the end of the simulation for all cases.

2.3.2 Dam Break Flow

Nomeritae et al. (2016) studied various dam break scenarios using an explicit incompressible SPH model similar to the model used in this study. Figure 2.7 shows the dam break simulation domain. The leading edge is defined as the distance to the wave front from the initial edge of the water column at t = 0 seconds. The residual height is defined as the remaining fluid column height at the edge of the domain. The SPH model was run with the same input parameters as the first case from Nomeritae et al. (2016), and compared to experimental data from Martin and Moyce (1952). The initial water column dimensions were 0.06 m by 0.12 m. The base simulation was run with h_{ker} = 1.2dp, dp = 0.005 m, and $dt = 5\text{x}10^{-4}$ seconds. To study the effect of these parameters, three additional simulations were run changing only one parameter with (1) h_{ker} = 1.4dp, (2) $dt = 1\text{x}10^{-4}$ seconds, and (3) dp = 0.0025 m. Figure 2.8 shows the leading edge and residual height. The values are normalized by the initial water column height, h, and time is multiplied by $(g/h)^{0.5}$. The SPH results are in excellent agreement with the experimental data, with only small variability between the cases with different parameters.

2.4 Validation of SPH Model of TLD with Damping Screens

The results of the SPH model of a TLD containing damping screens are compared to existing experimental shake table testing data obtained from Love and Tait (2010), Tait et al. (2005), and Love and Tait (2013). To illustrate the broad applicability of the model,

different TLD tank sizes, water depths, excitation amplitudes, and damping screens are investigated as outlined in Table 2.1.

Based on linear theory, the fundamental sloshing frequency of a rectangular tank is calculated as (Ibrahim, 2005):

$$\omega_1 = \sqrt{\frac{\pi g}{L}\tanh\left(\frac{\pi h}{L}\right)} \tag{2.24}$$

Each SPH case consisted of simulating a frequency sweep, where the TLD is excited by a sinusoidal base acceleration with a given amplitude X_0 at discrete frequencies ω_e (in radians/second) near the fundamental sloshing frequency of the TLD ω_1:

$$\ddot{X}(t) = -X_0\omega_e^2\sin(\omega_e t) \tag{2.25}$$

Each frequency was simulated for a total of 120 seconds with a timestep of 0.0005 seconds, allowing the TLD to reach the desired steady state response. After attaining steady state, the frequency response was determined by calculating peak values over each excitation cycle and taking an average. This allowed for comparison to experimental data in both the time and frequency domains, which is important for assessing the performance of a nonlinear TLD model. For all cases, the fluid in the tank was water. The kernel radius multiplier was set to $h_{ker} = 1.4dp$ for the vast majority of cases studied. In some instances where the excitation was small (i.e. the $h/L = 0.05$ and $X_0/L = 0.0026$ and 0.0052 cases in Section 2.4.3), the very low response of the TLD was impacted by numerical noise, causing the model to not capture the sloshing fluid motion. For these cases, $h_{ker} = 1.5dp$ was found to better capture the TLD response. If the SPH model is to be implemented for very small excitation cases in shallow tanks, tuning of the kernel radius may be necessary. In practice, the SPH model is unlikely to be used for very small sloshing responses, as computationally simpler models could adequately capture the response. For this study, it was determined that if the product of the kernel radius and particle spacing was less than the free surface wave height ($h_{ker}dp < \eta$) the model would not adequately capture the sloshing behaviour, and an increase in h_{ker} was necessary. The screens used the same Wendland fifth order

kernel function as the fluid (Wendland, 1995); however, their radius of influence is expected to be greater than that of the fluid particles, and thus the kernel radius multiplier h_{screen} was set to $3h_{ker}$. This value was found to provide good agreement with experimental data across the cases considered. For different screen geometries than those studied, tuning of the screen particle kernel radius multiplier h_{screen} will be required. This can be achieved by comparing to experimental data or results from other numerical models. Since experimental data is already required to determine the screen loss coefficient, this does not impact the applicability of the method. The damping screens considered in this study consisted of an array of small slats (see Figure 2.4). For small individual slats distributed across the tank height, the inertial screen force term in equation **(2.21)** is negligible since $C_m \rho t_{screen} S \ll 1$. Based on this, the inertial screen force is neglected in this study. For larger flow obstructions, it would be necessary to consider the impact of the added mass on the flow (Love & Haskett, 2018).

The experimental data has been low pass filtered in post-processing to remove noise from the signals. To facilitate comparison, the SPH results were also low pass filtered with a cut-off frequency of 5 Hz. Additionally, the data presented is normalized in accordance with the experimental data. Excitation frequency ratio is defined as:

$$\beta = \frac{\omega_e}{\omega_1} = \frac{f_e}{f_1} \tag{2.26}$$

Time is multiplied by excitation frequency, f_e, in Hz. Wave heights are divided by the still water depth in the tank, h. Forces are normalized by the maximum inertial force of the water in the TLD if it moved solidly:

$$F_w' = \frac{F_w}{m_w X_0 \omega_e^2}, F_{sw}' = \frac{F_{sw}}{m_w X_0 \omega_e^2}, F_{screen}' = \frac{F_{screen}}{m_w X_0 \omega_e^2} \tag{2.27}$$

where m_w is the total water mass, X_0 is the excitation amplitude in metres, F_w is the total water force in the TLD, $F_{sw} = F_w - m_w \ddot{X}$ is the sloshing force, and F_{screen} is the total screen force calculated by equation **(2.21)**.

2.4.1 Experimental Results from Love and Tait (2010)

Love and Tait (2010) completed experimental shake table testing of multiple rectangular TLDs equipped with damping screens to validate a nonlinear multi-modal TLD model. The SPH model results are compared to the experimental results measuring forces on the screens, wave height near the tank wall, and sloshing forces.

The first TLD tank considered had a fluid depth to tank length ratio *h/L* of 0.182, which corresponds to tank T2 in Love and Tait (2010). Three damping screens with C_l = 1.63 were placed at 25%, 50%, and 75% of the tank length. The initial SPH particle spacing was 0.012 m, resulting in approximately 3000 fluid particles. The SPH model was run for excitation values of $X_0/L = 0.005$ and $\beta = 1.01$. Figure 2.9 shows the time domain response of force acting on the screens at 25% and 50% of the tank length. The SPH model forces are in very good agreement with the experimental forces, indicating that the SPH model is capturing the effect of the screens well. Figure 2.10 shows the time domain response for the wave height near the tank wall and sloshing water force, with excellent agreement observed between the SPH and experimental results.

The second TLD considered had a fluid depth to tank length ratio *h/L* of 0.123, corresponding to tank T3 in Love and Tait (2010). Two damping screens with C_l equal to 2.16 were placed at 40% and 60% of the tank length. The initial SPH particle spacing was 0.007 m, resulting in approximately 2350 fluid particles. A frequency sweep consisting of 41 discrete frequencies ranging from 80% to 120% of the fundamental sloshing frequency was simulated using the SPH model. Figure 2.11 shows the frequency response for wave height (max and min) and sloshing forces. There is excellent agreement between the SPH and experimental wave troughs. The SPH model slightly underpredicts wave peaks at frequencies below $\beta = 1.00$ and slightly overpredicts them at frequencies above $\beta = 1.00$; however, the overall agreement is good. There is good agreement between the SPH and experimental sloshing forces, particularly near and above $\beta = 1.00$.

2.4.2 Experimental Results from Tait et al. (2005)

Tait et al. (2005) completed experimental shake table testing of a rectangular TLD equipped with screens to validate a nonlinear shallow water wave theory model. The ratio of water depth to tank length h/L = 0.123, which also corresponds to tank T3 from Love and Tait (2010). Two damping screens with C_l = 2.16 were placed at 40% and 60% of the tank length. The initial SPH particle spacing was 0.007 m. The SPH simulation was run at a frequency ratio β = 1.01 at three different excitation amplitude values of X_0/L = 0.005, 0.016, and 0.031.

Figure 2.12 shows the wave height and TLD tank force time domain response for the smallest excitation amplitude, X_0/L = 0.005. The SPH model shows excellent agreement with the experimental data for both wave height and water force. Figure 2.13 and Figure 2.14 show the time domain response for X_0/L = 0.016 and 0.031, respectively. The response is significantly more nonlinear than the previous case, and the SPH model shows excellent agreement with the experimental data for both excitation amplitudes. The SPH model captures both the peaks and troughs of the wave height well.

2.4.3 Experimental Results from Love and Tait (2013)

Love and Tait (2013) completed a parametric study on the response of a rectangular TLD with length L = 0.966 m. The initial water depth ratio h/L ranged from 0.05 to 0.25, and the excitation amplitude X_0/L ranged from 0.0026 to 0.0207. The initial particle spacing dp was set to 0.006 m. The TLD had two screens with C_l = 2.16 located at 40% and 60% of the tank length. SPH frequency sweeps were simulated at discrete frequencies ranging from 75% to 130% of the fundamental sloshing frequency of the tank for each case. For brevity, only selected representative results across the various water depths and excitation amplitudes are presented here.

2.4.3.1 Time Response

Selected results are presented in the time domain for each of the five water depths considered. Figure 2.15 shows the normalized wave height and sloshing water force response for h/L = 0.05, X_0/L = 0.0104, and β = 0.98. Both the wave heights and sloshing

water forces show a strongly nonlinear response with multiple peaks. The SPH model over-predicts the depths of the wave troughs; however, the agreement between the SPH model and experimental data is very good overall. Figure 2.16 shows the time response for h/L = 0.10, X_0/L = 0.0207, and β = 1.00. The SPH model shows excellent agreement with the experimental data, capturing not only the peak values of the response, but also the nonlinear waveform. The SPH model captures the main sloshing force peaks well, but slightly over-predicts the secondary peak values compared to the experimental data. Figure 2.17 shows the time response for h/L = 0.15, X_0/L = 0.0052, and β = 0.92. As the water depth increases, the nonlinearity of the response decreases. The SPH model shows very good agreement with the experimental data for sloshing forces. There is a slight phase shift between the experimental and SPH wave heights; however, the overall agreement is still good. Figure 2.18 shows the time response for h/L = 0.20, X_0/L = 0.0104, and β = 1.02. The SPH model shows excellent agreement with the experimental results. Finally, Figure 2.19 shows the time response for h/L = 0.25, X_0/L = 0.0026, and β = 1.04. The SPH model slightly under-predicts the wave heights and sloshing water forces; however, overall good agreement is shown between the SPH model and experimental data.

2.4.3.2 Frequency Response and Normalized Error

The frequency response allows for assessing the performance of the model across a range of excitation frequencies of interest, rather than considering individual responses in the time domain. Selected frequency response curves for the five water depths are presented, considering the peak and trough wave heights and the peak sloshing water forces. Figure 2.20 shows the frequency response for wave heights and sloshing forces corresponding to h/L = 0.05 and X_0/L = 0.0104. This case represents the shallowest TLD depth considered, which is expected to result in a strongly nonlinear response. The SPH model slightly over-predicts and under-predicts the peak wave heights and sloshing forces at certain frequencies. Overall, the SPH model results show good agreement with the experimental data. Figure 2.21 shows the frequency response for h/L = 0.15 and X_0/L = 0.0052. Excellent agreement is observed between the SPH results and the experimental data, particularly the sloshing water forces. Finally, Figure 2.22 shows the frequency

response for h/L = 0.25 and X_0/L = 0.0052. This is the deepest TLD water depth considered. The SPH model is in excellent agreement with the experimental data.

The normalized error between the SPH model and experimental data can be quantified as:

$$E^n = \sqrt{\frac{\sum_i \left(x_i^{SPH} - x_i^{exp}\right)^2}{\sum_i \left(x_i^{exp}\right)^2}} \tag{2.28}$$

where x_i^{SPH} and x_i^{exp} are the frequency response value at frequency i. Love and Tait (2013) considered an error value less than 0.10 to indicate acceptable model performance.

Capturing the sloshing force response is of primary importance for a TLD model as this force controls the motion of a structure. Figure 2.23 shows the normalized sloshing force error versus the excitation amplitude X_0/L for all cases that were investigated. Typically, numerical models can capture the TLD response well at low excitation amplitudes with moderate water depths, with model error increasing proportional to X_0/L due to increased nonlinearity. The opposite is observed for the SPH model, where the largest errors occurred at the smallest excitation amplitudes for each water depth. The normalized error for sloshing water forces was greater than 0.10 for only 2 cases when h/L = 0.05 and 0.10 and X_0/L = 0.0026, with a maximum value of 0.16. Based on these results, the SPH model captures the sloshing force response of the TLD acceptably for nearly all cases considered.

2.5 Conclusions

An explicit incompressible SPH model was presented for a TLD equipped with damping screens. An efficient novel SPH damping screen formulation based on Morison's formula was presented where the damping screen geometry does not need to be explicitly modelled, allowing for coarser particle spacing resulting in more efficient computational time. Explicitly modelling the screens in this study would require 50 times the number of particles, increasing the CPU time by a factor of approximately 700. The results of the SPH model were compared to existing experimental data for various cases in both the time

domain and frequency domain. Table 2.1 lists the full range of TLD parameters investigated. The following conclusions can be made:

1. The base SPH model shows good agreement with benchmark cases of a hydrostatic tank of water and a dam break simulation.
2. The SPH model of a TLD with screens shows good agreement with experimental results for forces measured on damping screens presented by Love and Tait (2010). This indicates that the SPH model captures the influence of the screens on the flow, despite not explicitly modelling the geometry of the screens.
3. When considering different excitation amplitudes X_0/L = 0.005, 0.016, and 0.031, the SPH model shows excellent agreement with experimental wave height and water force data from Tait et al. (2005).
4. The SPH model shows excellent agreement with both time domain and frequency response wave height and sloshing water force experimental data from Love and Tait (2013). The SPH model is shown to be suitable for fluid depths h/L between 0.05 and 0.25 and does not appear limited by excitation amplitude for the cases considered.

The SPH model has been validated against experimental data for a broad range of TLD scenarios in both the time domain and frequency domain. The proposed screen implementation has been shown to effectively capture the energy dissipation characteristics of damping screens in a TLD. The SPH model can be effectively used to study a TLD equipped with screens without limitation on water depth or excitation amplitude, providing a robust tool for understanding the fully nonlinear response of the system. Future research will couple this TLD model to a structure to evaluate its ability to represent structure-TLD interaction under large excitation amplitudes, where existing models tend to perform poorly.

2.6 Acknowledgment

The authors are thankful for the financial support provided by the Natural Sciences and Engineering Research Council of Canada (NSERC) and the Ontario Graduate Scholarship (OGS) program.

2.7 References

Adami, S., Hu, X. Y., & Adams, N. A. (2012). A generalized wall boundary condition for smoothed particle hydrodynamics. *Journal of Computational Physics, 231*(21), 7057-7075.

Aristodemo, F., Meringolo, D. D., & Veltri, P. (2016). A multi-node approach to simulate thin coastal structures in the SPH context. *Coastal Engineering Proceedings, 1*(35).

Bulian, G., Souto-Iglesias, A., Delorme, L., & Botia-Vera, E. (2009). Smoothed particle hydrodynamics (SPH) simulation of a tuned liquid damper (TLD) with angular motion. *Journal of Hydraulic Research, 48*(sup1), 28-39.

Cao, X. Y., Ming, F. R., & Zhang, A. M. (2014). Sloshing in a rectangular tank based on SPH simulation. *Applied Ocean Research, 47*, 241-254.

Chen, B. F., & Nokes, R. (2005). Time-independent finite difference analysis of fully non-linear and viscous fluid sloshing in a rectangular tank. *Journal of Computational Physics, 209*(1), 47-81.

Cho, J. R., & Lee, H. W. (2004). Non-linear finite element analysis of large amplitute sloshing flow in two-dimensional tank. *International Journal of Numerical Methods in Engineering, 61*(4), 514-531.

Chu, C. R., Wu, Y. R., Wu, T. R., & Wang, C. Y. (2018). Slosh-induced hydrodynamic force in a water tank with multiple baffles. *Ocean Engineering, 167*, 282-292.

Cummins, S. J., & Rudman, M. (1999). An SPH Projection Method. *Journal of Computational Physics, 152*, 584-607.

Deng, X., & Tait, M. J. (2008). Equivalent mechanical models of tuned liquid dampers with different tank geometries. *Canadian Journal of Civil Engineering, 35*(10), 1088-1101.

Gao, M. (2011). Numerical simulation of liquid sloshing in rectangular tanks using consistent particle method and experimental verification, PhD Thesis. 207. National University of Singapore.

Green, M. D., & Peiro, J. (2018). Long duration SPH simulations of sloshing in tanks with a low fill ratio and high stretching. *Computers and Fluids, 174*, 179-199.

Halabian, A. M., Karamnasab, A., & Chamani, M. R. (2019). A New Hybrid SPH-FEM Model to Evaluate Seismic Response of TSD Equipped-Structures. *Journal of Earthquake and Tsunami, 13*(2), 1-27.

Huang, S., Duan, W. Y., & Zhu, X. (2010). Time-domain simulation of tank sloshing pressure and experimental validation. *Journal of Hydrodynamics, Ser. B, 22*(5), 556-563.

Ibrahim, R. A. (2005). *Liquid Sloshing Dynamics.* Cambridge: Cambridge University Press.

Jiang, H., You, Y., Hu, Z., Zheng, X., & Ma, A. (2019). Comparative study on violent sloshing withwater jet flows by using the ISPH method. *Water (Switzerland), 11*, 2590.

Kaneko, S., & Ishikawa, M. (1999). Modeling of tuned liquid dampers with submerged nets. *Journal of Pressure Vessel Technology, 121*(3), 334-344.

Kaneko, S., & Yoshida, O. (1999). Modeling of Deepwater-Type Rectangular Tuned Liquid Damper With Submerged Nets. *ASME Journal of Pressure Vessel Technology, 121*(4), 413-422.

Kashani, A. H., Halabian, A. M., & Asghari, K. (2018). A numerical study of tuned liquid damper based on incompressible SPH method combined with TMD analogy. *Journal of Fluids and Structures, 82*, 394-411.

Love, J. S., & Haskett, T. C. (2018). Nonlinear modelling of tuned sloshing dampers with large internal obstructions: Damping and frequency effects. *Journal of Fluids and Structures, 79*, 1-13.

Love, J. S., & Tait, M. J. (2010). Nonlinear simulation of a tuned liquid damper with damping screens using a modal expansion technique. *Journal of Fluids and Structures, 26*(7-8), 1058-1077. doi:10.1016/j.jfluidstructs.2010.07.004

Love, J. S., & Tait, M. J. (2011). Non-linear multimodal model for tuned liquid dampers of arbitrary tank geometry. *International Journal of Nonlinear Mechanics, 46*(8), 1065-1075.

Love, J. S., & Tait, M. J. (2013). Parametric depth ratio study on tuned liquid dampers: Fluid modelling and experimental work. *Computers & Fluids, 79*, 13-26.

Marsh, A., Prakash, M., Semercigil, E., & Turan, O. F. (2011). A study of sloshing absorber geometry for structural control with SPH. *Journal of Fluids and Structures, 27*(8), 1165-1181.

Martin, J. C., & Moyce, W. J. (1952). Part IV. An Experimental Study of the Collapse of Liquid Columns on a Rigid Horizontal Plane. *Philosophical Transactions of the Royal Society A: Mathematical, Physical and Engineering Sciences, 244*(882), 312-324.

Monaghan, J. J. (1992). Smoothed Particle Hydrodynamics. *Annual Review of Astronomy and Astrophysics, 30*, 543-74.

Monaghan, J. J. (1994). Simulating free surface flows with SPH. *Journal of Computational Physics, 110*(2), 399-406.

Morison, J. R., O'Brien, M. P., Johnson, J. W., & Schaaf, S. A. (1950). The force exerted by surface waves on piles. *Petroleum Transactions AIME, 189*, 149-154.

Nomeritae, Daly, E., Grimaldi, S., & Bui, H. H. (2016). Explicit incompressible SPH algorithm for free-surface flow modelling: A comparison with weakly compressible schemes. *Advances in Water Resources, 97*, 156-167.

Shao, S., & Lo, E. Y. (2003). Incompressible SPH method for simulating Newtonian and non-Newtonian flows with a free surface. *Advances in Water Resources, 26*, 787-800.

Tait, M. J. (2008). Modelling and preliminary design of a structure-TLD system. *Engineering Structures, 30*(10), 2644-2655.

Tait, M. J., El Damatty, A. A., Isyumov, N., & Siddique, M. R. (2005). Numerical flow models to simulate tuned liquid dampers (TLD) with slat screens. *Journal of Fluids and Structures, 20*(8), 1007-1023.

Valizadeh, A., & Rudman, M. (2017). A numerical approach for simulating flow through thin porous media. *European Journal of Mechanics, B/Fluids, 65*, 31-44.

Violeau, D., & Rogers, B. D. (2016). Smoothed particle hydrodynamics (SPH) for free-surface flows: Past, present and future. *Journal of Hydraulic Research, 54*(1), 1-26.

Wendland, H. (1995). Piecewise polynomial, positive definite and compactly supported radial functions of minimal degree. *Advances in Computational Mathematics, 4*, 389-396.

Yeylaghi, S., Moa, B., Oshkai, P., Buckham, B., & Crawford, C. (2016). ISPH modelling of an oscillating wave surge converter using an OpenMP-based parallel approach. *Journal of Ocean Engineering and Marine Energy, 2*, 301-312.

Table 2.1: TLD Parameters Investigated

Experimental Data Source	**L (m)**	**X_{screen}/L**	**C_l**	**h/L**	**X_0/L**
Love and Tait (2010)	1.524	0.25, 0.50, 0.75	1.63	0.183	0.005
	0.966	0.40, 0.60	2.16	0.123	0.005
Tait et al. (2005)	0.966	0.40, 0.60	2.16	0.123	0.005, 0.016, 0.031
Love and Tait (2013)	0.966	0.40, 0.60	2.16	0.050	0.0026, 0.0052, 0.0104, 0.0207
				0.100	0.0026, 0.0052, 0.0104, 0.0207
				0.150	0.0026, 0.0052, 0.0104
				0.200	0.0026, 0.0052, 0.0104
				0.250	0.0026, 0.0052

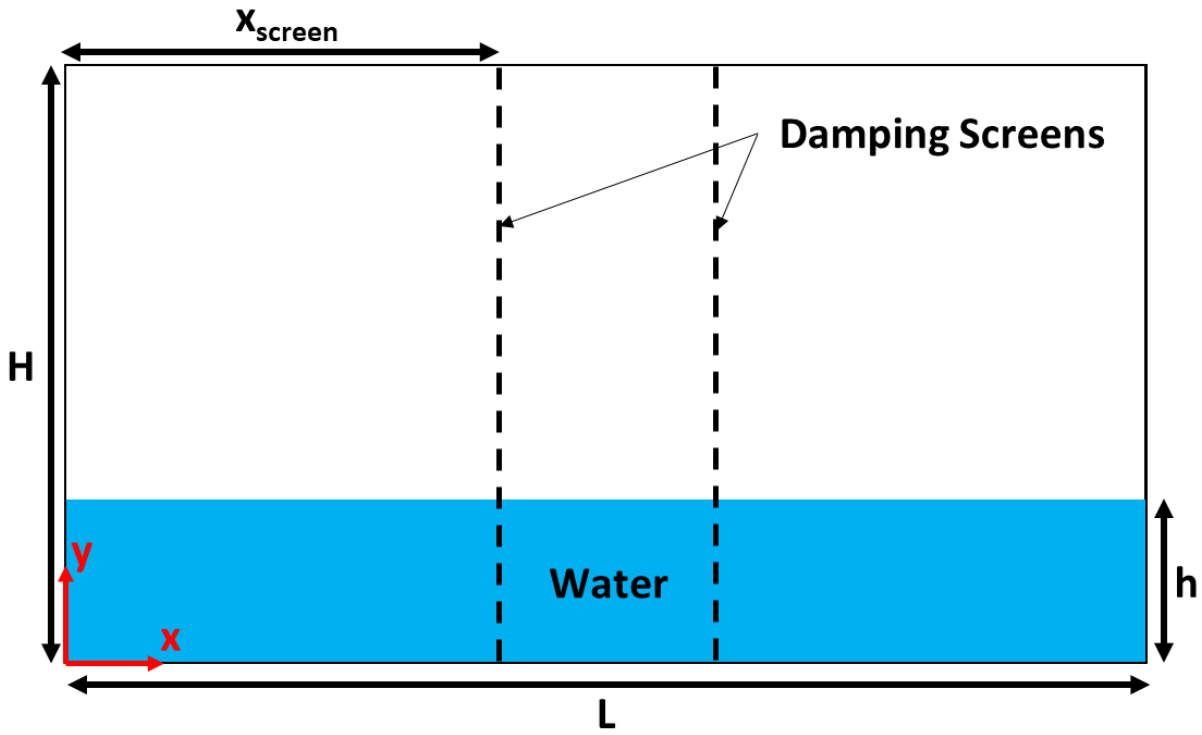

Figure 2.1: SPH domain definition for TLD with damping screens.

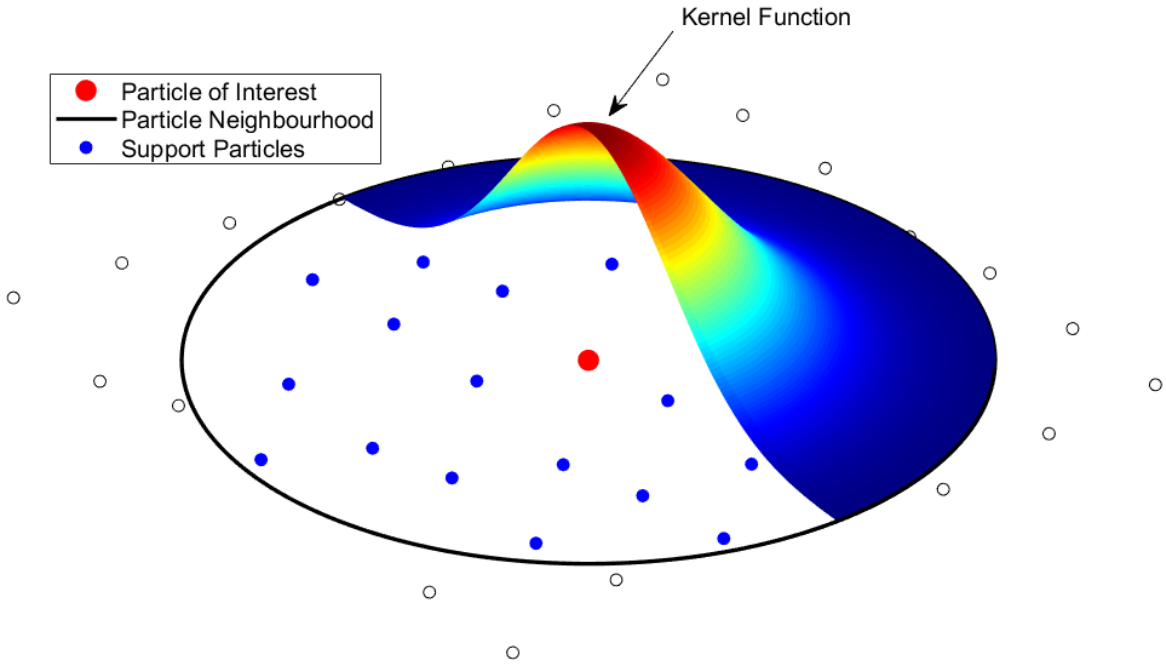

Figure 2.2: SPH discretization showing kernel function.

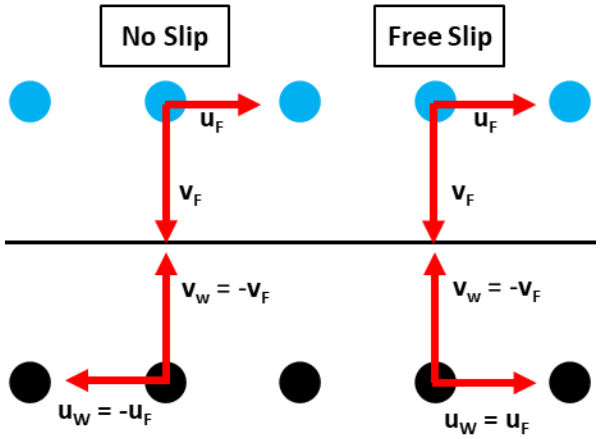

Figure 2.3: Illustration of free-slip and no-slip boundary velocity conditions.

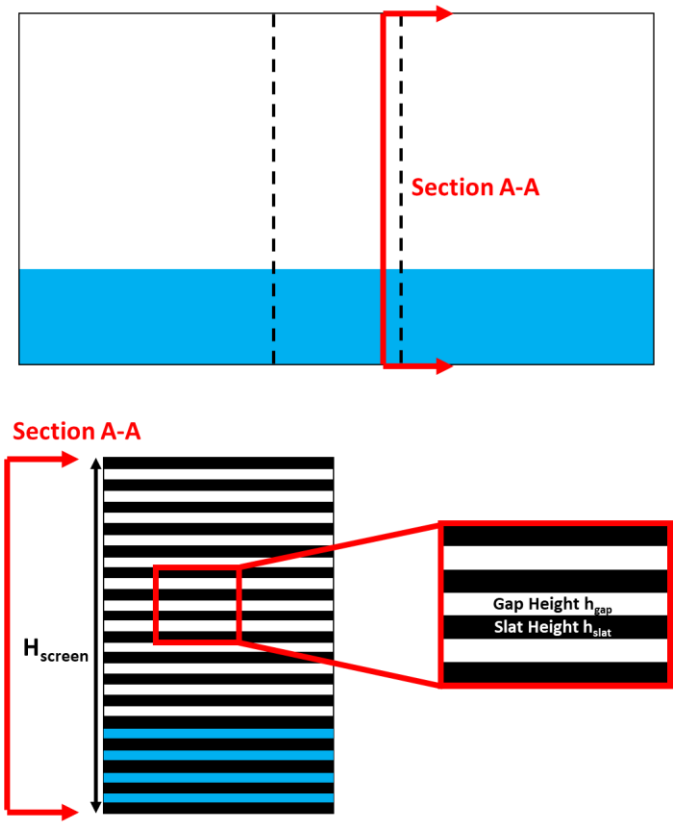

Figure 2.4: TLD slat screen schematic.

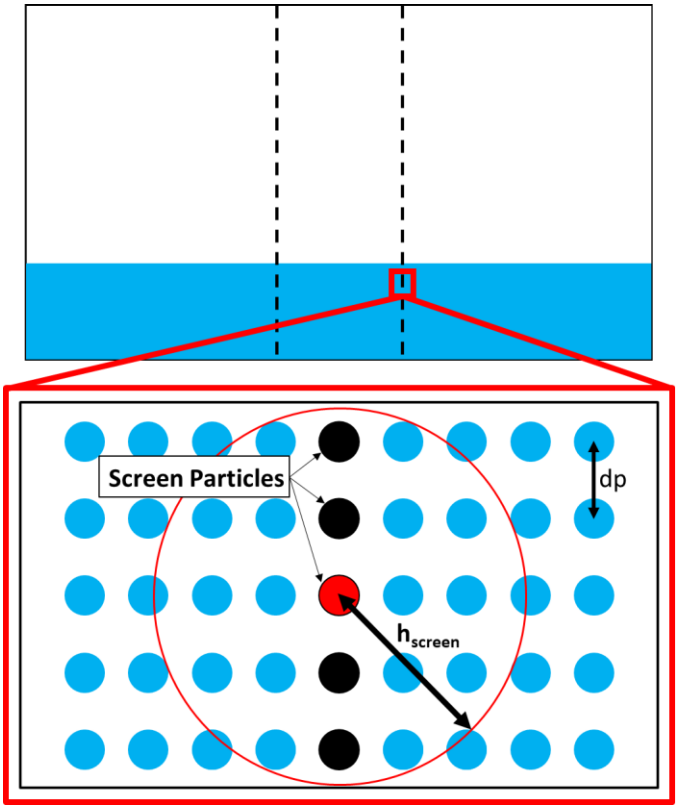

Figure 2.5: SPH screen discretization.

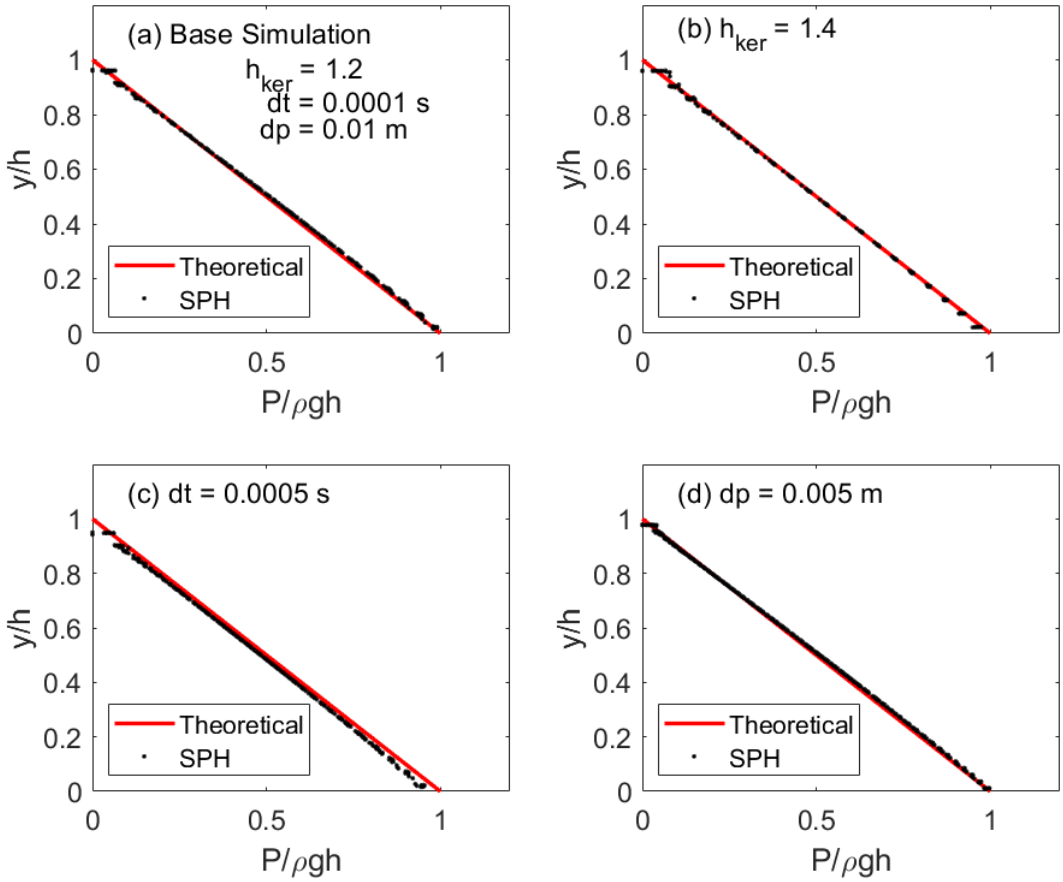

Figure 2.6: Pressure profile for hydrostatic tank at end (t = 10.0 seconds) of simulation for different h_{ker}, *dt*, and *dp* values.

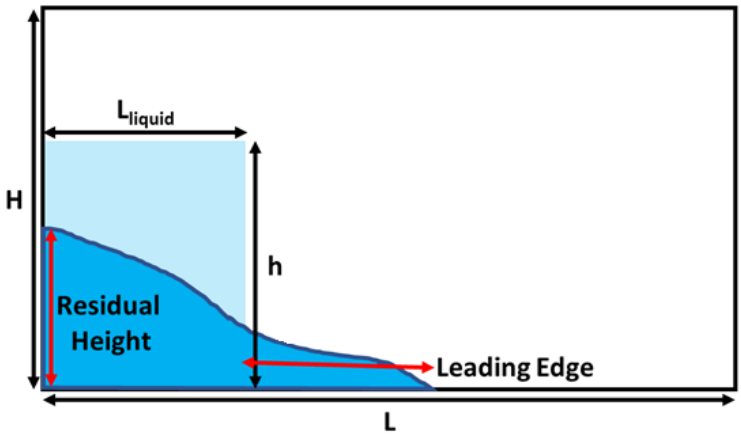

Figure 2.7: Dam break simulation domain.

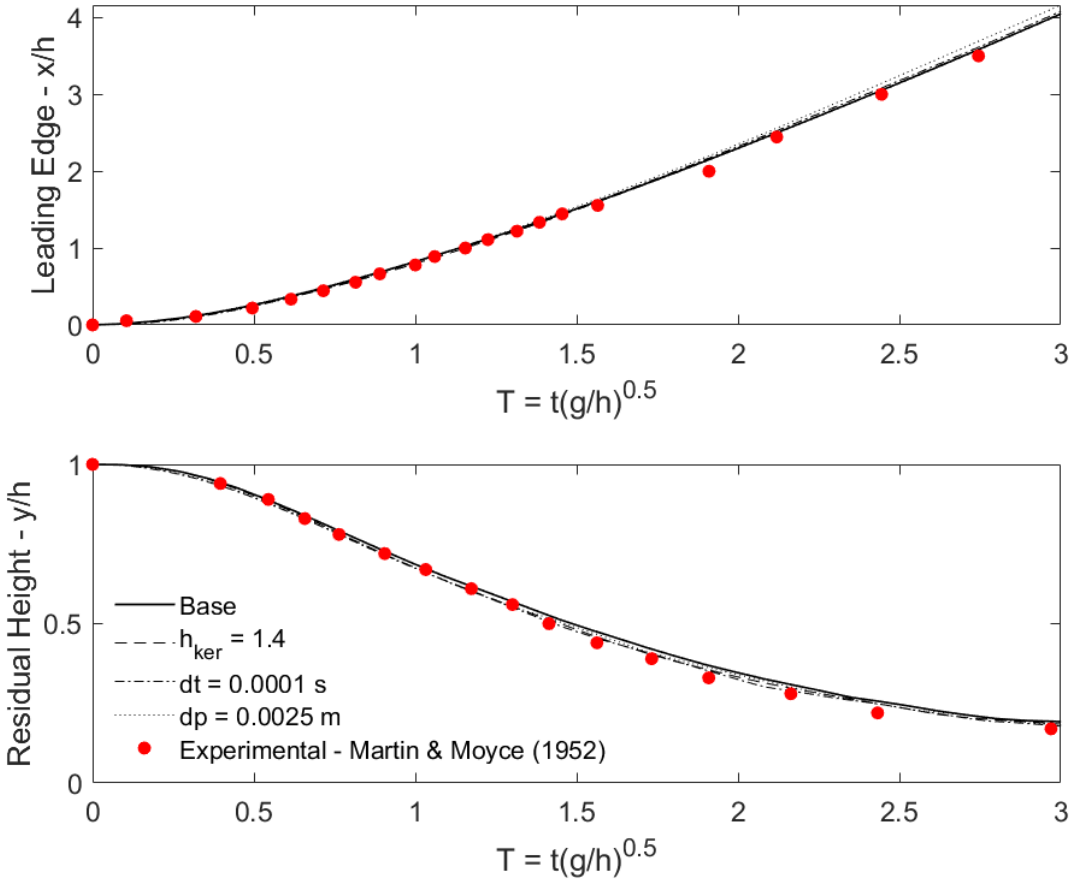

Figure 2.8: Dam Break Case 1 – Leading Edge and Residual Height, h = 0.12 m, L_{liquid}= 0.06 m.

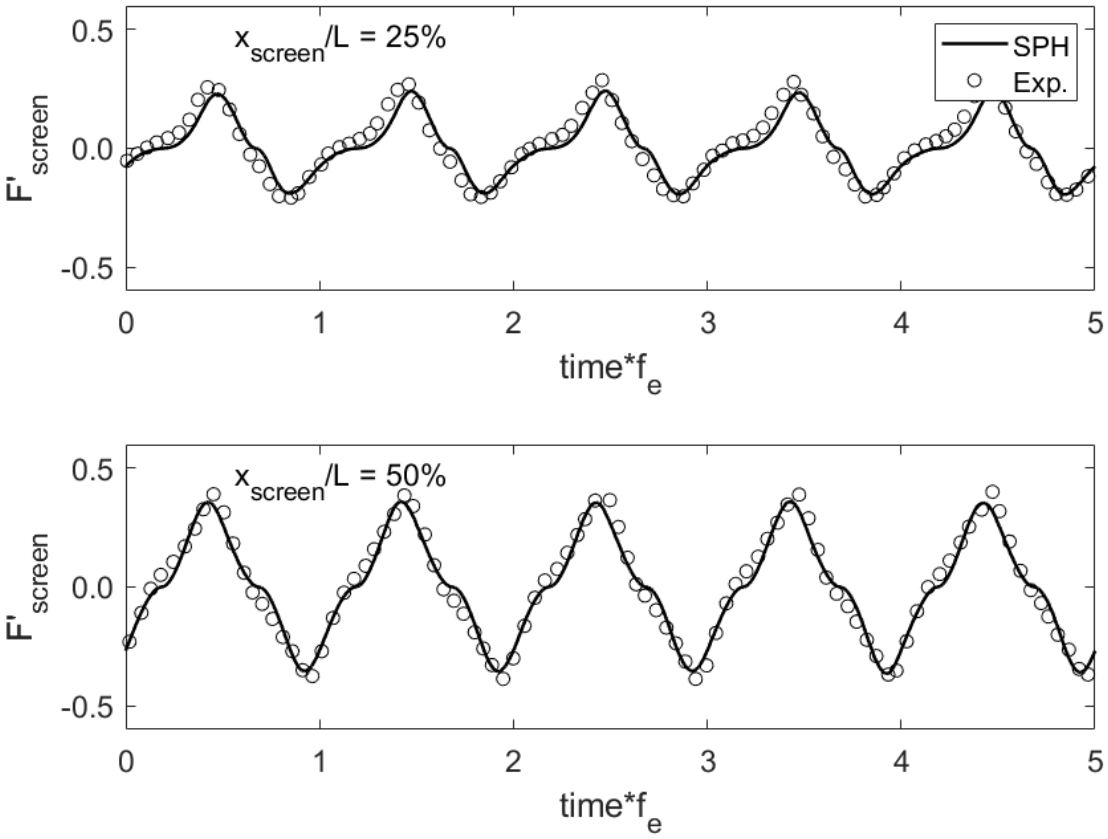

Figure 2.9: SPH screen force response history versus experimental results from Love and Tait (2010). h/L = 0.182, X_0/L = 0.005, β = 1.01.

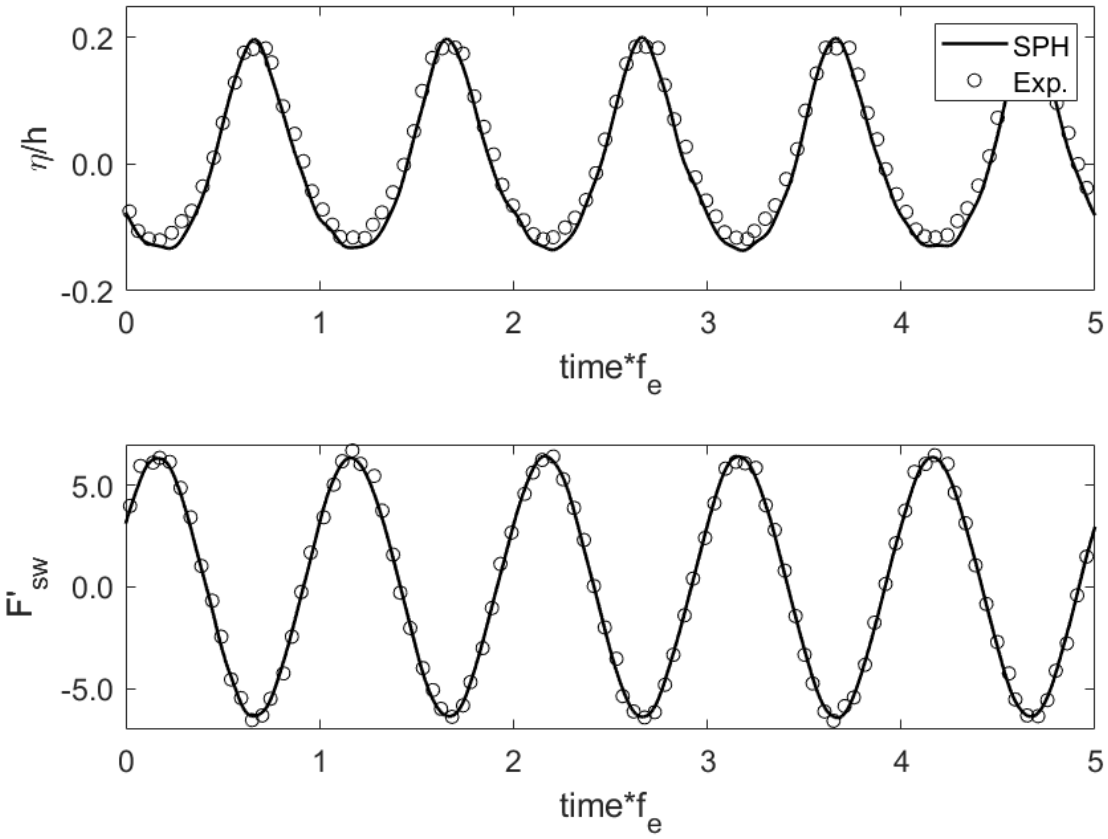

Figure 2.10: SPH wave height and sloshing force response history versus T2 experimental results from Love and Tait (2010). h/L = 0.182, X_0/L = 0.005, β = 1.01.

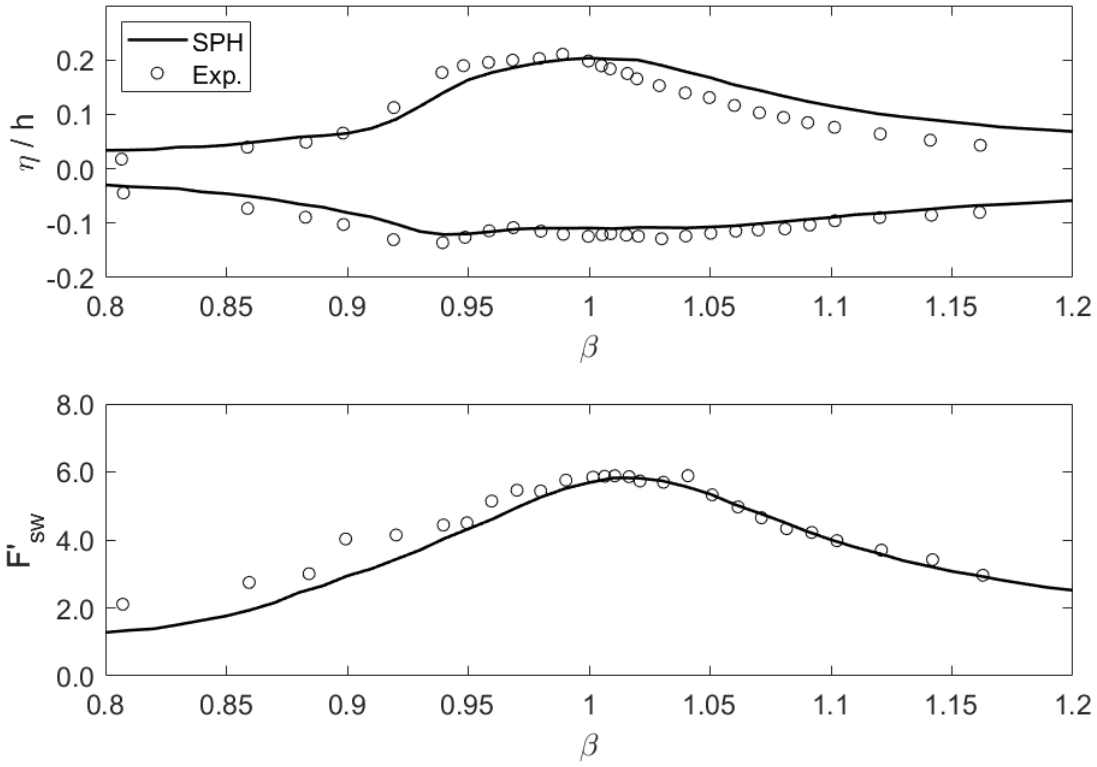

Figure 2.11: SPH wave height and sloshing force frequency response versus T3 experimental results from Love and Tait (2010). h/L = 0.123, X_0/L = 0.005.

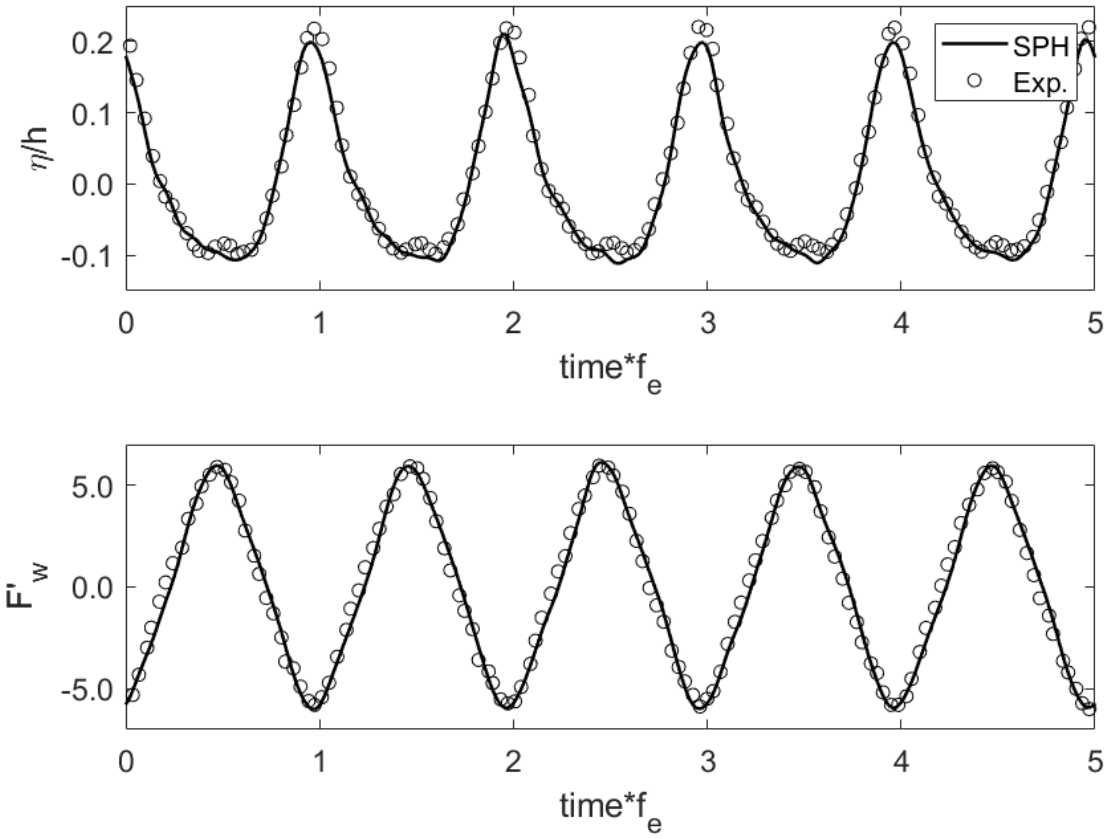

Figure 2.12: SPH wave height and sloshing force time response versus experimental results from Tait et al. (2005). h/L = 0.123, X_0/L = 0.005.

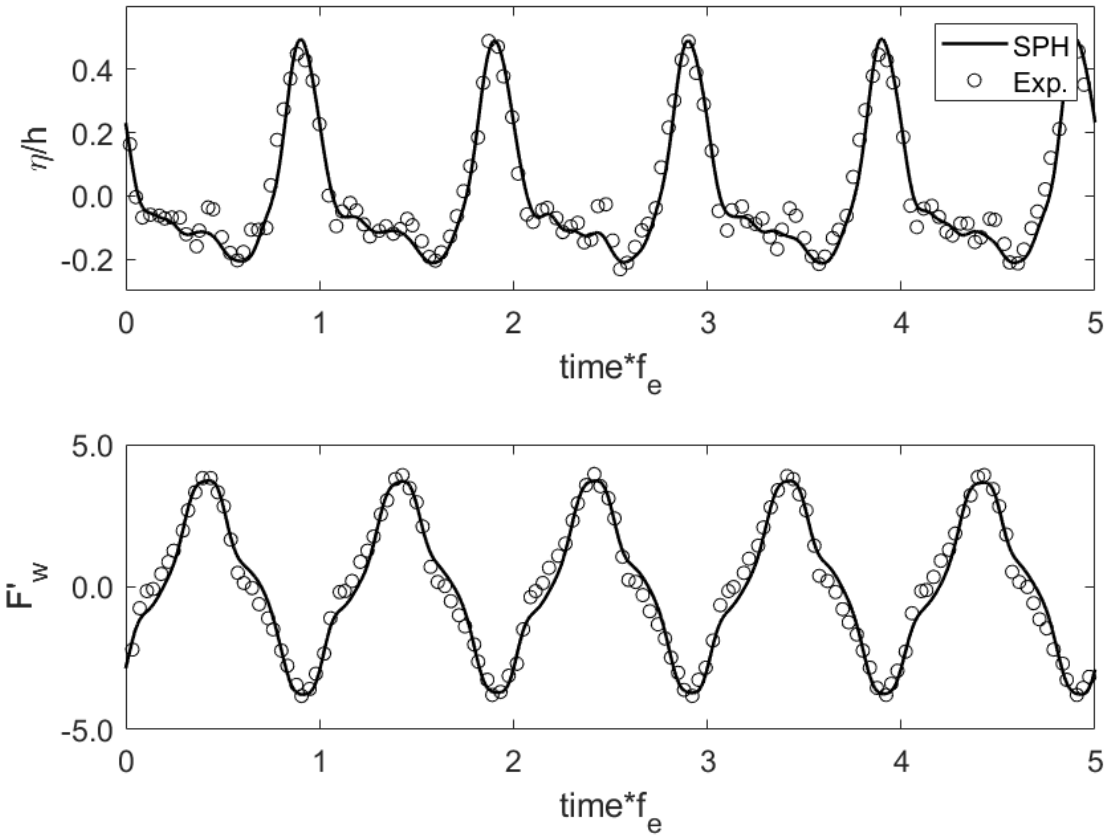

Figure 2.13: SPH wave height and sloshing force time response versus experimental results from Tait et al. (2005). h/L = 0.123, X_0/L = 0.016.

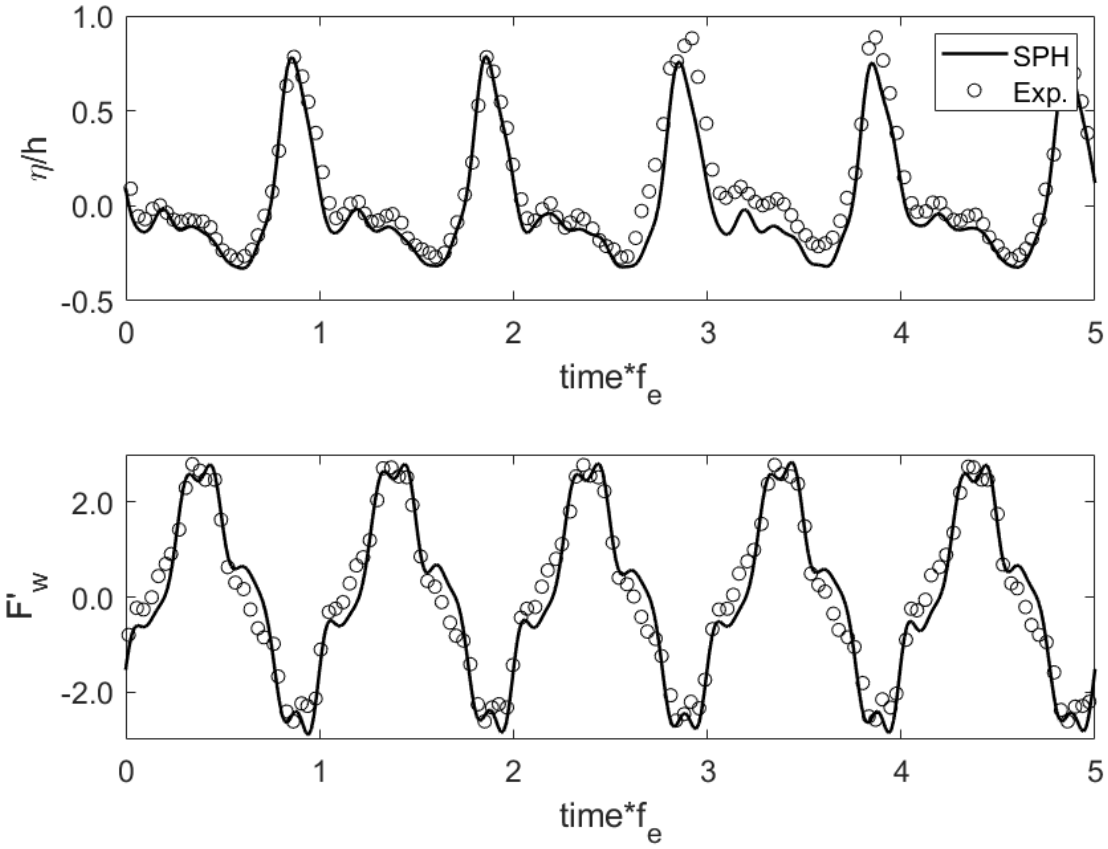

Figure 2.14: SPH wave height and sloshing force time response versus experimental results from Tait et al. (2005). h/L = 0.123, X_0/L = 0.031.

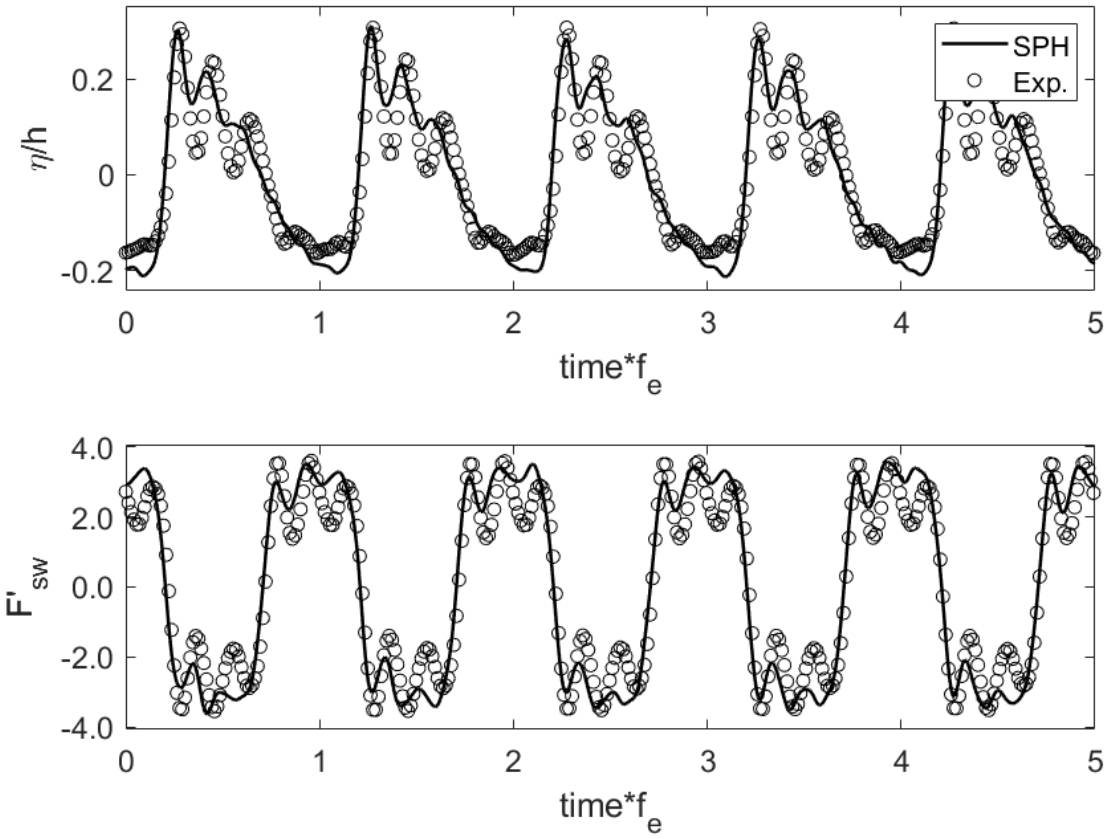

Figure 2.15: SPH wave height and sloshing force time response versus experimental results from Love and Tait (2013). h/L = 0.05, X_0/L = 0.0104, β = 0.98.

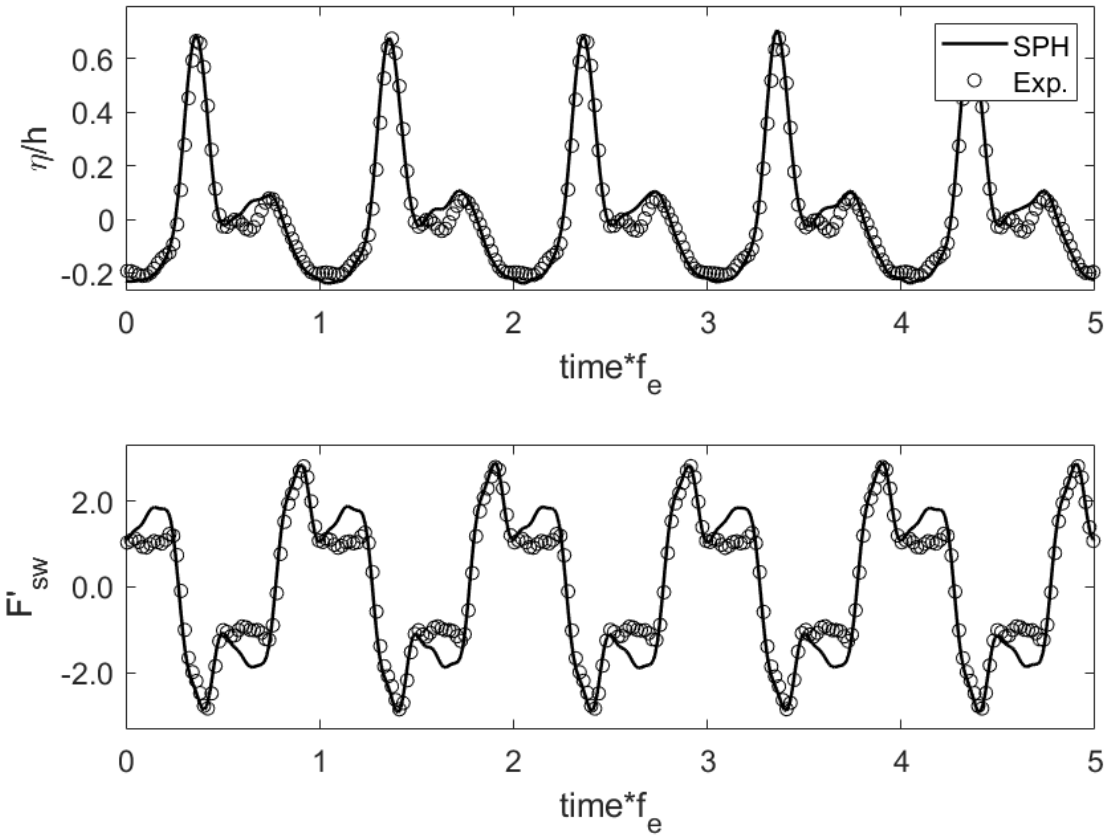

Figure 2.16: SPH wave height and sloshing force time response versus experimental results from Love and Tait (2013). h/L = 0.10, X_0/L = 0.0207, β = 1.00.

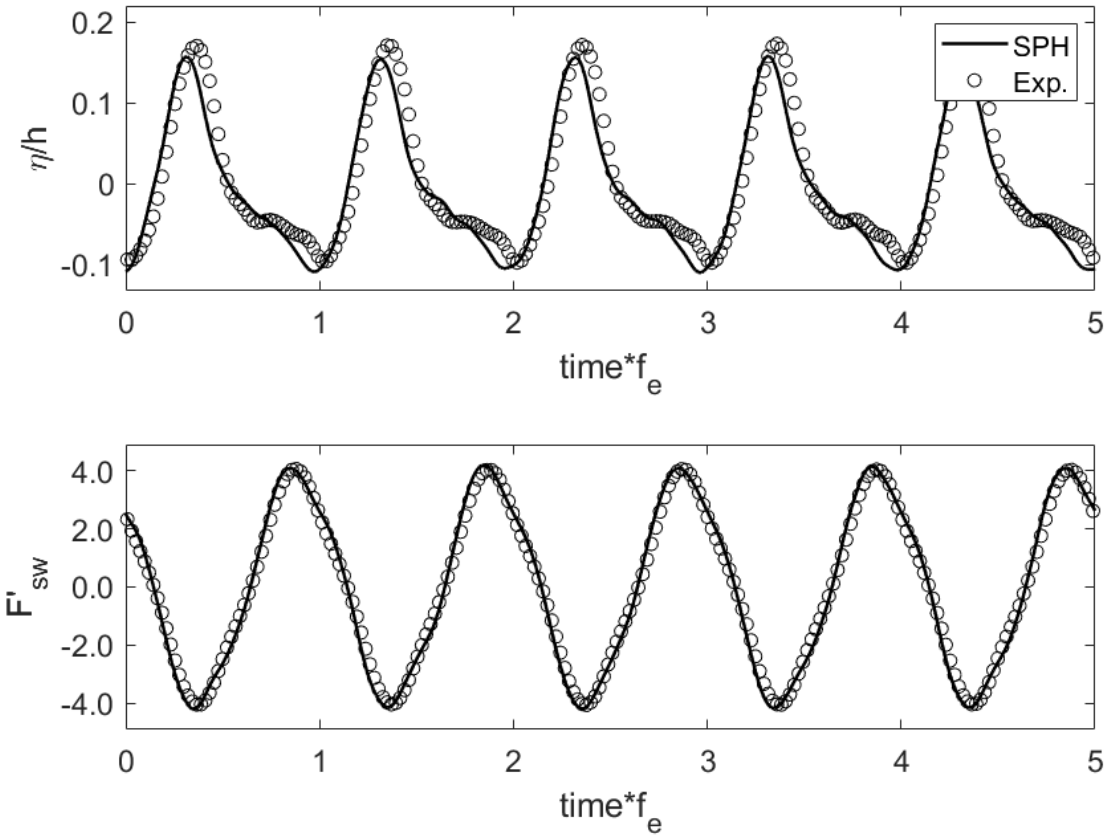

Figure 2.17: SPH wave height and sloshing force time response versus experimental results from Love and Tait (2013). h/L = 0.15, X_0/L = 0.0052, β = 0.94.

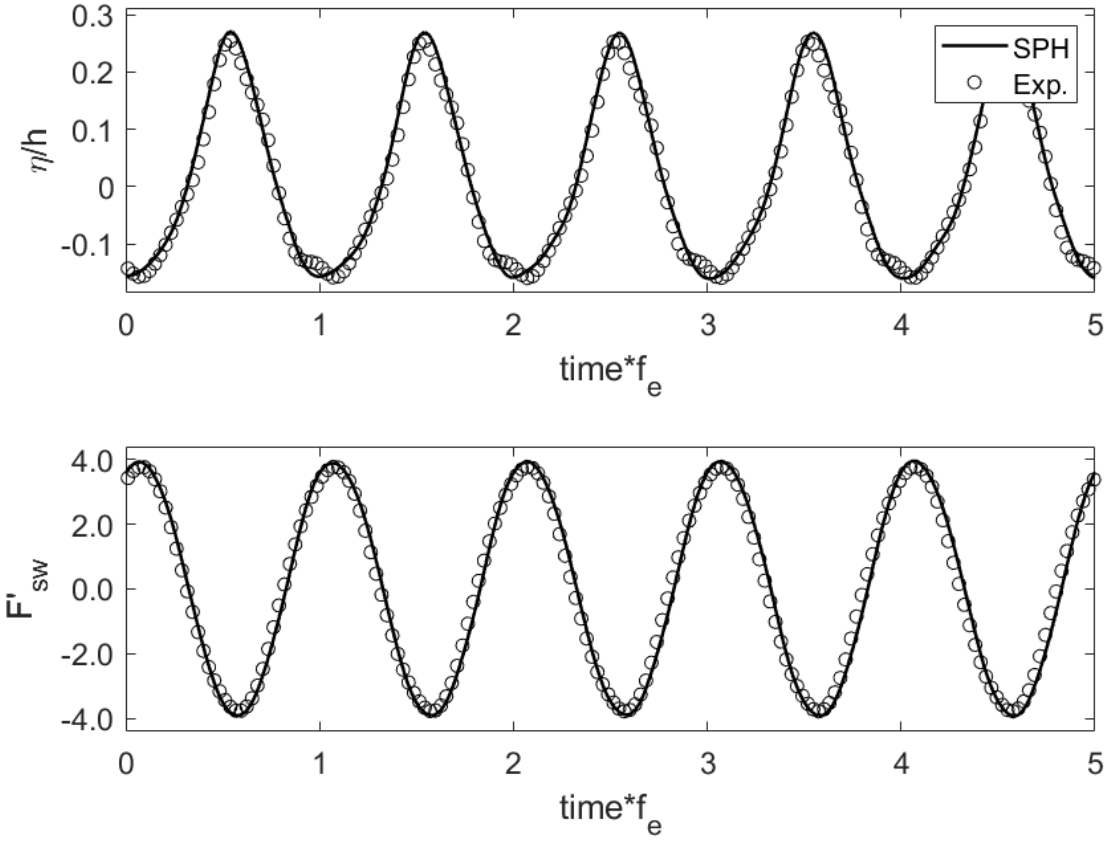

Figure 2.18: SPH wave height and sloshing force time response versus experimental results from Love and Tait (2013). h/L = 0.20, X_0/L = 0.0104, β = 1.02.

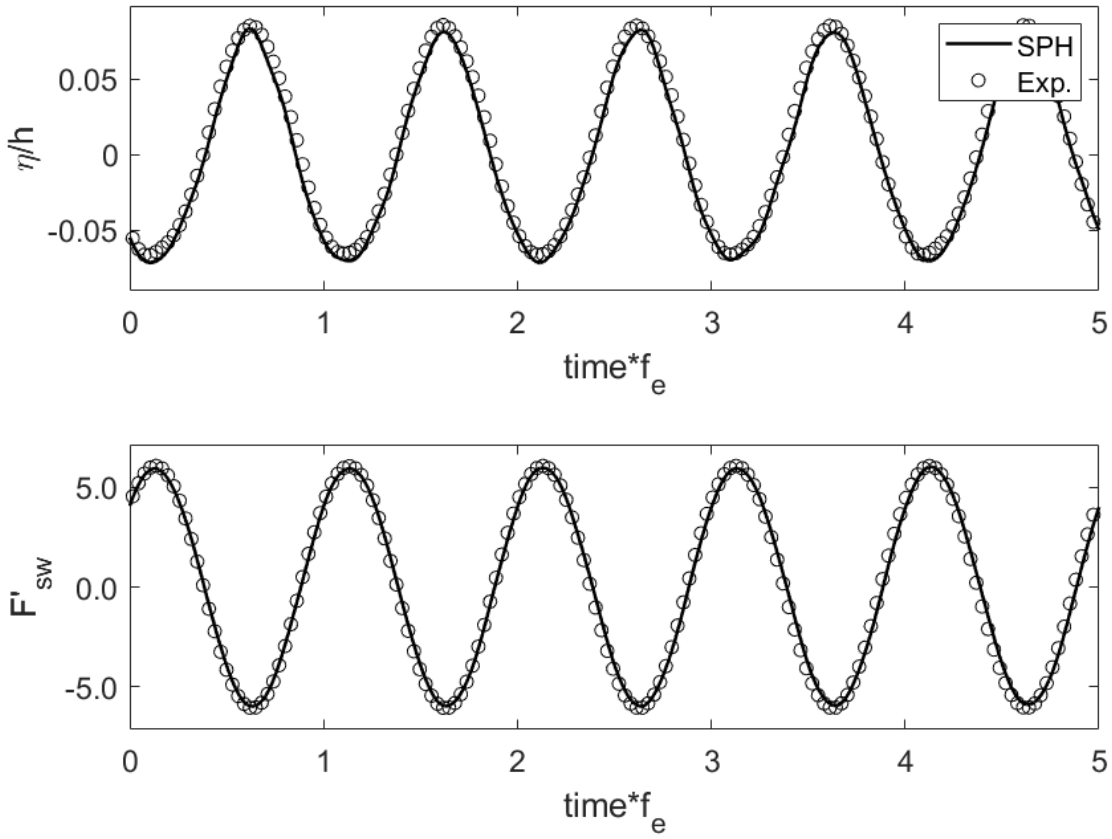

Figure 2.19: SPH wave height and sloshing force time response versus experimental results from Love and Tait (2013). h/L = 0.25, X_0/L = 0.0026, β = 1.04.

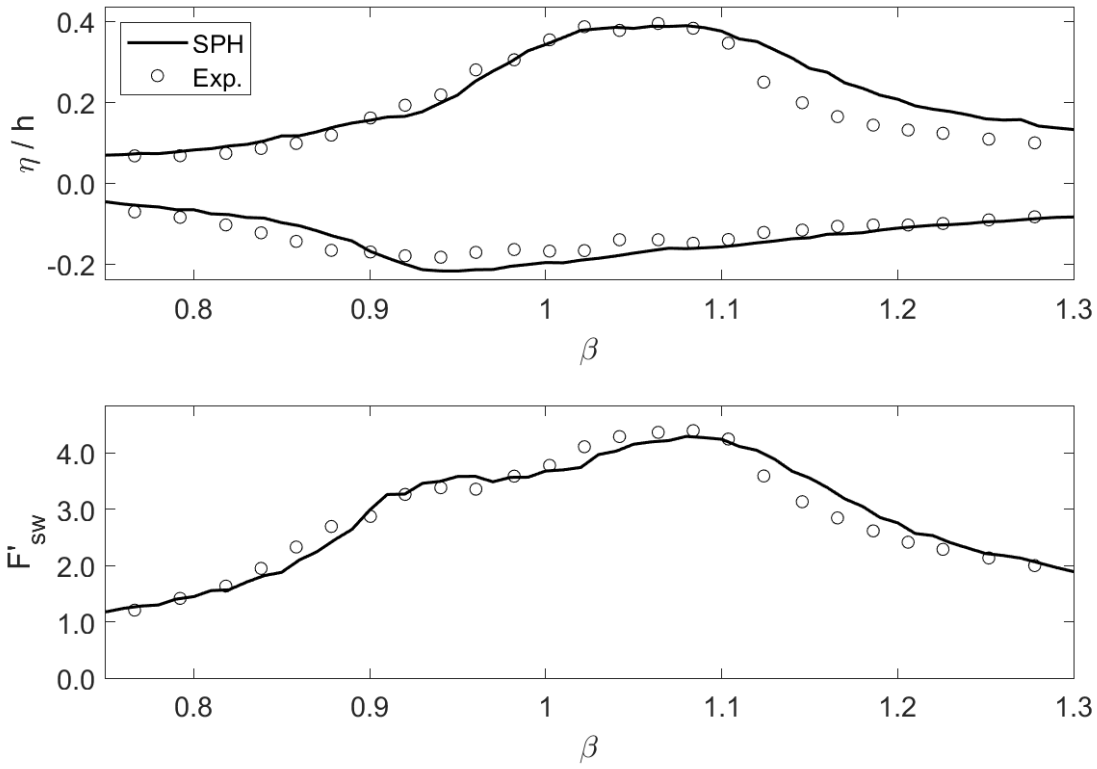

Figure 2.20: SPH wave height and sloshing force frequency response versus experimental results from Love and Tait (2013). h/L = 0.05, X_0/L = 0.0104.

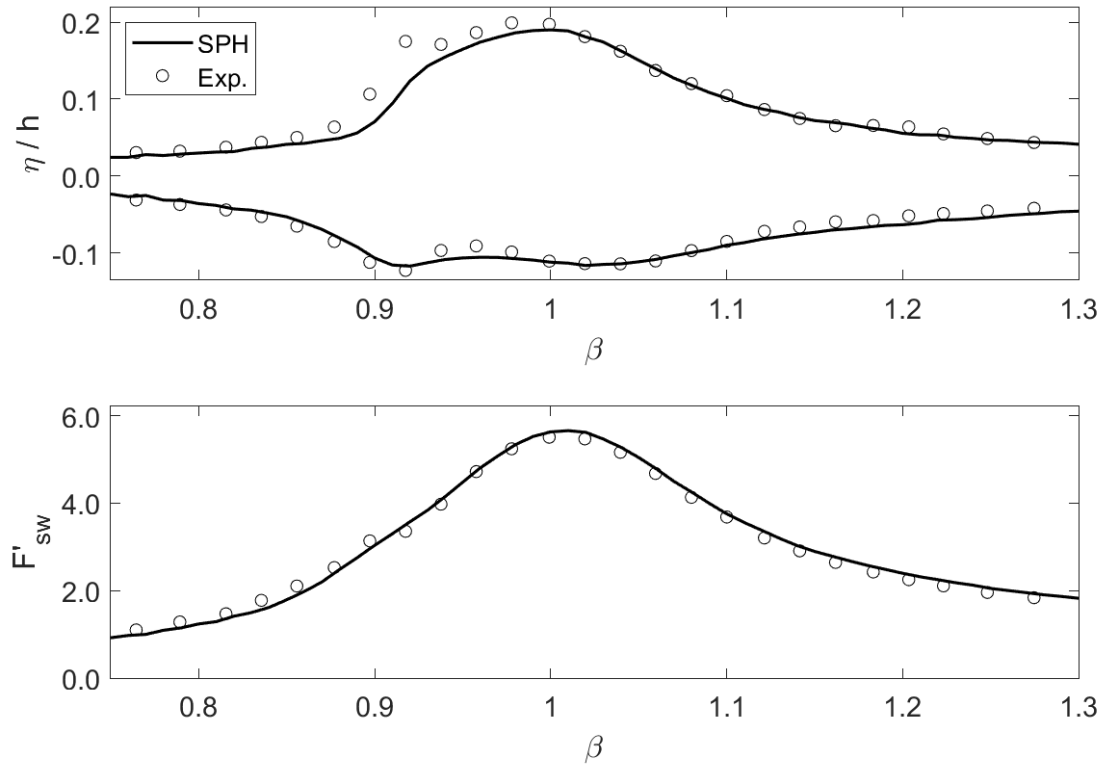

Figure 2.21: SPH wave height and sloshing force frequency response versus experimental results from Love and Tait (2013). h/L = 0.15, X_0/L = 0.0052.

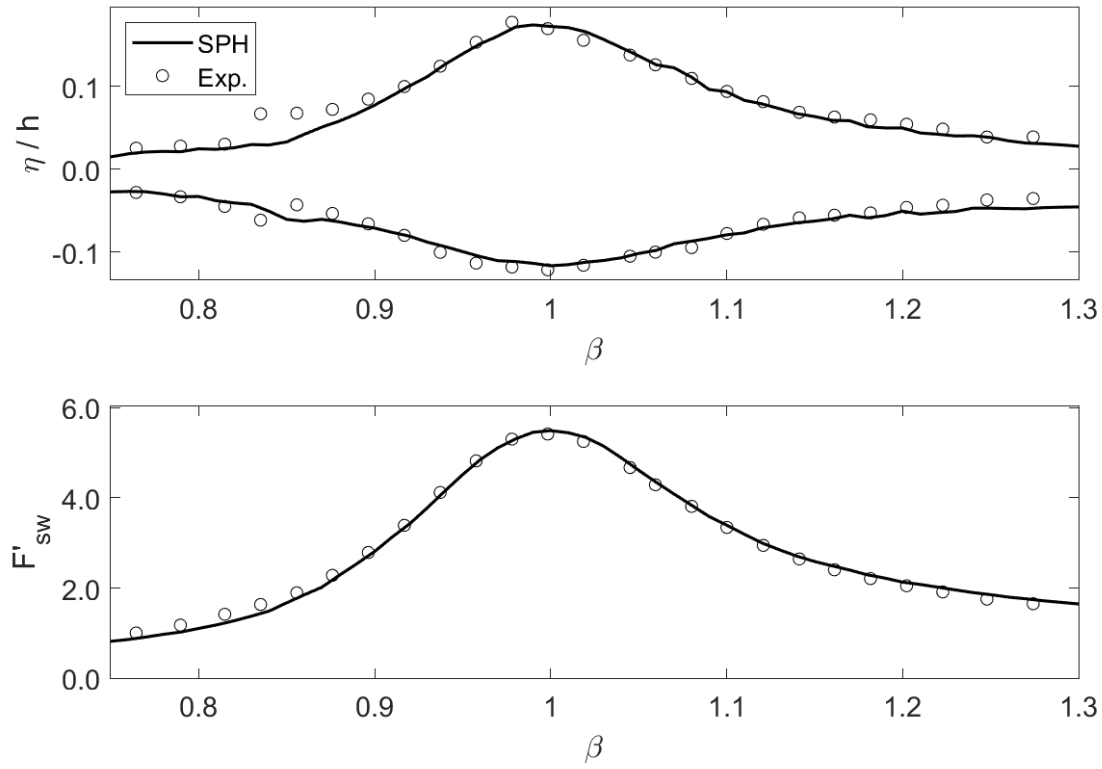

Figure 2.22: SPH wave height and sloshing force frequency response versus experimental results from Love and Tait (2013). h/L = 0.25, X_0/L = 0.0052.

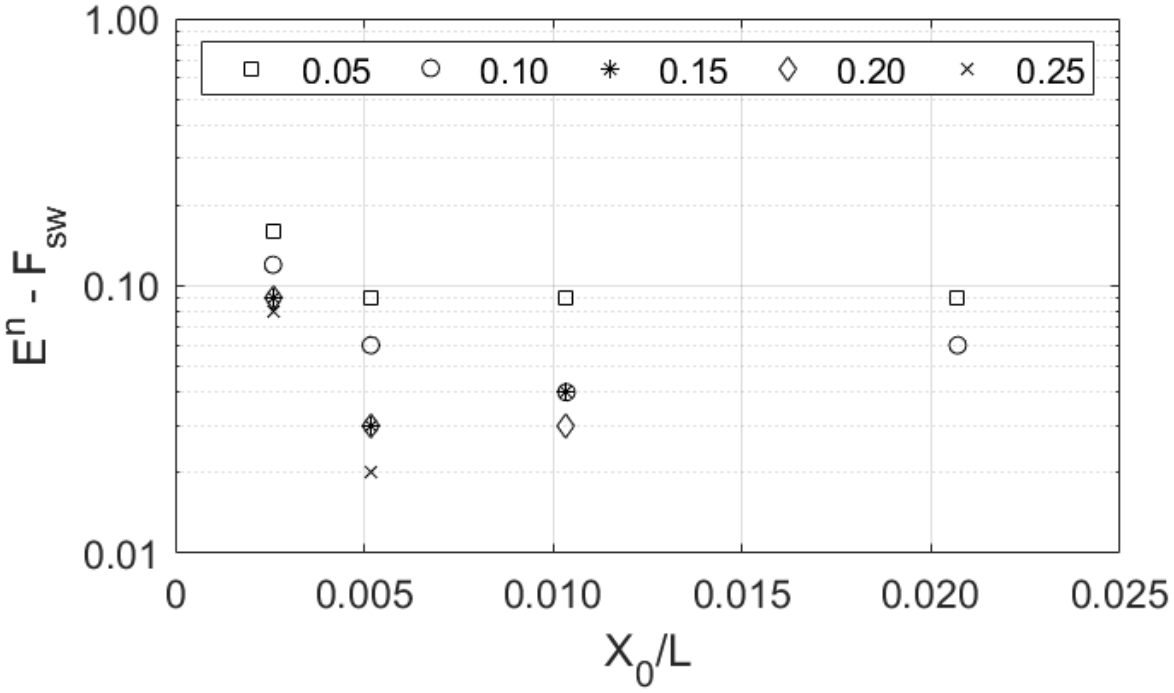

Figure 2.23: Normalized error between SPH and experimental sloshing force vs X_0/L. Legend indicates h/L value.

Chapter 3: Modelling the response of structure-tuned liquid damper systems under large amplitude excitation using SPH

McNamara K.P. and Tait M.J., "Modelling the response of structure-tuned liquid damper systems under large amplitude excitation using SPH." ASME Journal of Vibration and Acoustics 144 (2022): 011008, DOI: 10.1115/1.4051266

Abstract

The tuned liquid damper (TLD) is a system used to reduce the response of tall structures. Numerical modelling is a very important tool when designing TLDs. Many existing numerical models are capable of accurately capturing the structure-TLD system response at serviceability levels, covering the range where TLDs are primarily intended to perform. However, these models often have convergence issues when considering more extreme structural excitations. The goal of this study is to develop a structure-TLD model without convergence limitations at large amplitude excitations. A structure-TLD numerical model where the TLD is represented by a 2D incompressible SPH scheme is presented. The TLD contains damping screens which are represented by a force term based on the Morison equation. The performance of the model is assessed by comparing to experimental data for a structure-TLD system undergoing large amplitude excitations consisting of four-hour random signals and shorter transient signals. The model shows very good agreement with the experimental data for the structural response. The free surface response of the TLD is captured accurately by the model for the lower excitation forces considered, however as the excitation force is increased there are some discrepancies. The large amplitude excitations also result in SPH fluid particles penetrating the boundaries, resulting in degradation of the model performance over the four-hour simulations. Overall, the model is shown to capture the response of a structure-TLD system undergoing large amplitude excitations well.

KEYWORDS: tuned liquid damper (TLD), dynamic vibration absorber (DVA), damping screen, smoothed particle hydrodynamics (SPH), structure-TLD system.

3.1 Introduction

The tuned liquid damper (TLD) is a dynamic vibration absorber (DVA) that is employed to reduce the resonant response of tall and slender structures. In a TLD, a partially filled tank of liquid is installed near the top of a structure. The frequency of the TLD is tuned such that when the structure sways the liquid will slosh, generating a force that counteracts the motion of the building. TLD tanks typically include additional energy dissipating mechanisms, such as screens. The objective of a TLD is to reduce structural motion to a level acceptable by occupants, for example limiting structural acceleration to below the values set out in codes and standards, such as ISO 10137 [1]. The acceleration limits are generally defined for 1-year or 10-year return period events, indicating that a TLD is primarily intended to perform under serviceability conditions. However, for a TLD installed in structures located in regions prone to extreme loading events, such as hurricanes or earthquakes, it is imperative for the designer to understand the response of the TLD and structure-TLD system under large amplitude excitations.

Numerical modelling is an important tool in the TLD design process. Preliminary TLD design is often completed using simplified numerical models which determine feasibility and assist in sizing of the TLD. Equivalent mechanical models which can represent the TLD response linearly have been developed for various TLD tank shapes. Tait [2] presented an equivalent mechanical model for a rectangular TLD with screens alongside a methodology for preliminary structure-TLD system design. Tait and Deng [3] studied the performance of rectangular and cylindrical TLDs in structure-TLD systems. Love and Tait [4] presented an equivalent mechanical model for TLDs of arbitrary tank shape, and later coupled this model to a 2D structure [5]. These models are sufficient for preliminary design, however the TLD is an inherently nonlinear system and thus requires more sophisticated numerical models for detailed design.

Various models exist that can capture the nonlinear response of a TLD with damping screens. Kaneko and Ishikawa [6] developed a model for a TLD containing nets using shallow water wave theory and solved across the tank length using the finite difference

method, which was later adapted by Tait et al. [7] for a TLD with slat screens. These models have been shown to accurately capture the TLD response based on experimental testing, however there are amplitude limits above which convergence issues may arise. Love and Tait [8] presented a multi-modal model for a TLD of rectangular shape with screens. This model calculates the TLD response as a summation of sloshing modes with equations accounting for the nonlinear coupling between the modes. This nonlinear model was extended to TLDs of arbitrary dimensions [9], and coupled to a structure to study the structure-TLD system response [10]. The multi-modal model also has amplitude limitations for convergence, applicable liquid depth ranges, and at large excitations assumptions about the ordering of modal contributions may be invalid. These models are excellent at capturing the response of a TLD under service level loading, which allows for determination of the performance of the structure-TLD system within its target range of operation. However, these models do not always perform well under extreme loading scenarios.

To understand the response of the TLD at ultimate limit states and determine structural design quantities such as TLD tank forces and required freeboard, experimental testing on scale model tanks is often necessary. For example, Tait et al. [11] completed experimental studies on the response of a structure-TLD under large amplitude excitations. Shake table testing is commonly used to determine the performance of the TLD, however this testing can be time consuming and expensive. Numerical modelling is an attractive alternative to experimental testing, especially considering the availability and power of computing resources. The development of a numerical model capable of capturing the TLD response under extreme loading without amplitude limitation or convergence issues is the focus of this study.

The smoothed particle hydrodynamics (SPH) method is capable of modelling extreme sloshing responses. SPH is a Lagrangian meshless method which represents fluids as a series of particles. The method was originally developed by Gingold and Monaghan [12] and Lucy [13] for astrophysics applications. SPH has since been applied to numerous problems involving a free surface [14, 15]. The SPH method is particularly well suited to

model the response of sloshing fluids under extreme loading compared to other numerical models due to its inherent ability to define the free surface and capture phenomena such as wave breaking. There is no need for computationally expensive free surface tracking algorithms. SPH can also easily capture the response of sloshing fluids which impact the tank roof, which is a limitation of many other numerical models. Recent advances in the SPH method have allowed for capturing complicated fluid-structure interaction behavior in vibration problems, for example fluid vortex induced motion of solid bodies [16], slender structure vibration in viscous fluids [17], the interaction of fluids with elastic structures in both dam-break and sloshing experiments [18], and many more. These examples demonstrate the ability of the SPH method to capture complex flow interactions between structures and fluids. For a structure-TLD system, the TLD tank is rigid, and so modelling the interaction between the structure and TLD is not as complicated as other fluid-structure interaction problems. However, when the structure experiences a large response, the sloshing in the tank becomes highly nonlinear, making SPH an attractive method for capturing the sloshing behavior.

SPH models are typically broken down into weakly compressible (WCSPH) and incompressible (ISPH). ISPH can more accurately model the pressure field within a fluid compared to WCSPH, where special numerical treatment is often necessary to obtain a noise free pressure field. Since water is typically used in a TLD and is essentially incompressible, ISPH is particularly attractive for modelling a TLD. Various previous studies have modelled sloshing in TLDs using SPH [19, 20, 21], demonstrating that SPH can capture the response in sloshing tanks well, however these studies have focused on TLDs without damping screens or other interior tank damping elements. Kashani et al. [22] presented an ISPH model for a TLD with slat screens where the screen geometry was directly modelled. The results of this model were used to create an equivalent amplitude TMD model to capture the TLD response, which was compared to experimental data for a structure-TLD system. McNamara et al. [23] developed an explicit ISPH model for a rectangular TLD with slat screens where the screens were modelled macroscopically using a force term based on the Morison equation [24]. This allowed for much greater SPH

particle spacing, significantly reducing computational requirements. The model was compared to experimental shake table testing data for different rectangular TLDs with screens covering a range of tank dimensions, water depths, and excitation amplitudes, showing good agreement for all cases studied.

The goal of this study is to assess the performance of a structure-TLD numerical model under large excitations. This paper takes the ISPH model for a rectangular TLD from McNamara et al. [23] and couples it to a linear structure model. The structure is modelled as an equivalent single degree of freedom (SDOF) system with generalized properties. The model performance is assessed by comparing to experimental data for a structure-TLD system undergoing large excitations from Tait [25] and partially published in Tait et al. [11]. Two different types of structure excitation are considered: a four-hour random band limited white noise signal representative of wind excitation and a shorter transient excitation. For the random excitation, comparisons are made between the modelled and experimental response characteristics (root-mean-square and peak values) as well as response plots in the frequency and time domain. For the transient signal, the responses are compared in the time domain. Applicability and limitations of the model are discussed.

3.2 Structure – Tuned Liquid Damper System Model

A schematic of the structure-TLD system is shown in Figure 3.1. The response of tall structures to wind loading is often dominated by the first fundamental modes in sway and torsion. A TLD is typically installed to target a reduction in the response of one or multiple of these modes. The structure studied in this paper is modelled as an equivalent single degree of freedom (SDOF) system representing one of the fundamental sway modes. The equation of motion of this SDOF system undergoing force excitation with a TLD attached is given by:

$$M_s\ddot{X} + C_s\dot{X} + K_sX = F_{ext} + F_{TLD} \quad \textbf{(3.1)}$$

where M_s, C_s, and K_s are the structure generalized mass, damping, and stiffness, $\ddot{X}, \dot{X}$, and X are the structure acceleration, velocity, and displacement, F_{ext} is the applied external

force, and F_{TLD} is the TLD force defined in Section 3.2.1. The equation of motion is solved in time using the fourth order Runge-Kutta-Gill method. Rather than solving for the complete structure-TLD system, a substructuring approach is employed where the structure and TLD models interact at each timestep by passing back and forth the structural acceleration and TLD force.

The TLD is represented using an incompressible SPH model developed in-house by the authors. SPH was selected for its ability to inherently capture very large free surface responses without convergence issues unlike previous numerical models applied to TLDs. The actual TLD studied is three dimensional, however the model is restricted to two dimensions, which represents a slice of the TLD tank. This allows the model to represent the sloshing fluid undergoing uniaxial horizontal excitation parallel to the tank length. While the model will not capture any potential complex three dimensional effects such as swirling waves, the dominant behavior in a sloshing TLD with screens is a nonlinear standing wave which will be well represented by the SPH model. The domain of the model is shown in Figure 3.2. The TLD has dimensions of length *L*, height *H*, and water depth *h*. Vertically oriented damping screen(s) are placed at location(s) x_{screen} in the tank. Extensive details on the SPH model used in this study are presented in McNamara et al. [23]. The fluid response is governed by the Navier-Stokes equations for incompressible flow expressed in Lagrangian form:

$$\frac{D\rho}{Dt} + \rho\nabla\mathbf{u} = 0 \tag{3.2}$$

$$\frac{\mathrm{D}\mathbf{u}}{Dt} = -\frac{1}{\rho}\nabla P + v\nabla^2\mathbf{u} + \mathbf{g} \tag{3.3}$$

where *D/Dt* represents a Lagrangian derivative, ρ is the fluid density, **u** is the velocity (**bold** symbols indicate vector quantities), *P* is the fluid pressure, *v* is the fluid kinematic viscosity, and **g** is the external body force (gravity, applied excitation).

The governing equations are solved in an SPH framework by discretizing the fluid and boundaries using particles initially spaced at a distance *dp*. The properties of each particle (velocity, pressure, density) are calculated using the contributions from surrounding neighbour particles based on a smoothing kernel function [26]:

$$A_i = \sum_{j=1}^{N} A_j \frac{m_j}{\rho_j} W(r_i - r_j, h_{ker}) \tag{3.4}$$

where A_i is the quantity of interest, m_j is the particle mass, ρ_j is the particle density, W is the kernel function, and h_{ker} is the kernel function smoothing length. Expressions for the first and second order derivatives are given by Monaghan [26] and Cummins and Rudman [27], respectively as:

$$(\nabla A)_i = \rho_i \sum_{j=1}^{N} m_j \left(\frac{A_j}{\rho_j^2} + \frac{A_i}{\rho_i^2} \right) \nabla_j W_{ij} \tag{3.5}$$

$$\nabla . \left(\frac{1}{\rho} \nabla A \right)_i = \sum_{j=1}^{N} \left(\frac{8 m_j}{(\rho_i + \rho_j)^2} \frac{A_{ij} \boldsymbol{r_{ij}} . \boldsymbol{\nabla_i} W_{ij}}{r_{ij}^2 + \eta^2} \right) \tag{3.6}$$

where $\eta = 0.001 h_{ker}$ is a small factor to ensure a nonzero denominator.

This study uses the fifth order Wendland kernel in all SPH calculations [28]:

$$W(q) = W_c \begin{cases} (1 + 2q)\left(1 - \frac{q}{2}\right)^4 & 0 \le q \le 2 \\ 0 & q > 2 \end{cases} \tag{3.7}$$

where $q = \frac{|r_i - r_j|}{h_{ker}}$, $W_c = \frac{7}{\pi h_{ker}^2}$ for 2D simulations, and h_{ker} is the kernel function smoothing length, equal to 1.4*dp* in this study.

The SPH equations are solved in time using the projection method presented by Cummins and Rudman [27]. At each timestep, an intermediate velocity and position are calculated considering only the viscous and body forces:

$$\mathbf{u}^* = \mathbf{u}(t) + \left(v\nabla^2\mathbf{u} + \mathbf{g} + \ddot{\boldsymbol{X}} + \mathbf{F}_{\boldsymbol{screen}}\right)\Delta\mathrm{t} \tag{3.8}$$

$$\mathbf{r}^* = \mathbf{r}(t) + \mathbf{u}^*\Delta\mathrm{t} \tag{3.9}$$

where $v\nabla^2\mathbf{u}$ is the viscous force which is discretized using equation **(3.6)**, **g** is the gravitational acceleration, $\ddot{\boldsymbol{X}} = [\ddot{X}, 0]$ is the acceleration vector of the structure at the TLD location, and $\mathbf{F}_{\mathbf{screen}}$ is the force from the damping screens which is introduced in Section 3.2.2.

The intermediate velocity and position are used to calculate an intermediate density ρ^* [29], which leads to the calculation of fluid pressure by solving the pressure Poisson equation given by:

$$\boldsymbol{\nabla}.\left(\frac{\boldsymbol{\nabla}P}{\rho^*}\right) = \left(\frac{\boldsymbol{\nabla}.\boldsymbol{u}^*}{\Delta t}\right) \tag{3.10}$$

This equation is solved using an explicit approach from Yeylaghi et al. [30], with the addition of a pressure stabilizing term presented by Jiang et al. [31]. The velocity and position of each particle are then updated to enforce incompressibility:

$$\mathbf{u}(\mathrm{t}+\Delta\mathrm{t}) = \mathbf{u}^* + \left(-\frac{1}{\rho}\boldsymbol{\nabla}\mathrm{P}\right)\Delta\mathrm{t} \tag{3.11}$$

$$\mathbf{r}(\mathrm{t}+\Delta\mathrm{t}) = \mathbf{r}(\mathrm{t}) + \left(\frac{\mathbf{u}(\mathrm{t}+\Delta\mathrm{t}) + \mathbf{u}(\mathrm{t})}{2}\right)\Delta\mathrm{t} \tag{3.12}$$

The boundary conditions of the sloshing fluid in a TLD consist of the kinematic condition of zero velocity perpendicular to tank boundaries (i.e. $u_x = 0$ at the vertical tank walls and $u_y = 0$ at the tank bottom) and the dynamic condition of constant pressure on the free surface, equal to the atmospheric pressure in an open tank. In the SPH model the solid wall boundaries are modelled using multiple layers of boundary particles based on the method presented by Adami et al. [32], with a free-slip velocity condition since the tank walls are smooth and water is essentially inviscid. These boundary particles do not move throughout the simulation, but they do have a calculated pressure to prevent particle

penetration and are assigned a velocity during the prediction step. The velocity at the position of each boundary particle, $\mathbf{u}_{bnd}$, is calculated from the surrounding fluid particles using equation **(3.4)**. Velocity components are then determined parallel and perpendicular to the tank boundaries. The tank walls have x-velocity perpendicular and y-velocity parallel, whereas the tank floor has x-velocity parallel and y-velocity perpendicular. The boundary particle velocity parallel to the tank boundary is set equal to the parallel component of $\mathbf{u}_{bnd}$ to enforce the free-slip velocity profile. The boundary particle velocity perpendicular to the tank boundary is set opposite to the perpendicular component of $\mathbf{u}_{bnd}$ to enforce the kinematic boundary condition at the fluid-solid interface.

The dynamic condition of constant pressure on the free surface is implemented by calculating a numerical density which is only used to identify free surface fluid particles $\rho_{fi} = \sum_{j=1}^{N} m_j W_{ij}$ [30]. If the numerical density ρ_{fi} is less than 90% of the initial fluid density the particle is considered as a free surface particle and its pressure is set to zero. This occurs due to truncation of the kernel at the free surface.

3.2.1 TLD Force Calculation

The TLD force F_{TLD} in equation **(3.1)** is integral to the interaction between the structure and TLD. Since the SPH model is two dimensional, the force calculated is normalized by the TLD tank width, b. The actual TLD studied is three dimensional, and so this force is multiplied by the tank width when applied in equation **(3.1)**. The boundary particles do not move throughout the simulation, with the motion of the TLD accounted for by the acceleration of the structure $\ddot{X}$ being applied to the fluid particles in equation **(3.8)**. However, a numerical horizontal acceleration is calculated for each boundary particle in the tank walls based on the interaction with neighbouring fluid particles by the expression [33]:

$$a_{xj} = -\sum_f m_f \left(\frac{P_f}{\rho_f^2} + \frac{P_j}{\rho_j^2}\right) \nabla_f W_{jf} + \sum_f \nu \rho_f \left(\frac{8 m_f}{(\rho_f + \rho_j)^2} \frac{(u_f - u_j) \boldsymbol{r_{jf}} . \boldsymbol{\nabla_j} W_{jf}}{r_{jf}^2 + \eta^2}\right) + \ddot{X} \quad \textbf{(3.13)}$$

where the summation f is over the fluid particles, m_f is the fluid particle mass, P is the particle pressure, ρ is the particle density, ν is the kinematic viscosity, u_i is the horizontal particle velocity, $\mathbf{r_{jf}} = \mathbf{r_j} - \mathbf{r_f}$, $\eta = 0.001 h_{ker}$ and $\ddot{X}$ is the acceleration of the structure. The total TLD force is then calculated by summing the numerical acceleration times the mass of each wall boundary particle:

$$\frac{F_{TLD}}{b} = \sum_j m_j a_{xj} \quad \textbf{(3.14)}$$

where m_j is the mass of a single particle. The boundary particles have the same mass as the fluid particles.

3.2.2 Damping Screen Particles

The damping screens in the TLD studied consist of an array of small horizontal slats with a height of 5 mm spaced at 7 mm with a thickness of 1 mm [7]. The screens have a solidity of 42%, meaning that more than half of their area is open and allowing flow to pass through. As the fluid passes through the screen, the drag force on the slats induces a pressure loss proportional to fluid velocity squared, which leads to a drop in the height of the free surface across the screen. This action causes turbulence and dissipates energy in the sloshing fluid. Since the slats are small and distributed over the tank height, the added mass effect on the sloshing fluid is not significant. The drag characteristics of small slat screens are insensitive to the Reynolds number of the flow but can depend on the Keulegan-Carpenter (period) number. However, the screens studied have been shown to have constant loss characteristics for large Keulegan-Carpenter numbers [7], as will occur in the large amplitude excitations studied here. Compared to a TLD without screens, adding screens reduces the occurrence of higher order effects such as travelling waves and wave breaking,

and provides significant additional damping and improved performance for controlling structural motion.

In SPH, the screen geometry can be modelled explicitly using solid SPH particles, as was done by Kashani et al. [22], however this requires a very fine particle spacing for the screens considered (dp < 1 mm), leading to significant computational requirements. To reduce the computational time, a coarser particle spacing in the SPH simulation can be achieved by modelling the impact of the screens on the fluid flow without explicitly modelling the screen geometry. A novel macroscopic damping screen implementation for SPH was presented and validated with experimental data by McNamara et al. [23]. The screens are modelled by a line of screen particles with spacing dp equal to the initial fluid particle spacing. The screen particles interact with the fluid particles by applying a force (F_{screen} in equation **(3.8)**) based on the Morison equation [24] equal and opposite to the force that the fluid exerts on the screens. This is appropriate for screens that have known loss properties, and where the thickness is much less than the tank length, as is the case in this study.

The force that the fluid applies on each screen particle is calculated by [23]:

$$F_{screen-j} = \frac{1}{2} C_l \rho \left| U_{sc,j} \right| U_{sc,j} dp$$
$$U_{sc,j} = \sum_f \frac{m_f}{\rho_f} u_f W_{jf} \quad \textbf{(3.15)}$$

where C_l is the screen loss coefficient, ρ is the fluid density, $U_{sc,j}$ is the fluid velocity calculated at the screen particle location, and dp is the initial particle spacing. The smoothing length used in the kernel function W_{jf} is set to $h_{screen} = 3h_{ker}$. The force that the screen particles j apply on fluid particle f is weighted based on the kernel function as:

$$F_{screen-f} = -\sum_j F_{screen-j} \frac{W_{jf}}{\sum_f W_{jf}} \quad \textbf{(3.16)}$$

where *j* is summed over the neighbouring screen particles.

Since the damping screen particles are not explicitly modelled, and there is no added turbulence model, this method is not capable of capturing the complex and turbulent flow in the region of the screens. However, since the loss properties of the screens are known, and they are very thin relative to the length of the tank, the model does capture the overall resulting energy dissipation in the bulk flow. Additionally, the sloshing wave heights of primary interest are at the tank walls which are located away from the screens, outside the region of turbulence. Implementation of an efficient explicit screen geometry using solid particles and added turbulence model would be necessary for studies where the loss characteristics of the screens are unknown or the screen geometry significantly disrupts the sloshing flow.

3.2.3 SPH Model Parameters

This section will briefly discuss the SPH model parameters used in this study. Each simulation was run in series on a single CPU. The four-hour duration simulations took approximately two weeks to compute, and the shorter transient excitation simulations took approximately one hour. For all cases considered, the TLD was discretized in SPH using an initial particle spacing of dp = 7 mm. This value was selected as it provided a reasonable number of particles spaced along the tank length and across the fluid depth to capture the free surface deformation. It also provided an integer multiple of the tank length (966 mm) and water depth (119 mm), while staying within the bounds of the computational resources available to run the long four-hour simulations. For all cases, the kernel function smoothing length was set as $h_{ker} = 1.4dp$. The fluid was water, with a density of 1000 kg/m^3 and kinematic viscosity of 1x10^{-6} m^2/s.

The timestep was dt = 5x10^{-4} seconds and was fixed throughout the simulation. This was determined to provide adequate performance for several different validation test cases of the authors code, and also met the criteria that $dt \leq \min\left(\frac{0.1dp}{u_{max}}, \frac{0.1dp^2}{\nu}\right)$ for an incompressible SPH simulation [34], where u_{max} is the maximum fluid velocity.

The boundary particles and screen particles had the same spacing as the fluid particles, dp = 7 mm, and did not move throughout the simulation. Three layers of boundary particles were defined for each tank face to ensure complete kernel support for the fluid particles located near the walls and floor of the tank [32]. The screen particles were placed in a single vertical array at each screen location. The kernel function radius used for the screen particles was set to $h_{screen} = 3h_{ker}$ to capture the radius of screen influence. This value was determined based on tests to compare the model to experimental data for the TLD with screens that was studied. A different value may be appropriate for different screen geometries.

3.3 Structure-TLD Experimental Data

Experimental data for a structure-TLD system undergoing large excitations was obtained by Tait [25] and partially published in Tait et al. [11]. Experimental tests were completed for a large range of structure excitations, including those well above the serviceability levels that TLDs are primarily intended to perform at. Previous numerical models for TLDs often have convergence issues above certain structural response levels, limiting the ability to model large excitation scenarios numerically. The SPH TLD model does not have any excitation amplitude convergence limitations, however it is important to verify the accuracy of the model when the structural response is large as this has not previously been investigated.

Tait [25] studied various structure-TLD configurations experimentally under both 1D and 2D excitations. Extensive details on the experimental setup can be found in Tait [25] and Tait et al. [11]. The experimental structure was designed to represent the system schematic shown in Figure 3.1. The structure was represented by a cable suspended mass equal to M_s that was free to swing. The structure was connected to a rigid frame by several springs that were tensioned to provide the required stiffness of the structure, K_s. The properties of the structure were confirmed with free vibration testing [25]. The TLD consisted of a plexiglass tank mounted on top of the structure and partially filled with water. The displacement and acceleration of the structure were measured, as well as the wave

height at various locations in the TLD using capacitance-based wave probes. The mass of the tank and mounted instrumentation was accounted for in the total mass of the structure. The experimental structure was very lightly damped, and as such the structure-TLD system damping was almost entirely provided by the TLD. The focus of this study will be on structure-TLD systems undergoing 1D excitation with large amplitudes. In the experiments, the structure-TLD system was excited in one direction using an actuator that was connected to the structure through a driving spring, converting the displacement of the actuator to a force applied to the structure (representing F_{ext} in equation **(3.1)**). The data was sampled at a rate of 20 Hz and low-pass filtered with a 5 Hz cut-off frequency.

The experimental testing considered two different types of structural excitation. The first was a random band-limited white noise signal four hours in length, and the second was a shorter 35 second transient signal. Further details on the excitation will be provided in Sections 3.4.1 and 3.4.2. The properties of the structure studied are shown in Table 3.1. The TLD properties are shown in Table 3.2. The same TLD configuration was used for both excitation cases.

3.4 Model vs Experimental Comparisons

This section will assess the performance of the model by comparing to the experimental data.

3.4.1 Random Band-limited White Noise Excitation

The random excitation force consisted of a zero-mean signal of length four hours with frequency content ranging from 0.20 to 1.20 Hz (f/f_s ranging from 0.36 to 2.15). The normalized power spectrum of the excitation force is shown in Figure 3.3. A sample segment of the signal is shown in Figure 3.4. The excitation signal was scaled to three different root-mean-square (RMS) levels, σ_F = 165 N, 223 N, and 300 N (σ_F/K_s= 0.0030, 0.0040, and 0.0055). For reference, Tait et al. [11] estimated return periods for the different excitation levels considered in this study to be 335, 1400, and 6000-years by assuming that the hourly peak structural acceleration response was proportional to wind speed cubed.

These return periods are significantly greater than the serviceability levels that TLDs are typically designed for.

The RMS and peak structural response for the four-hour signal are provided in Table 3.3 for structural displacement and Table 3.4 for structural acceleration. The comparison between experimental and modelled responses shows very good agreement, with absolute percentage difference values between 0.3% and 11.8%. In some cases, the model over-predicted the response compared to the experimental data, and in some cases the model under-predicted the response. These results suggest that the model can accurately capture the overall structural response characteristics for a structure-TLD system undergoing large random signal excitations.

Since the excitation force contains many frequencies, it is important to analyze the performance of the model from a frequency domain perspective. The mechanical admittance function (MAF) of a structure indicates how the structure responds to different frequencies in a random excitation signal. The squared modulus of the MAF of a structure is defined by the expression:

$$|H_s(f)|^2 = \frac{S_{XX}(f)K_s^2}{S_{FF}(f)} \tag{3.17}$$

where $S_{FF}(f)$ and $S_{XX}(f)$ are the power spectra of the applied force and structural displacement response, and K_s is the structure generalized stiffness.

Figure 3.5 shows the squared MAF for the three excitation levels studied. The agreement between the experimental data and the model results is good. The model underestimates the peak experimental value by approximately 10% for each case. In Figure 3.5c there is a slight shift in the location of the peak of the curve. A linear structure with low damping and no TLD will have a single peak MAF. Typically for a structure-TLD system the MAF has multiple peaks. However, as the excitation force is increased to large values, the TLD becomes less effective, causing the MAF to return to a single peaked curve, as illustrated in Figure 3.5. The effective damping of a structure equipped with a TLD can

be calculated based on the area under the MAF [35]. Table 3.5 displays the calculated effective damping for the experimental and modelled results. The effective damping decreases as the value of σ_F/K_s increases, which is expected due to the corresponding reduction in TLD effectiveness. The model is within 8.3% of the experimental data for the three cases considered.

The ability of the model to capture the TLD wave height response at large excitations is also integral to verifying the performance of the model. The normalized wave height spectrum for the modelled and experimental data is shown in Figure 3.6. The model shows very good agreement with the experimental data for all three excitation levels. As was observed with the MAF, the model slightly under-predicts the peak value, with a difference of 5% for the σ_F/K_s = 0.0030 case, and a difference of 10% for the σ_F/K_s = 0.0040 and 0.0055 cases. The model shows very good agreement with the experimental data for the secondary peak in the spectra, which is a result of the nonlinear response of the TLD.

To illustrate the sloshing waves in the TLD, Figure 3.7 shows the SPH model wave profiles for various time instants from the σ_F/K_s = 0.0030 case. The particles are colored by their pressure value. The figure shows that the fluid pressure transitions smoothly from high values at the tank bottom to low values at the free surface. Since the pressure drop through the screens is dependent on fluid velocity squared, the effect of the screens on the wave height changes throughout the simulation. For example, at time = 3600, 10800, and 13800 seconds, the drop in wave height across the screens is visibly displayed in the positions of the particles, though it is not the same at each screen. Whereas for time = 7200 seconds, the screens do not appear to be impacting the flow significantly, indicating that the horizontal velocity was low at this time.

Response histories of the structural displacement and wave height illustrate the performance of the model in the time domain. Figure 3.8 shows a one-minute segment of the normalized response for the smallest excitation σ_F/K_s = 0.0030 case within the first ten minutes of the simulation. The modelled structural response is in excellent agreement with the experimental data. The modelled wave height response is in excellent agreement with

the experimental data, and can clearly capture the nonlinear response, though some of the peak values are under-predicted. Figure 3.9 shows another segment near the end of the excitation. Again, the modelled responses show excellent agreement with the experimental data, with some under-prediction of the peak values. This illustrates that the model performs well throughout the simulation despite the length (4 hours) and number of timesteps (28.8 million). Figure 3.10 shows a segment of the response history for the largest excitation σ_F/K_s = 0.0055 case during the first ten minutes of the simulation. Very good agreement is observed between the modelled and experimental responses. The discrepancies between the peak wave height values for some cycles are more significant than in the previous case. This is likely a result of the free surface being more chaotic under the larger excitation, leading to more splashing and three-dimensional sloshing effects not captured by the model. Figure 3.11 shows a segment of the response history near the end of the simulation. The agreement between the modelled and experimental responses is worse than in the previous cases, especially for the wave height. Compared to Figure 3.10, Figure 3.11 indicates that at this amplitude of excitation there is degradation of the model performance over the course of the long simulation. This is further discussed in Section 3.5.

3.4.2 Transient Excitation

The structure-TLD system was also studied experimentally under a shorter transient excitation by Tait [25]. A 35-second segment was extracted from the four-hour random signal discussed in Section 3.4.1. Figure 3.12 shows the transient signal normalized by the maximum applied force, F_0. Four values of F_0 were considered: 140 N, 415 N, 555 N, and 775 N.

Figure 3.13 shows the normalized structure displacement response. The model is in excellent agreement with the experimental data. Figure 3.14 shows the normalized wave height response. The model is in excellent agreement with the experimental data for the F_0 = 140 N and 415 N cases, capturing both the wave form and amplitude. For the F_0 = 555 N and 775 N cases the agreement between the model and experimental data is good initially.

Between the time of 10 and 15 seconds the model begins to deviate from the experimental data. This is the time where the structure is experiencing the greatest applied forces (see Figure 3.12). For the F_0 = 555 N case (Figure 3.14c) the model and experimental wave height data do not agree well from 12 to 25 seconds, however after this the agreement is improved. The F_0 = 775 N case (Figure 3.14d) shows poor agreement between 12 to 30 seconds, with better agreement after this point. This discrepancy may be a result of chaotic three-dimensional sloshing effects present in the tank under such large excitations that are not captured in the two-dimensional SPH model.

These results show that the model captures the structural response well under the transient motions considered. This indicates that the SPH model is accurately representing the controlling forces of the TLD (which impact the structural response), despite the discrepancies observed in the wave heights for the larger excitation cases.

3.5 Discussion on Model Performance

The model has been shown to agree well with experimental data for a structure-TLD system under long duration random and short duration transient excitations with large amplitudes. However, some discussion is warranted on the overall performance of the model and potential limitations on its use.

3.5.1 SPH Model Consistency for Very Long Simulations

In Section 3.4.1 it was noted that for the largest random excitation case, σ_F/K_s = 0.0055, the agreement between the modelled and experimental results was better near the start of the four-hour simulation than at the end. This was not observed for the other cases studied. The parameters for each of the three random simulations were identical except for the RMS applied force value. This result indicates degradation of the model performance over the length of the simulation when the excitation force passes a certain threshold. To investigate the cause of the discrepancy over the length of the simulation for the σ_F/K_s = 0.0055 case, the SPH simulation results were further analyzed.

In the SPH model the boundary conditions are only approximately satisfied, which can result in fluid particles penetrating the boundaries [36]. This is generally a small percentage of the fluid particles (1% to 2%) which does not significantly impact the results for a short simulation. Figure 3.15 shows the percentage of fluid particles outside the domain boundaries for each of the three excitation cases at various times in the four-hour simulation. The percentage of particles outside the domain at the end of the simulation was 0.6%, 4%, and 34% for the σ_F/K_s = 0.0030, 0.0040, and 0.0055 cases, respectively. With 34% of the fluid particles outside the domain in the σ_F/K_s = 0.0055 case, the TLD effectively became mistuned from the structure by the end of the simulation, which could be the cause of the more significant discrepancies compared to the start of the simulation. This result clearly indicates that the current boundary conditions in the model have a limit on their ability to contain the fluid which is impacted by both the excitation amplitude and the simulation duration. For a shorter simulation, the loss of particles through the boundary would be insignificant, however the length of simulation considered in this study is much longer than most SPH simulations, which are generally limited to at most a few minutes of time.

It is clear from these results that above a certain RMS excitation force threshold, the SPH model boundary particles do not contain the fluid particles effectively over long simulations. Additionally, as the RMS excitation force increases, the rate of particle loss increases. The excitation forces considered are very large. However, if the SPH model is to be used accurately at these excitation forces, care must be taken to ensure containment of the fluid particles. Implementation of different or additional boundary conditions, such as a repulsive force method [14], may improve the performance of the model.

3.5.2 Accuracy of 2D Simulations

It is typical to model a rectangular TLD using a two-dimensional numerical model, which effectively captures a slice of the TLD fluid. Tait et al. [37] demonstrated that the response of a rectangular TLD undergoing 2D excitation can be de-coupled into that of two TLDs undergoing 1D excitation, and this principal can be applied to models as well. The

2D SPH model implemented in this study was found to accurately capture the structural controlling actions of the TLD. This was demonstrated by good agreement with experimental data for the structural response across the amplitudes studied for both the random and transient excitation cases. Since the controlling action of a TLD is generated primarily by the fundamental mode of sloshing, most numerical models can capture this behavior adequately.

The free surface response is significantly more complicated to model. As the excitation increases, the degree of sloshing nonlinearity increases, resulting in significant higher order effects such as splashing, jetting, and wave breaking. Additionally, despite experiencing only 1D excitation, the experimental structure was not constrained from moving in the direction perpendicular to the excitation, which can lead to nonlinear excitation of 3D sloshing effects in the TLD. The SPH model was found to capture the free surface response well at the lower excitation forces studied in both the random and transient cases. As the excitation forces were increased, the model agreement with the experimental wave height was decreased for some cycles (for example see Figure 3.10 and Figure 3.14) despite good agreement with the structural response. It is postulated that this is to some extent due to the 3D sloshing effects that are not captured by the 2D SPH model.

These results indicate that the model captures the structural response well in a structure-TLD system under large excitation. However, the wave height response is not as accurately captured as the excitation force increases. In situations where accurate modelling of the free surface is imperative, using a 3D SPH model may provide improved results, though there would also be a significant increase in computational runtime.

3.6 Conclusions

This study presented a structure-TLD system model intended to capture the response of the system undergoing large amplitude excitations beyond the values typically possible with other numerical models. The structure was represented by an equivalent linear SDOF and coupled to a TLD represented by a 2D SPH model. The performance of the model was assessed by comparing to experimental data obtained by Tait [25] and published in Tait et

al. [11] for a structure-TLD system undergoing both long duration random band-limited white noise excitation and short duration transient excitation. The following conclusions can be made from the results of this study:

1. For random white noise excitation, the model captured the response of the structure-TLD system accurately for the σ_F/K_s = 0.0030 and 0.0040 cases when considering the peak and RMS response, frequency response plots, and time domain response histories. The good agreement between the model and experimental data was maintained throughout the four-hour simulation time. The effective damping ratio of the structure-TLD system was well predicted by the model. For the σ_F/K_s = 0.0055 case, the peak and RMS responses and frequency response plots were accurately captured by the model, however the agreement between the model and experimental data was found to degrade over the length of the simulation.
2. The loss of fluid particles through solid boundaries was found to impact the results of the SPH model over the four-hour simulations. As the random white noise excitation RMS force was increased, the SPH boundary particles were unable to adequately contain the fluid. Care must be taken when using the model under very large excitation amplitudes. The implementation of different or additional solid boundary conditions may improve this result.
3. For the shorter transient excitation, the model captured the structure response well over the range of excitation forces studied. For F_0 = 140 N and 415 N, the TLD wave height showed good agreement between the model and experimental data. For the F_0 = 555 N and 775 N cases, the model did not accurately capture the wave heights for certain cycles.

These results indicate that the model can be used to study a structure-TLD system under large amplitude random and transient excitations. This model can capture excitations that would generally result in convergence issues for other numerical model types. Care must be taken when applying the current 2D SPH model to extremely large excitation cases, as the model may not always capture the free surface response.

Further advancements such as the implementation of additional boundary conditions and/or extension to a 3D SPH model are expected to improve the performance of the SPH model.

3.7 Acknowledgment

The authors are thankful for the financial support provided by the Natural Sciences and Engineering Research Council of Canada (NSERC) and the Ontario Graduate Scholarship (OGS) program. This research was enabled in part by support provided by Compute Ontario (www.computeontario.ca) and Compute Canada (www.computecanada.ca).

3.8 References

[1] International Organization for Standardization, *ISO 10137*, 2007.

[2] M. J. Tait, "Modelling and preliminary design of a structure-TLD system," *Engineering Structures*, vol. 30, no. 10, pp. 2644-2655, 2008.

[3] M. J. Tait and X. Deng, "The performance of structure-tuned liquid damper systems with different tank geometries," *Structural Control and Health Monitoring*, vol. 17, no. 3, pp. 254-277, 2008.

[4] J. S. Love and M. J. Tait, "Equivalent Linearized Mechanical Model for Tuned Liquid Dampers of Arbitrary Tank Shape," *Journal of Fluids Engineering*, vol. 133, no. 6, pp. 1065-1075, 2011.

[5] J. S. Love and M. J. Tait, "Equivalent mechanical model for tuned liquid damper of complex tank geometry coupled to a 2D structure," *Structural Control and Health Monitoring*, vol. 21, pp. 43-60, 2014.

[6] S. Kaneko and M. Ishikawa, "Modeling of tuned liquid dampers with submerged nets," *Journal of Pressure Vessel Technology*, vol. 121, no. 3, pp. 334-344, 1999.

[7] M. J. Tait, A. A. El Damatty, N. Isyumov and M. R. Siddique, "Numerical flow models to simulate tuned liquid dampers (TLD) with slat screens," *Journal of Fluids and Structures*, vol. 20, no. 8, pp. 1007-1023, 2005.

[8] J. S. Love and M. J. Tait, "Nonlinear simulation of a tuned liquid damper with damping screens using a modal expansion technique," *Journal of Fluids and Structures*, vol. 26, no. 7-8, pp. 1058-1077, 2010.

[9] J. S. Love and M. J. Tait, "Non-linear multimodal model for tuned liquid dampers of arbitrary tank geometry," *International Journal of Nonlinear Mechanics*, vol. 46, no. 8, pp. 1065-1075, 2011.

[10] J. S. Love and M. J. Tait, "The response of structures equipped with tuned liquid dampers of complex geometry," *JVC/Journal of Vibration and Control*, vol. 21, no. 6, pp. 1171-1187, 2015.

[11] M. J. Tait, N. Isyumov and A. A. El Damatty, "Performance of Tuned Liquid Dampers," *Journal of Engineering Mechanics*, vol. 134, no. 5, pp. 417-427, 2008.

[12] R. A. Gingold and J. J. Monaghan, "Smoothed particle hydrodynamics: theory and application to non-spherical stars," *Monthly Notices of the Royal Astronomical Society*, vol. 181, pp. 375-389, 1977.

[13] L. Lucy, "A numerical approach to the testing of the fission hypothesis," *The Astronomical Journal*, vol. 82, no. 12, pp. 1013-1024, 1977.

[14] J. J. Monaghan, "Simulating free surface flows with SPH," *Journal of Computational Physics,* vol. 110, no. 2, pp. 399-406, 1994.

[15] D. Violeau and B. D. Rogers, "Smoothed particle hydrodynamics (SPH) for free-surface flows: Past, present and future," *Journal of Hydraulic Research,* vol. 54, no. 1, pp. 1-26, 2016.

[16] P. N. Sun, A. Colagrossi, D. Le Touzé and A. M. Zhang, "Extension of the δ-Plus-SPH model for simulating Vortex-Induced-Vibration problems," *Journal of Fluids and Structures,* vol. 90, pp. 19-42, 2019.

[17] A. Tafuni and I. Sahin, "Non-linear hydrodynamics of thin laminae undergoing large harmonic oscillations in a viscous fluid," *Journal of Fluids and Structures,* vol. 52, pp. 101-117, 2015.

[18] P. N. Sun, D. Le Touzé, G. Oger and A. M. Zhang, "An accurate FSI-SPH modeling of challenging fluid-structure interaction problems in two and three dimensions," *Ocean Engineering,* vol. 221, p. 108552, 2021.

[19] G. Bulian, A. Souto-Iglesias, L. Delorme and E. Botia-Vera, "Smoothed particle hydrodynamics (SPH) simulation of a tuned liquid damper (TLD) with angular motion," *Journal of Hydraulic Research,* vol. 48, no. sup1, pp. 28-39, 2009.

[20] A. Marsh, M. Prakash, E. Semercigil and O. F. Turan, "A study of sloshing absorber geometry for structural control with SPH," *Journal of Fluids and Structures,* vol. 27, no. 8, pp. 1165-1181, 2011.

[21] M. D. Green and J. Peiro, "Long duration SPH simulations of sloshing in tanks with a low fill ratio and high stretching," *Computers and Fluids,* vol. 174, pp. 179-199, 2018.

[22] A. H. Kashani, A. M. Halabian and K. Asghari, "A numerical study of tuned liquid damper based on incompressible SPH method combined with TMD analogy," *Journal of Fluids and Structures,* vol. 82, pp. 394-411, 2018.

[23] K. P. McNamara, B. N. Awad, M. J. Tait and J. S. Love, "Incompressible smoothed particle hydrodynamics model of a rectangular tuned liquid damper containing screens," *Journal of Fluids and Structures,* vol. 103, p. 103295, 2021.

[24] J. R. Morison, M. P. O'Brien, J. W. Johnson and S. A. Schaaf, "The force exerted by surface waves on piles," *Petroleum Transactions AIME,* vol. 189, pp. 149-154, 1950.

[25] M. J. Tait, *The Performance of 1-D and 2-D Tuned Liquid Dampers,* Ph.D. Thesis. University of Western Ontario, 2004.

[26] J. J. Monaghan, "Smoothed Particle Hydrodynamics," *Annual Review of Astronomy and Astrophysics,* vol. 30, pp. 543-74, 1992.

[27] S. J. Cummins and M. Rudman, "An SPH Projection Method," *Journal of Computational Physics,* vol. 152, pp. 584-607, 1999.

[28] H. Wendland, "Piecewise polynomial, positive definite and compactly supported radial functions of minimal degree," *Advances in Computational Mathematics,* vol. 4, pp. 389-396, 1995.

[29] Nomeritae, E. Daly, S. Grimaldi and H. H. Bui, "Explicit incompressible SPH algorithm for free-surface flow modelling: A comparison with weakly compressible schemes," *Advances in Water Resources,* vol. 97, pp. 156-167, 2016.

[30] S. Yeylaghi, B. Moa, P. Oshkai, B. Buckham and C. Crawford, "ISPH modelling of an oscillating wave surge converter using an OpenMP-based parallel approach," *Journal of Ocean Engineering and Marine Energy,* vol. 2, pp. 301-312, 2016.

[31] H. Jiang, Y. You, Z. Hu, X. Zheng and A. Ma, "Comparative study on violent sloshing withwater jet flows by using the ISPH method," *Water (Switzerland),* vol. 11, p. 2590, 2019.

[32] S. Adami, X. Y. Hu and N. A. Adams, "A generalized wall boundary condition for smoothed particle hydrodynamics," *Journal of Computational Physics,* vol. 231, no. 21, pp. 7057-7075, 2012.

[33] DualSPHysics, *DualSPHysics v5.0 Guide,* 2020.

[34] S. Shao and E. Y. Lo, "Incompressible SPH method for simulating Newtonian and non-Newtonian flows with a free surface," *Advances in Water Resources,* vol. 26, no. 7, pp. 787-800, 2003.

[35] B. J. Vickery and A. G. Davenport, "An investigation of the behaviour in wind of the proposed centrepoint tower," Research Report BLWT-1-70, Sydney, Australia, 1970.

[36] J. J. Monaghan, "On the Problem of Penetration in Particle Methods," *Journal of Computational Physics,* vol. 82, pp. 1-15, 1989.

[37] M. J. Tait, A. A. El Damatty and N. Isyumov, "An investigation of tuned liquid dampers equipped with damping screens under 2D excitation," *Earthquake Engineering and Structural Dynamics,* vol. 34, no. 7, pp. 719-735, 2005.

Table 3.1: Structure Generalized Properties

Property		**Random**	**Transient**
Generalized Mass	M_s (kg)	4480	4040
Generalized Stiffness	K_s (N/m)	55100	49656
Generalized Damping	C_s (Ns/m)	31	14
Natural Frequency	f_s (Hz)	0.558	0.558

Table 3.2: Tuned Liquid Damper Properties

Property		**Value**
Tank Length	L (mm)	966
Tank Height	H (mm)	420
Tank Width	b (mm)	966
Fluid Depth	h (mm)	119
Screen Loss Coefficient	C_l	2.16
Screen Locations	X_{screen}/L	0.40 0.60

Table 3.3: Structural Displacement Response from Random Excitation (RMS and Peak)

σ_F/K_s	σ_X (mm)			$\widehat{X}$ (mm)		
	Exp.	**Model**	**%Diff**	**Exp.**	**Model**	**% Diff**
0.0030	12.8	12.4	3.52%	54.4	54.2	0.29%
0.0040	18.7	18.0	3.96%	80.7	79.1	2.03%
0.0055	27.1	28.3	-4.35%	115.6	129.2	-11.8%

Table 3.4: Structural Acceleration Response from Random Excitation (RMS and Peak)

σ_F/K_s	$\sigma_{\ddot{X}}$ (milli-g)			$\hat{\ddot{X}}$ (milli-g)		
	Exp.	**Model**	**%Diff**	**Exp.**	**Model**	**% Diff**
0.0030	16.0	15.6	2.81%	71.5	69.1	3.43%
0.0040	23.0	22.5	2.09%	102.0	102.4	-0.40%
0.0055	33.1	35.6	-7.61%	144.1	160.7	-11.5%

Table 3.5: Effective Damping of Structure-TLD System

σ_F/K_s	ζ_{eff} (%)		
	Exp.	**Model**	**% Diff**
0.0030	2.39	2.57	-7.53%
0.0040	2.05	2.22	-8.29%
0.0055	1.79	1.66	7.26%

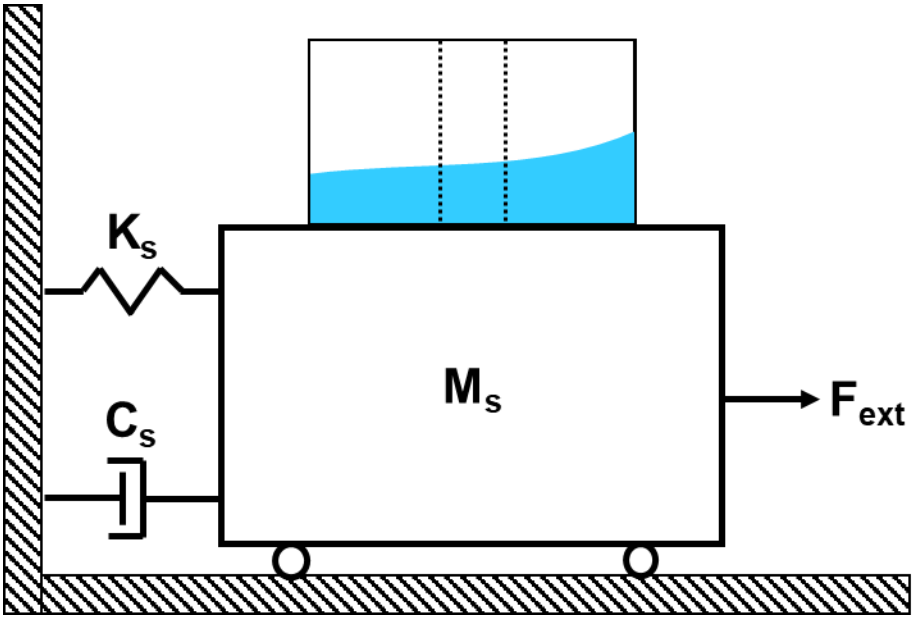

Figure 3.1: Structure – Tuned Liquid Damper System Schematic.

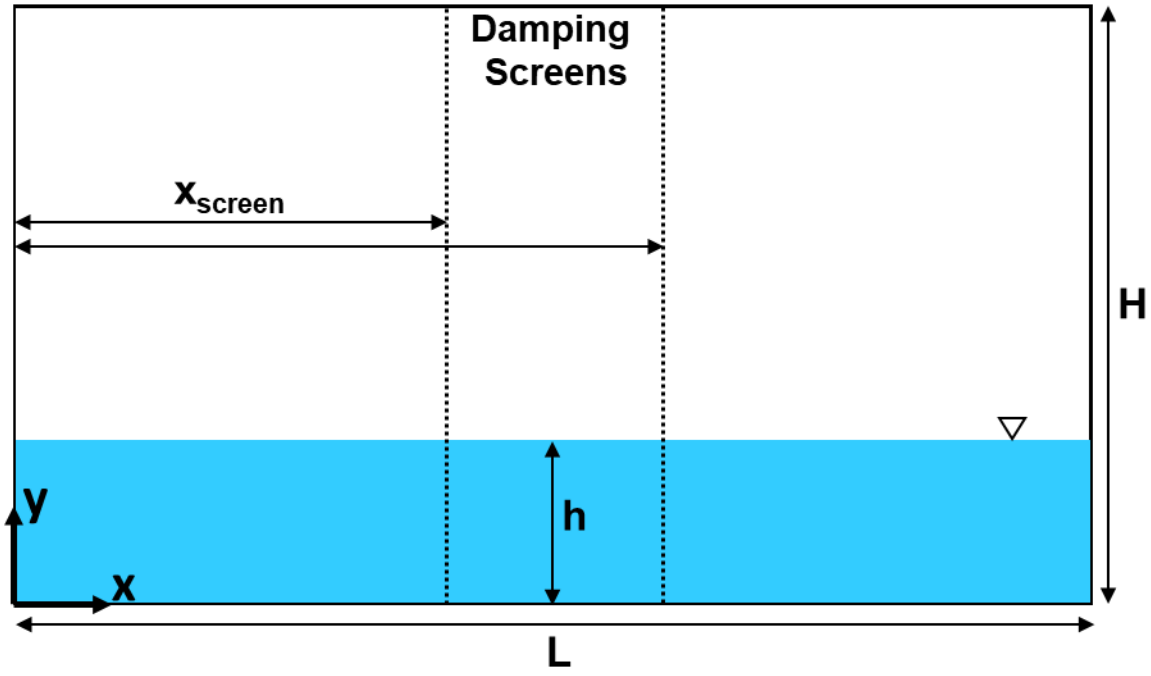

Figure 3.2: TLD with Damping Screens SPH Domain Definition.

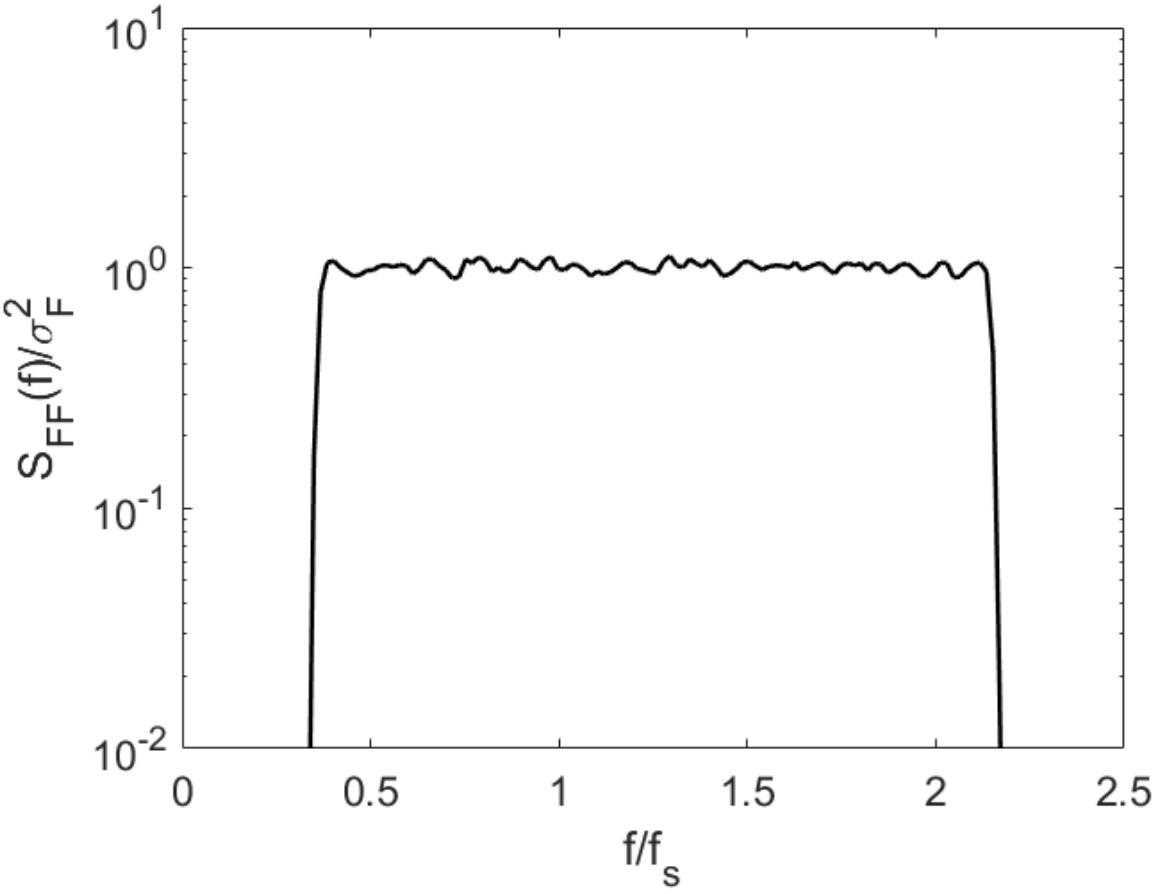

Figure 3.3: Power spectrum of band-limited white noise excitation signal (normalized).

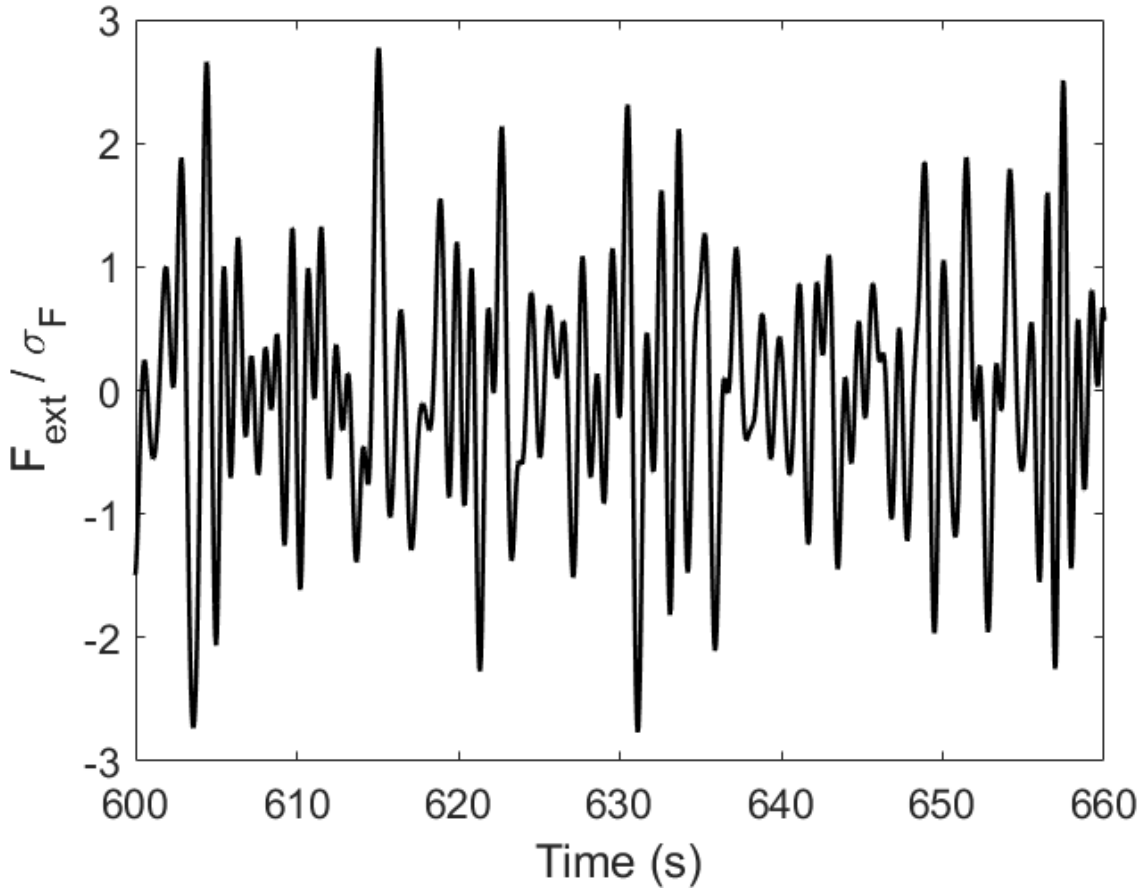

Figure 3.4: Example segment of random white noise excitation signal.

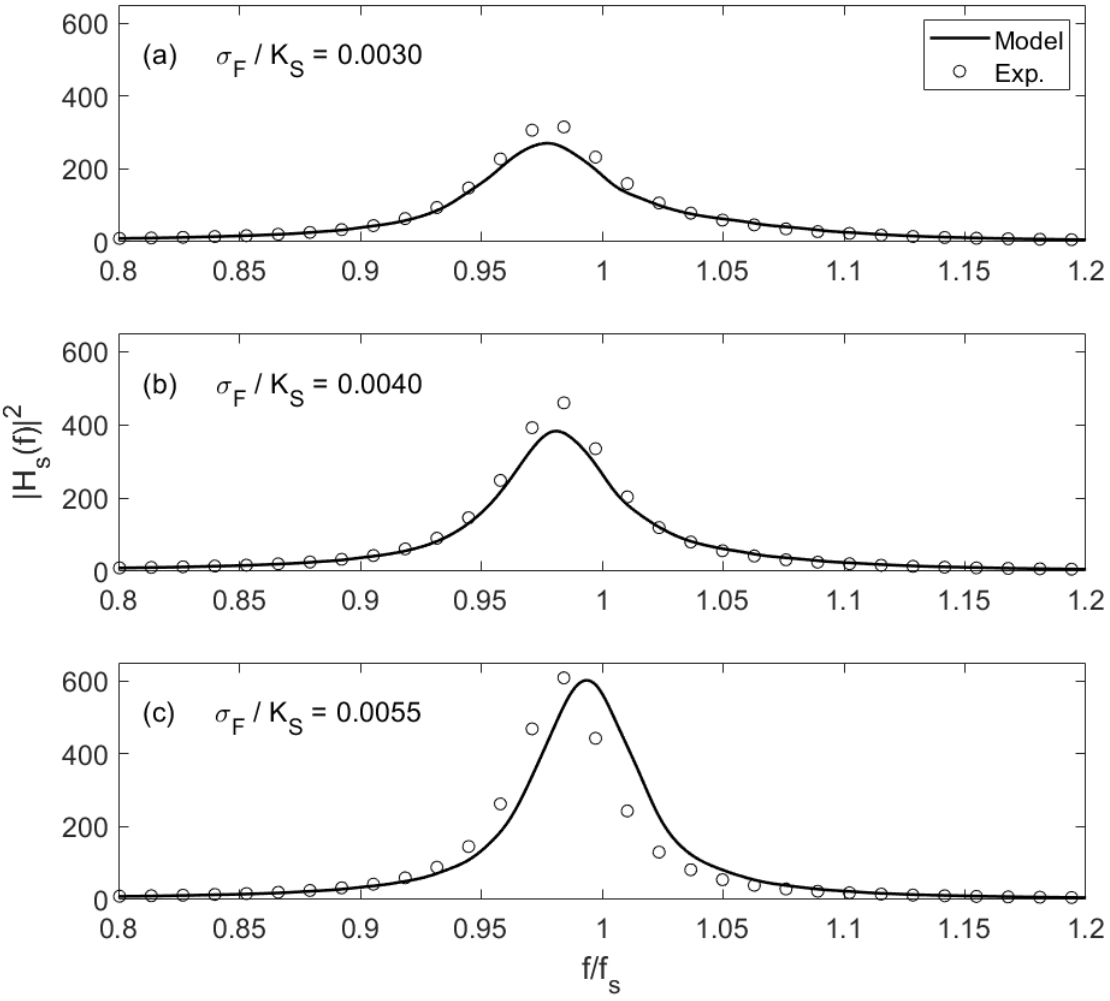

Figure 3.5: Model vs experimental structure MAF for band-limited white noise excitation.

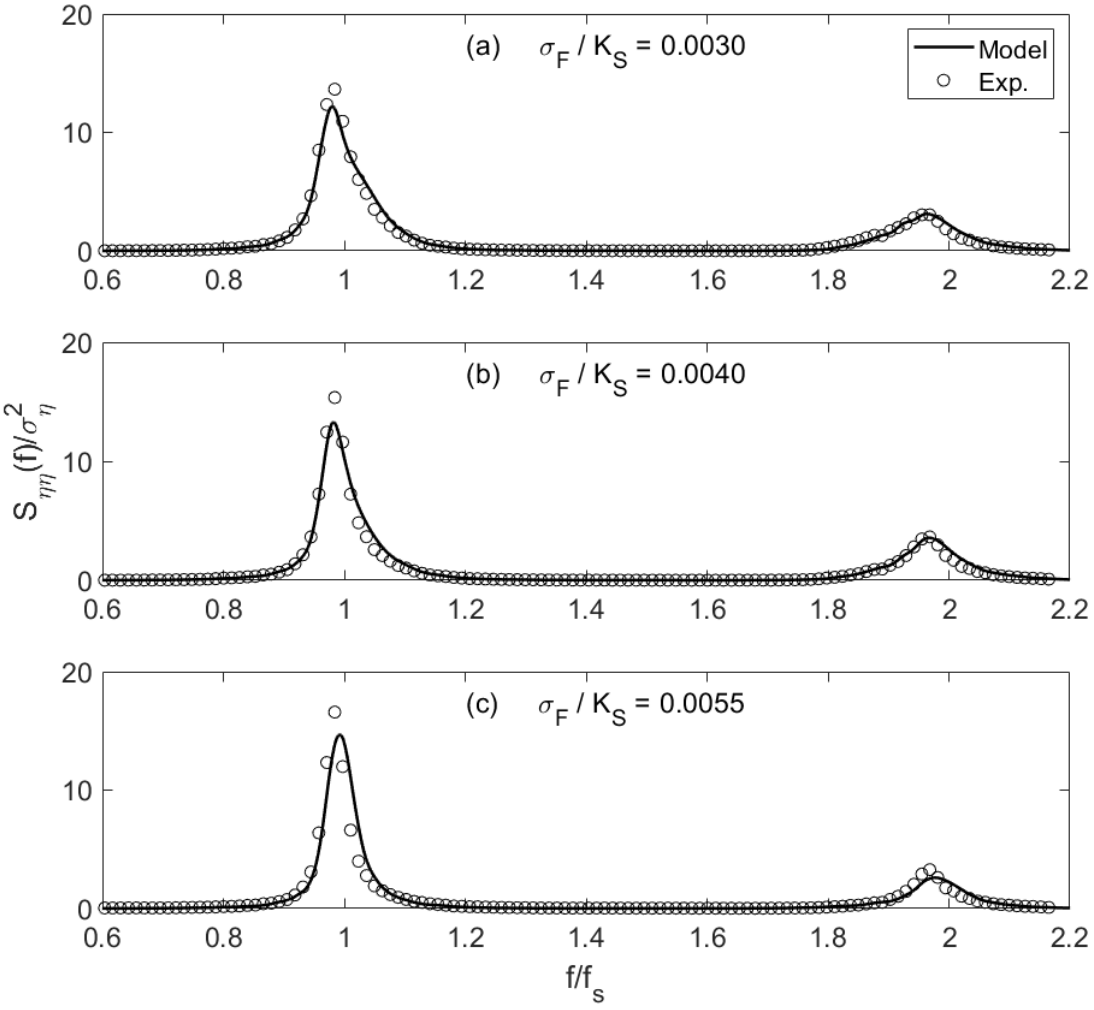

Figure 3.6: Model vs experimental normalized wave height spectra for band-limited white noise excitation.

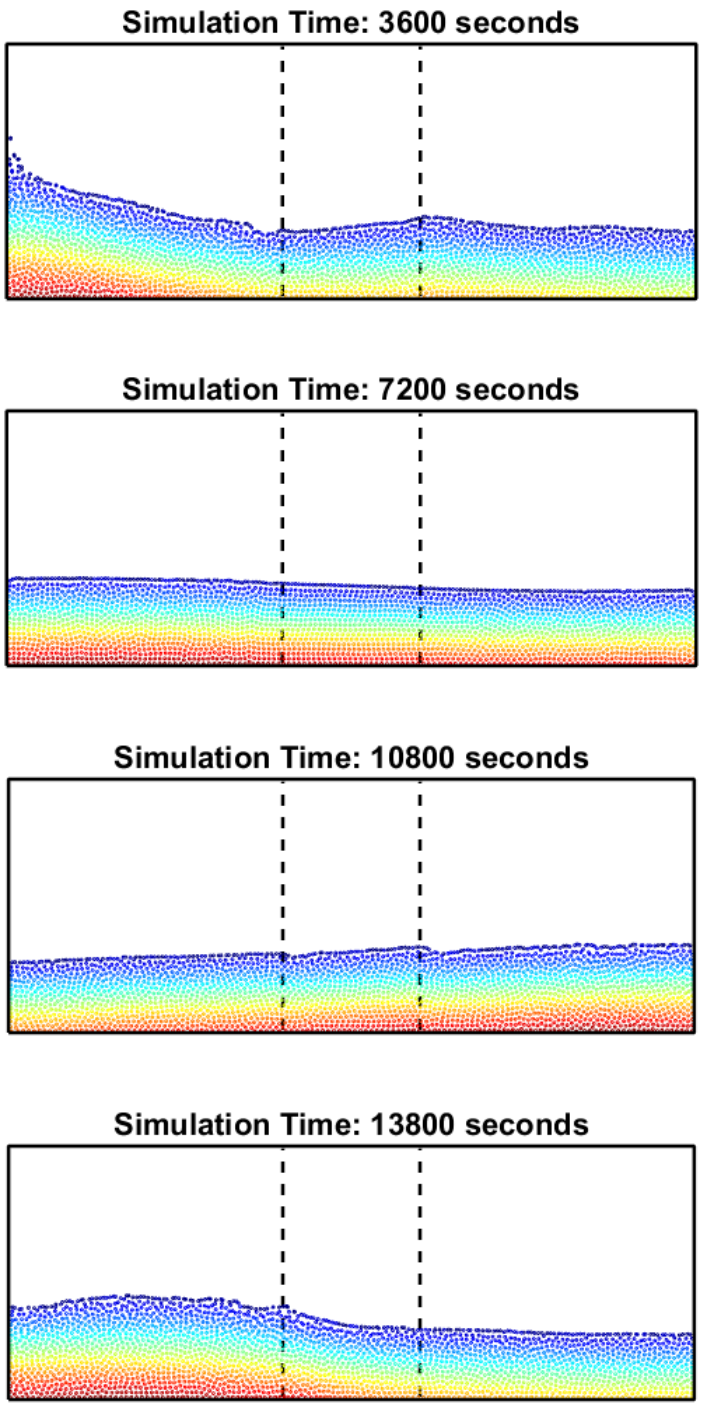

Figure 3.7: SPH wave profiles at various time instants for $\sigma_F/K_s = 0.0030$. Particles are colored by pressure value.

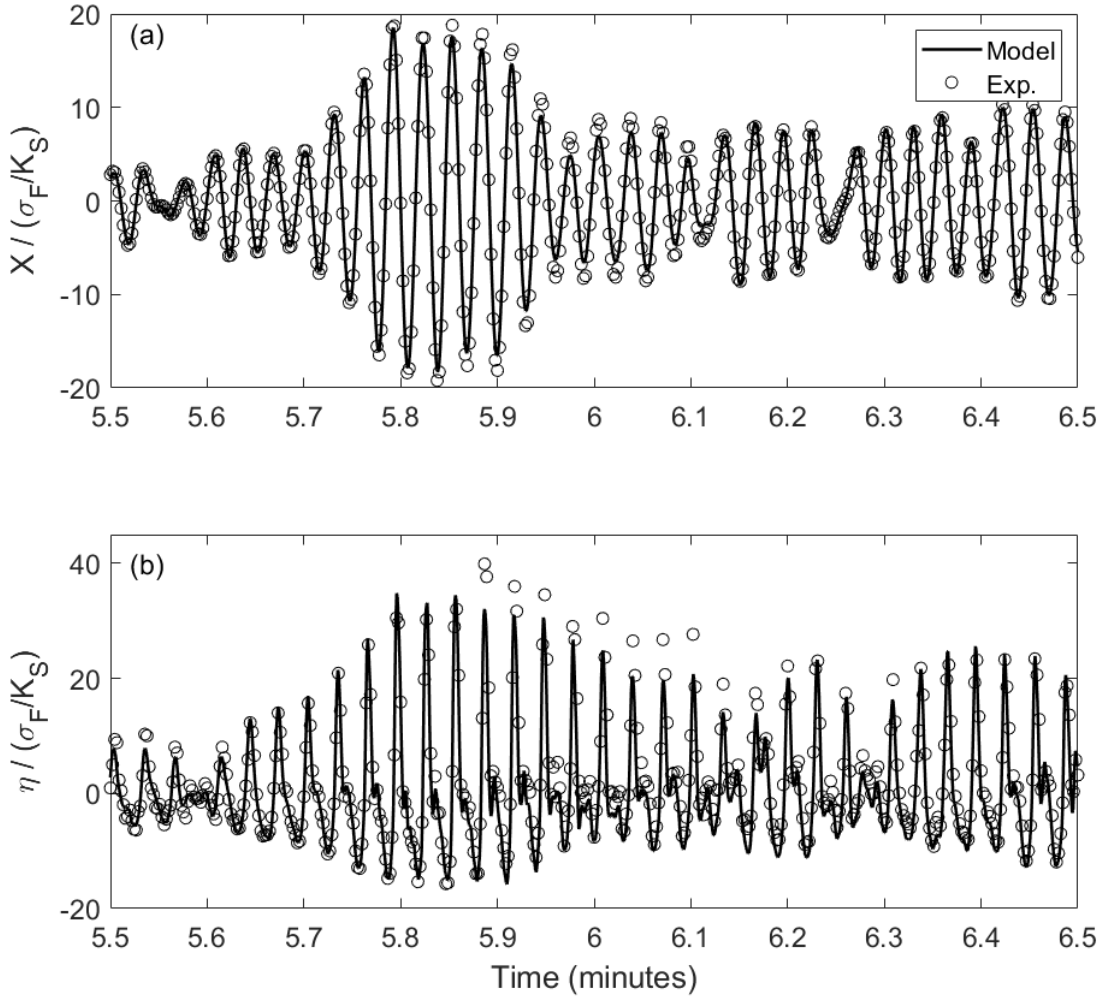

Figure 3.8: Model vs experimental response history for σ_F/K_s = 0.0030 near start of simulation.

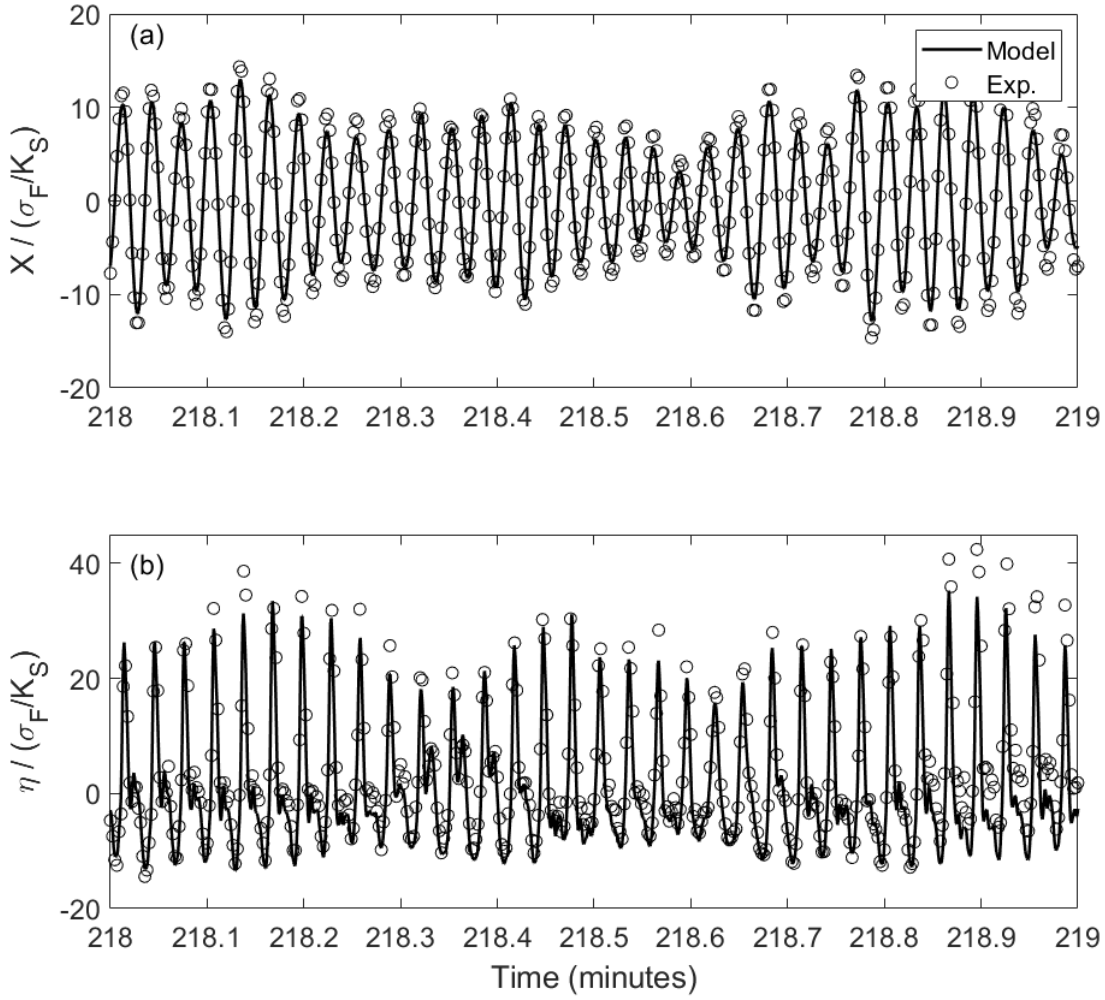

Figure 3.9: Model vs experimental response history for $\sigma_F/K_s = 0.0030$ near end of simulation.

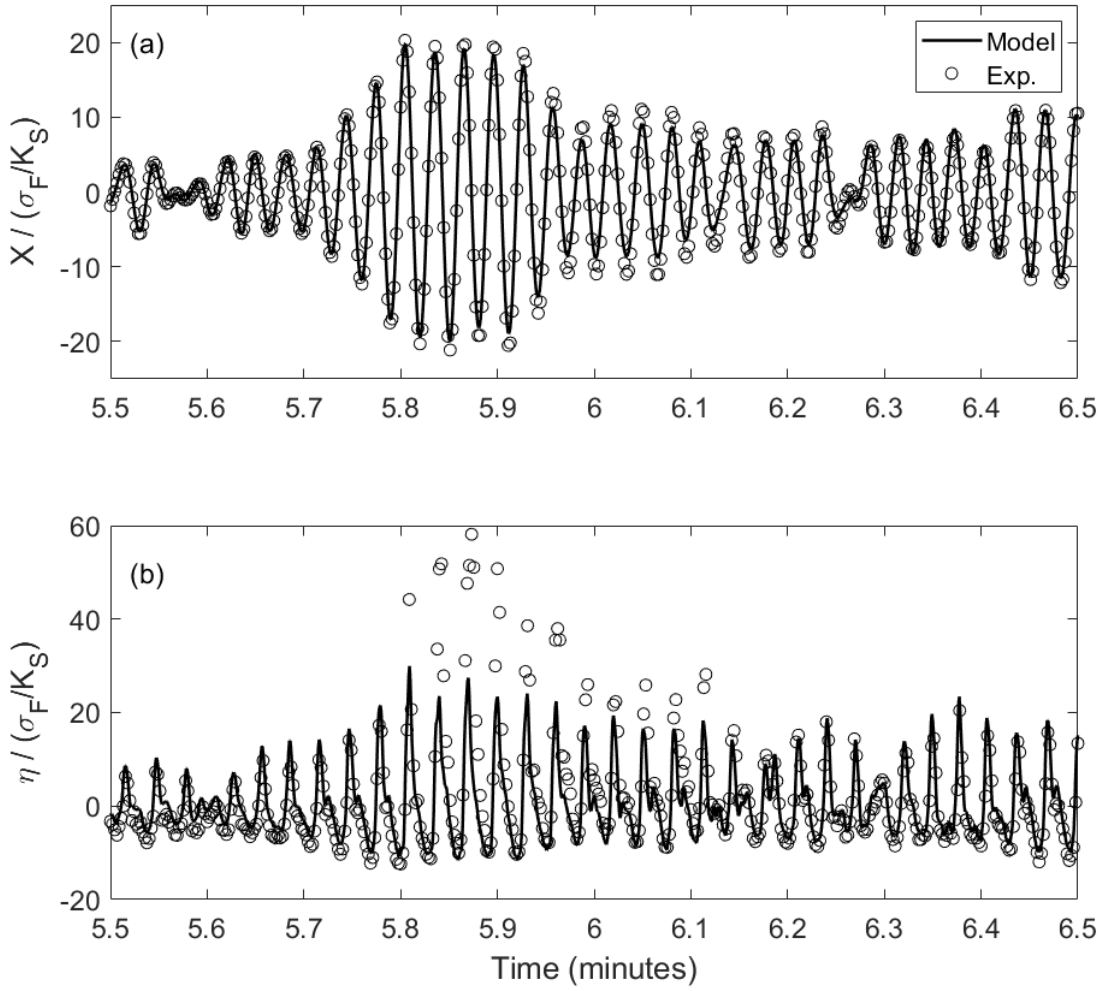

Figure 3.10: Model vs experimental response history for σ_F/K_s = 0.0055 near start of simulation.

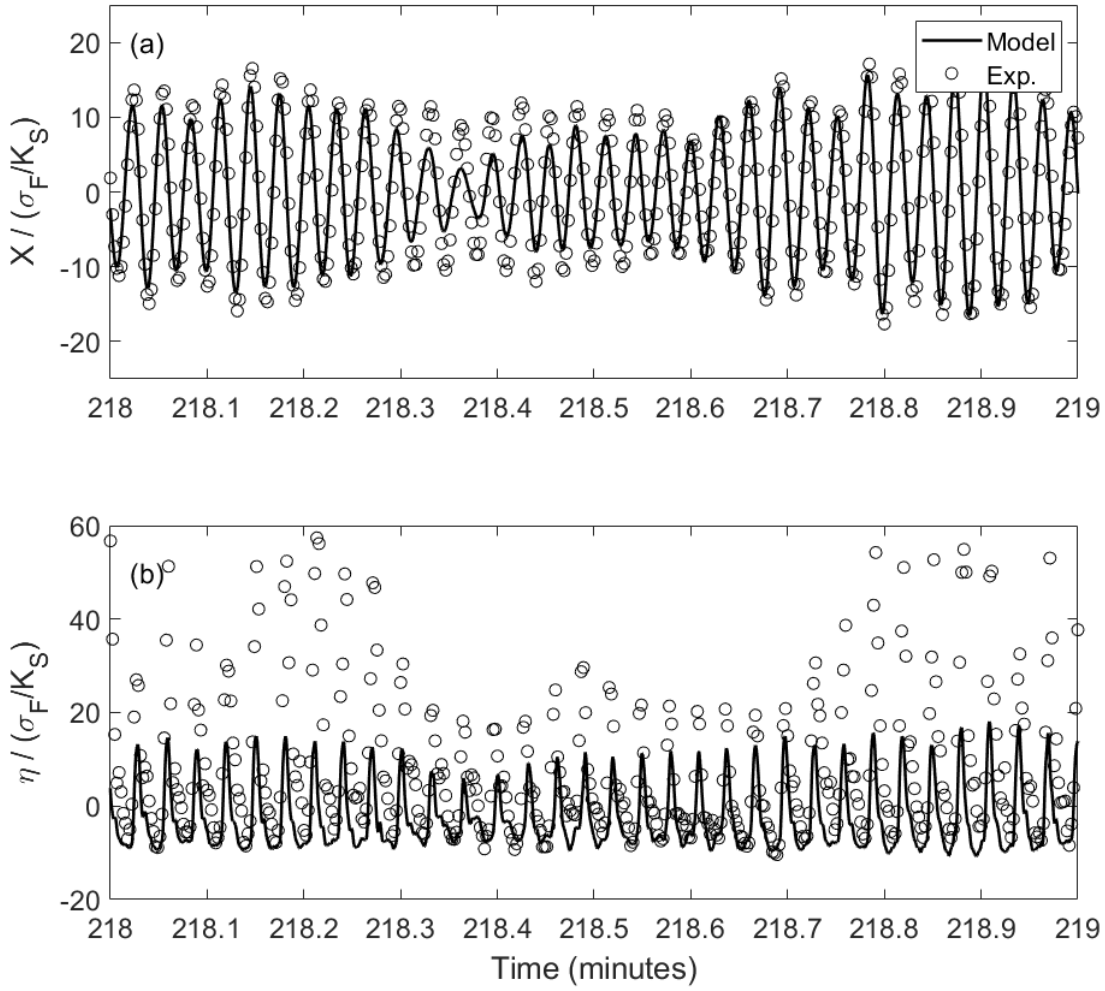

Figure 3.11: Model vs experimental response history for σ_F/K_s = 0.0055 near end of simulation.

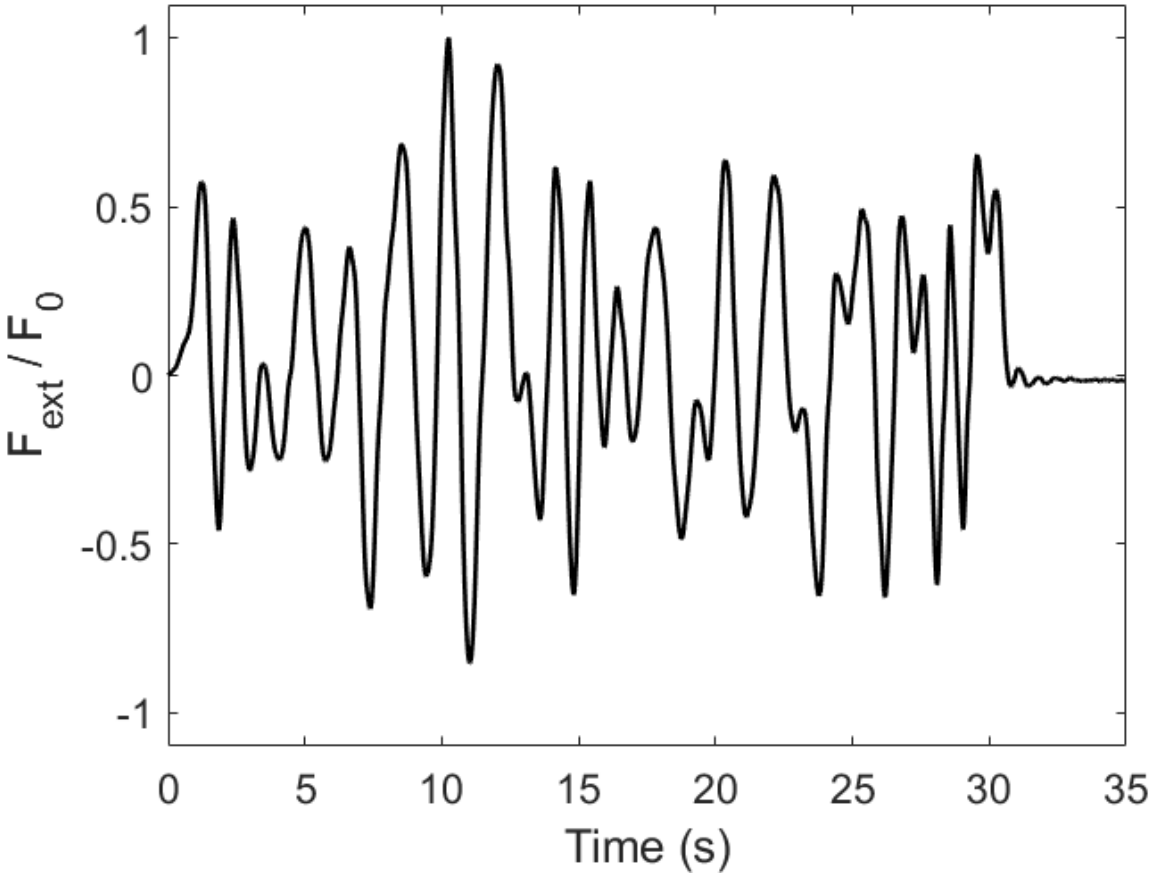

Figure 3.12: Transient excitation force signal (normalized).

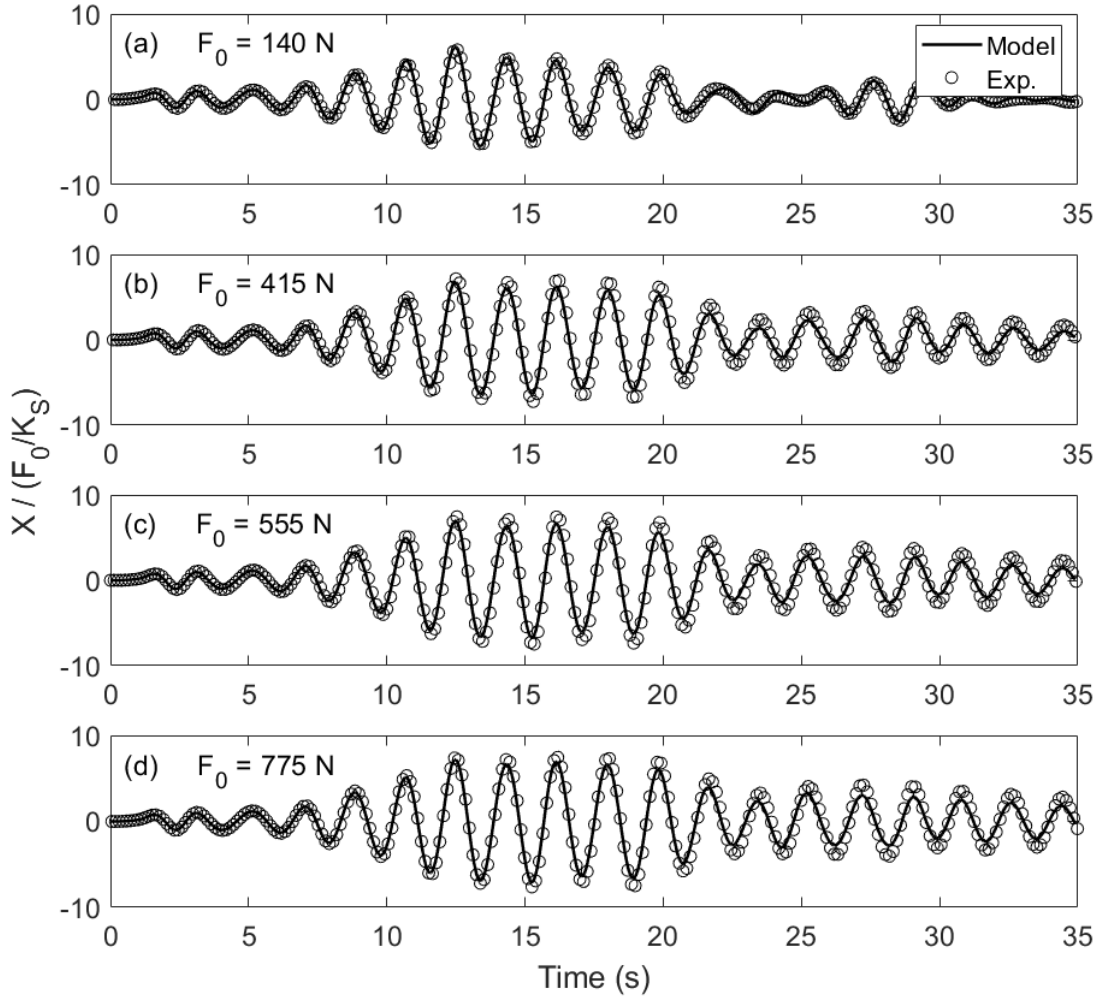

Figure 3.13: Model vs experimental structure response for different transient excitation amplitudes.

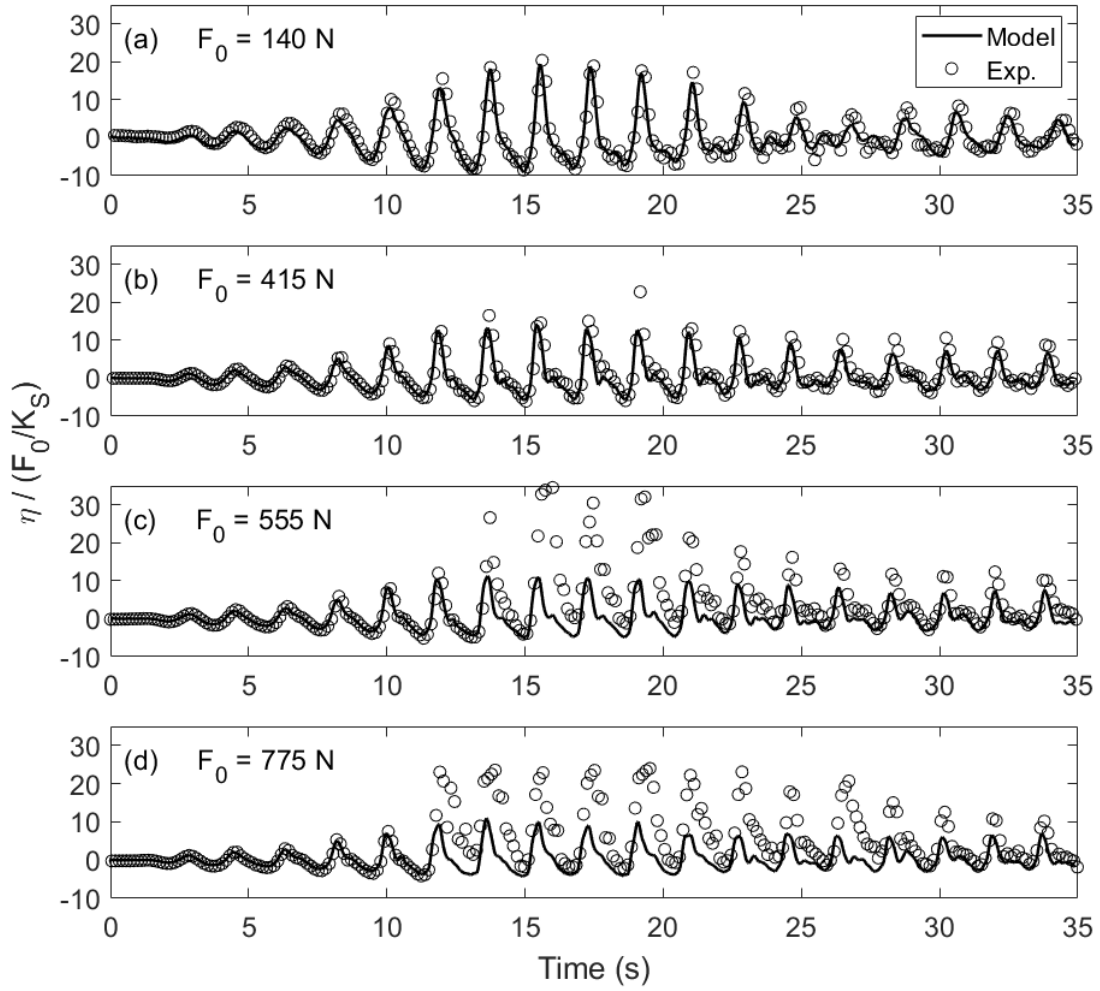

Figure 3.14: Model vs experimental wave height response for different transient excitation amplitudes.

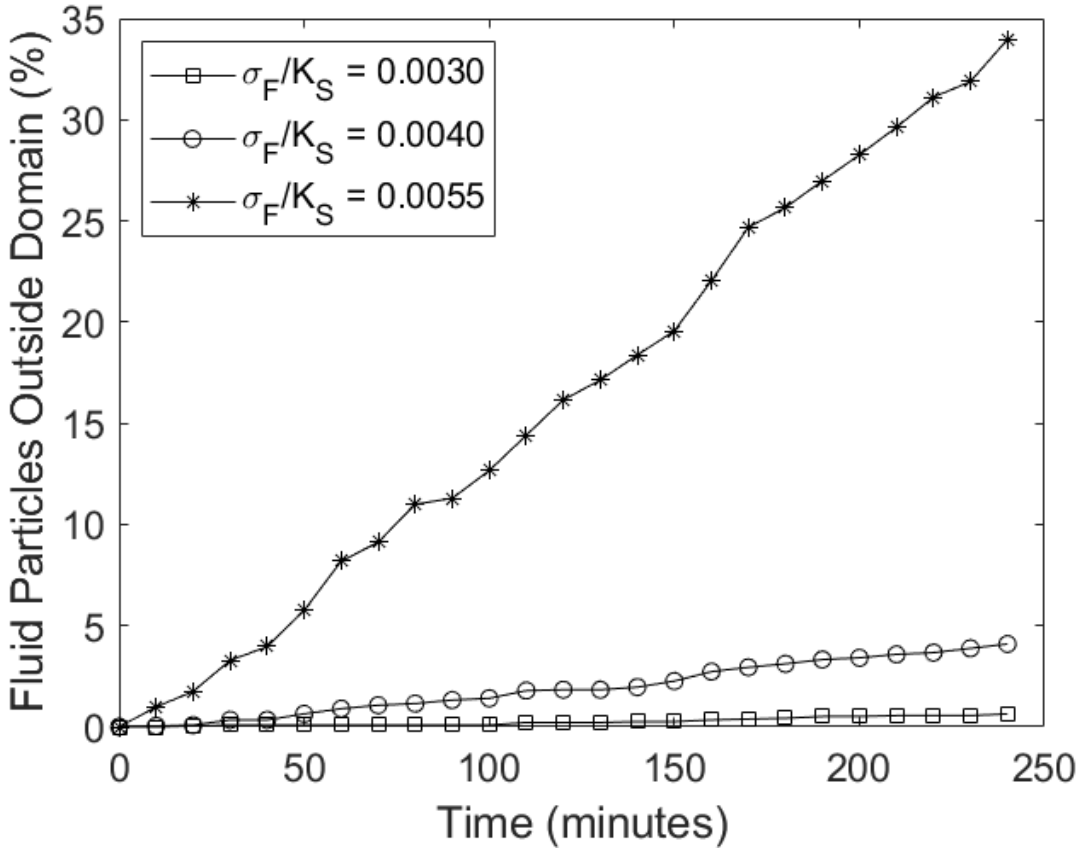

Figure 3.15: SPH fluid particles outside domain vs simulation time.

Chapter 4: Mitigating SPH fluid particle loss for multiple-hour duration large amplitude sloshing simulation

Abstract

The smoothed particle hydrodynamics (SPH) method is attractive for modelling large amplitude sloshing liquid simulations due to its ability to capture complex free surface phenomena. Various methods exist to implement solid boundary conditions in SPH. It is commonly accepted that a small percentage of SPH fluid particles may penetrate the solid boundaries and escape the domain. The impact of this on simulation results is minor for the typical short durations SPH is applied to. In some cases, it is necessary to carry out a long duration simulation to obtain a statistically significant result. An example of this is studying the response of a structure-tuned liquid damper (TLD) system subject to random wind loading. For simulations of multiple-hour duration, the minor loss of fluid particles through solid boundaries can become significant. An explicit incompressible SPH model is used to study the response of a structure-TLD system subject to a long duration random wind load excitation. Loss of fluid particles is observed in the simulations when the sloshing response is large and splashing occurs at the tank walls. Four modifications to the solid boundary implementation are investigated: 1) increasing the number of boundary particle layers, 2) reducing the kernel function radius for calculating boundary particle velocities as implemented by Muta et al. [1], 3) introducing a buffer zone to neglect certain fluid-boundary particle interactions as proposed by Green [2], and 4) a conditional test which returns fluid particles outside the boundaries to inside the tank. The modified boundary conditions improve the containment of fluid particles over the course of the simulations. This significantly improves agreement with experimental data for a structure-TLD system compared to the base simulation.

KEYWORDS: smoothed particle hydrodynamics, solid boundary conditions, sloshing, tuned liquid damper.

4.1 Introduction

The development of numerical models for sloshing liquid in tanks has seen significant work in recent years. The nonlinearity of sloshing fluids undergoing external excitation can be complicated to capture numerically, resulting in the need for experimental testing. However, increases in computational power have made numerical modelling attractive and efficient. When simulating a sloshing liquid in a tank, there are a few physical quantities of particular interest. Accurately capturing the free surface wave heights is important for selecting tank dimensions and freeboard between the still water surface and tank ceiling. Fluid-induced pressures and forces acting on tank boundaries are needed for structural design and are used in cases where the tank controls the motion of a structure, such as an antiroll tank on a large vessel, or a tuned liquid damper (TLD) in a tall building.

The smoothed particle hydrodynamics (SPH) method has been applied in recent years to simulate problems involving a free surface. The Lagrangian formulation of SPH is particularly attractive for cases with large deformation of the free surface as it is not necessary to re-mesh the domain or use computationally expensive free surface tracking methods. SPH was originally developed for simulating astrophysics problems by Gingold and Monaghan [3] and Lucy [4]. Monaghan [5] proposed application of the SPH method to free surface problems by introducing solid boundaries and controlling the fluid compressibility by relating density and pressure with a stiff equation of state. This is commonly denoted as the weakly compressible SPH (WCSPH) method. An incompressible SPH (ISPH) scheme was proposed by Cummins and Rudman [6]. Violeau and Rogers [7] provide a thorough review of SPH applications for free surface flows.

SPH has been applied to sloshing liquid in tanks in various studies. Delorme et al. [8] compared tank wall pressures obtained from SPH to experimental data for sloshing liquid in a rigid tank. The sloshing response of shallow TLDs was investigated by Bulian et al. [9] and Marsh et al. [10] using SPH. Cao et al. [11] investigated the response of sloshing liquid in a tank both with and without a vertical baffle. The response of sloshing liquid in a tank subjected to earthquake excitation was investigated by Kusic et al. [12]. Green et al.

[13, 14] simulated the 2D and 3D liquid sloshing response in various tanks for multiple-minute duration simulations. A tuned liquid damper with damping screens explicitly modelled using SPH particles was investigated by Kashani et al. [15]. McNamara et al. [16] studied a TLD with damping screens modelled using ghost particles based on the Morison equation. McNamara and Tait [17] coupled the SPH model to a structure to investigate the system response for a 4-hour simulation.

Accurate description of solid boundaries is important for simulating sloshing liquid in tanks. Many methods for implementing solid boundary conditions in SPH have been proposed. These methods are generally divided into three main groups: ghost/dummy particle boundaries, applied force boundaries, and semi-analytical boundaries. Ghost/dummy particle boundaries place multiple layers of solid boundary particles outside the fluid domain. The pressure and velocity of these particles is solved based on the fluid response. The pressure of the boundary particles works to contain the fluid particles, and it is also possible to capture a free-slip or no-slip velocity condition. Different implementations of ghost/dummy particles have been presented, such as Marrone et al. [18], Adami et al. [19] and English et al. [20]. These boundary particles have the benefit of ensuring a complete fluid particle neighbourhood, which addresses kernel truncation issues for fluid particles near the solid boundaries. Applied force boundaries were first proposed by Monaghan [5]. These boundary conditions work by using a repulsive force that only acts on fluid particles that are close to solid boundaries. This method is computationally efficient; however, it can lead to unphysical gaps between the solid boundary and fluid particles. The issue of truncated fluid particle neighbourhoods near tank boundaries is also not accounted for. Semi-analytical boundary conditions, for example Leroy et al. [21], apply the boundary conditions by modifying the SPH operators and governing equations, which removes the need to add layers of boundary particles. This method addresses the issue of truncated particle neighbourhoods directly, however, the implementation can be complicated depending on the geometry of the boundaries.

Despite significant research into solid boundary treatment in SPH, it is commonly accepted that some fluid particles may penetrate the boundaries throughout a simulation. Green et al. [13, 14, 2] found good agreement between SPH and experimental results for 5-minute duration sloshing simulations in a WCSPH code using the boundary particles proposed by Adami et al. [19], however, some minor loss of fluid particles was reported by Green [2]. For certain applications, such as studying a structure-TLD system subject to random wind loading, it is necessary to simulate a long duration response history to achieve a statistically significant result. McNamara and Tait [17] completed 4-hour duration simulations of a structure-TLD system undergoing large amplitude excitations, where the boundary particles from Adami et al. [19] were applied to an explicit ISPH code. Up to 35% of the fluid particles were lost through the boundaries throughout the simulations. This effect was found to become more significant as the amplitude of excitation was increased.

The focus of this study is on mitigating the loss of fluid particles when using SPH for long duration simulations. An explicit ISPH code developed by the authors is used for the simulations. Solid boundary particles are implemented based on Adami et al. [19] with a free-slip boundary velocity condition. Four methods to mitigate loss of fluid particles are investigated, specifically:

1) Increasing the number of boundary particle layers beyond those required for complete fluid particle neighbourhoods,
2) Reducing the kernel support radius for calculation of boundary particle velocities to better represent the velocity nearest to the tank walls, as implemented by Muta et al. [1],
3) Addition of a buffer zone where certain fluid-boundary particle interactions are neglected, as proposed by Green [2], and
4) A conditional test where fluid particles outside the domain are simply returned to inside the tank boundaries.

The methods are compared by simulating the response of a structure-TLD system subject to a 3.75-hour duration band limited white noise excitation signal representative of

wind loading. The performance of the different methods at containing the fluid particles is assessed. The impact of modifying the boundary conditions on the structure-TLD response is also investigated.

4.2 Incompressible Smoothed Particle Hydrodynamics Model

This section details the SPH model code used in this study to simulate the response of a structure-TLD system. A schematic of the system is shown in Figure 4.1. The structure is represented by a mass-spring-dashpot system. The dynamic response of the structure is governed by the equation of motion:

$$M_s\ddot{X} + C_s\dot{X} + K_sX = F_{ext} + F_{TLD} \quad \textbf{(4.1)}$$

where M_s is the generalized mass, C_s is the generalized damping, K_s is the generalized stiffness, X is the structure displacement (an overdot represents differentiation with respect to time), F_{ext} is the externally applied excitation, and F_{TLD} is the force of sloshing water from the TLD.

The code was developed using an explicit incompressible SPH implementation. The simulation is limited to two dimensions. The domain is discretized using SPH particles with an initial spacing equal to *dp*. Three types of particles are used to represent the fluid, solid boundaries, and TLD damping screens, as shown in Figure 4.2. A substructuring method is applied to solve the structure-TLD system response. Equation **(4.1)** is solved in time using the 4th order Runge-Kutta-Gill method. The resulting structure acceleration is applied to the TLD in the SPH model, which is solved to find the TLD response. The force generated by the sloshing water F_{TLD} is then applied back to the structure in the next timestep. Since the TLD tank is assumed rigid and the timestep is small, this method appropriately captures the fluid-structure interaction, rather than solving for the coupled system response directly.

4.2.1 Fluid Response

The fluid response is governed by the incompressible Lagrangian formulation of the Navier-Stokes equations, represented by the continuity and momentum equations:

$$\frac{D\rho}{Dt} + \rho\nabla\mathbf{u} = 0 \tag{4.2}$$

$$\frac{\mathrm{D}\mathbf{u}}{Dt} = -\frac{1}{\rho}\nabla P + v\nabla^2\mathbf{u} + \mathbf{g} \tag{4.3}$$

where *D/Dt* is the Lagrangian derivative, ρ is the fluid density (1000 kg/m^3 for water), **u** is the velocity vector, *P* is the fluid pressure, v is the kinematic viscosity (1x10^{-6} m^2/s for water), and **g** is a vector of external body forces, including gravity and applied excitation. **Bold** symbols denote a vector quantity in this notation.

In SPH a smoothing kernel function is used to calculate the properties of each particle based on contributions from neighbouring particles. The fifth order Wendland kernel function is used in this study [22]:

$$W(q) = W_c \begin{cases} (1+2q)\left(1-\frac{q}{2}\right)^4 & 0 \le q \le 2 \\ 0 & q > 2 \end{cases} \tag{4.4}$$

where $q = \frac{|\boldsymbol{r_i} - \boldsymbol{r_j}|}{h_{ker}}$, $W_c = \frac{7}{\pi h_{ker}^2}$ for 2D simulations, and h_{ker} is the smoothing length which is a function of the initial particle spacing *dp*. In this study h_{ker} = 1.4*dp*.

The terms in the momentum equation are discretized using SPH operators as [23, 6]:

$$\frac{1}{\rho_i}\nabla P_i = \sum_{j=1}^{N} m_j \left(\frac{P_j}{\rho_j^2} + \frac{P_i}{\rho_i^2}\right)\nabla_j W_{ij} \tag{4.5}$$

$$v\nabla^2\mathbf{u_i} = v\rho_i \sum_{j=1}^{N}\left(\frac{8m_j}{(\rho_i+\rho_j)^2}\frac{(\mathbf{u_i}-\mathbf{u_j})\cdot\boldsymbol{r_{ij}}}{r_{ij}^2+\eta^2}\nabla_j W_{ij}\right) \tag{4.6}$$

where $m_j = \rho(dp)^{ndim}$ is the mass of each particle (*ndim* = 2 for a 2D simulation), $\boldsymbol{r_{ij}} = \boldsymbol{r_i} - \boldsymbol{r_j}$, $r_{ij} = |\boldsymbol{r_{ij}}|$, and $\eta = 0.001h_{ker}$ is a small value to ensure a nonzero denominator.

All summations include fluid particles and boundary particles within the neighbourhood of the particle of interest.

Figure 4.3(a) shows the neighbourhood of various fluid particles in the SPH domain, where the circle surrounding a particle indicates the kernel support radius q_{max} = 2. The fluid particles are ensured to have a complete neighbourhood by placing multiple rows of boundary particles around the domain which are used in the kernel function summations. The exception to this is fluid particles near the free surface, where the neighbourhood is truncated. Boundary particles are further discussed in Section 4.2.2.

The governing equations are integrated in time according to the projection method for incompressible SPH from Cummins and Rudman [6]. An intermediate fluid velocity and position are calculated by including only the viscous and body forces from equation **(4.3)**:

$$\boldsymbol{u}^* = \boldsymbol{u}(t) + \left(v\nabla^2\boldsymbol{u} + \boldsymbol{g} + \ddot{\boldsymbol{X}} + \boldsymbol{F}_{\boldsymbol{screen}}\right)\Delta t \tag{4.7}$$

$$\boldsymbol{r}^* = \boldsymbol{r}(t) + \boldsymbol{u}^*\Delta t \tag{4.8}$$

where $v\nabla^2\mathbf{u}$ represents the viscous interaction force, $\boldsymbol{g}$ is gravitational acceleration, $\ddot{\boldsymbol{X}}$ is the external acceleration applied to the fluid, and $\mathbf{F}_{\boldsymbol{screen}}$ is a screen force from TLD damping screens which is described in Section 4.2.4.

From Nomeritae et al. [24], the intermediate fluid velocity and position are then used to calculate an intermediate fluid density by discretizing equation **(4.2)**:

$$\rho_i^* = \rho - \Delta t \sum_{j=1}^{N} m_j \left(\mathbf{u}_\mathbf{i}^* - \mathbf{u}_\mathbf{j}^*\right) \cdot \nabla_j W_{ij} \tag{4.9}$$

The intermediate particle values are used to solve for the fluid pressure with an explicit approach. The pressure Poisson equation (PPE) combines the density-invariant and divergence-free implementations for incompressible SPH based on Jiang et al. [25]:

$$\boldsymbol{\nabla}.\left(\frac{\boldsymbol{\nabla}P}{\rho^*}\right) = \alpha\frac{\rho_0 - \rho^*}{\rho_0 \Delta \mathrm{t}^2} + (1-\alpha)\frac{\boldsymbol{\nabla}.\boldsymbol{u}^*}{\Delta t} \tag{4.10}$$

where α is a blending parameter equal to 0.01 in this study. The PPE is discretized as [26]:

$$\sum_{j=1}^{N} A_{ij}P_{ij} = (1-\alpha)\left(\frac{-1}{\Delta t}\right)\sum_{j=1}^{N} B_{ij} + \alpha\frac{\rho_0 - \rho^*}{\Delta \mathrm{t}^2}$$
$$A_{ij} = \frac{8m_j}{\left(\rho_i^* + \rho_j^*\right)^2}\frac{\boldsymbol{r_{ij}}.\boldsymbol{\nabla_i}W_{ij}}{r_{ij}^2 + \eta^2}, B_{ij} = \frac{m_j}{\rho_j^*}(\boldsymbol{u_j^*} - \boldsymbol{u_i^*})\boldsymbol{\nabla_j}W_{ij} \tag{4.11}$$

Assuming that the timestep is small, the pressure of each particle at time $t+\Delta t$ is calculated based on the pressure of neighbouring particles at time t, and the PPE is rearranged resulting in the explicit expression:

$$P_i(t+\Delta t) = \frac{\sum_{j=1}^{N} A_{ij}P_j(t) + (1-\alpha)\left(\frac{-1}{\Delta t}\right)\sum_{j=1}^{N} B_{ij} + \alpha\frac{\rho_0 - \rho^*}{\Delta \mathrm{t}^2}}{\sum_{j=1}^{N} A_{ij}} \tag{4.12}$$

If a particle pressure calculated by equation **(4.12)** is negative, it is set to zero since negative pressures are not physically possible in the simulations considered [24].

To identify the free surface particles and enforce the dynamic boundary condition of $P = 0$, a numerical density is calculated for each fluid particle [26]:

$$\rho_{fi} = \sum_{j=1}^{N} m_j W_{ij} \tag{4.13}$$

As shown in Figure 4.3(a), particles near the free surface will not have complete neighbourhoods, which results in a calculated density less than the initial fluid density ρ. Particles with densities calculated by equation **(4.13)** to be less than 90% of the initial fluid density are considered to be free surface particles, and their pressure is set to zero at each timestep. The density calculated by equation **(4.13)** is only used for identifying the free surface.

Once the pressure has been calculated, particle velocities, positions, and densities are updated to enforce incompressibility of the fluid. The velocity and position of the particles at time $t+\Delta t$ are calculated as:

$$\boldsymbol{u}(t+\Delta t) = \boldsymbol{u}^* - \left(\frac{1}{\rho^*}\boldsymbol{\nabla} P\right)\Delta t \tag{4.14}$$

$$\boldsymbol{r}(t+\Delta t) = \boldsymbol{r}(t) + \left(\frac{\boldsymbol{u}(t+\Delta t) + \boldsymbol{u}(t)}{2}\right)\Delta t \tag{4.15}$$

The fluid density is re-set at the end of each timestep to the initial value ρ [24].

4.2.2 Solid Boundary Particles

The solid boundaries of the TLD tank are represented in this study using multiple layers of fixed dummy particles based on the methodology of Adami et al. [19]. The boundary particles not only work to contain the fluid particles within the tank, but they also ensure complete fluid particle neighbourhoods (see Figure 4.3(a)) and can be made to represent either a no-slip or a free-slip boundary velocity condition.

The number of boundary particle layers (*nbl*) is determined to provide a complete fluid particle neighbourhood: $nbl = q_{max}h_{ker}/dp$, where q_{max} is the kernel support radius. The calculated value of *nbl* is rounded up to the nearest integer and is dependent on the simulation parameters. For this study, q_{max} = 2.0 for the 5th order Wendland kernel and h_{ker}/dp = 1.4. Thus, 2.8 layers of boundary particles are necessary, which is rounded up to 3 layers. These particles are created at the start of the simulation with the same initial spacing as the fluid particles, *dp*. The boundary particles have the same mass and density as the fluid particles. Due to the incompressible SPH formulation, the boundary particle density is held constant throughout the simulation, rather than being evolved in time as described for WCSPH by Adami et al [19]. Additionally, the boundary particles are fixed and do not move throughout the simulation. The motion of the TLD is instead accommodated by the external excitation term applied to the fluid particles in equation **(4.7)**.

Following the calculation of fluid particle pressure at each timestep, the pressure of each boundary particle is calculated by [19]:

$$P_j = \frac{\sum_{i=1}^{N} P_i W_{ji} + \mathbf{g}(\sum_{i=1}^{N} \rho_i r_{ji} W_{ji})}{\sum_{i=1}^{N} W_{ji}} \quad \textbf{(4.16)}$$

A boundary particle velocity is also calculated before the projection step and again before the calculation of fluid pressure. This is achieved by first calculating the velocity at each boundary particle location based on the neighbouring fluid particles:

$$\boldsymbol{u}_j = \frac{\sum_{i=1}^{N} \boldsymbol{u}_i W_{ji}}{\sum_{i=1}^{N} W_{ji}} \quad \textbf{(4.17)}$$

To enforce the boundary condition of zero fluid velocity normal to the tank boundaries, the boundary particle velocity component perpendicular to the tank wall is set as the reflection of the value calculated by equation **(4.17)**. For example, at a vertical wall, the horizontal x-component of boundary particle velocity will be set to $-u_{j-x}$. Similarly, at a horizontal boundary, the vertical z-component of boundary particle velocity will be set to $-u_{j-z}$. The boundary particles can accommodate either a no-slip or a free-slip condition. In this study a free-slip condition is used, and thus the boundary velocity component parallel to the boundary is set equal to the value calculated by equation **(4.17)**.

In all calculations involving the boundary particles, only the neighbouring fluid particles are considered. This means that the boundary particles do not interact with other boundary particles in the SPH summations. This leads to incomplete boundary particle neighbourhoods, as shown in Figure 4.3(b). To accommodate this, the calculations of pressure and velocity are normalized by the summation of the kernel function $\sum_{i=1}^{N} W_{ji}$. As a default, the boundary particles have the same kernel function support radius q_{max} as the fluid particles.

4.2.3 Boundary Condition Modifications

The boundary particles presented by Adami et al. [19] have been successfully applied to several SPH simulations covering various phenomena. In previous work by the authors, it was determined that for very large sloshing amplitudes over multiple-hour durations there is the potential for fluid particles to escape through the solid boundaries [17]. Though the number of fluid particles lost per minute was small, over the course of a multiple-hour duration simulation this leads to a significant number of particles outside the TLD tank. Similar behavior was reported by Green [2] who completed sloshing simulations of multiple-minute duration. To mitigate the particle loss observed, four methods of modifying the boundary conditions are tested in this study:

1) **Increasing the number of boundary particle layers from 3 to 4.** Despite the number of boundary particle layers being sufficient to provide a complete fluid particle neighbourhood, the additional layer of particles is expected to help contain the fluid. This method will be denoted as *nbl = 4*.
2) **Reducing the kernel support radius for boundary particle velocity calculation in equation (4.17).** Instead of a kernel radius of q_{max} = 2.0, the kernel radius will be reduced to q_{max} = 1.0. This is expected to better represent the reflection of fluid velocity perpendicular to the boundaries by increasing the contributions of fluid particles closest to the wall. This method was used by Muta et al. [1] and will be denoted as *qb = 1.0*.
3) **Introduce a buffer zone condition where fluid-boundary interactions can be neglected.** This method was proposed by Green [2], and intended to neglect interactions between fluid and boundary particles if the fluid is already moving away from the boundary. This is determined by the condition $\boldsymbol{u_i} \cdot (\boldsymbol{x_i} - \boldsymbol{x_j}) > 0$, where subscript *i* indicates a fluid particle and *j* a boundary particle. If this condition is true, the interaction between the fluid and boundary particle pair is neglected. This method will be denoted as the *buffer zone*.
4) **Create a conditional check to return fluid particles to the domain.** In this case, at the end of each timestep the position of each fluid particle is checked relative to

the tank boundaries. If the position is outside the tank by a distance greater than the initial particle spacing *dp*, the fluid particle position is simply reflected back into the tank. This method does not have a physical basis but is very simple to implement. This will be denoted as the *conditional* method.

4.2.4 Damping Screen Particles and TLD Force Calculation

The damping screens are represented in SPH as a series of ghost particles using the methodology presented and validated by McNamara et al. [16]. This implementation can capture the loss of energy from the sloshing fluid passing through the screens without explicitly modelling the screen geometry, which would require a very small particle spacing. A single line of ghost particles is placed vertically at the location of the screen spaced with the same initial distance as the fluid particles *dp*. The only interaction between the screen particles and fluid particles is the $\boldsymbol{F_{screen}}$ term in equation **(4.7)**. The force that the fluid applies on the screen ghost particles is calculated based on the Morison equation for force on a submerged object in oscillating flow [16]:

$$F_{screen-j} = \frac{1}{2} C_l \rho \left| U_{sc,j} \right| U_{sc,j} dp$$
$$U_{sc,j} = \sum_i \frac{m_i}{\rho_i} u_i W_{ji} \tag{4.18}$$

where C_l is the screen loss coefficient and $U_{sc,j}$ is the horizontal fluid velocity calculated at screen particle j. The summation is over the neighbouring fluid particles. The equal and opposite force exerted on the fluid by the screens is then calculated using the kernel function as:

$$F_{screen-i} = -\sum_j F_{screen-j} \frac{W_{ji}}{\sum_f W_{ji}} \tag{4.19}$$

where the summation is over the neighbouring screen particles.

To account for the interaction between the TLD and the structure, the sloshing water force generated by the fluid must be calculated (F_{TLD} in equation **(4.1)**). Different methods for calculating this force were compared by Green [2], and it was determined that the most effective method was to consider the interaction of the solid boundary particles with their neighbouring fluid particles. This is achieved by solving the momentum equation for the solid boundary particles and multiplying the result by the particle mass:

$$F_{TLD} = b\sum_j m_j\left(-\sum_i m_i\left(\frac{P_i}{\rho_i^2}+\frac{P_j}{\rho_j^2}\right)\nabla_f W_{ji} + \sum_i \nu\rho_i\left(\frac{8m_i}{(\rho_i+\rho_j)^2}\frac{(u_j-u_i)\boldsymbol{r_{ji}}.\boldsymbol{\nabla_j} W_{ji}}{r_{ji}^2+\eta^2}\right)+\ddot{X}\right) \qquad \textbf{(4.20)}$$

where a subscript *i* refers to a fluid particle, and *j* refers to a boundary particle. The total force is multiplied by the tank breadth *b*. This is necessary since the tank is modelled in two dimensions with a unit width while the actual TLD has three dimensions.

4.3 Simulation Parameters and Sensitivity Study

This section outlines the simulation parameters used in this study. The structure had generalized properties: M_s = 4480 kg, C_s = 31 Ns/m, and K_s = 5.51x10^4 N/m, resulting in a natural frequency of 0.558 Hz. The TLD tank was square in plan, with length and breadth equal to 0.966 m. The liquid inside the tank was water with an initial fluid depth of 0.119 m, resulting in a TLD natural frequency of 0.546 Hz. Damping screens with a screen loss coefficient C_l = 2.16 were located at 40% and 60% of the tank length.

The structure was subjected to a 3.75-hour duration band limited white noise signal representative of wind loading. The frequency content of the signal was between 0.2 and 1.2 Hz. Figure 4.4 shows the first 30-minutes of the excitation force and the normalized power spectrum of the full signal, scaled by the root-mean-square excitation force, σ_F. This study is focused on large excitation forces, where splashing is likely to occur in the TLD leading to fluid particle loss. The excitation force was scaled to two RMS values: σ_F = 165 N and 300 N. These values result in structure responses beyond the typical range of performance for a TLD. A total of 10 simulations were completed, consisting of the base simulation (no modification to boundary conditions) and the four methods described in Section 4.2.3 at each of the two RMS force values.

The SPH model parameters were selected based on the previous work by the authors validating the SPH model with experimental data for a TLD [16] and structure-TLD system [17]. The SPH fluid, boundary, and screen particles were discretized with an initial particle spacing dp = 7.0 mm. This value was selected to provide an integer number of particles across the fluid depth and tank length, while ensuring sufficient resolution to capture the sloshing behavior. The total number of fluid particles was 2,346. The kernel function smoothing radius was selected as $h_{ker} = 1.4dp$ for the fluid particles and boundary particles. For the screen particles, the smoothing radius was set to $h_{screen} = 3.0h_{ker}$ to better account for the flow in the region of the screens by considering a larger neighbourhood of fluid particles. The timestep was held constant throughout the simulations and set to $dt = 5\text{x}10^{-4}$ seconds. To conserve storage space and improve computational runtime, the SPH results, such as structure displacement and TLD wave height, were output every 100 timesteps or every 0.05 seconds. The TLD wave height was measured at 5% of the tank length by determining the location of the free surface using equation **(4.13)** at an array of calculation points across the height of the tank.

A sensitivity study was completed to ensure the initial particle spacing and simulation timestep were appropriate for the structure-TLD system. The first two minutes of the base simulation was run with an RMS force of σ_F = 300 N. Figure 4.5 shows a five second segment of the normalized structure displacement and wave height comparing initial particle spacings dp = 3.5, 7.0, and 14.0 mm. The structure displacement is nearly identical for the three cases. Slight variation is observed in the wave heights; however, the wave form is very similar for each case. Figure 4.6 shows the same segment comparing simulation timesteps $dt = 2.5\text{x}10^{-4}$, $5.0\text{x}10^{-4}$, and $1.0\text{x}10^{-3}$ seconds with dp = 7.0 mm. The results are nearly identical for all three cases for both the structural displacement and the TLD wave height. Based on these results, the selection of dp = 7.0 mm and $dt = 5\text{x}10^{-4}$ seconds is deemed appropriate for this study.

4.4 Results

4.4.1 Fluid Particle Loss

Prior to evaluating the performance of modifying the boundary conditions for mitigating fluid particle loss, it is necessary to discuss the conditions leading to fluid particle loss in the base simulations. The loss of fluid particles was previously observed by the authors to occur only for large amplitude sloshing simulations, and the number of fluid particles outside the tank domain increased with increasing excitation amplitude [17]. The cause of the boundary particles being unable to contain the sloshing fluid particles is attributed to the occurrence of splashing at the tank walls. When the sloshing response is large, small amounts of fluid will splash each cycle when the fluid impacts the tank walls. In the SPH simulations, this leads to a small number of particles running up at the walls away from the bulk of the fluid. This is illustrated in Figure 4.7 which shows the particle positions from the base simulation with σ_F = 300 N at two times. The sloshing response is significant, and splashing is observed at the top left corner of the tank.

The splashing of these small numbers of particles away from the bulk of the flow causes two issues with the solid boundary particle calculations. First, due to the lack of neighbouring particles, these fluid particles will be determined to be free surface particles by equation **(4.13)**, resulting in their pressure being set to zero. This causes the boundary particle pressure calculated from equation **(4.16)** to also be zero. The pressure of the boundary particles works to repel the fluid particles and contain them within the tank. When the boundary particle pressure is zero this is not possible, and this allows the fluid particles to approach closely to the boundary particles. Figure 4.8 shows the fluid and boundary particles coloured by their pressures corresponding to the first case from Figure 4.7. At the bottom of the tank the particle pressures transition smoothly from the fluid to the boundaries, however at the top of the tank where the splashing particles are located, the boundary particle pressures are zero.

This effect on boundary particle pressure alone is not expected to result in significant loss of fluid particles. However, the calculation of boundary particle velocity must also be

considered. The boundary particle velocity normal to the tank boundaries is calculated from the surrounding fluid particles, and then reflected to enforce the condition of zero velocity normal to the boundary. If there are isolated fluid particles with velocities moving away from the tank boundaries, this will result in the calculated boundary particle velocity being directed outward from the tank, causing the fluid particle to become attracted to it. To illustrate this, the velocity normal to the vertical wall boundary particles was calculated for the same case shown in Figures 4.7 and 4.8. The calculated normal velocities for the first layer of boundary particles at the top corner of the tank are shown in Figure 4.9. Significant velocities pointing outward from the tank are observed at the top corner where there are only a few fluid particles present. In comparison, lower in the tank where more fluid particles are located, the boundary velocity is nearly zero.

As a result of the issues identified with boundary particle pressure and velocity calculations, it is possible for the splashing fluid particles to become stuck to the boundary particles, and eventually be forced out of the tank. This represents an unphysical behavior and is a consequence of the method employed to calculate boundary particle values. Of the proposed methods, reducing the boundary particle kernel support radius (qb = 1.0) and implementation of the buffer zone method address this problem directly.

4.4.2 Performance of Modified Boundary Conditions

This section discusses the performance of the four methods for mitigating loss of fluid particles over the duration of the 3.75-hour simulations. The number of fluid particles outside the TLD tank was counted every five minutes throughout the simulations. Figure 4.10 plots the percentage of fluid particles outside the tank versus time. For both values of σ_F, the base simulation has the most fluid particles outside the tank. When σ_F = 165 N, only 0.9% of the fluid particles are outside of the tank at the end of the simulation, which is a small number that is not likely to significantly impact the overall simulation results. However, when σ_F = 300 N, 30.8% of the fluid particles are outside of the tank at the end of the simulation, leading to a significant change in the overall simulation results. Increasing the number of boundary particle layers in the nbl = 4 method reduces the

percentage of particles outside the tank to 0.26% for σ_F = 165 N and 20.0% for σ_F = 300 N, respectively. This is a significant improvement over the base simulation, but still requires further improvement. Increasing the number of layers of boundary particles also increases the computational time due to the additional particle interactions.

The remaining three methods performed very well at containing the fluid particles inside the tank. Reducing the kernel function support radius in the qb = 1.0 method led to no particles outside the tank when σ_F = 165 N, and only 0.9% when σ_F = 300 N. These values are well within an acceptable limit for particle loss. The best performance was observed for the conditional and buffer zone methods. In both cases, the fluid particles were completely contained within the tank over the course of the simulations. From the results, the methods with the best performance for containing the fluid particles within the domain are the qb = 1.0, buffer zone, and conditional methods.

The base simulation was observed in Figure 4.9 to result in boundary particle velocities pointing outward from the tank, causing an attraction of the fluid particles. To compare the results of the modified boundary conditions for this behavior, the same case is shown in Figure 4.11 at time = 105 minutes for the σ_F = 300 N excitation. For the qb = 1.0 method, the boundary particle velocities at the very top corner are zero since the fluid particles are not close enough to be included in the summations. This is an improvement over the base simulation, though there appears to be larger horizontal velocities further down the tank wall, and some velocities pointing outward from the tank. The conditional method has velocities directed outside the tank like the base simulation, though the magnitude is smaller. This behavior is expected since this method does not modify the actual boundary particle calculations. The buffer zone method is effective in ensuring that the boundary particle velocities are only acting inward to the tank, since the fluid particle interactions causing the velocity to point outward are neglected. Overall, the modified boundary conditions result in differences to the calculation of boundary particle velocities, though only the buffer zone method appears to fix the issue of outward directed velocities.

4.4.3 Impact of Modified Boundary Conditions on Results

It is necessary to identify the impact that modifying the boundary conditions has on the structure-TLD system response to ensure the simulations are still physically capturing the behavior of the system. This section will focus on comparing the base simulation to the three methods which best contained the fluid particles throughout all simulations: qb = 1.0, conditional, and buffer zone. The discussion will be limited to the σ_F = 300 N cases since the improvement in simulation results is more significant than the σ_F = 165 N cases.

Figure 4.12 shows the fluid particles coloured by their pressure at time = 10 minutes into the simulation. The results between the base simulation, qb = 1.0, and conditional methods are observed to be very similar, and the pressure transitions smoothly from high values at the bottom of the tank to low values at the free surface. The buffer zone results show a similar wave profile; however, the fluid pressure field has been degraded and does not appear to be physically correct. Figure 4.13 shows the same cases at time = 20 minutes. At this time the TLD response is less significant. Again, the response is very similar for the base simulation, qb = 1.0, and conditional methods and the pressure field shows smooth transitions across the fluid depth. The buffer zone method results show a degraded pressure field. Since these two times are relatively early in the total simulation time, the impact of particle loss on the base simulation is not significant. Figure 4.14 shows the response in the TLD much later in the simulations at time = 175 minutes. The difference between the base simulation and other methods is more significant. Similar behavior is observed for the buffer zone method as in the previous cases. Based on these results, the buffer zone method appears to lead to issues with fluid pressure, despite containing the fluid particles completely within the tank. It is postulated that while the buffer zone corrects the boundary velocity issues near splashing fluid particles, it may also erroneously neglect boundary-fluid particle interactions in the bulk of the flow that impact the overall results. Further investigation into the cause of this is warranted. However, since both the qb = 1.0 and conditional methods effectively contained the fluid particles, the remaining results will focus on these methods.

Figure 4.15 shows the TLD wave height over the entire 3.75-hour duration for the base simulation as well as the qb = 1.0 and conditional methods. The RMS wave height is denoted by the horizontal line. The impact of fluid particle loss on the base simulation can be observed by the downward drifting of the signal over time. In effect the TLD has become detuned from the structure as the fluid mass is decreased which causes a reduction in the TLD natural frequency. In comparison, there is no drifting observed in the wave height signal for the qb = 1.0 method, despite some minor fluid particle loss. The same is true of the conditional method, where no fluid particles are lost throughout the simulation.

To further illustrate the impact of fluid particle loss on the results, comparison is made to experimental data for the structure-TLD system from Tait [27]. Figure 4.16 shows a segment of the structure displacement and TLD wave height at time = 15 minutes into the simulation. At this time only 1.45% of the fluid particles are outside the TLD in the base simulation. The response for the base simulation, qb = 1.0, and conditional methods is shown. The structure response is nearly identical for all three methods. Minor differences are observed for the peak TLD wave heights, but the results overall are very similar. All three methods show very good agreement with the experimental data. Figure 4.17 makes the same comparison at time = 180 minutes into the simulation. At this time 24.3% of the fluid particles are outside the TLD in the base simulation, and the agreement with the experimental data is poor. In contrast, the responses of the qb = 1.0 and conditional methods show very good agreement with the experimental data. Additionally, the two methods show nearly identical responses to one another, indicating that these modifications to the boundary conditions did not impact the SPH model ability to capture the response of the structure-TLD system.

4.5 Conclusions

This study investigated strategies to mitigate the loss of fluid particles through solid boundaries during long duration SPH simulations. A structure-TLD system was modelled. The TLD was represented using an incompressible SPH method. Solid boundaries were modelled using fixed dummy particles with a free-slip velocity condition. The structure-

TLD system was subject to a 3.75-hour duration band limited white noise force excitation representative of wind loading scaled to two different RMS force levels. This study compared four methods to improve the ability of the boundary particles to contain the fluid particles.

For the base simulations without modification, it was determined that when splashing of the water in the TLD occurs at the tank boundaries, it is possible for SPH fluid particles to become attracted to the boundaries. This leads to the fluid particles eventually being forced outside of the tank. This behavior is especially prominent when the excitation amplitude is large and splashing of the water occurs in many cycles. When σ_F = 165 N, a total of 0.9% of the fluid particles were outside the TLD tank at the end of the simulation. Increasing σ_F to 300 N led to a total of 30.8% of the fluid particles to be outside of the TLD tank at the end of the simulation.

The four methods studied to mitigate fluid particle loss were all found to improve the performance of the SPH model, though the effectiveness of each method varied. Increasing the number of boundary layers beyond the value required to ensure complete fluid particle neighbourhoods (nbl = 4 method) reduced the percentage of fluid particles outside the TLD tank at the end of the simulations, though the percentage was still significant when σ_F = 300 N. Reducing the kernel support radius of the boundary particle velocity calculation (qb = 1.0 method) was very effective at containing the fluid particles within the TLD tank, with <1% loss of fluid particles when σ_F = 300 N. The buffer zone method which neglected certain boundary-fluid particle interactions and the conditional method which simply put fluid particles from outside the tank back in were both completely effective at containing the fluid particles within the tank, with no fluid particles lost throughout the simulations.

The impact of modifying the boundary conditions on the structure-TLD response was investigated. The buffer zone method was found to degrade the pressure field within the TLD, leading to unphysical values. Further investigation related to the cause of this is warranted. Both the qb = 1.0 and conditional methods were found to accurately capture the response of the structure-TLD system throughout the 3.75-hour simulations. Comparisons

to experimental data showed excellent agreement both near the start and multiple hours into the simulation time.

The results of this study show that simple modifications to the SPH boundary particle implementation can be applied to improve the results of large amplitude sloshing simulations with multiple hour duration. Implementation of one or more of the methods studied to mitigate the loss of fluid particles is recommended for very long duration SPH sloshing simulations where splashing of the fluid is expected.

4.6 Acknowledgment

The authors are thankful for the financial support provided by the Natural Sciences and Engineering Research Council of Canada (NSERC) and the Ontario Graduate Scholarship (OGS) program. This research was enabled in part by computing support provided by Compute Ontario (www.computeontario.ca) and Compute Canada (www.computecanada.ca).

4.7 References

[1] A. Muta, P. Ramachandran and P. Negi, "An efficient, open source, iterative ISPH scheme," *Computer Physics Communications,* vol. 255, p. 107283, 2020.

[2] M. D. Green, *Sloshing simulations with the smoothed particle hydrodynamics (SPH) method,* PhD Thesis, Imperial College London, 2017.

[3] R. A. Gingold and J. J. Monaghan, "Smoothed particle hydrodynamics: theory and application to non-spherical stars," *Monthly Notices of the Royal Astronomical Society,* vol. 181, pp. 375-389, 1977.

[4] L. Lucy, "A numerical approach to the testing of the fission hypothesis," *The Astronomical Journal,* vol. 82, no. 12, pp. 1013-1024, 1977.

[5] J. J. Monaghan, "Simulating free surface flows with SPH," *Journal of Computational Physics,* vol. 110, no. 2, pp. 399-406, 1994.

[6] S. J. Cummins and M. Rudman, "An SPH Projection Method," *Journal of Computational Physics,* vol. 152, pp. 584-607, 1999.

[7] D. Violeau and B. D. Rogers, "Smoothed particle hydrodynamics (SPH) for free-surface flows: Past, present and future," *Journal of Hydraulic Research,* vol. 54, no. 1, pp. 1-26, 2016.

[8] L. Delorme, A. Colagrossi, A. Souto-Iglesias, R. Zamora-Rodriguez and E. Botia-Vera, "A set of canonical problems in sloshing, Part I: Pressure field in forced roll-comparison between experimental results and SPH," *Ocean Engineering,* vol. 36, no. 2, pp. 168-178, 2009.

[9] G. Bulian, A. Souto-Iglesias, L. Delorme and E. Botia-Vera, "Smoothed particle hydrodynamics (SPH) simulation of a tuned liquid damper (TLD) with angular motion," *Journal of Hydraulic Research,* vol. 48, no. sup1, pp. 28-39, 2009.

[10] A. Marsh, M. Prakash, E. Semercigil and O. F. Turan, "A study of sloshing absorber geometry for structural control with SPH," *Journal of Fluids and Structures,* vol. 27, no. 8, pp. 1165-1181, 2011.

[11] X. Y. Cao, F. R. Ming and A. M. Zhang, "Sloshing in a rectangular tank based on SPH simulation," *Applied Ocean Research,* vol. 47, pp. 241-254, 2014.

[12] M. S. Kusic, J. Radnic, N. Grgic and A. Harapin, "Sloshing in medium size tanks caused by earthquake studied by SPH," *Građevinar,* vol. 70, no. 8, pp. 671-684, 2018.

[13] M. D. Green and J. Peiro, "Long duration SPH simulations of sloshing in tanks with a low fill ratio and high stretching," *Computers and Fluids,* vol. 174, pp. 179-199, 2018.

[14] M. D. Green, Y. Zhou, J. M. Dominguez, M. G. Gesteira and J. Peiro, "Smooth particle hydrodynamics simulations of long-duration violent three-dimensional sloshing in tanks," *Ocean Engineering,* vol. 229, p. 108925, 2021.

[15] A. H. Kashani, A. M. Halabian and K. Asghari, "A numerical study of tuned liquid damper based on incompressible SPH method combined with TMD analogy," *Journal of Fluids and Structures,* vol. 82, pp. 394-411, 2018.

[16] K. P. McNamara, B. N. Awad, M. J. Tait and J. S. Love, "Incompressible smoothed particle hydrodynamics model of a rectangular tuned liquid damper containing screens," *Journal of Fluids and Structures,* vol. 103, p. 103295, 2021.

[17] K. P. McNamara and M. J. Tait, "Modelling the response of structure-tuned liquid damper systems under large amplitude excitation using SPH," *Journal of Vibration and Acoustics,* vol. 144, p. 011008, 2022.

[18] S. Marrone, M. Antuono, A. Colagrossi, G. Colicchio, D. Le Touze and G. Graziani, "δ-SPH model for simulating violent impact flows," *Computer Methods in Applied Mechanics and Engineering,* vol. 200, pp. 1526-1542, 2011.

[19] S. Adami, X. Y. Hu and N. A. Adams, "A generalized wall boundary condition for smoothed particle hydrodynamics," *Journal of Computational Physics,* vol. 231, no. 21, pp. 7057-7075, 2012.

[20] A. English, J. M. Dominguez, R. Vacondio, A. J. Crespo, P. K. Stansby, S. J. Lind, L. Chiapponi and M. Gomez-Gesteira, "Modified dynamic boundary conditions (mDBC) for general-purpose smoothed particle hydrodynamics (SPH): application to tank sloshing, dam break and fish pass problems," *Computational Particle Methods,* 2021.

[21] A. Leroy, D. Violeau, M. Ferrand and C. Kassiotis, "Unified semi-analytical wall boundary conditions applied to 2-D incompressible SPH," *Journal of Computational Physics,* vol. 261, pp. 106-129, 2014.

[22] H. Wendland, "Piecewise polynomial, positive definite and compactly supported radial functions of minimal degree," *Advances in Computational Mathematics,* vol. 4, pp. 389-396, 1995.

[23] J. J. Monaghan, "Smoothed Particle Hydrodynamics," *Annual Review of Astronomy and Astrophysics,* vol. 30, pp. 543-74, 1992.

[24] Nomeritae, E. Daly, S. Grimaldi and H. H. Bui, "Explicit incompressible SPH algorithm for free-surface flow modelling: A comparison with weakly compressible schemes," *Advances in Water Resources,* vol. 97, pp. 156-167, 2016.

[25] H. Jiang, Y. You, Z. Hu, X. Zheng and A. Ma, "Comparative study on violent sloshing withwater jet flows by using the ISPH method," *Water (Switzerland),* vol. 11, p. 2590, 2019.

[26] S. Yeylaghi, B. Moa, P. Oshkai, B. Buckham and C. Crawford, "ISPH modelling of an oscillating wave surge converter using an OpenMP-based parallel approach," *Journal of Ocean Engineering and Marine Energy*, vol. 2, pp. 301-312, 2016.

[27] M. J. Tait, *The Performance of 1-D and 2-D Tuned Liquid Dampers,* Ph.D. Thesis. University of Western Ontario, 2004.

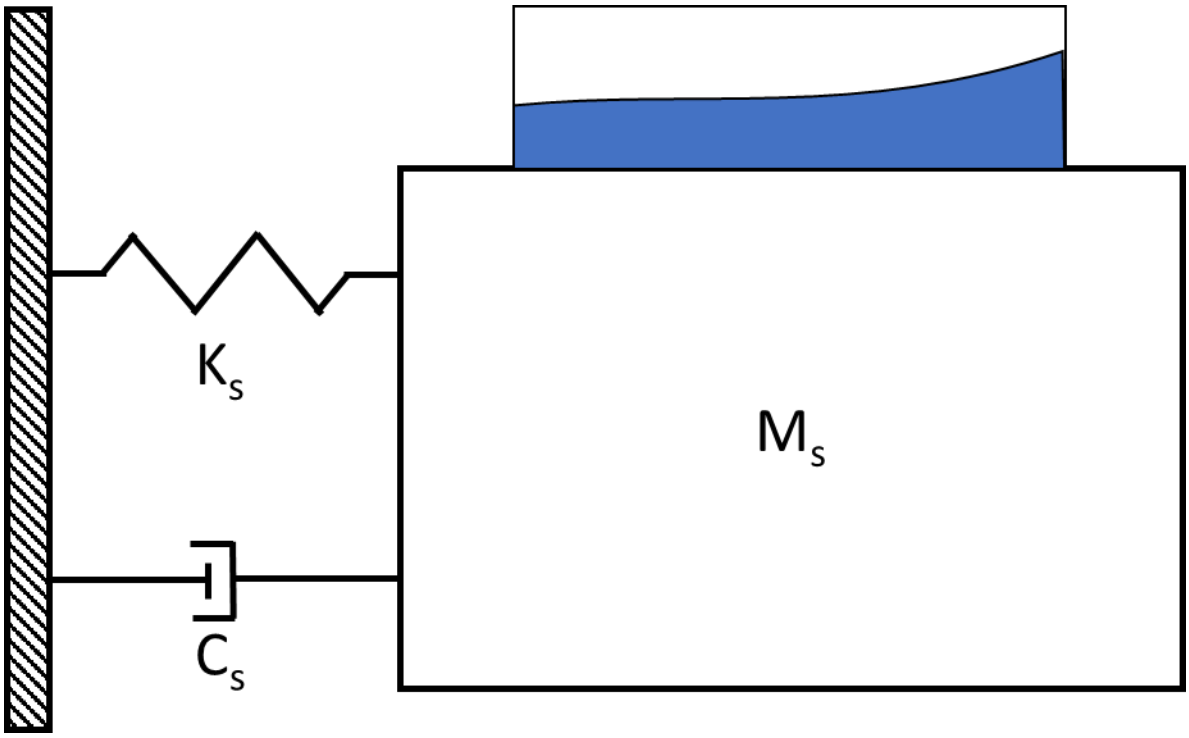

Figure 4.1: Structure-TLD System Schematic

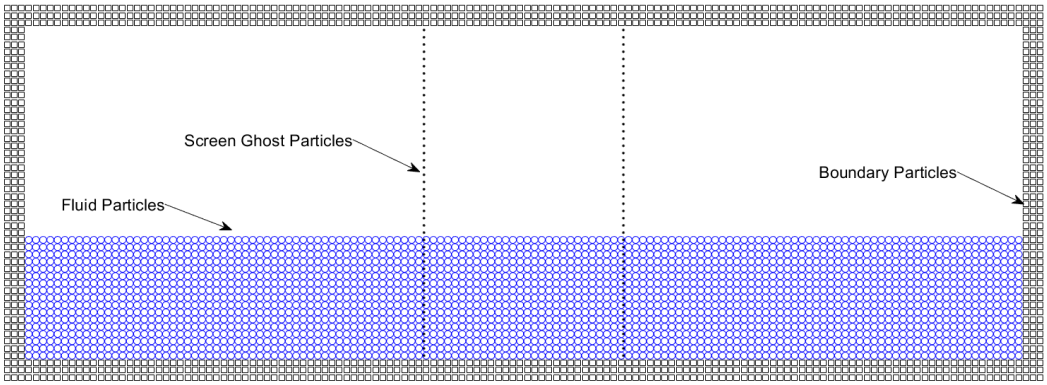

Figure 4.2: Initial SPH Particle Discretization

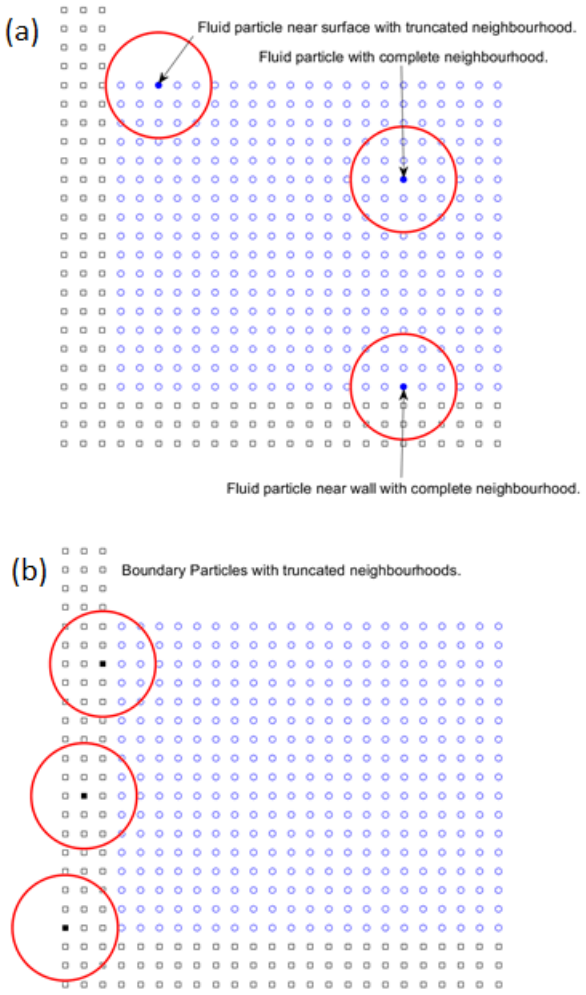

Figure 4.3: SPH Particle Neighbourhoods: (a) fluid particles, (b) boundary particles

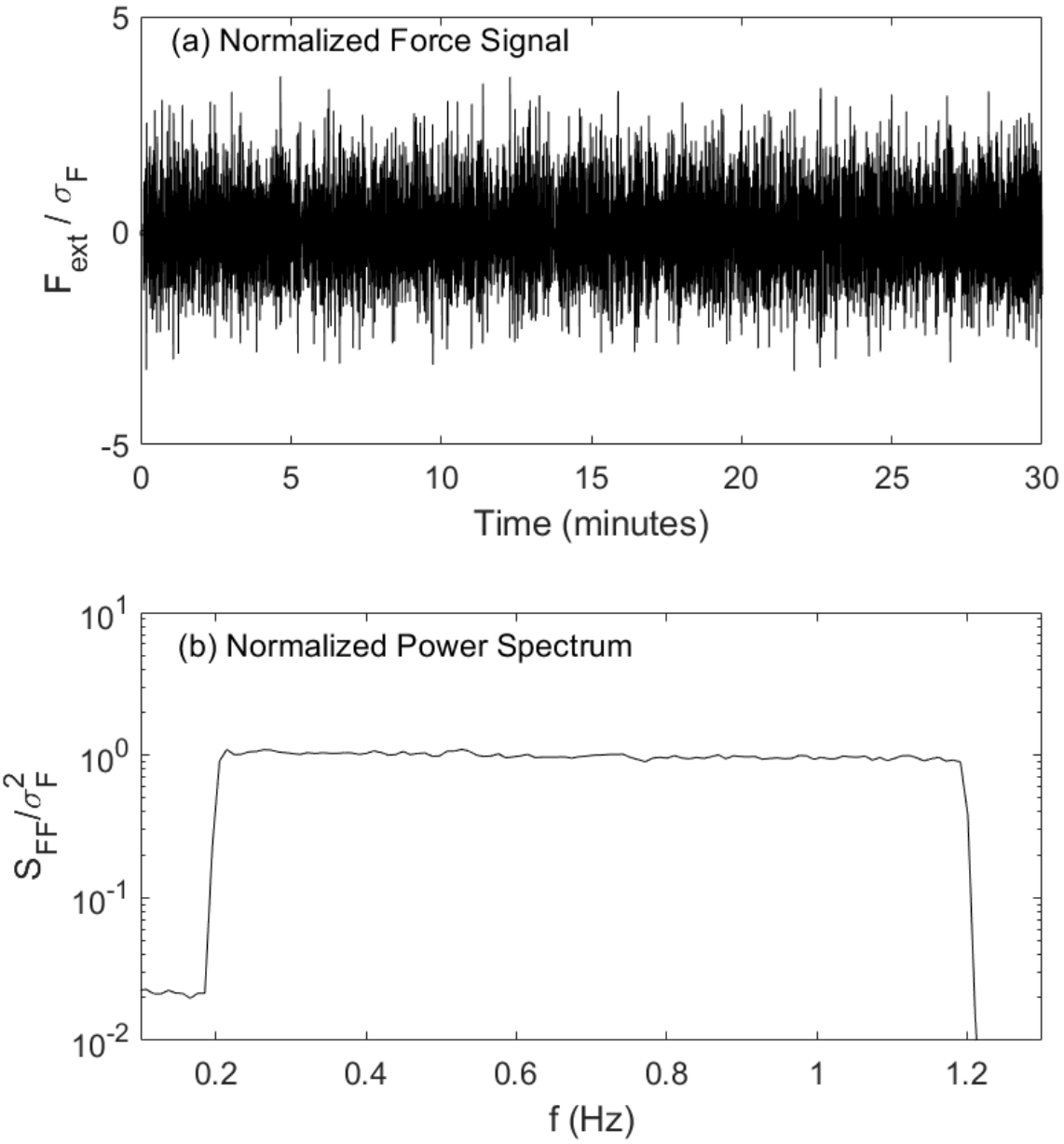

Figure 4.4: Band-limited White Noise Force Excitation Signal: (a) time history, (b) power spectrum

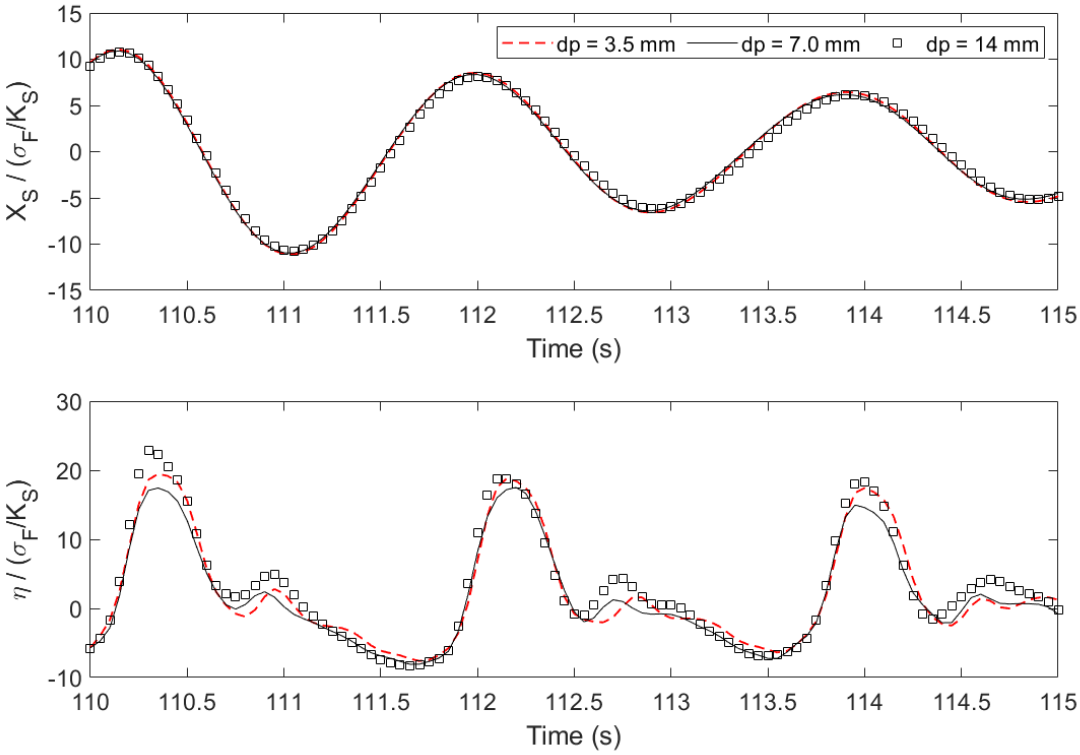

Figure 4.5: Normalized structure displacement (X_S) and wave height (η) for initial particle spacing dp = 3.5, 7.0, and 14.0 mm

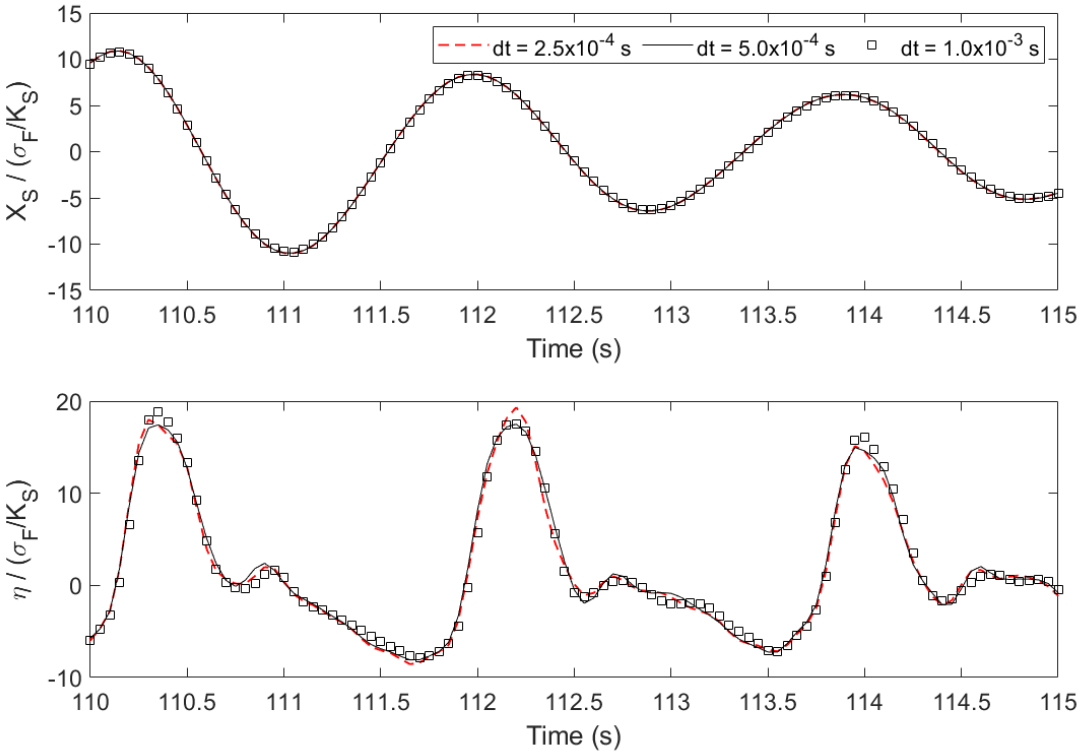

Figure 4.6: Normalized structure displacement (X_S) and wave height (η) for timestep dt = 5.0x10^{-4}, 2.5x10^{-4}, and 1.0x10^{-3} seconds

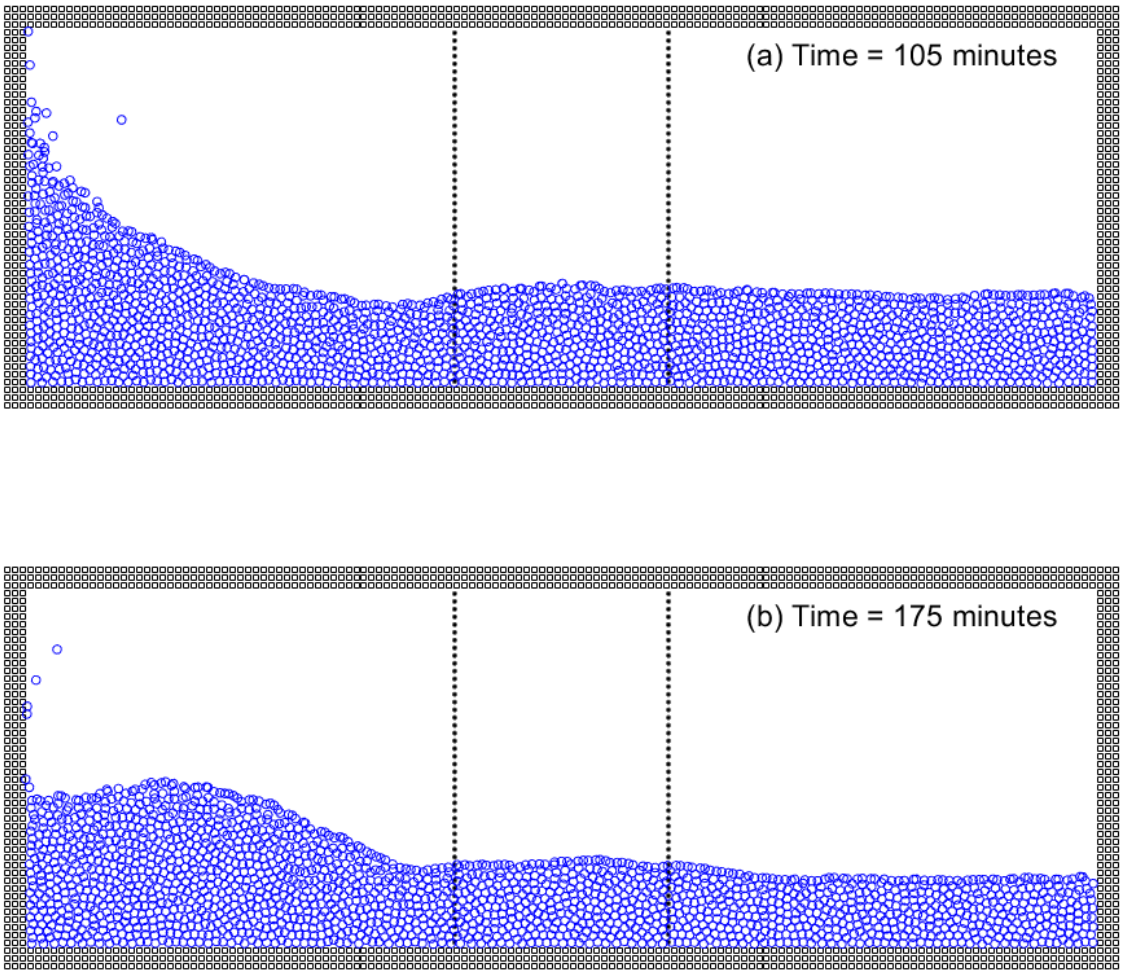

Figure 4.7: Particle Positions from σ_F = 300 N base simulation showing splashing at top left corner

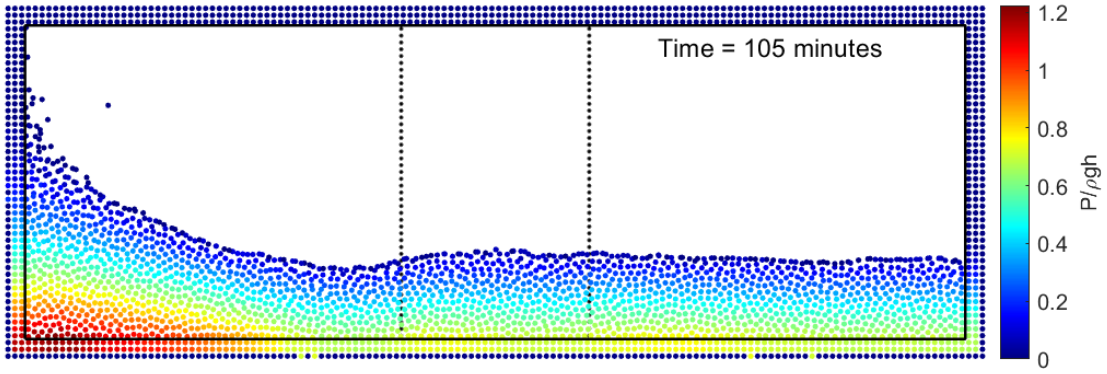

Figure 4.8: Particle Pressures from σ_F = 300 N base simulation

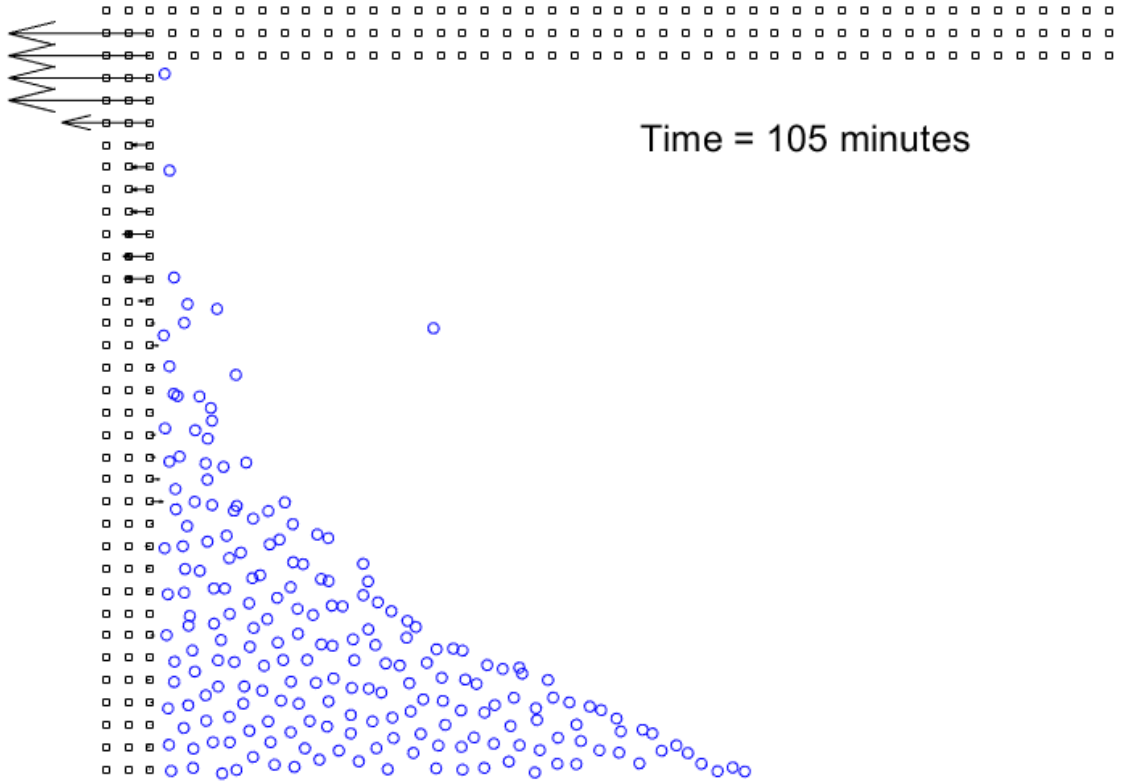

Figure 4.9: Wall boundary particle normal velocities (denoted by arrows) from σ_F = 300 N base simulation

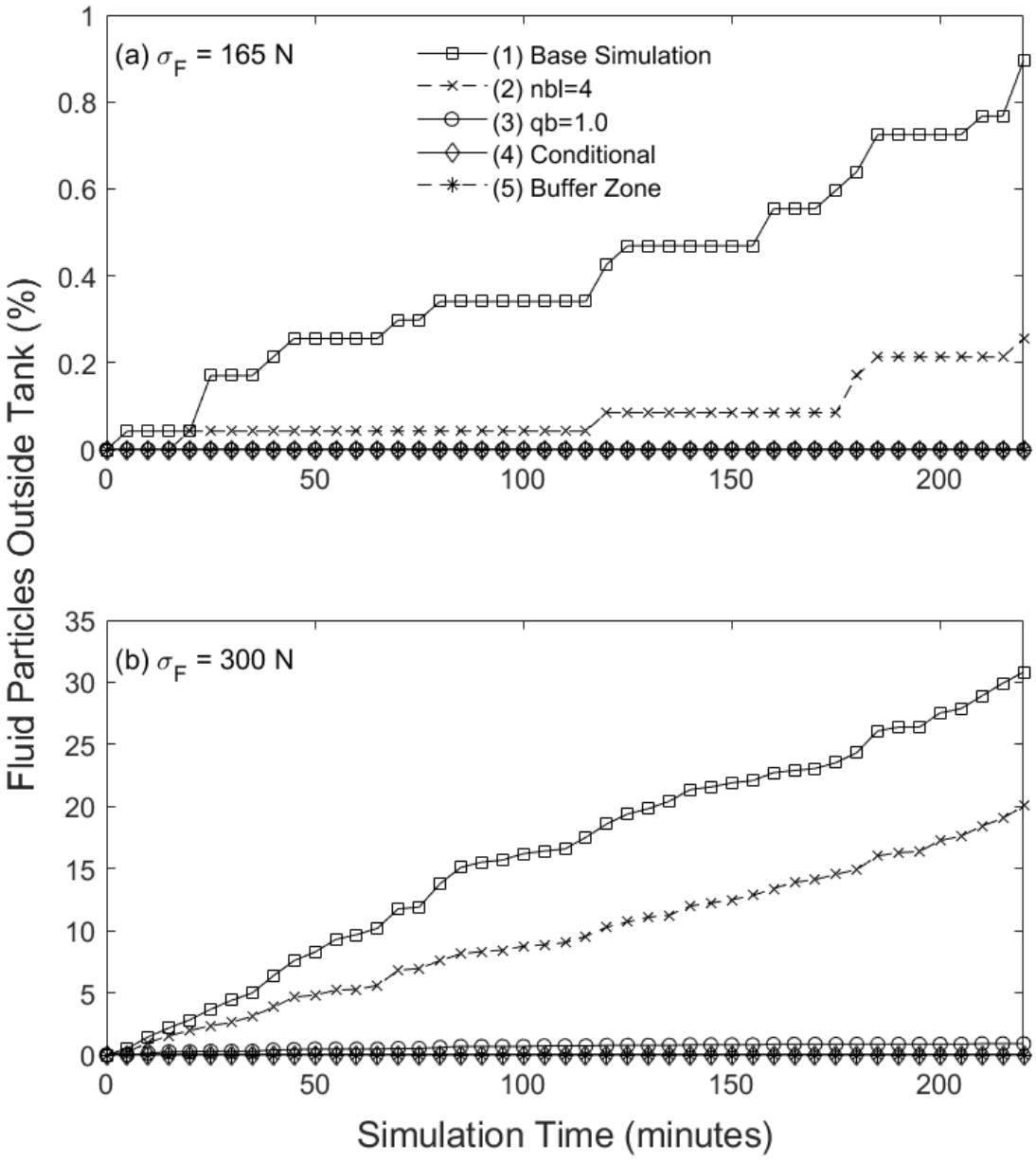

Figure 4.10: Percentage of fluid particles outside domain vs. simulation time: (a) σ_F = 165 N, (b) σ_F = 300 N

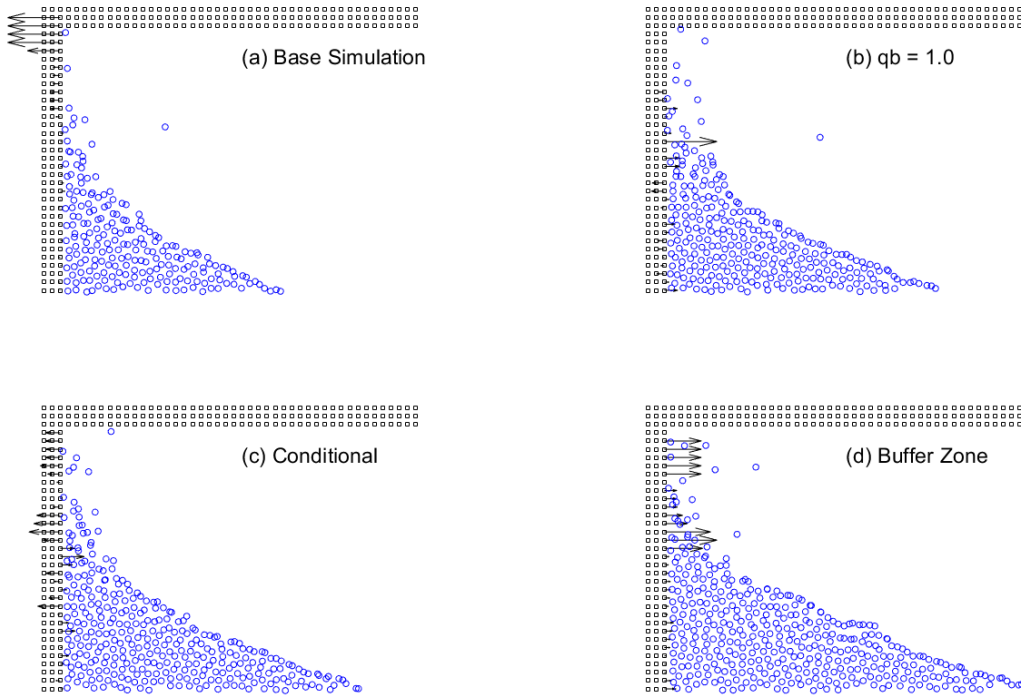

Figure 4.11: Boundary particle normal velocities (indicated by arrows) at time = 105 minutes and σ_F = 300 N: (a) base simulation, (b) qb = 1.0, (c) conditional, and (d) buffer zone

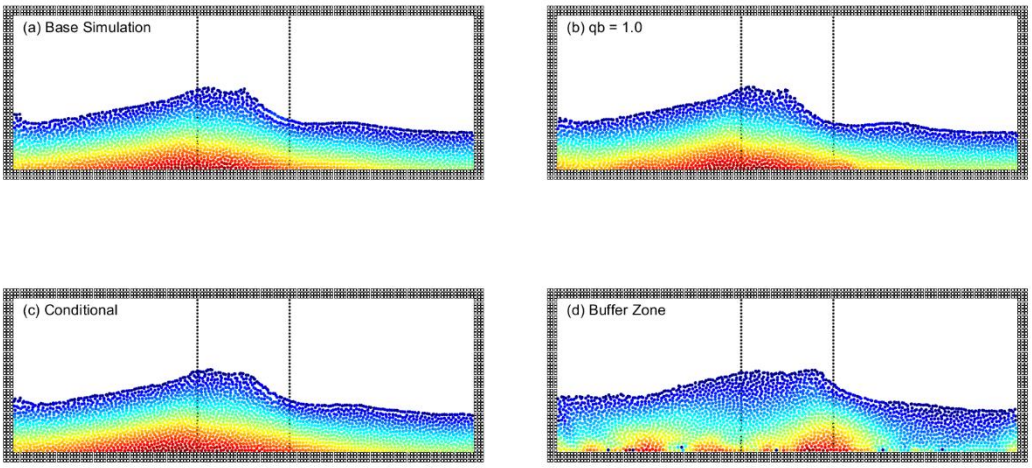

Figure 4.12: Fluid particles (coloured by pressure) at time = 10 minutes and σ_F = 300 N: (a) base simulation, (b) qb = 1.0, (c) conditional, and (d) buffer zone

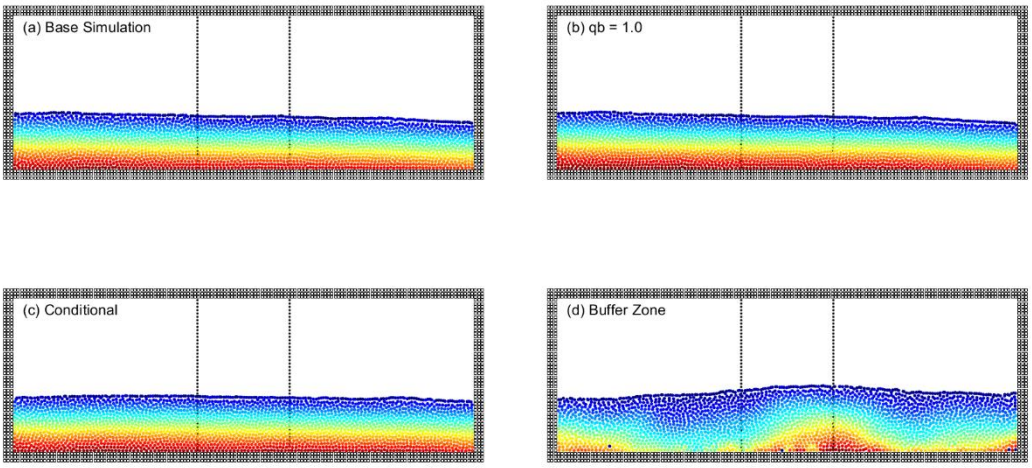

Figure 4.13: Fluid particles (coloured by pressure) at time = 20 minutes and σ_F = 300 N: (a) base simulation, (b) qb = 1.0, (c) conditional, and (d) buffer zone

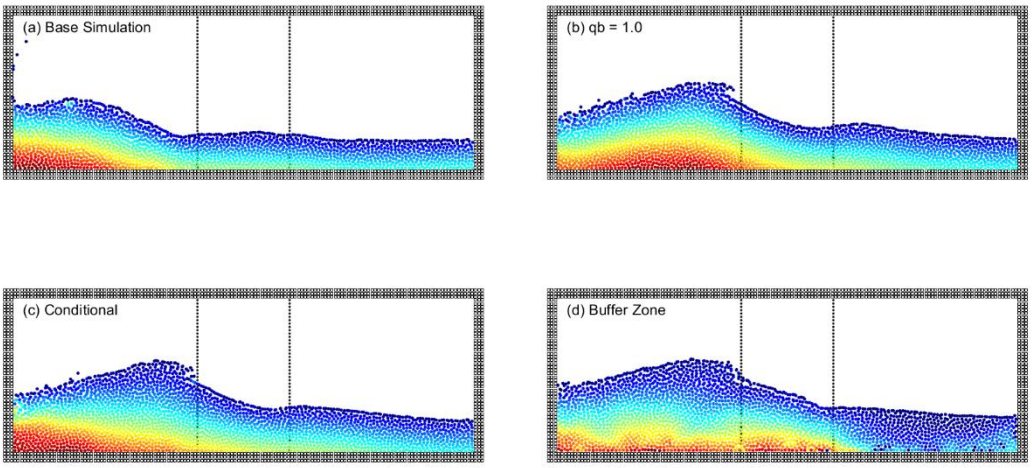

Figure 4.14: Fluid particles (coloured by pressure) at time = 175 minutes and σ_F = 300 N: (a) base simulation, (b) qb = 1.0, (c) conditional, and (d) buffer zone

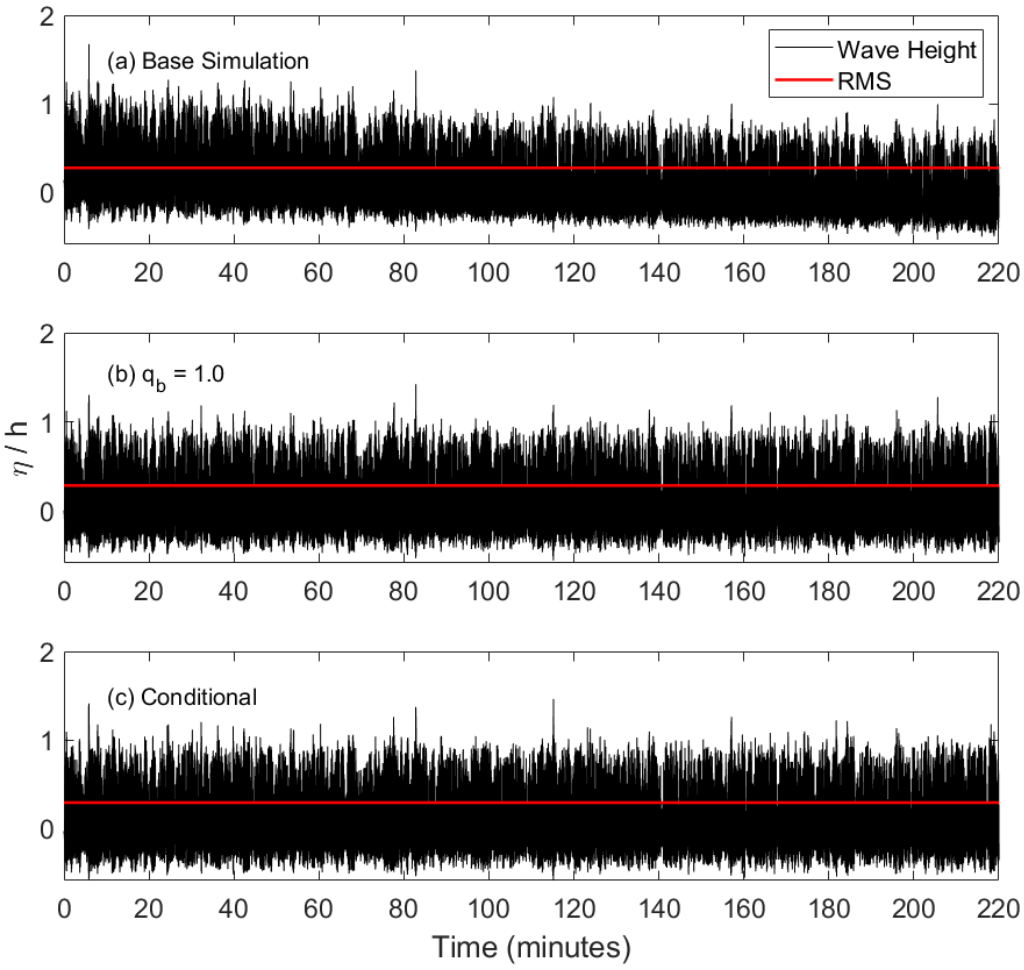

Figure 4.15: TLD Wave Height Response History for σ_F = 300 N: (a) base simulation, (b) qb = 1.0, (c) conditional

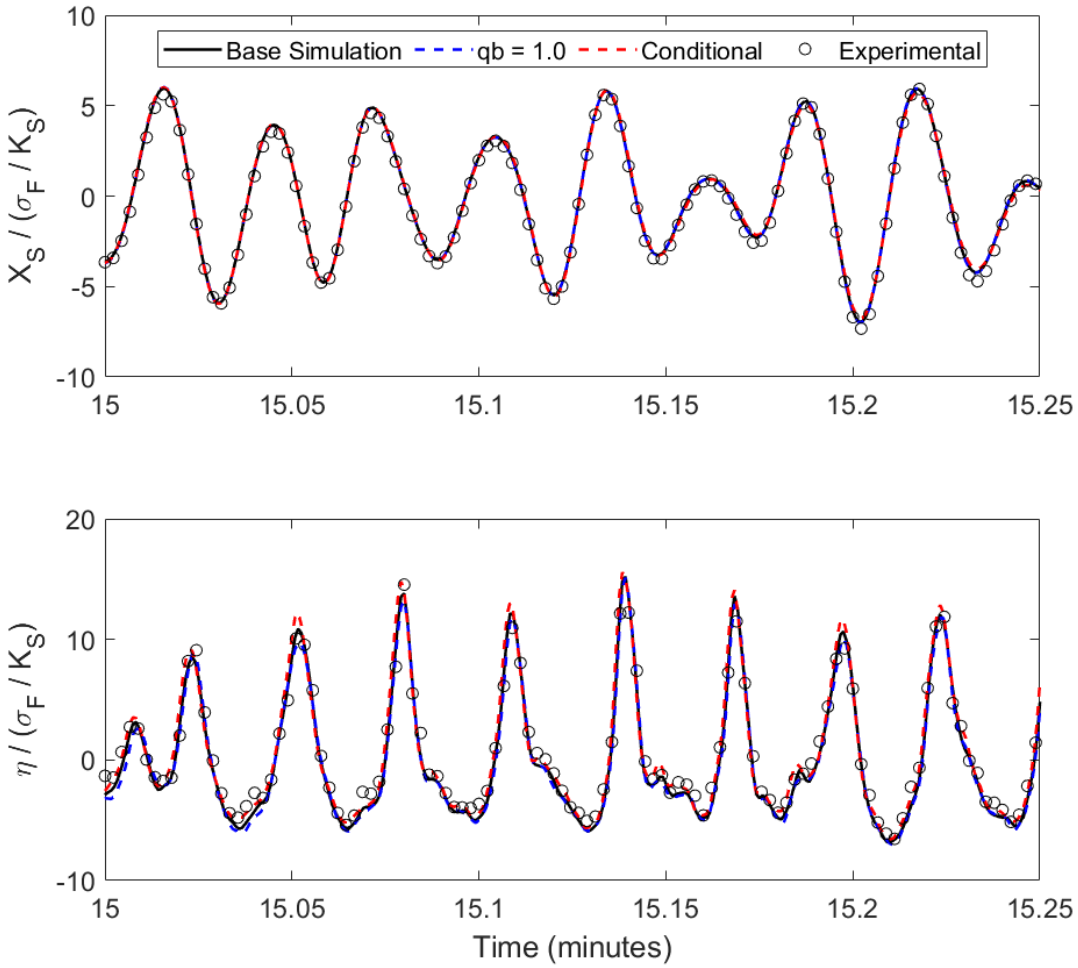

Figure 4.16: Structural Displacement and TLD Wave Height Response History for σ_F = 300 N at simulation time = 15 minutes

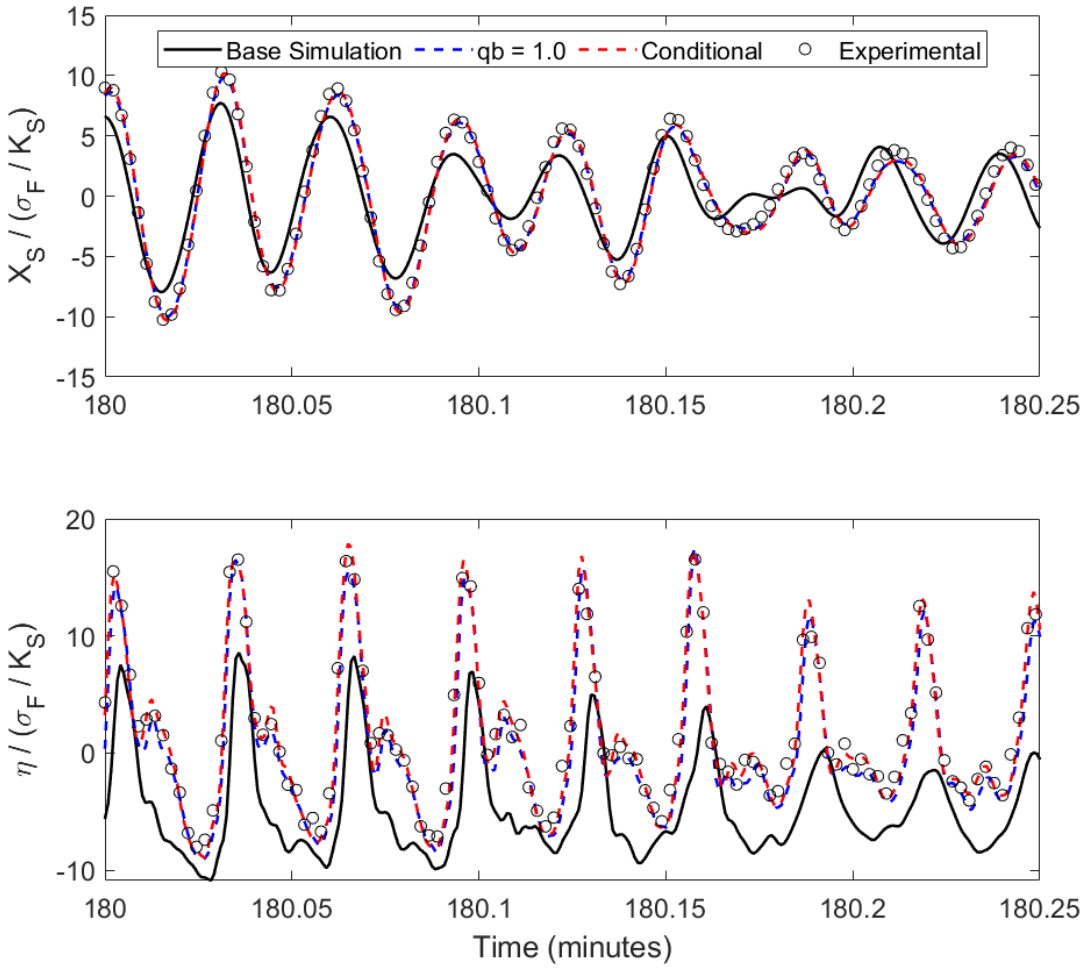

Figure 4.17: Structural Displacement and TLD Wave Height Response History for σ_F = 300 N at simulation time = 180 minutes

Chapter 5: Numerical investigation of the response of structures equipped with a limited freeboard tuned liquid damper

Abstract

The tuned liquid damper (TLD) uses liquid sloshing in a tank to suppress unwanted wind-induced vibration of a flexible structure. The tank interior height is traditionally selected such that sloshing waves do not impact the tank ceiling by providing sufficient freeboard between the free surface and the tank ceiling. To optimize a TLD for a space with height constraints, it is possible to design the tank to have intentionally limited freeboard. This study numerically investigates the response of a structure equipped with a limited freeboard TLD using an incompressible smoothed particle hydrodynamics (SPH) model. Seven excitation force intensities are studied at nine different freeboard heights. The SPH results are used to assess the performance of the limited freeboard TLD. In general, limiting freeboard is found to reduce the effectiveness of the TLD. When the fundamental sloshing mode is not constrained by the tank ceiling, the TLD performs comparably well to its unlimited freeboard counterpart. If the fundamental sloshing mode is constrained by the tank ceiling, the motion reduction performance of the TLD is affected. The equivalent damping ratio of the fundamental sloshing mode is evaluated from the SPH results. An equivalent linear mechanical model that can be used for preliminary feasibility studies of the system with limited freeboard is presented. Additional TLD damping due to ceiling impact proportional to the reduction in wave height is introduced. The mechanical model is found to reasonably capture the structure response when compared to the SPH results.

KEYWORDS: tuned liquid damper (TLD), dynamic vibration absorber (DVA), smoothed particle hydrodynamics (SPH), structure-TLD system, sloshing tank ceiling impact.

5.1 Introduction

The tuned liquid damper (TLD) is well established as an effective system for controlling the wind-induced motion of a tall structure. A TLD consists of a partially filled tank of liquid installed in a structure near the location of maximum modal response. TLDs can be of various shapes, ranging from simple rectangular or circular tanks to more complex shapes designed to conform to space restrictions. In all cases, the plan dimensions and liquid depth of a TLD are selected to tune the natural sloshing frequency to be close to the natural frequency of the targeted structural mode. The height of a TLD is generally selected to ensure sufficient freeboard is provided such that the sloshing water does not impact the ceiling during common wind events. If the TLD wave impacts the tank ceiling, this can lead to significant fluid induced pressures and forces, which may complicate the structural design of the tank. Moreover, there is limited knowledge on the change in TLD performance if ceiling impact occurs. As a result, the design height of TLD tanks is typically conservative, which can take up valuable space (height) in a building. Designing TLDs with intentionally limited freeboard is an attractive option to fit the tank(s) into structures with limited available height. The behavior of limited freeboard TLDs is not well understood. Developing a better understanding of the performance of TLDs with limited freeboard would increase the practicality and attractiveness of TLDs for many structures.

The behavior of sloshing liquids impacting the walls and ceiling in a tank has received considerable attention in both experimental and numerical studies. Several experimental studies have been completed on the pressure distribution in a sloshing tank [1, 2]. Brizzolara et al. [3] compared experimental sloshing pressure data to various numerical models. Kusić et al. [4] simulated circular and rectangular tanks with fill levels of 67% and 95% of the tank height subject to seismic excitation. Kabiri et al. [5] simulated sloshing in a limited freeboard tank using the lattice Boltzmann method and validated this model with experimental data. Studies on the seismic design of storage tanks have resulted in several simplified numerical models created to account for tank ceiling impacts [6, 7]. These studies have focused on deeper tanks and forms of external excitations that are not typical for a structure-TLD system subjected to wind excitation.

Few studies have investigated the response of a limited freeboard TLD. Fujino et al. [8] completed free vibration tests on a circular TLD to determine the impact of limited freeboard on performance and suggested an optimal value of freeboard ranging from 1.0 to 1.5 times the fluid depth. Tait et al. [9] completed experimental testing on a structure-limited freeboard system with a rectangular TLD and found that the TLD performance was reduced when freeboard was less than 50% of the water depth. Numerical modelling of a limited freeboard TLD is necessary to broadly study the performance of the system. Most numerical methods previously applied to modelling a TLD are not capable of capturing the response when ceiling impact occurs without assumptions about the physical behavior. Faltinsen and Rognebakke [10] presented a multi-modal method capable of accounting for ceiling impact. A linear damping term was introduced based on the energy dissipated by the sloshing water hitting the ceiling each cycle. A slamming-based analogy was used to calculate the energy dissipation. There are limits to the applicability of this model depending on tank geometry and TLD water depth.

More robust computational fluid dynamics methods can account for the ceiling impact directly. The smoothed particle hydrodynamics (SPH) method is particularly attractive for modelling a TLD with ceiling impact, as it is inherently capable of handling complex free surface phenomena. SPH is a Lagrangian meshless method that discretizes the fluid using many particles. Several previous studies have investigated the response of a TLD using SPH. Marsh et al. [11] used a weakly compressible SPH model to study the behavior of TLDs. Green and Peiró [12] modelled a rectangular tank with the same properties as a shallow TLD studied by Reed et al. [13]. Kashani et al. [14] used an incompressible SPH model to capture the response of a TLD with screens and determined equivalent properties for a linearized TMD model. The screen geometry was modelled explicitly using particles. Halabian et al. [15] coupled a weakly compressible SPH model to a multi-degree-of-freedom structural model to study the system response when subjected to seismic loading. McNamara et al. [16] presented and validated an incompressible SPH model for a TLD with screens that were modelled macroscopically using a Morison equation-based force term. This implementation allowed for a greater initial particle spacing compared to

previous studies. McNamara and Tait [17] investigated the response of a structure-TLD system undergoing large amplitude excitation using SPH and found good agreement with experimental data.

This study numerically investigates the response of a structure-TLD system when the tank has limited freeboard. The novelty of this work is the completion of an extensive assessment of the system response and performance, which has not been considered in previous studies to the knowledge of the authors. The structure is modelled using modal analysis as an equivalent linear single degree of freedom system, and the TLD is represented by a 2D incompressible SPH model. The SPH model is validated for a sloshing tank with ceiling impact using experimental data from Faltinsen and Rognebakke [10]. A total of 63 structure-TLD system simulations are completed. The structure-TLD system is subject to a four-hour duration band-limited white noise force excitation representative of wind loading. Seven different RMS force levels are considered with nine different tank freeboards. The response and performance of the structure TLD system is discussed with specific focus on the effects of limited freeboard. A linearized equivalent mechanical model intended for preliminary feasibility studies of limited freeboard TLDs is presented. The mechanical model structural response is compared to the SPH results.

5.2 Structure – Tuned Liquid Damper Model

Figure 5.1 shows a schematic of the structure-TLD system considering both unlimited and limited freeboard TLDs. The TLD tank in this study is defined by a length L, breadth b, height H, and water depth h, with damping screens located at 40% and 60% of the tank length. The TLD response is described numerically using a two-dimensional incompressible SPH model. The two-dimensional model represents a slice of the three-dimensional TLD. The tank breadth is accounted for in the TLD forces by multiplying the calculated values by b. The response of the liquid in the TLD is described by the Lagrangian form of the incompressible Navier-Stokes equations:

$$\frac{D\rho}{Dt} + \rho\nabla\boldsymbol{u} = 0 \tag{5.1}$$

$$\frac{D\boldsymbol{u}}{Dt} = -\frac{1}{\rho}\nabla P + v\nabla^2\boldsymbol{u} + \boldsymbol{g} \tag{5.2}$$

where ρ is the fluid density, $\boldsymbol{u}$ is the fluid velocity vector, P is the fluid pressure, v is the fluid kinematic viscosity, and $\boldsymbol{g}$ is the external force vector, which included gravity.

The Navier-Stokes equations are discretized by a series of particles covering the domain of the fluid and boundaries. The particles are initially spaced at a distance *dp*. A smoothing kernel function is used to calculate the properties of each particle based on its surrounding neighbours. For this study, the fifth order Wendland kernel is used [18]:

$$W(q) = W_c \begin{cases} (1+2q)\left(1-\frac{q}{2}\right)^4 & 0 \le q \le 2 \\ 0 & q > 2 \end{cases} \tag{5.3}$$

where $q = \frac{|r_i - r_j|}{h_{ker}}$, $W_c = \frac{7}{\pi h_{ker}^2}$, and h_{ker} is the smoothing length, equal to 1.4*dp* for all cases. The first order divergence terms are discretized based on Monaghan [19], and the Laplacian operator is discretized based on Cummins and Rudman [20].

The discretized Navier-Stokes equations are integrated in time by applying a two-step projection method [20]. Intermediate particle velocities $\boldsymbol{u}^*$ and positions $\boldsymbol{r}^*$ are calculated based on the viscous and body force terms in equation **(5.2)**:

$$\boldsymbol{u}^* = \boldsymbol{u}(t) + \left(v\nabla^2\boldsymbol{u} + \boldsymbol{g} + \ddot{\boldsymbol{X}} + \boldsymbol{F}_{\boldsymbol{screen}}\right)\Delta t \tag{5.4}$$

$$\boldsymbol{r}^* = \boldsymbol{r}(t) + \boldsymbol{u}^*\Delta t \tag{5.5}$$

where $\ddot{\boldsymbol{X}} = [\ddot{X}, 0]$ is the acceleration vector of the structure at the TLD location determined using equation **(5.9)**, and $\boldsymbol{F}_{\boldsymbol{screen}}$ is the force from the damping screens, which is calculated based on McNamara et al. [16].

Pressure of the fluid particles is determined by an explicit approach to solving the pressure Poisson equation from Yeylaghi et al. [21]. An additional pressure stabilizing term presented by Jiang et al. [22] is included, which balances maintaining a divergence-free velocity field and density-invariant conditions for incompressibility. With the calculated pressure values, the particle velocity and position are updated at the end of the timestep:

$$\boldsymbol{u}(t+\Delta t) = \boldsymbol{u}^{*} + \left(-\frac{1}{\rho}\boldsymbol{\nabla} P\right)\Delta t \tag{5.6}$$

$$\boldsymbol{r}(t+\Delta t) = \boldsymbol{r}(t) + \left(\frac{\boldsymbol{u}(t+\Delta t) + \boldsymbol{u}(t)}{2}\right)\Delta t \tag{5.7}$$

Boundary particles representing the TLD tank walls are modelled based on Adami et al. [23]. The boundary particles do not move throughout the simulation. Pressure is solved for each boundary particle to prevent penetration of the fluid particles, and a boundary velocity is calculated to provide a free slip condition at the fluid-boundary interface. The free surface pressure boundary condition is applied at each time step by identifying the free surface particles using a numerical density based on Yeylaghi et al. [21].

The force generated by the water in the TLD is calculated based on solving the momentum equation for the wall boundary particles in the x-direction and multiplying by their mass [24]:

$$F_{TLD} = b\sum_{j} m_j \left(-\sum_{f} m_f \left(\frac{P_f}{\rho_f^2} + \frac{P_j}{\rho_j^2}\right)\nabla_f W_{jf} + \sum_{f} \nu\rho_f \left(\frac{8m_f}{(\rho_f+\rho_j)^2}\frac{(u_j-u_f)\boldsymbol{r_{jf}}.\boldsymbol{\nabla_j} W_{jf}}{r_{jf}^2+\eta^2}\right) + \ddot{X}\right) \tag{5.8}$$

where m_j is the particle mass, u_j is the horizontal velocity, $\boldsymbol{r_{jf}} = \boldsymbol{r_j} - \boldsymbol{r_f}$ is the position vector, $r_{jf} = |r_j - r_f|$ is the distance between particles, and η is a small value to ensure a nonzero denominator. The summation of j is over the vertical wall boundary particles at each end of the tank and the summation of f is over the neighbouring fluid particles. The boundary particles have the same mass as the fluid particles. The force is multiplied by the

tank breadth *b* to account for the third dimension of the TLD that is modelled as a unit width in SPH.

The SPH model of the TLD is coupled to a structure represented as a single degree of freedom system using modal analysis. The equation of motion for the structure is defined by:

$$M_s\ddot{X} + C_s\dot{X} + K_sX = F_{ext} + F_{TLD} \quad \textbf{(5.9)}$$

where M_s is the generalized mass, C_s is the generalized damping, and K_s is the generalized stiffness of the structure. X is the structural displacement. F_{ext} is the external applied force, and F_{TLD} is the TLD tank force from equation **(5.8)**. The structural response is integrated in time using the 4th order Runge-Kutta-Gill method. At each timestep the structure-TLD system response is solved using a substructuring method, where the structural response is calculated according to equation **(5.9)**. The resulting structural acceleration $\ddot{X}$ is passed to the SPH model as a base acceleration of the tank in equation **(5.4)**. The SPH model then calculates the TLD response and returns the TLD force F_{TLD} to be applied to the structure at the next timestep.

5.2.1 SPH Model Validation

The SPH model performance was previously validated with experimental data for screen-equipped TLDs in McNamara et al. [16] and structure-TLD systems in McNamara and Tait [17]. The TLD in these studies had unlimited freeboard, and thus no ceiling impact occurred. Faltinsen and Rognebakke [10] presented experimental data for free surface elevations in a sloshing water tank undergoing horizontal harmonic excitation where ceiling impact occurred. The experimental data is used to evaluate the SPH model when there is ceiling impact. The tank had dimensions of length 1.73 m and height 1.02 m. This sloshing tank was modelled in SPH using an initial particle spacing of 0.01 m and a timestep of $5\text{x}10^{-4}$ seconds. The free surface elevation was measured near the tank end wall.

Figure 5.2 shows the free surface elevation normalized by the water depth for two representative cases. Figure 5.2(a) corresponds to a water depth of 0.60 m (*h/L* = 35%),

excitation amplitude of 0.032 m, and excitation frequency of 1.11 times the fundamental sloshing frequency of the tank. For this case ceiling impact occurs only in select cycles. The SPH model results are in good agreement with the experimental data. Figure 5.2(b) corresponds to a water depth of 0.50 m (h/L = 29%), excitation amplitude of 0.05 m, and excitation frequency of 1.03 times the fundamental sloshing frequency of the tank. Following the first two cycles, repeated ceiling impacts occur. The SPH model appears to slightly under-predict the duration of the ceiling impact, as evidenced by the narrower flat region corresponding to the water contacting the ceiling at the wave measurement location. However, the overall agreement between the SPH model and experimental data is very good.

Figure 5.3 shows the SPH particle positions during ceiling impact from the second case. The fluid particles are well contained by the boundary particles and fill the top corner of the tank upon impact without any unphysical gaps. Based on these results, the SPH model is able to capture the dynamics of sloshing fluid in a tank with ceiling impact.

5.3 Model Setup and Parameters

This section details the model setup and parameters investigated in this study. The structure generalized properties were M_s = 4480 kg, C_s = 31 Ns/m (ζ_s = 0.1%) and K_s = 55.1 kN/m, corresponding to a natural frequency f_s = 0.558 Hz. The TLD dimensions were L = b = 0.966 m, with a fluid depth h = 0.119 m, corresponding to a natural frequency of 0.546 Hz. Damping screens with screen loss coefficient C_l = 2.16 were located at 40% and 60% of the tank length. The structure-TLD system has a mass ratio μ = 1.9%, and a tuning ratio Ω = 98%, which is near optimal for this system according to optimal design formulae [25]. The available freeboard in the tank is defined as $G = H - h$ and will be normalized by the fluid depth G/h for presentation herein. In addition to the unlimited freeboard case with no tank ceiling ($G/h = \infty$), eight values of limited freeboard were studied ranging from G/h = 0.10 to 1.0. The structure-TLD system was subject to a four-hour duration band-limited white noise force with frequency content ranging from 0.2 to 1.2 Hz. Due to the amplitude dependent damping in a TLD, there is a value of root-mean-square (RMS) excitation force

that results in optimal TLD damping. This value is denoted as $\sigma_F^{(opt)}$, and for this study was equal to 52.4 N. Seven RMS excitation force values were studied with normalized values $\sigma_F' = \sigma_F/\sigma_F^{(opt)}$ ranging from 0.25 to 4.25.

The TLD was discretized in the SPH model using an initial particle spacing *dp* of 7 mm, resulting in a total of 2346 fluid particles. The screens were represented by dummy particles discretized with the same initial particle spacing, and a kernel function radius h_{ker} equal to three times that of the fluid particles based on McNamara et al. [16]. The number of boundary particles and screen particles were dependent on the tank height for a given case. The time step used in all cases was equal to $5x10^{-4}$ seconds. The time domain results, such as structural displacement or TLD wave height, were output every 100 timesteps (0.05 seconds). Each simulation took approximately 260 hours of computational time, which is a result of the long duration of the simulation and the current serial implementation of the code.

5.4 Structure – TLD System Response

5.4.1 Result Normalization

It is first necessary to define the quantities that are used to evaluate the structure-TLD system response. The simplest key performance indicators for a structure-TLD system subject to a random force excitation are the root-mean-squared (RMS) and peak values of the system responses (i.e. structural displacement, TLD wave height). To remove the influence of transients the first ten minutes of the simulation are ignored, and the RMS and peak values are determined from the remaining signal.

The mechanical admittance function (MAF) of a structure defines the relationship between excitation force and structural response for each frequency in a random signal. A TLD operates by modifying the MAF of the structure to which it is attached. The squared modulus of the MAF for the structure studied can be defined by [26]:

$$|H_s(f)|^2 = \frac{S_{XX}(f)K_s^2}{S_{FF}(f)} \tag{5.10}$$

where $S_{FF}(f)$ and $S_{XX}(f)$ are the spectra of the applied force and structural displacement, respectively.

The effective damping can be used to quantify the performance of a TLD. It is defined as the amount of damping the uncontrolled structure requires to achieve the same response level as the TLD equipped structure. It can be calculated from the expression [27]:

$$\zeta_{eff} = \zeta_s \frac{\sigma_x^2}{\sigma_{x-damped}^2} \tag{5.11}$$

where ζ_s is the structural damping ratio (0.1% in this study), σ_x is the RMS structural displacement without the TLD, and $\sigma_{x\text{-}damped}$ is the RMS structural response with the TLD.

Finally, to compare the performance of a TLD with limited freeboard to the same TLD with unlimited freeboard, a TLD freeboard efficiency factor is defined:

$$\Psi_{FB} = \frac{\zeta_{eff}^{(G/h)}}{\zeta_{eff}^{(\infty)}} \tag{5.12}$$

where $\zeta_{eff}^{(G/h)}$ is the effective damping for a structure-TLD system with limited freeboard G/h, and $\zeta_{eff}^{(\infty)}$ is the effective damping for a structure-TLD system with unlimited freeboard ($G/h = \infty$). When $\Psi_{FB} = 1$, the motion reduction performance of the limited freeboard TLD is the same as that of the unlimited freeboard TLD. When $\Psi_{FB} < 1$, the performance of the TLD is reduced by the limited available freeboard.

5.4.2 Root-Mean-Square and Peak Responses

The TLD wave height was measured at $x/L = 0.05$ and $x/L = 0.50$, capturing the response near the tank end wall and the mid-tank, respectively. Figure 5.4 shows the peak wave height measured for each simulation. The tank ceiling limits the maximum possible wave height and is indicated by the dashed line. When σ_F' increases, the wave height in the

TLD also increases, as does the number of simulations in which ceiling impact occurs. For the wave height measured at the tank wall (Figure 5.4(a)), when $\sigma_F' = 0.25$ (the smallest value studied), ceiling impact only occurs at $G/h = 0.10$, whereas when $\sigma_F' = 4.25$ (the largest value studied), ceiling impact occurs for every limited freeboard case considered. In several cases, ceiling impact occurs at the mid-tank as well (Figure 5.4(b)), though this is less frequent.

Figure 5.5 shows the RMS and peak values of structural displacement for each case studied. The values are normalized by the results from the unlimited freeboard case when $G/h = \infty$. When $\sigma_F' < 1.00$ there is limited ceiling impact, and the structural response is insensitive to limiting the TLD freeboard. When $\sigma_F' \geq 1.00$, the structural response for the limited freeboard TLD is greater than the unlimited freeboard TLD. For $G/h \geq 0.50$, the normalized structural response was approximately one for all values of σ_F', indicating that either ceiling impact did not occur, or the occurrence did not lead to a significant change to the structural response. When $G/h < 0.50$, the structural response for the limited freeboard TLD can be up to three times larger than the unlimited freeboard TLD. The ratios of limited to unlimited freeboard structural displacement are similar for the RMS and peak values, indicating that the effects of limited freeboard are comparable for both.

5.4.3 Freeboard Influence on Structure Response

Figure 5.6 displays the squared mechanical admittance function (MAF) for $\sigma_F' = 1.00$ and 1.90. Each plot displays four freeboard values, $G/h = 0.10$, 0.20, 0.50, and ∞ (unlimited). The unlimited freeboard curve shown in Figure 5.6(a) corresponds to the optimal TLD performance case, with optimal damping and no effects from ceiling impact. Reducing the freeboard to $G/h = 0.50$ does not significantly change the MAF, and when $G/h = 0.20$ there is only a slight change in the curve. However, when $G/h = 0.10$, the curve has transitioned from a double peak to a single peak. Figure 5.6(b) shows the MAF for $\sigma_F' = 1.90$. When $\sigma_F' > 1$, the amplitude dependent TLD damping is greater than the optimal value, and the system performance is slightly reduced. As in the previous case, reducing the freeboard to $G/h = 0.50$ does not significantly change the MAF. There is a more

noticeable change when G/h = 0.20, and the MAF clearly shows a dramatically different response consisting of a single, larger peak when G/h = 0.10. Both cases demonstrate that the TLD is not performing effectively when freeboard is very limited, however the value of G/h at which the system response changes significantly is dependent on the excitation amplitude, σ_F'.

Figure 5.7(a) shows the effective damping of the structure-TLD system, computed using equation **(5.11)**, as a function of G/h. The decrease in effective damping quantifies the reduction in TLD performance when freeboard is limited. The effective damping is nearly constant when $G/h \geq 0.50$ for all values of σ_F'. When $\sigma_F' < 1.00$, the effective damping remains constant or even slightly increases as freeboard is reduced. The small increase is likely attributed to additional damping obtained when the water impacts the ceiling, which increases the TLD damping towards optimal when $\sigma_F' < 1.00$. When $\sigma_F' \geq 1.00$ and $G/h < 0.50$, the effective damping decreases due to there being more than optimal TLD damping. The most significant decrease is observed when G/h reduces from 0.20 to 0.10.

Figure 5.7(b) shows the TLD freeboard efficiency ratio for each case considered. For $G/h > 0.50$ the limited freeboard TLD is as effective as the unlimited freeboard case for all excitation amplitudes (Ψ_{FB} approximately 1). For $G/h < 0.50$ the effectiveness of the TLD is reduced, with a minimum Ψ_{FB} value of 0.11 corresponding to the largest excitation case of $\sigma_F' = 4.25$. This shows that for the range of excitation amplitudes considered, the worst-case limited freeboard TLD effectiveness is only 11% of the unlimited freeboard TLD, which is a significant reduction.

5.4.4 Time Domain Response

Looking at the structure-TLD system response in the time domain allows for direct observation of the impact of freeboard on the response. This section will present portions of the time domain response for the unlimited freeboard case ($G/h = \infty$) and the smallest freeboard studied (G/h = 0.10), which will be referred to as the limited freeboard case.

Response histories for σ_F' = 1.00 and 1.90 are presented, corresponding to the same cases shown in Figure 5.6. A one-minute segment occurring between time = 5000 and 5060 seconds is presented. The responses are normalized by σ_F/K_s.

Figure 5.8 shows the response for σ_F' = 1.00. In this case there are several cycles where ceiling impact occurs. The responses are generally in-phase between the two cases, however there are differences between the peak values each cycle. In some cycles the displacement of the structure with the limited freeboard TLD is less than the unlimited freeboard TLD. It is postulated that minor additional damping provided by waves impacting the ceiling may reduce the structural response for some cycles. However, the displacement of the structure with the unlimited freeboard TLD is overall less than with the limited freeboard TLD. Figure 5.9 shows the response for σ_F' = 1.90. In this case ceiling impact occurs during almost every cycle. The amount that the wave height is limited by the tank ceiling varies, however with a few exceptions the structure displacement cycle amplitudes are greater for the limited freeboard case than the unlimited freeboard case. In some cycles, the limited freeboard structural displacement is out of phase with the unlimited freeboard displacement.

5.5 Equivalent Mechanical Model for Structure Response

The development of simplified numerical models is important for preliminary TLD design and feasibility studies. Due to the complexity of the SPH method and associated computational requirements, the model presented would not be used for preliminary studies. This section describes a simplified linearized mechanical model of the structure-TLD system where the TLD damping is modified to account for limited freeboard.

Tait [28] presented a procedure for preliminary design of a structure-TLD system using an equivalent linearized mechanical model resulting in a two degree of freedom spring-mass-dashpot system. The response of the system subjected to a force excitation *F(t)* can be described by the equations of motion:

$$\begin{bmatrix} (M_S' + m_{eq}) & m_{eq} \\ m_{eq} & m_{eq} \end{bmatrix} \begin{Bmatrix} \ddot{X} \\ \ddot{x}_r \end{Bmatrix} + \begin{bmatrix} C_s & 0 \\ 0 & c_{eq} \end{bmatrix} \begin{Bmatrix} \dot{X} \\ \dot{x}_r \end{Bmatrix} + \begin{bmatrix} K_s & 0 \\ 0 & k_{eq} \end{bmatrix} \begin{Bmatrix} X \\ x_r \end{Bmatrix} = \begin{Bmatrix} F(t) \\ 0 \end{Bmatrix} \quad \textbf{(5.13)}$$

where m_{eq}, c_{eq}, and k_{eq} are the equivalent TLD mass, stiffness, and damping, C_s and K_s are the structure damping and stiffness, and $M'_S = M_s + m_w - m_{eq}$, where M_s is the structure mass and m_w is the total water mass in the TLD. X is the structure response, and x_r is the equivalent TLD response variable defined by:

$$x_r = \Gamma q = \frac{4}{\pi} \tanh\left(\frac{\pi h}{L}\right) q \quad \textbf{(5.14)}$$

where Γ is a modal participation factor and q is the wave height measured at the TLD tank wall. Full details on the definitions of these terms are provided by Tait [28].

Equation **(5.13)** can be solved in the frequency domain. The structure-TLD mass ratio is defined as $\mu = m_{eq}/M'_s$. To determine the MAF of the coupled system, the structure and equivalent TLD responses are assumed to be of the form $X(t) = H_S(\omega)exp(i\omega t)$ and $x_r(t) = H_r(\omega)exp(i\omega t)$, where i is the imaginary number. H_S and H_r are complex frequency response functions defined by McNamara [29] as:

$$H_S(\omega) = \frac{-B_2\omega^2 + B_1 i\omega + B_0}{A_4\omega^4 - A_3 i\omega^3 - A_2\omega^2 + A_1 i\omega + A_0} \quad \textbf{(5.15)}$$

$$H_r(\omega) = \frac{B_2\omega^2}{A_4\omega^4 - A_3 i\omega^3 - A_2\omega^2 + A_1 i\omega + A_0} \quad \textbf{(5.16)}$$

$$A_0 = \omega_S^2 \omega_{TLD}^2$$

$$A_1 = 2\zeta_s \omega_s \omega_{TLD}^2 + 2\zeta_{TLD}\omega_S^2 \omega_{TLD}$$

$$A_2 = \omega_{TLD}^2 + 4\zeta_s\zeta_{TLD}\omega_s\omega_{TLD} + \omega_S^2 + \mu\omega_{TLD}^2 \quad \textbf{(5.17)}$$

$$A_3 = 2\zeta_{TLD}\omega_{TLD} + 2\zeta_S\omega_S + 2\mu\zeta_{TLD}\omega_{TLD}$$

$$A_4 = 1$$

$$B_0 = \omega_S^2 \omega_{TLD}^2$$

$$B_1 = 2\zeta_{TLD}\omega_s\omega_{TLD}^2 \quad \textbf{(5.18)}$$

$$B_2 = \omega_s^2$$

where ω_s is the structure's natural frequency including the non-sloshing fluid mass, ζ_s is the structural damping ratio, and ω_{TLD} is a nonlinear amplitude dependent TLD natural frequency from Cassolato et al. [30].

The TLD damping ratio, $\zeta_{TLD,}$ is calculated as:

$$\zeta_{TLD} = \zeta_w + \zeta_{eq} + \zeta_{FB} \quad \textbf{(5.19)}$$

where ζ_w and ζ_{eq} are the damping associated with liquid viscosity and the equivalent linearized amplitude dependent screen damping which are both defined in Tait (2008). ζ_{FB} is the additional damping due to limited freeboard which is introduced in Section 5.5.2.

The variance of the structure and equivalent TLD can be calculated as [29]:

$$\sigma_s^2 = S_0\pi\left(\frac{\frac{B_0^2}{A_0}(A_2A_3 - A_1A_4) + A_3(B_1^2 - 2B_0B_2) + A_1B_2^2}{A_1(A_2A_3 - A_1A_4) - A_0A_3^2}\right) \quad \textbf{(5.20)}$$

$$\sigma_r^2 = S_0\pi\left(\frac{A_1B_2^2}{A_1(A_2A_3 - A_1A_4) - A_0A_3^2}\right) \quad \textbf{(5.21)}$$

where S_0 is the spectral amplitude and the constants A_i and B_i are defined in equations **(5.17)** and **(5.18)**.

The RMS TLD wave height can then be calculated from:

$$\sigma_q = \Gamma\sigma_r \quad \textbf{(5.22)}$$

5.5.1 Limited Freeboard TLD Damping Evaluation

The SPH model results indicate that a TLD with limited freeboard may be less effective than its unlimited freeboard counterpart. Energy is dissipated in the TLD when the wave impacts the tank ceiling, which leads to an increase in the TLD damping ratio. This increased damping causes the TLD to become less effective at controlling structural motion. This section evaluates the damping ratio of the TLD with limited freeboard based on the SPH results.

The equivalent mechanical model only represents the fundamental sloshing mode. To remove the effects of higher sloshing modes from the TLD response, a lowpass filter is applied to the SPH wave height with a cut-off frequency equal to 1.5 times the TLD natural frequency. The resulting filtered wave response is denoted by $q_1(t)$. The structure acceleration and TLD wave height response histories can be used to evaluate the equivalent damping ratio of the fundamental sloshing mode using the methodology presented by Love and Tait [27]. First, the wave height response is differentiated numerically to obtain the fundamental mode velocity response, $\dot{q}_1(t)$. The equivalent damping ratio of the fundamental TLD sloshing mode can then be evaluated by the expression:

$$\zeta_1 = -\frac{\Gamma}{2\omega_{TLD}} \frac{E\left[\ddot{X}\dot{q}_1\right]}{E[\dot{q}_1^2]} \tag{5.23}$$

where ω_{TLD} is the fundamental sloshing frequency in rad/s, $E[\,]$ denotes the expected value, $\ddot{X}$ is the structural acceleration response, $\dot{q}_1$ is the fundamental sloshing mode velocity, and Γ is the modal participation factor defined by equation **(5.14)**.

Figure 5.10 shows the values of ζ_1 calculated by equation **(5.23)** from the SPH results for σ_F' = 0.50, 1.00, and 1.90. The damping ratio increases as the freeboard is reduced, verifying that the impact of the water with the tank ceiling is introducing additional energy dissipation to the TLD. The value of freeboard (*G/h*) where the damping begins to increase depends on the excitation force σ_F'.

The change in TLD damping associated with ceiling impact depends on the amount of freeboard (*G/h*) and the RMS of the band-limited excitation force (σ_F'). To incorporate these values into one parameter, the ratio $\hat{q}_1^{(\infty)}/G$ can be used, where $\hat{q}_1^{(\infty)}$ represents the average one-hour peak TLD wave height for the fundamental sloshing mode in an unlimited freeboard TLD, and G is the available tank freeboard. A value of $\hat{q}_1^{(\infty)}/G \geq 1$ indicates that the tank ceiling is constraining the first mode of sloshing in a limited freeboard case. It is common in wind engineering to consider peak values with an associated averaging time, for example the ten-minute or one-hour peak. The average one-hour peak TLD wave height $\hat{q}_1^{(\infty)}$ is determined by averaging the maximum value of $q_1(t)$ from each hour of the signal.

5.5.2 Calculation of ζ_{FB}

The additional TLD damping due to limited freeboard, ζ_{FB}, can be calculated from the SPH results by:

$$\zeta_{FB} = \zeta_1^{(G/h)} - \zeta_1^{(\infty)} \tag{5.24}$$

where $\zeta_1^{(\infty)}$ is the TLD damping for the unlimited freeboard case, and $\zeta_1^{(G/h)}$ is the TLD damping when freeboard is limited to *G/h*. Both values are calculated from the SPH results by equation **(5.23)**.

The energy dissipated by water impacting the tank ceiling is inherently incorporated into the SPH model. To allow the linearized mechanical model to capture the effects of limited freeboard, an equivalent freeboard damping parameter must be introduced. For cases where damping forces can not be easily calculated, it is convenient to approximate an equivalent viscous damping ratio. The following empirical relationship was determined for the additional damping due to freeboard:

$$\zeta_{FB} = \frac{1}{9\pi}\left(\frac{\hat{q}_1^{(\infty)}}{G} - 1\right) \tag{5.25}$$

This expression only applies when $\hat{q}_1^{(\infty)}/G \geq 1.00$, otherwise $\zeta_{FB} = 0$.

Figure 5.11 shows the calculated values of ζ_{FB} from the SPH results as well as the empirical fit. The fit shows good agreement with the SPH results. When $\hat{q}_1^{(\infty)}/G \leq 1.00$, the freeboard damping from the SPH results is either zero or very small, indicating that when the fundamental sloshing mode does not impact the tank ceiling, there is limited additional TLD damping due to limited freeboard. That is, even if some liquid impacts the tank ceiling, the TLD performance is not significantly affected unless the amplitude of the fundamental sloshing mode exceeds the tank freeboard. As $\hat{q}_1^{(\infty)}/G$ increases above 1.00, ζ_{FB} increases due to the additional damping from ceiling impacts. The values of ζ_{FB} show a correlation with $\hat{q}_1^{(\infty)}/G$. This indicates that the change in TLD damping is proportional to the amount that the fundamental mode of sloshing is constrained by the tank ceiling.

To incorporate the additional freeboard damping into the mechanical model, it is necessary to determine the 1-hour peak TLD wave height for the unlimited freeboard case, $\hat{q}_1^{(\infty)}$. The unlimited freeboard RMS wave height, $\sigma_q^{(\infty)}$, can be calculated directly by equation **(5.22)**. A peak factor is commonly used in wind engineering to relate the RMS and peak response values:

$$\hat{q}_1^{(\infty)} = PF\sigma_q^{(\infty)} \tag{5.26}$$

where *PF* is the peak factor. The peak factor for wind loading typically falls within the range of 2 to 4 for a one-hour averaging time. The average peak factor from the SPH model results with unlimited freeboard was 3.11. For this investigation, a value of *PF* = 3.0 was used. When SPH results are unavailable, the peak factor can be calculated using the frequency domain methodology from Love and Tait [31] or a suitable nonlinear TLD model. Thus, the TLD freeboard damping in the mechanical model is calculated as:

$$\zeta_{FB} = \frac{1}{9\pi}\left(\frac{PF\sigma_q^{(\infty)}}{G} - 1\right) = \frac{1}{9\pi}\left(\frac{3\sigma_q^{(\infty)}}{G} - 1\right) \tag{5.27}$$

5.5.3 Equivalent Mechanical Model Results

To evaluate the mechanical model with the incorporation of limited freeboard, three levels of excitation force, σ_F' = 1.00, 1.50, and 1.90, and three freeboard levels G/h = 0.15, 0.20, and ∞ were considered. The equivalent mechanical model is not expected to accurately capture the wave height response of the TLD, as it does not directly account for the impact of limited freeboard on the wave forms. The wave height is less critical to calculate when the level of freeboard is prescribed as a constraint. By incorporating the overall behavior of the structure-limited freeboard TLD system, the model is intended to produce a suitable preliminary result for the response of the structure, allowing the model to be applied to initial design or feasibility studies.

Figure 5.12 shows the structure frequency response function determined by the mechanical model and SPH results. The mechanical model shows good agreement with the SPH model results for all cases. The RMS structural displacements are compared between the mechanical model and SPH results in Table 5.1. For all cases considered, the mechanical model slightly under-predicts the RMS structural displacement compared to the SPH results. The maximum relative error between the mechanical model and SPH results is -6%.

Figure 5.13 shows the TLD damping ratio ζ_1 calculated by the mechanical model (equation **(5.19)**) and evaluated from the SPH results (equation **(5.23)**). When the freeboard is significantly limited (G/h = 0.10) the equivalent mechanical model under-predicts the TLD damping. Overall, the mechanical model results show very good agreement with the SPH values. This indicates that the mechanical model is capturing the overall energy dissipation of the limited freeboard TLD.

The equivalent mechanical model shows good agreement with the SPH model results for the structure-TLD system studied. The mechanical model is intended only to provide a preliminary understanding of the performance of a limited freeboard TLD. For detailed TLD design with limited freeboard it would be necessary to use the SPH model or some other method capable of directly capturing the ceiling impact.

5.6 Conclusions

The response of a structure-limited freeboard TLD system was studied numerically by coupling an equivalent linear single degree of freedom structure to a TLD using a 2D incompressible SPH model. The SPH model was validated for a limited freeboard tank using experimental data from Faltinsen and Rognebakke [10]. The structure was subjected to a four-hour band-limited white noise excitation with a range of intensities. A total of 63 simulations were completed. An equivalent linearized mechanical model for the structure-limited freeboard TLD system was presented, including a calculation of the additional TLD damping provided by ceiling impact. Several conclusions can be made from the results of this study:

1. The limited freeboard TLD was less effective at reducing structural motion than the unlimited freeboard TLD. The displacement of the structure with a limited freeboard TLD was up to three times that of the structure with an unlimited freeboard TLD when considering both the RMS and peak values.
2. When TLD freeboard was significantly limited, the structural mechanical admittance function transitioned from a double peaked response to a single peak. This corresponded with a decrease in effective damping and reduction in TLD effectiveness. At the extreme, the effectiveness of the limited freeboard TLD was found to be only 11% of the unlimited freeboard TLD.
3. The limited freeboard TLD was demonstrated to be comparably effective to the unlimited freeboard TLD in cases when the fundamental sloshing mode was not constrained by the presence of the tank ceiling. When the fundamental sloshing mode was constrained by the tank ceiling, additional damping achieved from ceiling impact led to a reduction in TLD effectiveness.
4. The equivalent mechanical model including damping from limited TLD freeboard showed good agreement with the SPH model results. The calculated RMS structural displacement was within 6% of the SPH model results. The equivalent mechanical model captured the overall TLD damping well when $G/h > 0.10$ for the system studied.

This paper has numerically studied the reduction in TLD effectiveness when freeboard is reduced. For cases where limited space is available for a TLD, it may not be possible to provide the required freeboard to avoid sloshing wave impacts with the tank ceiling. The equivalent mechanical model can be used preliminarily to assess the feasibility of a limited freeboard TLD in these scenarios. To capture the full structure-TLD response, the SPH model should be used, however this requires significant computational effort. This study investigated a single structure-TLD system. Further research looking at the impact of other system parameters, such as TLD depth ratio (h/L) and structure-TLD mass ratio (μ) is required to generalize the results of this study broadly to limited freeboard TLDs. The SPH model presented can be easily applied to these scenarios.

5.7 Acknowledgment

The authors are thankful for the financial support provided by the Natural Sciences and Engineering Research Council of Canada (NSERC) and the Ontario Graduate Scholarship (OGS) program. This research was enabled in part by computing support provided by Compute Ontario (www.computeontario.ca) and Compute Canada (www.computecanada.ca).

5.8 References

[1] H. Akyildiz and E. Ünal, "Experimental investigation of pressure distribution on a rectangular tank due to the liquid sloshing," *Ocean Engineering,* vol. 32, pp. 1503-1516, 2005.

[2] F. Pistani and K. Thiagarajan, "Experimental measurements and data analysis of the impact pressures in a sloshing experiment," *Ocean Engineering,* vol. 52, pp. 60-74, 2012.

[3] S. Brizzolara, L. Savio, M. Viviani, Y. Chen, P. Temarel, N. Couty, S. Hoflack, L. Diebold, N. Moirod and A. Souto Iglesias, "Comparison of experimental and numerical sloshing loads in partially filled tanks," *Ships and Offshore Structures,* vol. 6, no. 1-2, pp. 15-43, 2011.

[4] M. S. Kusic, J. Radnic, N. Grgic and A. Harapin, "Sloshing in medium size tanks caused by earthquake studied by SPH," *Građevinar,* vol. 70, no. 8, pp. 671-684, 2018.

[5] M. M. Kabiri, M. R. Nikoomanesh, P. N. Danesh and M. A. Gourdarzi, "Numerical and Experimental Evaluation of Sloshing Wave Force Caused by Dynamic Loads in Liquid Tanks," *ASME Journal of Fluids Engineering,* vol. 141, no. 11, pp. 1-24, 2019.

[6] P. K. Malhotra, "Sloshing loads in liquid-storage tanks with insufficient freeboard," *Earthquake Spectra,* vol. 21, no. 4, pp. 1185-1192, 2005.

[7] M. A. Goudarzi, S. R. Sabbagh-Yazdi and W. Marx, "Seismic analysis of hydrodynamic sloshing force on storage tank roofs," *Earthquake Spectra,* vol. 26, no. 1, pp. 131-152, 2010.

[8] Y. Fujino, B. Pacheco, P. Chaiseri and L. M. Sun, "Parametric Studies on Tuned Liquid Damper (TLD) Using Circular Containers by Free-Oscillation Experiments," *Structural Engineering/Earthquake Engineering,* vol. 5, no. 2, pp. 381-391, 1988.

[9] M. J. Tait, N. Isyumov and A. A. El Damatty, "Tuned Liquid Dampers to Mitigate Wind-Induced Motions of Buildings," in *Structures Congress*, 2006.

[10] O. M. Faltinsen and O. F. Rognebakke, "Sloshing and slamming in tanks," in *Hydronav'99-Manouevring'99*, Gdansk-Ostrada, Poland, 1999.

[11] A. Marsh, M. Prakash, E. Semercigil and O. F. Turan, "A study of sloshing absorber geometry for structural control with SPH," *Journal of Fluids and Structures,* vol. 27, no. 8, pp. 1165-1181, 2011.

[12] M. D. Green and J. Peiro, "Long duration SPH simulations of sloshing in tanks with a low fill ratio and high stretching," *Computers and Fluids,* vol. 174, pp. 179-199, 2018.

[13] D. Reed, J. Yu, H. Yeh and S. Gardarsson, "Investigation of Tuned Liquid Dampers Under Large Amplitude Excitation," *Journal of Engineering Mechanics,* vol. 124, no. 4, pp. 405-413, 1998.

[14] A. H. Kashani, A. M. Halabian and K. Asghari, "A numerical study of tuned liquid damper based on incompressible SPH method combined with TMD analogy," *Journal of Fluids and Structures,* vol. 82, pp. 394-411, 2018.

[15] A. M. Halabian, A. Karamnasab and M. R. Chamani, "A New Hybrid SPH-FEM Model to Evaluate Seismic Response of TSD Equipped-Structures," *Journal of Earthquake and Tsunami,* vol. 13, no. 2, pp. 1-27, 2019.

[16] K. P. McNamara, B. N. Awad, M. J. Tait and J. S. Love, "Incompressible smoothed particle hydrodynamics model of a rectangular tuned liquid damper containing screens," *Journal of Fluids and Structures,* vol. 103, p. 103295, 2021.

[17] K. P. McNamara and M. J. Tait, "Modelling the response of structure-tuned liquid damper systems under large amplitude excitation using SPH," *Journal of Vibration and Acoustics,* vol. 144, p. 011008, 2022.

[18] H. Wendland, "Piecewise polynomial, positive definite and compactly supported radial functions of minimal degree," *Advances in Computational Mathematics,* vol. 4, pp. 389-396, 1995.

[19] J. J. Monaghan, "Smoothed Particle Hydrodynamics," *Annual Review of Astronomy and Astrophysics,* vol. 30, pp. 543-74, 1992.

[20] S. J. Cummins and M. Rudman, "An SPH Projection Method," *Journal of Computational Physics,* vol. 152, pp. 584-607, 1999.

[21] S. Yeylaghi, B. Moa, P. Oshkai, B. Buckham and C. Crawford, "ISPH modelling of an oscillating wave surge converter using an OpenMP-based parallel approach," *Journal of Ocean Engineering and Marine Energy,* vol. 2, pp. 301-312, 2016.

[22] H. Jiang, Y. You, Z. Hu, X. Zheng and A. Ma, "Comparative study on violent sloshing withwater jet flows by using the ISPH method," *Water (Switzerland),* vol. 11, p. 2590, 2019.

[23] S. Adami, X. Y. Hu and N. A. Adams, "A generalized wall boundary condition for smoothed particle hydrodynamics," *Journal of Computational Physics,* vol. 231, no. 21, pp. 7057-7075, 2012.

[24] M. D. Green, *Sloshing simulations with the smoothed particle hydrodynamics (SPH) method,* PhD Thesis, Imperial College London, 2017.

[25] G. B. Warburton, "Optimum absorber parameters for various combinations of response and excitation parameters," *Earthquake Engineering and Structural Dynamics,* vol. 10, pp. 381-401, 1982.

[26] M. J. Tait, N. Isyumov and A. A. El Damatty, "Performance of Tuned Liquid Dampers," *Journal of Engineering Mechanics,* vol. 134, no. 5, pp. 417-427, 2008.

[27] J. S. Love and M. J. Tait, "Estimating the added effective damping of SDOF systems incorporating multiple dynamic vibration absorbers with nonlinear damping," *Engineering Structures,* vol. 130, pp. 154-161, 2017.

[28] M. J. Tait, "Modelling and preliminary design of a structure-TLD system," *Engineering Structures,* vol. 30, no. 10, pp. 2644-2655, 2008.

[29] R. J. McNamara, "Tuned Mass Dampers for Buildings," *ASCE Journal of the Structural Division,* vol. 103, no. 9, pp. 1785-1798, 1977.

[30] M. R. Cassolato, J. S. Love and M. J. Tait, "Modelling of a tuned liquid damper with inclined damping screens," *Structural Control and Health Monitoring,* vol. 18, pp. 674-681, 2011.

[31] J. S. Love and M. J. Tait, "Frequency domain prediction of peak nonlinear wave heights of structure-TLD systems," *Engineering Structures,* vol. 194, pp. 1-10, 2019.

Table 5.1: RMS Structure Displacements (in mm) from SPH and Equivalent Mechanical Model

	SPH			**Mech. Model**			**% Error**		
G/h σ'_F	**0.15**	**0.20**	∞	**0.15**	**0.20**	∞	**0.15**	**0.20**	∞
1.00	3.42	3.39	3.37	3.37	3.35	3.35	-1.4%	-1.3%	-0.6%
1.50	5.30	5.15	5.02	5.11	5.02	4.97	-3.6%	-2.7%	-1.1%
1.90	7.41	7.01	6.71	6.97	6.79	6.62	-6.0%	-3.1%	-1.3%

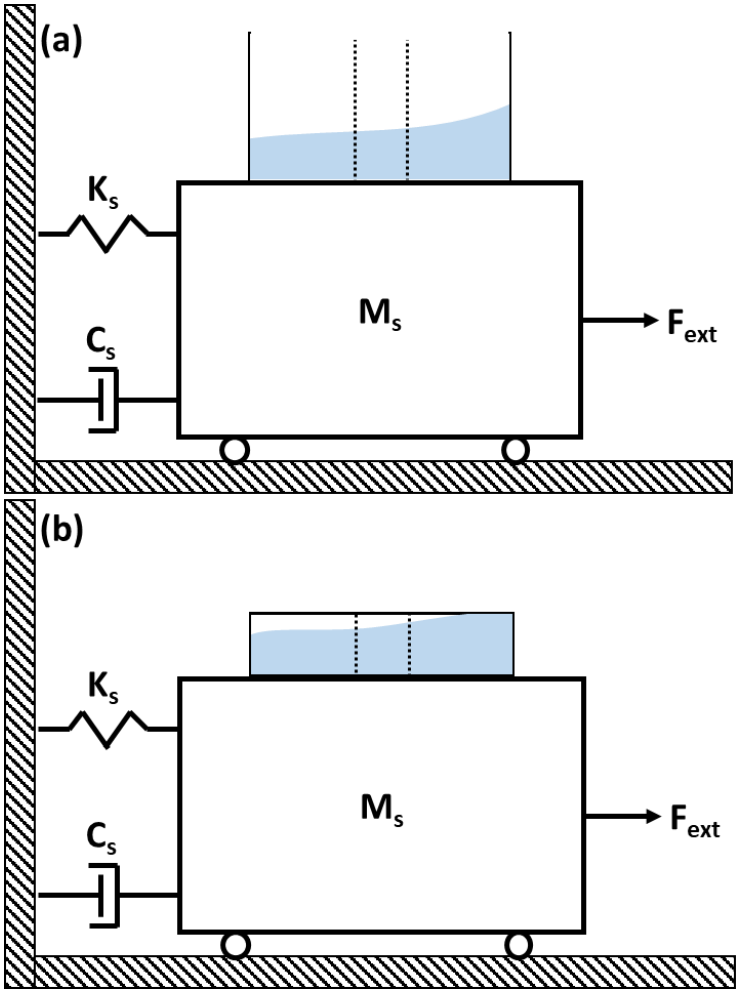

Figure 5.1: Structure – TLD system with (a) unlimited and (b) limited freeboard.

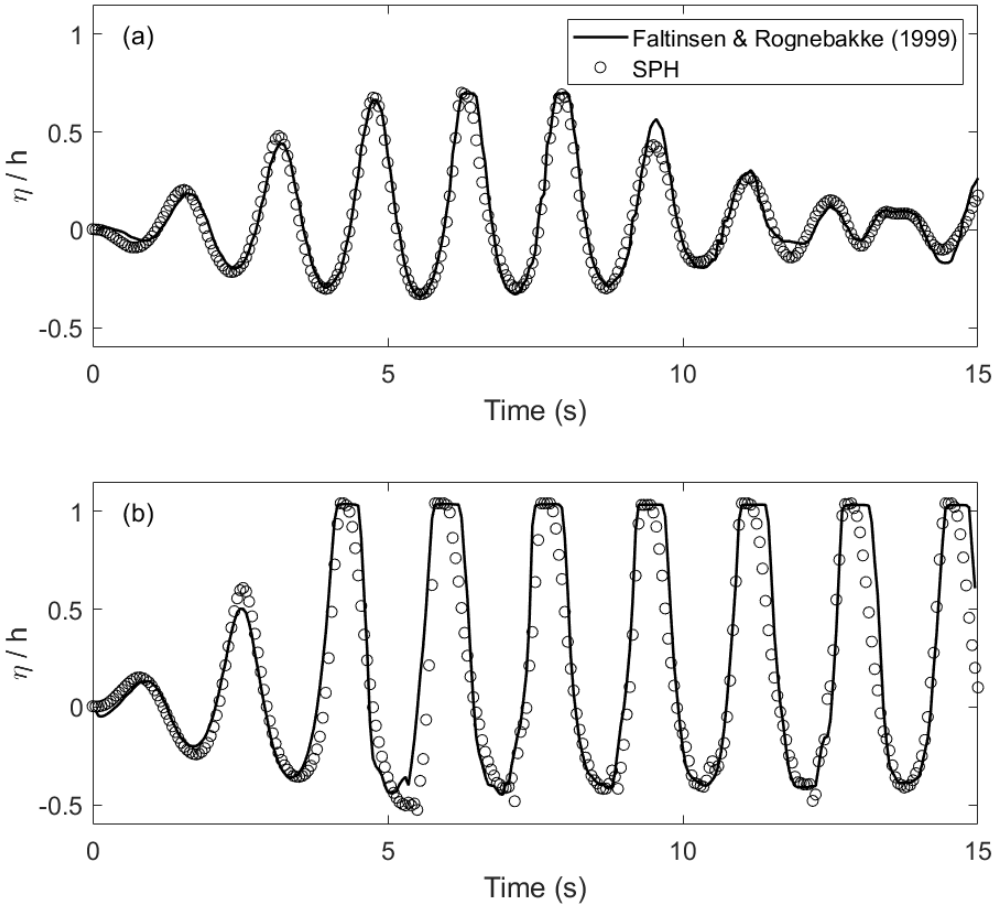

Figure 5.2: Normalized wave height comparison between SPH model and experimental data from Faltinsen and Rognebakke [10].

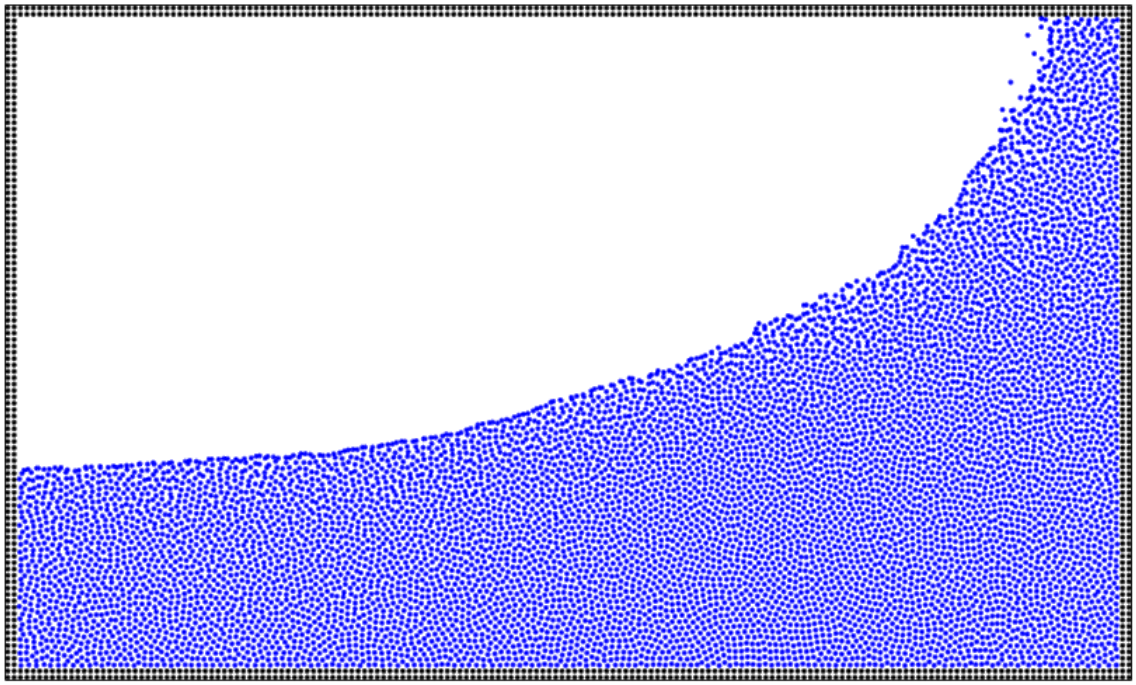

Figure 5.3: SPH particle positions showing ceiling impact.

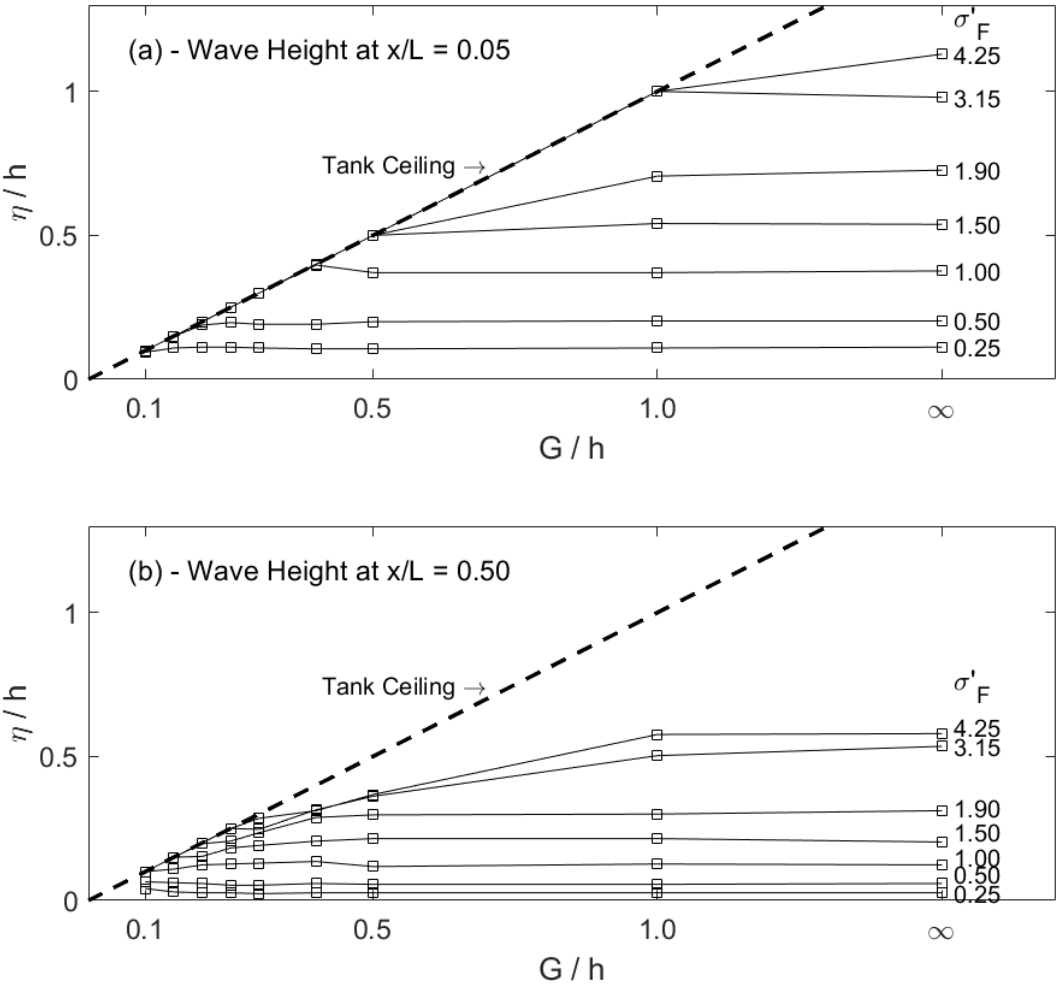

Figure 5.4: Peak wave heights measured at tank-end and mid-tank for all cases studied.

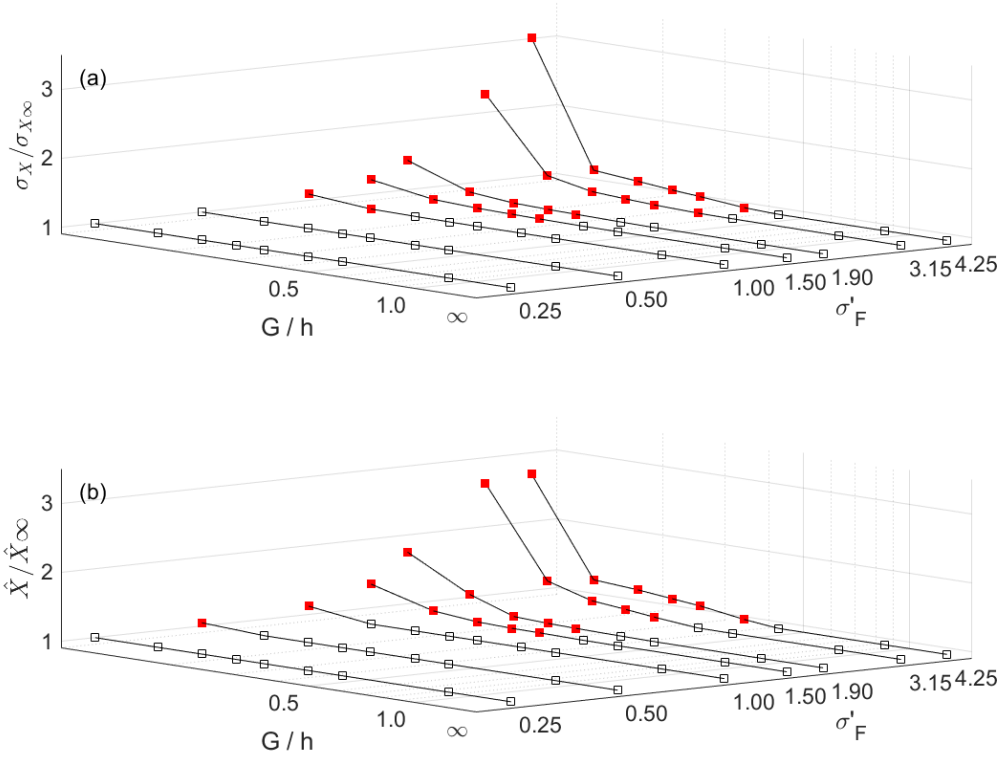

Figure 5.5: Structural response normalized by the unlimited freeboard (G/h = ∞) response. (a) RMS displacement, (b) peak displacement. Values greater than 1.0 indicated by red square ■.

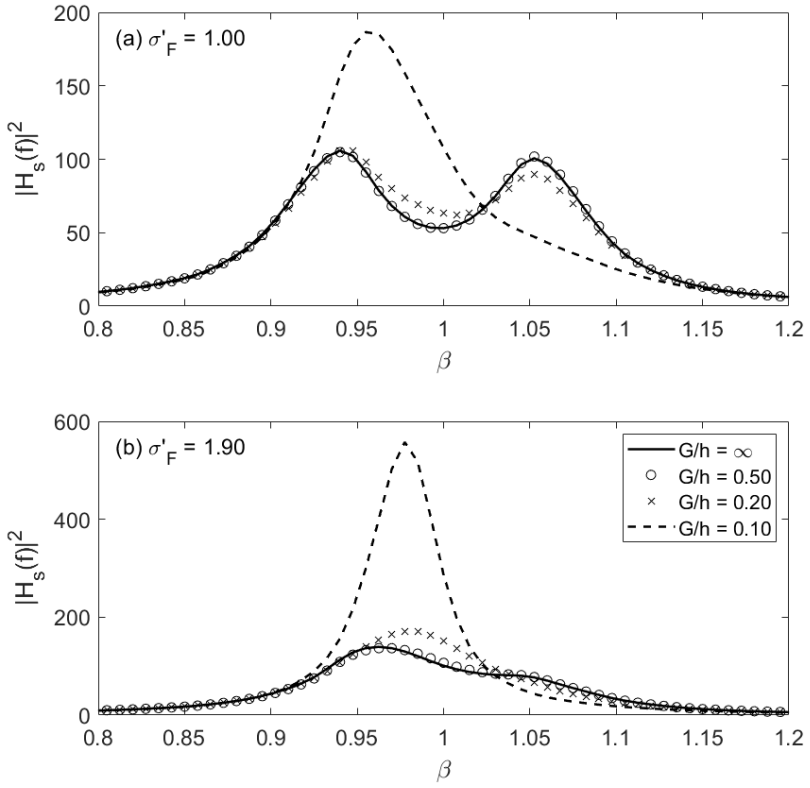

Figure 5.6: Squared modulus of mechanical admittance function for different G/h and $\boldsymbol{\sigma'_F}$, where $\beta = f/f_s$.

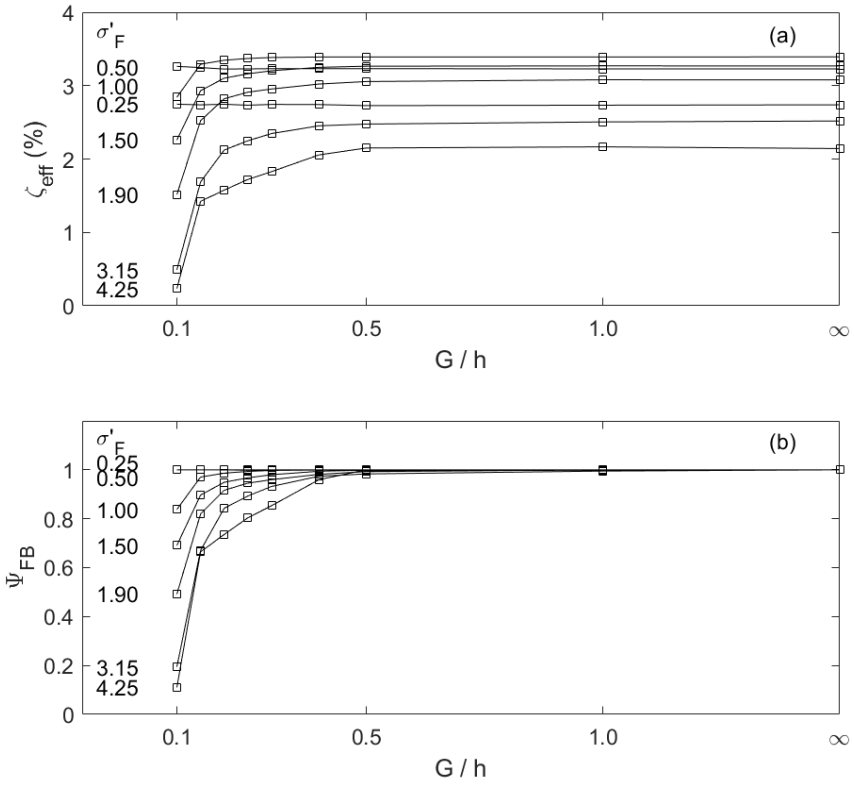

Figure 5.7: (a) effective damping and (b) TLD freeboard efficiency versus G/h.

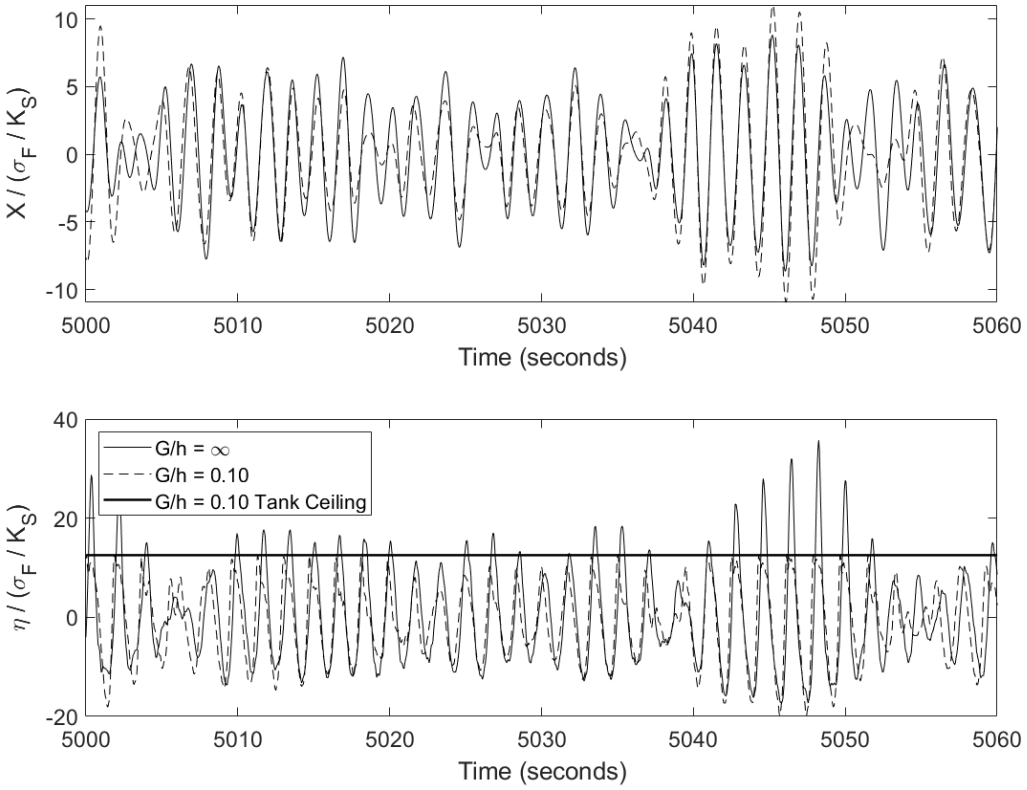

Figure 5.8: normalized structure and wave height response for $\boldsymbol{\sigma'_F}$ = 1.00.

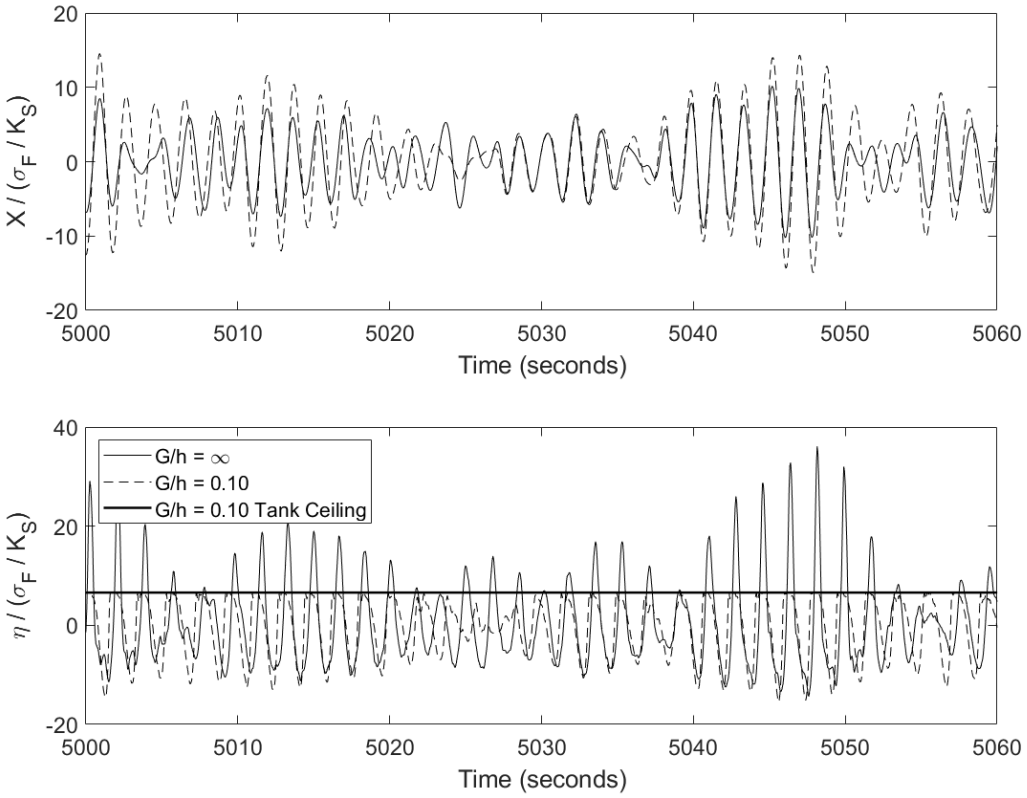

Figure 5.9: normalized structure and wave height response for $\boldsymbol{\sigma'_F}$ = 1.90.

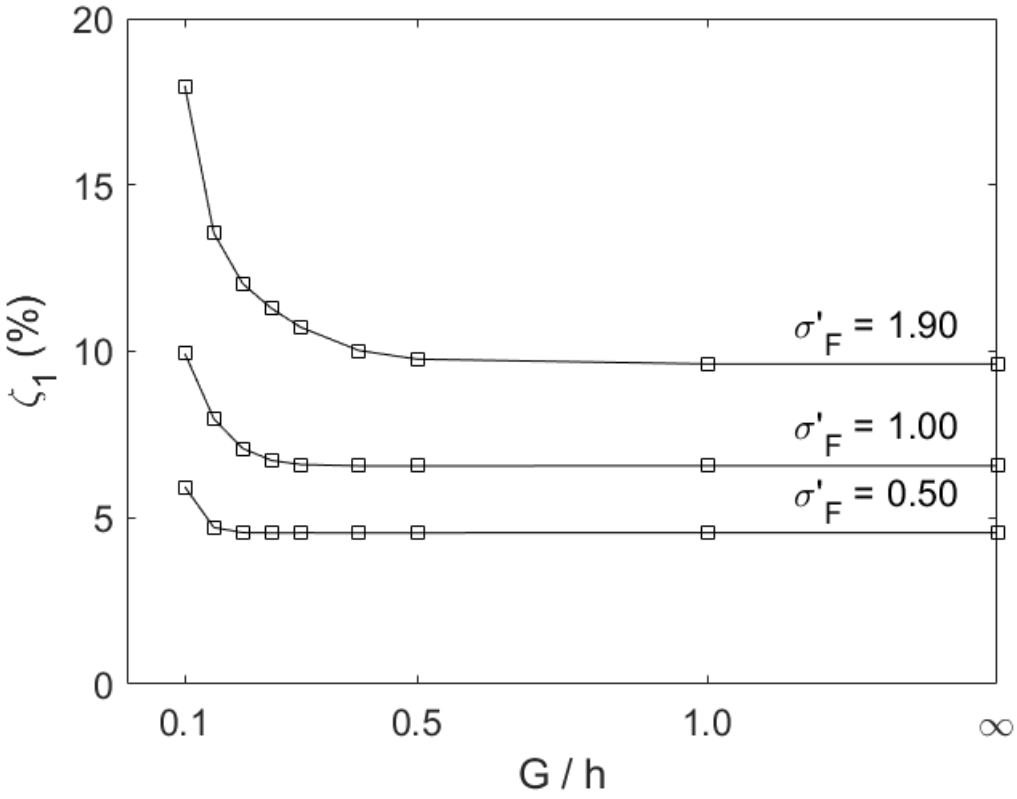

Figure 5.10: Fundamental sloshing mode damping ratio ζ_1 versus freeboard from SPH results.

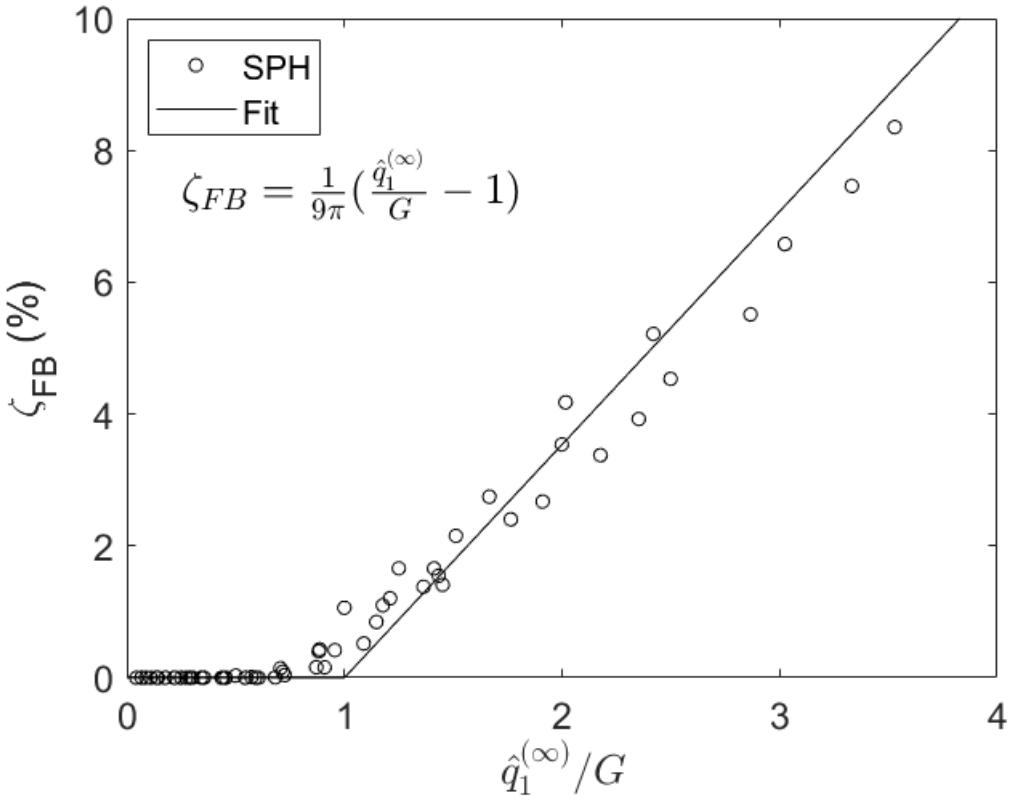

Figure 5.11: Freeboard damping ζ_{FB} versus normalized fundamental mode hourly peak wave height.

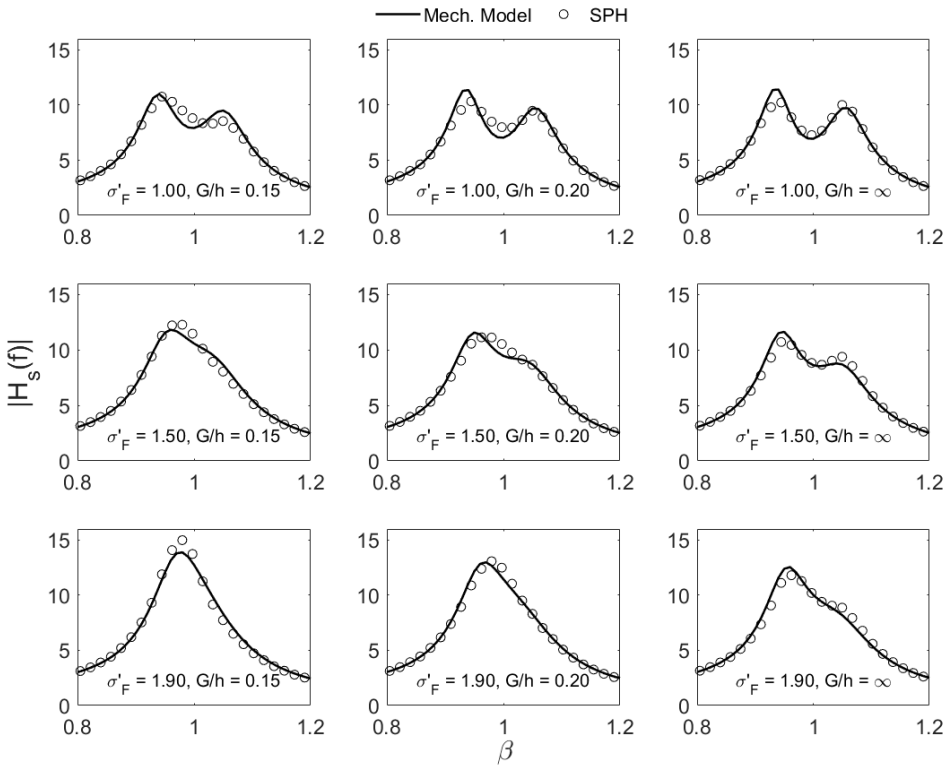

Figure 5.12: Comparison of structure frequency response function from SPH and equivalent mechanical model.

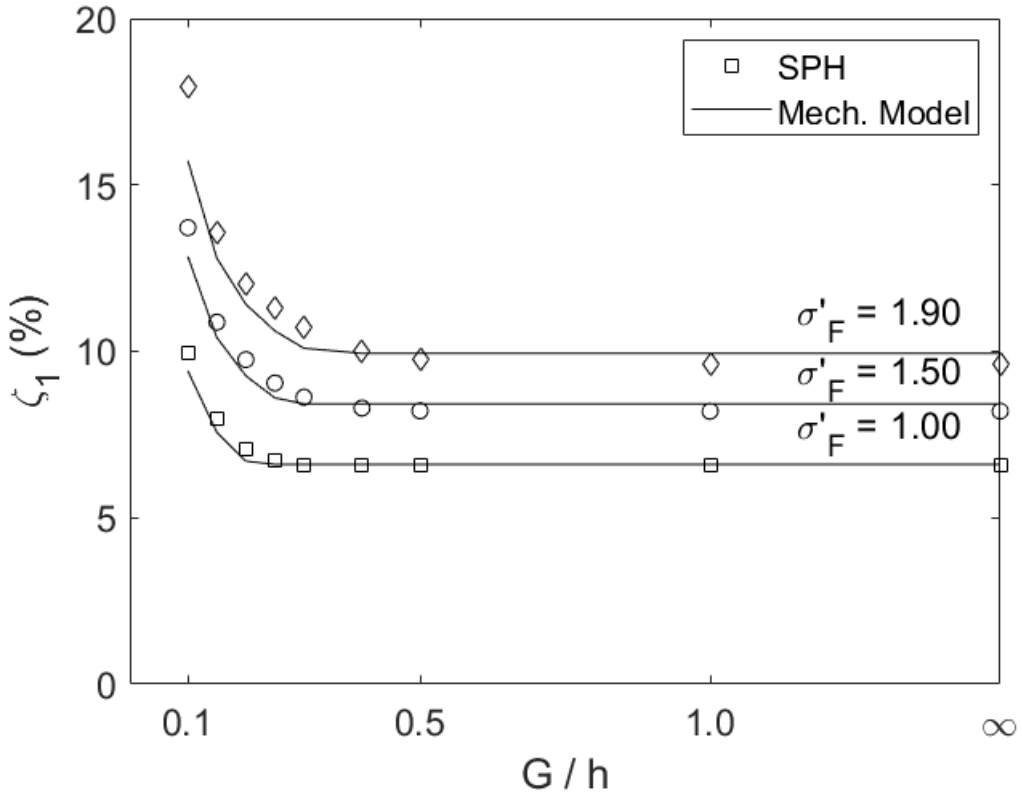

Figure 5.13: Fundamental sloshing mode damping ratio from mechanical model and SPH results.

Chapter 6: Nonlinear modelling of series-type pendulum tuned mass damper-tuned liquid damper

Abstract

The nonlinear response of a series-type pendulum tuned mass damper-tuned liquid damper (TMD-TLD) system is investigated in this study. In this system, the TLD is mounted on the pendulum TMD in series to remove the need for costly viscous damping elements. Since the response of the TMD is greater than that of the primary structure, the TLD experiences a significant base motion, leading to a highly nonlinear response that is difficult to model. The fully nonlinear pendulum TMD equation of motion is modelled without linearizing assumptions. The TLD is represented by an incompressible smoothed particle hydrodynamics (SPH) model that can capture large sloshing responses. The nonlinear model results are compared to shake table testing data for a TMD-TLD system and a linear equivalent mechanical model. Four system configurations are considered. The nonlinear model shows good agreement with the experimental data for the TMD displacement and TLD wave heights in both the time and frequency domain. The nonlinear model shows improved agreement compared to the linear model for all cases studied, especially for the TLD wave heights. The impact of simplifying the pendulum TMD equation of motion by the small angle assumption is investigated for two cases. The results indicate that the simplified pendulum equation does not properly capture the frequency of the TMD in the TMD-TLD system, and results in a reduction in calculated TLD wave heights compared to the fully nonlinear equation. It is therefore critical to consider the fully nonlinear pendulum TMD response to capture the TMD-TLD behavior.

KEYWORDS: tuned mass damper, tuned liquid damper, nonlinear pendulum, nonlinear dynamics, structural control, smoothed particle hydrodynamics.

6.1 Introduction

The installation of a dynamic vibration absorber (DVA) to control wind-induced vibrations of flexible structures has become increasingly common in recent years. Various configurations of DVAs have been applied to structures ranging from supertall buildings to offshore wind turbines. One DVA is the tuned mass damper (TMD), which consists of an auxiliary mass attached to the primary structure. The TMD is often represented as a pendulum or spring-mass-dashpot. The TMD frequency is tuned by appropriate choice of the pendulum length or TMD mass and stiffness, and energy dissipation is typically introduced using viscous dampers. Another commonly applied DVA is the tuned liquid damper (TLD), also known as the tuned sloshing damper (TSD). A TLD consists of a partially filled tank of liquid that is free to slosh. The TLD frequency is established through the appropriate choice of tank plan dimensions and liquid depth. When the primary structure vibrates, the liquid inside the TLD sloshes. Energy is dissipated within shallow TLDs through wave breaking and sloshing impact [1]. For intermediate- and deep-water TLDs additional damping mechanisms such as nets [2], screens [3], or paddles [4] are introduced to dissipate energy. The optimal natural frequency of the DVA is typically determined using design formulae based on the ratio of the DVA mass to the generalized mass of the targeted mode of vibration of the structure [5, 6, 7]. The response of a properly tuned DVA will have a phase lag from the primary structure response. The DVA therefore opposes the response of the structure, resulting in significant reductions in overall structural motion.

A large percentage of the cost and complexity of TMD design and installation is due to the viscous dampers which provide energy dissipation to the system. Removing the need for these components would decrease the cost and fabrication complexity of TMDs. The response of linear series-type TMDs, where multiple TMD masses are connected in series, has been investigated [8, 7]. These systems have been demonstrated to provide increased performance compared to a traditional TMD of the same total mass. However, the cost associated with the TMD system design, fabrication and installation is more significant than a traditional TMD, and viscous dampers or some other energy dissipating mechanism

are still required. To remove the need for expensive viscous dampers, a series-type TMD-TLD system has been proposed [9]. In this system, the TLD is mounted on the TMD mass. The sloshing response of the TLD provides damping to the TMD. A similar system was proposed by Cao [10], where a tuned liquid column damper (TLCD) was connected in series with a TMD. The study focused on improving the performance of traditional TLCD systems, however, with the appropriate selection of mass ratios the system would behave as a series-type TMD-TLCD. Love and Lee [9] found the series-type TMD-TLD provided improved performance and robustness compared to traditional TMD or TLD systems with the same total mass. The system was further investigated for a pendulum TMD by Love et al. [11]. An equivalent mechanical model was developed and compared to shake table testing data. The presence of the TLD was found to increase the TMD frequency. The model showed good agreement with experimental data when the TLD liquid was deep and wave heights were moderate. At large responses and shallow liquid depths, the model did not fully capture the system response due to the significant TLD nonlinearity.

To properly tune the series TMD-TLD system expressions presented by Asami [7] for two DVAs in series can be used. In an optimal system, the mass ratio of the TLD to the TMD will be double that of the TMD to the structure. The optimal natural frequency of the TMD will be slightly greater than that of the structure, and the optimal natural frequency of the TLD will be slightly less than that of the structure. The optimal performance of the TMD-TLD system occurs when the TMD has negative damping, however this is not achievable in a passive system, and thus the TMD should have as close to zero damping as possible. A suitable model which can account for nonlinear TLD frequency hardening [1], added mass effects of TLD damping elements [4], and the TLD influence on the TMD frequency [11] should be employed to confirm proper tuning and performance of the system.

The response of a pendulum TMD has been investigated in many studies [6, 12, 13, 14]. Simplifying assumptions are often employed, such as limiting the TMD response to small angles. This linearizes the pendulum equation of motion to the standard form for the

dynamic response of a spring-mass-dashpot system and will provide accurate results when the TMD response is small. However, at large responses, significant discrepancies between nonlinear and linearized pendulum TMD models have been demonstrated, illustrating the importance of nonlinear modelling for fully capturing the system response [13].

The base motion of a TLD installed in a TMD-TLD system will be significantly greater than a traditional TLD for the same structural response since the motion of the TMD is amplified compared to the structure [11]. The vertical motion of the pendulum TMD does not linearly excite sloshing in the TLD but can increase the TLD response nonlinearly [15]. As a result, the TLD in a TMD-TLD system can experience a highly nonlinear response even for moderate primary structure responses. Numerical models of varying complexity have been developed for the nonlinear response of a TLD. A multi-modal method introduced by Faltinsen et al. [16] was extended to TLDs equipped with damping screens by Love and Tait [17]. This method represents the TLD response as a summation of nonlinearly coupled modes of sloshing and has been extended to study various tank shapes [18] and structure-TLD systems [19]. Other studies have solved the nonlinear TLD response using depth-averaged shallow water wave theory equations, such as Kaneko and Ishikawa [2] and Tait et al. [20], who included the influence of TLD damping elements through a pressure drop term. These models perform well at typical TLD serviceability excitations, however at large amplitudes convergence is difficult to achieve, and assumptions inherent to the methods and equations may become invalid. Additionally, many models have limits of applicability based on TLD liquid depth. Therefore, these existing models may not adequately capture the TMD-TLD system response. Selection of a nonlinear model capable of representing the TLD response at large amplitudes is imperative to accurate modelling of the TMD-TLD system.

The smoothed particle hydrodynamics (SPH) method is capable of modelling highly nonlinear free surface flows at large amplitudes. SPH solves the Navier-Stokes equations using a Lagrangian framework where the fluid is discretized by a series of particles. The properties of each particle are calculated based on the values of neighbouring particles

weighted by a smoothing kernel function. Various extensive reviews on the SPH method have been published, for example Liu and Liu [21], Vacondio et al. [22], and Violeu and Rogers [23] for specific application to free surface flows. SPH has been applied to shallow TLDs [24, 25] as well as TLDs equipped with screens [26, 27]. McNamara and Tait [28] investigated the response of structure-TLD systems under large amplitude excitations and compared to experimental data. Though the SPH method may be computationally intensive relative to the other TLD sloshing models, it can capture large sloshing responses and does not have specific limitations on liquid depth or excitation amplitude. This makes SPH attractive for capturing the highly nonlinear TLD response in the TMD-TLD system.

This study presents a nonlinear model for the series type pendulum TMD-TLD system. The fully nonlinear TMD equation of motion is solved without any linearizing assumptions. The TLD is represented by an explicit incompressible SPH model where both the horizontal and vertical excitation of the pendulum TMD are included. TLD damping elements are represented through a ghost particle force term based on the Morison equation considering both the drag induced loss and added mass inertia terms. The model response is compared to experimental shake table data for the system covering a range of TMD-TLD properties and excitation amplitudes. The nonlinear model is compared to the linear equivalent mechanical model from Love et al. [11]. Finally, the impact of simplifying the pendulum TMD equation of motion based on the small angle assumption is investigated.

6.2 Numerical Modelling

The nonlinear and linear equivalent mechanical models of the series-type pendulum TMD-TLD system are introduced in this section. A schematic of the system is shown in Figure 6.1. The TMD is subject to a horizontal base acceleration excitation $\ddot{X}(t)$. The response of the TMD is represented by the angle $\theta(t)$. The length of the pendulum cable is defined as L_c. The TMD is assumed to have linear viscous damping. In the following expressions, the response variables are functions of time, but the time variable (t) is neglected from the notation for brevity.

6.2.1 Pendulum TMD Model

The nonlinear equation of motion for the pendulum TMD is developed by applying Lagrange's equation. The total kinetic and potential energies of the TMD subject to a horizontal base excitation are defined as:

$$\begin{aligned} T &= \frac{1}{2} m_{TMD} \left[\left(\dot{X} + L_c \dot{\theta} \sin(\theta) \right)^2 + \left(L_c \dot{\theta} \cos(\theta) \right)^2 \right] \\ &= \frac{1}{2} m_{TMD} \left[\dot{X}^2 + 2 \dot{X} L_c \dot{\theta} \cos(\theta) + L_c^2 \dot{\theta}^2 \right] \end{aligned} \tag{6.1}$$

$$V = m_{TMD} g L_c (1 - \cos(\theta)) \tag{6.2}$$

where m_{TMD} is the mass of the TMD, and an overdot represents differentiation with respect to time.

The Lagrangian is defined as the difference in kinetic and potential energies:

$$L = T - V \tag{6.3}$$

The equation of motion with respect to the TMD coordinate θ can then be found from the expression:

$$\frac{d}{dt} \frac{\partial L}{\partial \dot{\theta}} - \frac{\partial L}{\partial \theta} = Q \tag{6.4}$$

The non-conservative force Q is defined as:

$$Q = F_D + F_{TLD} = c_{TMD} L_c^2 \dot{\theta} \cos^2(\theta) + F_{TLD} \tag{6.5}$$

where F_D is the viscous damping force of the TMD, c_{TMD} is the TMD damping coefficient, and F_{TLD} is the TLD force which is yet to be determined.

Substituting the quantities into equation **(6.4)** and after algebraic manipulation and simplification, the nonlinear equation of motion governing the pendulum TMD response is given as:

$$\ddot{\theta} = -\frac{\ddot{X}}{L_c}\cos(\theta) + \frac{F_{TLD}}{m_{TMD}L_c} - 2\zeta_{TMD}\omega_{TMD}\dot{\theta}\cos^2(\theta) - \omega_{TMD}^2\sin(\theta) \quad \textbf{(6.6)}$$

where ω_{TMD} and ζ_{TMD} are the TMD natural frequency and damping coefficient defined by:

$$\omega_{TMD} = \sqrt{\frac{g}{L_c}}, \zeta_{TMD} = \frac{c_{TMD}}{2\omega_{TMD}m_{TMD}} \quad \textbf{(6.7)}$$

When solving the dynamic response of a pendulum it is common to simplify equation **(6.6)** by assuming the value of θ is small such that $\cos(\theta) \approx 1$ and $\sin(\theta) \approx \theta$. In this study the fully nonlinear equation is solved without this assumption.

Based on the calculated value of θ, the horizontal (X_{TMD}) and vertical displacement (Z_{TMD}) and acceleration of the pendulum TMD are calculated as:

$$X_{TMD} = L_c\sin(\theta), Z_{TMD} = L_c(1 - \cos(\theta)) \quad \textbf{(6.8)}$$

$$\ddot{X}_{TMD} = \ddot{\theta}L_c\cos(\theta) - \dot{\theta}^2L_c\sin(\theta), \ddot{Z}_{TMD} = \ddot{\theta}L_c\sin(\theta) + \dot{\theta}^2L_c\cos(\theta) \quad \textbf{(6.9)}$$

6.2.2 SPH TLD Model

Figure 6.2 shows a definition of the TLD domain. The origin is defined at the bottom left corner of the tank. The TLD tank has dimensions length *L*, height *H*, and breadth *b* (into the page), with an initial depth of liquid *h*. In this study the liquid inside the TLD is water. Three vertical damping elements are included at locations $x_j/L = 25\%$, 50%, and 75%. The damping elements provide additional energy dissipation to the TLD based on a loss coefficient determined empirically by Love and Haskett [4]. The TLD is represented by an incompressible SPH model developed in-house by the authors. For computational efficiency, the model is limited to two-dimensions, with the TLD modelled as a unit width, which can later be scaled by the actual breadth *b* to determine the proper forces. Essential details of the model implementation are described in this section, however, readers are referred to McNamara et al. [27] and McNamara and Tait [28] for an extensive overview of the model implementation.

The governing equations for the TLD response are the Lagrangian form of the Navier-Stokes equations:

$$\frac{D\rho}{Dt} + \rho\nabla\mathbf{u} = 0 \tag{6.10}$$

$$\frac{\mathrm{D}\mathbf{u}}{Dt} = -\frac{1}{\rho}\nabla P + v\nabla^2\mathbf{u} + \mathbf{f_b} \tag{6.11}$$

where *D/Dt* is the Lagrangian derivative, ρ is fluid density, **u** is the fluid velocity vector (herein, vector quantities are represented as **bold** symbols), *P* is fluid pressure, v is fluid kinematic viscosity, and $\mathbf{f_b}$ is the body force (gravity and applied tank acceleration).

The TLD domain is discretized in SPH using a series of particles representing the fluid, solid tank boundaries, and TLD damping elements. The particles are initially spaced at a distance *dp*. In the SPH method the governing equations are discretized as summations over neighbouring particles weighted using a smoothing kernel function. The fifth order Wendland kernel function is used in this study [29]:

$$W(q) = W_c \begin{cases} (1+2q)\left(1-\frac{q}{2}\right)^4 & 0 \le q \le 2 \\ 0 & q > 2 \end{cases} \tag{6.12}$$

where $q = \frac{|\boldsymbol{r_{ij}}|}{h_{ker}} = \frac{|\boldsymbol{r_i} - \boldsymbol{r_j}|}{h_{ker}}$, $\boldsymbol{r_i}$ is the position vector of particle i, $W_c = \frac{7}{\pi h_{ker}^2}$, and h_{ker} is the kernel function smoothing length.

The first-order derivative term is discretized based on Monaghan [30], and the second order derivative term is discretized based on Cummins and Rudman [31] as:

$$(\nabla A)_i = \rho_i \sum_{j=1}^{N} m_j \left(\frac{A_j}{\rho_j^2} + \frac{A_i}{\rho_i^2}\right)\nabla_j W_{ij} \tag{6.13}$$

$$\nabla.\left(\frac{1}{\rho}\nabla A\right)_i = \sum_{j=1}^{N}\left(\frac{8m_j}{\left(\rho_i+\rho_j\right)^2}\frac{A_{ij}\boldsymbol{r_{ij}}.\boldsymbol{\nabla_i}W_{ij}}{r_{ij}^2+\eta^2}\right) \tag{6.14}$$

where A_i is the quantity of interest for particle i, ρ_i is the particle density, m_i is the particle mass, and $\eta = 0.001h_{ker}$ is a small value to ensure a nonzero denominator.

The discretized governing equations are integrated in time using the projection method from Cummins and Rudman [31]. An intermediate value of velocity and position is calculated for each fluid particle neglecting the pressure gradient term in the momentum equation:

$$\mathbf{u}^* = \mathbf{u}(t) + \left(v\nabla^2\mathbf{u} + \mathbf{g} + \ddot{\boldsymbol{X}}_{\mathbf{TMD}} + \mathbf{F}_{\boldsymbol{DE}}\right)\Delta\mathrm{t} \tag{6.15}$$

$$\mathbf{r}^* = \mathbf{r}(t) + \mathbf{u}^*\Delta\mathrm{t} \tag{6.16}$$

where $\Delta\mathrm{t}$ is the timestep, $\mathbf{g}$ is the gravitational acceleration, $\ddot{\boldsymbol{X}}_{\boldsymbol{TMD}} = [\ddot{X}_{TMD}, \ddot{Z}_{TMD}]$ is the acceleration vector of the TMD to which the tank is rigidly connected, determined from equation **(6.9)**, and $\mathbf{F}_{\boldsymbol{DE}}$ is the force from the TLD damping elements which is introduced in equation **(6.26)**.

From the intermediate velocity and position, an intermediate density ρ^* is calculated for each fluid particle. The pressure of each fluid particle is solved using an explicit method from Yeylaghi et al. [32], including a density-invariant correction based on Jiang et al. [33]:

$$\boldsymbol{\nabla}.\left(\frac{\boldsymbol{\nabla}P}{\rho^*}\right) = \alpha\frac{\rho_0-\rho^*}{\rho_0\Delta\mathrm{t}^2} + (1-\alpha)\frac{\boldsymbol{\nabla}.\boldsymbol{u}^*}{\Delta t} \tag{6.17}$$

where $\alpha = 0.01$ is a blending parameter.

When the pressure value has been calculated, the fluid particle density is corrected to the initial value ρ, and the velocities and positions of each fluid particle are corrected to include the pressure gradient term and enforce incompressibility:

$$\boldsymbol{u}(t+\Delta t) = \boldsymbol{u}^* - \left(\frac{1}{\rho^*}\boldsymbol{\nabla} P\right)\Delta t \tag{6.18}$$

$$\boldsymbol{r}(t+\Delta t) = \boldsymbol{r}(t) + \left(\frac{\boldsymbol{u}(t+\Delta t) + \boldsymbol{u}(t)}{2}\right)\Delta t \tag{6.19}$$

The solid TLD tank boundaries are implemented using multiple layers of fixed dummy particles based on Adami et al. [34]. These particles do not move throughout the simulation since the base motion of the TLD is applied directly to the fluid particles. At each timestep the pressure of the solid boundary particles is calculated from neighbouring fluid particles. To enforce a free-slip velocity boundary condition, a numerical velocity is calculated for each boundary particle. Finally, to apply the dynamic boundary condition of constant fluid pressure on the free surface, a numerical density is calculated for each fluid particle [32]:

$$\rho_{fi} = \sum_{j=1}^{N} m_j W_{ij} \tag{6.20}$$

If the numerical density value is calculated to be less than 90% of the initial fluid density, the fluid particle is identified as a free surface particle and its pressure is set to zero.

Rather than directly modelling the geometry of the TLD damping elements, they are represented by an array of ghost particles located at each damping element location in the tank. The ghost particles interact with the fluid particles only through the $\mathbf{F}_{\boldsymbol{DE}}$ term from equation **(6.15)**. This implementation was proposed for TLD screens by McNamara et al. [27], and significantly reduces the computational requirements for the SPH simulations by allowing a much greater particle spacing while still capturing the damping characteristics of the TLD. To apply this method, the loss coefficient and added mass coefficient of the damping elements must be known. The loss coefficient for the TLD damping elements in this study was determined empirically by Love and Haskett [4]. The added mass coefficient is calculated theoretically from Wendel [35].

The force that the fluid particles exert on the damping elements is calculated based on the Morison equation [36]. Since the damping elements are vertical, only the resultant horizontal force is considered. The spacing between the TLD damping element ghost particles is set equal to the initial fluid particle spacing *dp*. The total force acting on each TLD damping element is calculated as the summation of the force for each ghost particle:

$$F_{DE} = \sum_j F_{DE-j} = \frac{1}{2} C_l \rho \sum_j \left| U_{DE,j} \right| U_{DE,j} dp + C_m \rho \sum_j A_{DE,j} dp \qquad \textbf{(6.21)}$$

where j is summed over the damping element ghost particles, C_l is the loss coefficient, C_m is the added mass coefficient, $U_{DE,j}$ is the horizontal fluid velocity and $A_{DE,j}$ is the horizontal fluid acceleration calculated at ghost particle j:

$$U_{DE,j} = \sum_f \frac{m_f}{\rho_f} u_f W_{jf} \, , A_{DE,j} = \frac{U_{DE,j} - U_{DE,j}(t - \Delta t)}{\Delta t} \qquad \textbf{(6.22)}$$

where f is summed over neighbouring fluid particles, and W_{jf} is the kernel function. The same kernel function is used for the fluid, boundary, and damping element particles.

When the force of the fluid acting on the damping element is calculated, the equal and opposite force is applied back to the fluid particles in equation **(6.15)** weighted by the SPH kernel function:

$$F_{DE-f} = -\sum_j F_{DE-j} \frac{W_{jf}}{\sum_f W_{jf}} \qquad \textbf{(6.23)}$$

It is important to note that this implementation captures the loss and added mass characteristics of the damping elements, however it does not directly model the physical flow in the region of the elements. For cases where the loss and added mass coefficients are unknown, or the flow in the region of the damping elements must be finely resolved, a different implementation may be necessary.

6.2.3 TMD-TLD Substructuring

The response of the combined TMD-TLD system is solved using a substructuring method. At each timestep, the TMD acceleration is determined by solving equation **(6.6)**. The TMD acceleration in the horizontal and vertical directions is then applied to the TLD in equation **(6.15)**, and the TLD response is calculated by the SPH model. At the end of the timestep, the resulting TLD force components are calculated by summing the mass times acceleration of each fluid particle:

$$F_{TLD-X} = -b \sum_j m_j \left[\frac{u_x(t) - u_x(t-\Delta t)}{\Delta t} + \ddot{X}_{TMD} \right] \quad \textbf{(6.24)}$$

$$F_{TLD-Z} = -b \sum_j m_j \left[\frac{u_z(t) - u_z(t-\Delta t)}{\Delta t} + \ddot{Z}_{TMD} + g \right] \quad \textbf{(6.25)}$$

where *b* is the actual breadth of the TLD tank. The resultant TLD force is then calculated from the components based on the angle of the pendulum TMD:

$$F_{TLD} = F_{TLD-X} \cos(\theta) + F_{TLD-Z} \sin(\theta) \quad \textbf{(6.26)}$$

The TLD force is applied back to the TMD in equation **(6.6)**, and the process is repeated for the next timestep.

The solution to the TMD response defined by equation **(6.6)** was found using the 4th order Runge-Kutta-Gill method. The timestep used to solve both the TMD and TLD response was held constant at 5x10^{-4} seconds, which was found to provide accurate and stable results. For all cases studied, the SPH particles were discretized using an initial spacing *dp* of 7 mm, which allowed for an integer number of particles across the tank length, and sufficient particles across the water depth to capture the sloshing response.

6.2.4 Linear Equivalent Mechanical Model

The linear equivalent mechanical model was presented by Love et al. [11] for the pendulum TMD-TLD system. This model represents the TMD-TLD using a two degree of

freedom system as shown in Figure 6.3. The response of the system subject to a base excitation $\ddot{X}(t)$ is defined by the system of equations:

$$\begin{bmatrix} (m'_{TMD} + m_{eq}) & m_{eq} \\ m_{eq} & m_{eq} \end{bmatrix} \begin{Bmatrix} \ddot{X}_{TMD} \\ \ddot{x}_r \end{Bmatrix} + \begin{bmatrix} c_{TMD} & 0 \\ 0 & c_{eq} \end{bmatrix} \begin{Bmatrix} \dot{X}_{TMD} \\ \dot{x}_r \end{Bmatrix} + \begin{bmatrix} k'_{TMD} & 0 \\ 0 & k_{eq} \end{bmatrix} \begin{Bmatrix} X_{TMD} \\ x_r \end{Bmatrix} = -\begin{Bmatrix} m'_{TMD} + m_{eq} \\ m_{eq} \end{Bmatrix} \ddot{X} \tag{6.27}$$

where X_{TMD} represents the horizontal displacement of the TMD and x_r represents the response of the equivalent TLD mass.

The equivalent TMD mass and stiffness are defined to account for the TLD water mass [11]:

$$\begin{aligned} m'_{TMD} &= m_{TMD} + m_{water} - m_{eq} \\ k'_{TMD} &= (m'_{TMD} + m_{eq}) \frac{g}{L_c} \end{aligned} \tag{6.28}$$

The equivalent TLD mass and stiffness are defined from Tait [37]:

$$\begin{aligned} m_{eq} &= \frac{8\rho b L^2}{\pi^3} \tanh\left(\frac{\pi h}{L}\right) \\ k_{eq} &= \frac{8\rho b L g}{\pi^2} \tanh^2\left(\frac{\pi h}{L}\right) \end{aligned} \tag{6.29}$$

Finally, c_{TMD} is the linear viscous damping coefficient of the TMD, and c_{eq} is an equivalent amplitude dependent viscous TLD damping [37]. The response of the linear equivalent mechanical model can readily be found in the frequency domain using an iterative solution method to account for the amplitude dependent TLD damping.

6.3 Experimental Study Parameters

Four TMD-TLD system configurations were studied experimentally. Details on the experimental setup were previously reported in Love et al. [11]. Figure 6.4 shows a picture

of the experimental setup. A stiff steel test frame was installed on the shake table. The shake table provided a uniaxial excitation to the test frame, representing the base acceleration applied to the TMD. The pendulum TMD had a total mass of 1251 kg, which was held constant in each configuration. The TMD was hung from the test frame using four cables, and the length of cable was adjusted through a moveable tuning brace to achieve different TMD frequencies. Due to the configuration of the pendulum cables, the TMD mass experienced a horizontal and vertical translation without rotation of the mass, unlike in a simple pendulum configuration where some rotation would also occur. The frequency of the TMD was determined by the available length of cable, which was limited by the height of the test frame and the gap between the TMD mass and outer frame. In an optimal passive system, the TMD will have zero inherent damping [7]. As this is not physically achievable, the pendulum TMD was designed to have very low damping, and the damping ratio of the TMD was determined to be between 0.33% and 0.5% through free vibration testing. A rectangular TLD tank with dimensions of length 889 mm and breadth 785 mm was mounted to the TMD mass. The depth of water in the TLD was varied to provide different natural frequencies, targeting optimal tuning ratios based on the mass ratios of the TLD and TMD [7]. Damping elements were installed to increase the damping within the TLD. The parameters of each TMD-TLD configuration are shown in Table 6.1.

A total of sixteen frequency sweep tests were completed, consisting of four tests for each TMD-TLD configuration. For each test, the shake table was excited by a sine wave displacement with constant amplitude X_0, as shown in Table 6.1. The frequency of the sine wave was varied in discrete intervals ranging from 80% to 120% of the TMD natural frequency. At each frequency, the system was given sufficient time to achieve a steady state response, after which the response was recorded for 120 seconds. The frequency was then increased to the next discrete frequency, and the process repeated. The data was acquired using a dynamic system with a sampling frequency of 50 Hz. A 10 Hz anti-aliasing lowpass filter was applied. The displacement of the shake table and TMD were measured using string potentiometers, and their accelerations were also recorded using accelerometers.

Wave heights were measured at each end of the TLD tank using capacitance type wave probes.

6.4 Results

This section compares the results of the models and experimental testing for selected representative tests. Since the nonlinear model is solved in the time domain, its results can be compared to the recorded time series of the experimental data. Frequency response plots of the linear model and nonlinear model are compared to those obtained from the experimental data. One test from each TMD-TLD configuration is shown, covering a range of the parameters studied. For presentation, the results are normalized by the shake table amplitude, X_0, time is normalized by multiplying by the excitation frequency f, and excitation frequency is normalized by the TMD natural frequency through the parameter $\beta = f/f_{TMD}$.

6.4.1 Time Domain

The first results correspond to TMD-TLD configuration #1. Figure 6.5 shows the time response for Test #3 and $\beta = 0.96$ at a shake table amplitude of 5.0 mm. The TMD displacement calculated by the numerical model is in excellent agreement with the experimental data. The experimental wave heights are observed to have varying peak values at each cycle, indicating that the TLD did not achieve a truly steady state response, however, the numerical model is in good agreement with the wave form.

Figure 6.6 shows the time response for Test #8 and $\beta = 1.08$ with a shake table amplitude of $X_0 = 7.0$ mm. This is the largest excitation studied for TMD-TLD configuration #2. This configuration is the same as the previous case, however the width of the damping elements was increased which provides significantly more energy dissipation within the TLD. The model is in excellent agreement with both the experimental TMD displacement and the TLD wave height.

Figure 6.7 shows the time response for Test #10 and $\beta = 0.94$ with a shake table amplitude $X_0 = 2.5$ mm. This corresponds to TMD-TLD configuration #3 which had the

shallowest water depth and smallest damping element width. The peak TMD displacements are slightly under-predicted by the model. Despite this, the model shows excellent agreement with the experimental wave heights.

Finally, Figure 6.8 shows the time response for Test #16 and $\beta = 0.91$ with a shake table amplitude $X_0 = 7.0$ mm. This corresponds to TMD-TLD configuration #4 which had the deepest water depth and largest damping element width, leading to a less chaotic TLD response. In this case, the model is in reasonable agreement with the experimental data, though the peak values of both TMD displacement and TLD wave height are under-predicted.

6.4.2 Frequency Response

This section presents the frequency response of the TMD displacement and TLD wave height for the experimental data, nonlinear model, and linear equivalent mechanical model. The frequency response is determined by calculating the average peak value per cycle from the steady state response at each discrete excitation frequency for the experimental data and nonlinear model. The steady state response of the linear equivalent mechanical model is solved directly. Since the linear model is only capable of representing a single mode of TLD sloshing, each wave height plot includes an additional series with the experimental wave heights filtered to remove the influence of higher mode sloshing harmonics. This was achieved by applying a lowpass filter with a cut-off frequency 50% greater than the excitation frequency in post processing. The presented cases follow from those shown in the time domain.

Figure 6.9 shows the frequency response from Test #3. The linear model shows good agreement with the experimental TMD displacement when $\beta < 0.90$ but does not capture the shape of the frequency response curve above this excitation frequency. The nonlinear model is in much better agreement with the experimental TMD displacement. The linear model shows good agreement with the filtered TLD wave heights. In this case the unfiltered TLD wave heights are much greater in value than the filtered wave heights. The nonlinear

model is in good agreement with the experimental wave heights when $\beta > 0.90$ but under-predicts the value at lower frequencies.

Figure 6.10 shows the frequency response for Test #8, which corresponds to the largest shake table amplitude studied for TMD-TLD configuration #2, X_0 = 7.0 mm. Unlike in the previous case, the frequency response curve for both the TMD displacement and TLD wave height has a single peak value, which results from the large amplitude response and correspondingly large TLD amplitude-dependent damping provided by the damping elements. The linear model captures the shape of the TMD displacement frequency response well, but the peak value of the curve occurs at a higher frequency than the experimental data. The nonlinear model is in very good agreement with the experimental data for TMD displacement. For TLD wave height, the nonlinear model shows good agreement with the experimental data when $\beta > 0.90$ but under-predicts the values at lower frequencies. The linear model shows reasonable agreement with the filtered wave heights but under-predicts the values for most frequencies.

Figure 6.11 shows the frequency response for Test #10 corresponding to TMD-TLD configuration #3 and X_0 = 2.5 mm. The experimental frequency response for the TMD displacement shows three distinct peaks. The shape of the frequency response curve is captured well by the nonlinear model, however there are some discrepancies in the values compared to the experimental data across the range of frequencies. In contrast, the linear model shows only a double peaked response and poor agreement with the experimental data. The experimental frequency response for TLD wave height is observed to increase across the range of frequencies, with a sudden drop in response near $\beta = 1.16$. This behavior is common in TLDs with shallow depth and low damping. The nonlinear model shows very similar behavior, though there are some discrepancies between the wave height values. The linear model shows reasonable agreement with the filtered TLD wave heights.

Figure 6.12 shows the frequency response for Test #16 corresponding to TMD-TLD configuration #4 and X_0 = 7.0 mm. The TMD displacement from the nonlinear model is in reasonable agreement with the experimental data. The linear model shows a similar overall

response trend, though the frequency at which the peak TMD displacement occurs is greater than the experimental data. Despite the reasonable agreement with the TMD displacement, the TLD wave heights are mostly under-predicted by the nonlinear model, though the shape of the frequency response curve is similar. The linear model also under-predicts the filtered TLD wave height data.

6.4.2.1 Forces and Energy Dissipated per Cycle

The forces and energy dissipated per cycle of the TMD and TLD are of interest to understand the system behavior. The forces were not measured directly during the experimental testing, however they can be evaluated from the nonlinear model results.

Figure 6.13 shows the frequency response of the different TLD force components calculated from the nonlinear model results. The static inertial portion of F_{TLD-Z} equal to the mass of water times gravitational acceleration was removed for presentation as this is constant across all frequencies. The forces are normalized by the maximum inertial force of the total water mass if it moved rigidly with the TMD: $F' = F_{TLD}/m_w|\ddot{X}_{TMD}|$, where $|\ddot{X}_{TMD}|$ is the amplitude of TMD acceleration. The X-direction component of force is representative of the resultant force in a traditional TLD where only horizontal motion is considered. Due to the phase differences between the force components, at some frequencies the resultant TLD force F_{TLD} is less than the X-direction component, and at some frequencies it is greater. For all four tests the peak X-direction force is greater than the peak resultant force, indicating that the pendulum TMD vertical motion decreases the resultant TLD forces slightly. In all cases the Z-component of force is less than the X-component.

The interaction force between the structure and TMD-TLD system is sum of the inertial force of the TMD mass and the TLD force. This can be approximated by:

$$F_{TMD-TLD} = -m_{TMD}\ddot{X}_{TMD} + F_{TLD} \quad \textbf{(6.30)}$$

Due to the complicated phase angle relationships between the applied excitation, TMD, and TLD, the forces alone do not give an indication of the damping performance of the system. In an ideal system the TMD will have zero damping, and energy from the structure will be transferred to the TMD-TLD and dissipated from the damping provided by the TLD. Unlike in a linear TMD system, the damping of the TMD-TLD is amplitude dependent. The energy dissipated per cycle can be used as an indication of the damping, and is calculated by integration of the force-displacement curves:

$$E_{d-TMD-TLD} = \int_T F_{TMD-TLD} dX$$

$$E_{d-TLD} = \int_T F_{TLD} dX \tag{6.31}$$

where X is the base displacement of the structure (the shake table in experimental tests). The values of energy dissipated per cycle represent the energy dissipated by the TMD-TLD system and TLD only from the structure. For an optimized passive series type TMD-TLD system, the TMD should have zero damping, though realistically some amount of damping will always be present. Since the TMD has very low inherent damping (< 0.5% of critical), most of the energy dissipation in the system should be provided by the TLD. This can be verified by comparing the frequency response curves for each value of energy dissipation. The energy dissipated per cycle is normalized by the maximum kinetic energy of the TMD and TLD masses if they moved rigidly with the structure (shake table):

$$E'_d = \frac{E_d}{0.5(m_{TMD} + m_w)\left|\dot{X}\right|^2} \tag{6.32}$$

where $\left|\dot{X}\right|$ is the amplitude of the applied base velocity.

Figure 6.14 shows the frequency response of normalized energy dissipated per cycle. The value of $E'_{d-TMD-TLD}$ was evaluated from the experimental results by using the

measured acceleration of the TMD mass to approximate $F_{TMD-TLD}$. Similar observations can be made for each test presented. The model results for $E'_{d-TMD-TLD}$ are in comparable agreement with the experimental data to what was presented in the previous section. Only a minor amount of energy is dissipated by the TLD from the shake table input, as indicated by the small values of the E'_{d-TLD} curve, and the energy dissipated is close to zero when β = 1.0 for each test. Significantly more energy is dissipated per cycle by the combined TMD-TLD response shown by $E'_{d-TMD-TLD}$ despite the low inherent TMD damping. These results indicate that the energy from the structure (shake table) is transferred to the TMD-TLD system, where it is dissipated by the TLD response.

6.5 Impact of Simplified Pendulum Equation

To determine the importance of considering the fully nonlinear pendulum response, this section will study the impact of simplifying the pendulum equation of motion on the response of the TMD-TLD system. By assuming that the angle of the pendulum θ is small and therefore $\cos(\theta) \approx 1$ and $\sin(\theta) \approx \theta$, equation **(6.6)** reduces to the form:

$$\ddot{\theta} = -\frac{\ddot{X}}{L_c} + \frac{F_{TLD}}{m_{TMD}L_c} - 2\zeta_{TMD}\omega_{TMD}\dot{\theta} - \omega_{TMD}^2\theta \qquad \textbf{(6.33)}$$

Further defining $\theta = X_{TMD}/L$, $\dot{\theta} = \dot{X}_{TMD}/L$, and $\ddot{\theta} = \ddot{X}_{TMD}/L$, the equation of motion reduces to the equation for a base excited single degree of freedom (SDOF) oscillator:

$$\ddot{X}_{TMD} = -\ddot{X} + \frac{F_{TLD}}{m_{TMD}} - 2\zeta_{TMD}\omega_{TMD}\dot{X}_{TMD} - \omega_{TMD}^2 X_{TMD} \qquad \textbf{(6.34)}$$

The horizontal motion of the pendulum is still captured by the simplified equation of motion; however, the vertical motion is assumed to be small and is neglected. To assess the applicability of the simplified equation of motion, the maximum TMD angle measured in each of the experimental tests is plotted in Figure 6.15 versus $\sin(\theta)$ and $\cos(\theta)$. The results show that $\sin(\theta)$ is approximately equal to θ for all the experimental tests, as indicated by lining up with the 1 to 1 line on the plot. The value of $\cos(\theta)$ deviates slightly from 1 at large θ values, but the maximum error is less than 2%. Based on this, the

assumption of small TMD angles appears valid when considering only the TMD response measured experimentally. However, it is necessary to determine the impact that simplifying the TMD equation has on both the TLD and the combined TMD-TLD system responses.

The TMD equation of motion in the nonlinear model was replaced with the simplified form, and the simulations were run for Tests #8 and #10. All other parameters in the SPH model were held constant. Figure 6.16 shows the frequency response for Test #8. The simplified model has a shifted frequency compared to the nonlinear model, which is expected as the simplified model neglects the impact of the TLD vertical force on the pendulum TMD response. The shape of the TMD displacement frequency response curve is similar between the models, however the maximum TMD displacement for the simplified model is 4% greater than the nonlinear model. The TLD wave height frequency response curve is also shifted, and the wave heights are significantly reduced compared to the nonlinear model. The maximum wave height for the simplified model is reduced by 24% compared to the nonlinear model. Figure 6.17 shows the frequency response for Test #10. Again, the simplified model has a shifted frequency compared to the nonlinear model. For this test, the maximum TMD displacement calculated by the simplified model is 10% less than the nonlinear model. The TLD wave heights are reduced for most frequencies, with a maximum wave height that is 23% less than the nonlinear model.

Overall, the simplified model appears to capture the TMD displacement response reasonably, though it does not account for the shifted TMD frequency which is critical to tuning the TMD-TLD system to the primary structure. Additionally, simplifying the pendulum equation of motion causes the model to under-predict the TLD wave heights with an error of approximately 25%. Though the vertical motion of the TMD does not linearly excite sloshing in the TLD [15], the TLD response can be excited nonlinearly, which clearly causes an increase in the TLD wave heights.

6.6 Conclusions

This paper investigated the nonlinear response of a series-type pendulum TMD-TLD system subject to a base excitation. A fully nonlinear pendulum TMD model was coupled

to an incompressible SPH model of a TLD with damping elements. The results of the nonlinear model were compared to experimental shake table testing data for the system and a linear equivalent mechanical model. Finally, the impact on the response of simplifying the pendulum TMD equation was investigated. The following conclusions can be made from this work:

1. The nonlinear model captures the response of the pendulum TMD and TLD in the time domain across a range of system parameters. Some discrepancies exist due to the highly nonlinear response of the system.
2. Good agreement was demonstrated between the nonlinear model and experimental testing data considering the frequency response of TMD displacement and TLD wave height. At some frequencies, the nonlinear model under-estimated the response, however it provided improved agreement compared to the linear equivalent mechanical model, especially for calculation of TLD wave heights.
3. The frequency response of TLD forces from the nonlinear model indicated that including the vertical pendulum motion modified the forces compared to a traditional TLD undergoing only horizontal motion. The peak resultant TLD force was less than the peak X-component force for all cases. Due to the low inherent TMD damping, a small amount of energy was dissipated per cycle by the TMD alone, with significantly more energy dissipated by the combined TMD-TLD system. The TMD-TLD damping is therefore provided primarily by the TLD response.
4. The shake table testing results indicated that applying a small angle simplification to the pendulum TMD equations would be valid based on the TMD response alone. Two cases were simulated with a simplified TMD equation of motion. The results indicated that simplifying the pendulum TMD does not accurately capture the TMD frequency, which is critical to proper tuning of the system. The peak TMD displacement was modified by approximately 5-10%. Additionally, the calculated TLD wave heights were reduced by approximately 25% compared to the nonlinear model for both cases. It is therefore critical to consider the fully nonlinear pendulum TMD equation to capture the system response.

The results of this study indicate that the nonlinear model can be used to reasonably capture the response of the series-type pendulum TMD-TLD system across a range of parameters. The presented model can be used to further investigate the performance of the system by coupling to a structure.

6.7 Acknowledgment

The authors gratefully acknowledge the funding provided by the Ontario Centres of Excellence (OCE) Voucher for Innovation and Productivity I (VIP I) program for the experimental testing portion of this work and the financial support provided by the Natural Sciences and Engineering Research Council of Canada (NSERC) and the Ontario Graduate Scholarship (OGS) program. This research was enabled in part by computing support provided by Compute Ontario (www.computeontario.ca) and Compute Canada (www.computecanada.ca). The authors would also like to thank the staff of the McMaster Applied Dynamics Laboratory for their assistance throughout the experimental testing.

6.8 References

[1] D. Reed, J. Yu, H. Yeh and S. Gardarsson, "Investigation of Tuned Liquid Dampers Under Large Amplitude Excitation," *Journal of Engineering Mechanics,* vol. 124, no. 4, pp. 405-413, 1998.

[2] S. Kaneko and M. Ishikawa, "Modeling of Tuned Liquid Damper With Submerged Nets," *Journal of Pressure Vessel Technology,* vol. 121, no. 3, pp. 334-344, 1999.

[3] M. J. Tait, N. Isyumov and A. A. El Damatty, "Performance of Tuned Liquid Dampers," *Journal of Engineering Mechanics,* vol. 134, no. 5, pp. 417-427, 2008.

[4] J. S. Love and T. C. Haskett, "Nonlinear modelling of tuned sloshing dampers with large internal obstructions: Damping and frequency effects," *Journal of Fluids and Structures,* vol. 79, pp. 1-13, 2018.

[5] G. B. Warburton, "Optimum absorber parameters for various combinations of response and excitation parameters," *Earthquake Engineering and Structural Dynamics,* vol. 10, pp. 381-401, 1982.

[6] R. R. Gerges and B. J. Vickery, "Optimum design of pendulum-type tuned mass dampers," *Structural Design of Tall and Special Buildings,* vol. 14, no. 4, pp. 353-368, 2005.

[7] T. Asami, "Optimal Design of Double-Mass Dynamic Vibration Absorbers Arranged in Series or in Parallel," *Journal of Vibration and Acoustics,* vol. 139, no. 1, p. 011015, 2017.

[8] L. Zuo, "Effective and Robust Vibration Control Using Series Multiple Tuned-Mass Dampers," *Journal of VIbration and Acoustics,* vol. 131, no. 3, p. 031003, 2009.

[9] J. S. Love and C. S. Lee, "Nonlinear Series-Type Tuned Mass Damper-Tuned Sloshing Damper for Improved Structural Control," *Journal of Vibration and Acoustics,* vol. 141, p. 021006, 2019.

[10] Q. H. Cao, "Vibration Control of Structures by an Upgraded Tuned Liquid Column Damper," *Journal of Engineering Mechanics,* vol. 147, no. 9, p. 04021052, 2021.

[11] J. S. Love, K. P. McNamara, M. J. Tait and T. C. Haskett, "Series-type pendulum tuned mass damper-tuned sloshing damper," *Journal of Vibration and Acoustics,* vol. 142, p. 011003, 2019.

[12] A. J. Roffel, S. Narasimhan and T. Haskett, "Performance of Pendulum Tuned Mass Dampers in Reducing the Responses of Flexible Structures," *Journal of Structural Engineering,* vol. 139, no. 12, p. 04013019, 2013.

[13] K. Xu, X. Hua, W. Lacarbonara, Z. Huang and Z. Chen, "Exploration of the Nonlinear Effect of Pendulum Tuned Mass Dampers on Vibration Control," *Journal of Engineering Mechanics,* vol. 147, no. 8, p. 04021047, 2021.

[14] P. Soltani and A. Deraemaeker, "Pendulum tuned mass dampers and tuned mass dampers: Analogy and optimum parameters for various combinations of response and excitation parameters," *Journal of VIbration and Control,* 2021.

[15] O. M. Faltinsen and A. N. Timokha, Sloshing, New York: Cambridge University Press, 2009.

[16] O. M. Faltinsen, O. F. Rognebakke, I. A. Lukovsky and A. N. Timokha, "Multidimensional modal analysis of nonlinear sloshing in a rectangular tank with finite water depth," *Journal of Fluid Mechanics,* vol. 407, pp. 201-234, 2000.

[17] J. S. Love and M. J. Tait, "Nonlinear simulation of a tuned liquid damper with damping screens using a modal expansion technique," *Journal of Fluids and Structures,* vol. 26, no. 7-8, pp. 1058-1077, 2010.

[18] J. S. Love and M. J. Tait, "Non-linear multimodal model for tuned liquid dampers of arbitrary tank geometry," *International Journal of Non-Linear Mechanics,* vol. 46, no. 8, pp. 1065-1075, 2011.

[19] J. S. Love and M. J. Tait, "The response of structures equipped with tuned liquid dampers of complex geometry," *JVC/Journal of Vibration and Control,* vol. 21, no. 6, pp. 1171-1187, 2015.

[20] M. J. Tait, A. A. El Damatty, N. Isyumov and M. R. Siddique, "Numerical flow models to simulate tuned liquid dampers (TLD) with slat screens," *Journal of Fluids and Structures,* vol. 20, no. 8, pp. 1007-1023, 2005.

[21] M. B. Liu and G. R. Liu, "Smoothed particle hydrodynamics (SPH): An overview and recent developments," *Archives of Computational Methods in Engineering,* vol. 17, no. 1, pp. 25-76, 2010.

[22] R. Vacondio, C. Altomare, M. De Leffe, X. Hu, D. Le Touze, S. Lind, J. Marongiu, S. Marrone, B. D. Rogers and A. Souto-Iglesias, "Grand challenges for Smoothed Particle Hydrodynamics numerical schemes," *Computational Particle Mechanics,* vol. 8, no. 3, pp. 575-588, 2021.

[23] D. Violeau and B. D. Rogers, "Smoothed particle hydrodynamics (SPH) for free-surface flows: Past, present and future," *Journal of Hydraulic Research,* vol. 54, no. 1, pp. 1-26, 2016.

[24] A. Marsh, M. Prakash, E. Semercigil and O. F. Turan, "A study of sloshing absorber geometry for structural control with SPH," *Journal of Fluids and Structures,* vol. 27, no. 8, pp. 1165-1181, 2011.

[25] M. D. Green and J. Peiro, "Long duration SPH simulations of sloshing in tanks with a low fill ratio and high stretching," *Computers and Fluids,* vol. 174, pp. 179-199, 2018.

[26] A. H. Kashani, A. M. Halabian and K. Asghari, "A numerical study of tuned liquid damper based on incompressible SPH method combined with TMD analogy," *Journal of Fluids and Structures,* vol. 82, pp. 394-411, 2018.

[27] K. P. McNamara, B. N. Awad, M. J. Tait and J. S. Love, "Incompressible smoothed particle hydrodynamics model of a rectangular tuned liquid damper containing screens," *Journal of Fluids and Structures,* vol. 103, p. 103295, 2021.

[28] K. P. McNamara and M. J. Tait, "Modelling the response of structure-tuned liquid damper systems under large amplitude excitation using SPH," *ASME Journal of Vibration and Acoustics,* vol. 144, p. 011008, 2022.

[29] H. Wendland, "Piecewise polynomial, positive definite and compactly supported radial functions of minimal degree," *Advances in Computational Mathematics,* vol. 4, pp. 389-396, 1995.

[30] J. J. Monaghan, "Smoothed Particle Hydrodynamics," *Annual Review of Astronomy and Astrophysics,* vol. 30, pp. 543-74, 1992.

[31] S. J. Cummins and M. Rudman, "An SPH Projection Method," *Journal of Computational Physics,* vol. 152, pp. 584-607, 1999.

[32] S. Yeylaghi, B. Moa, P. Oshkai, B. Buckham and C. Crawford, "ISPH modelling of an oscillating wave surge converter using an OpenMP-based parallel approach," *Journal of Ocean Engineering and Marine Energy,* vol. 2, pp. 301-312, 2016.

[33] H. Jiang, Y. You, Z. Hu, X. Zheng and A. Ma, "Comparative study on violent sloshing withwater jet flows by using the ISPH method," *Water (Switzerland),* vol. 11, p. 2590, 2019.

[34] S. Adami, X. Y. Hu and N. A. Adams, "A generalized wall boundary condition for smoothed particle hydrodynamics," *Journal of Computational Physics,* vol. 231, no. 21, pp. 7057-7075, 2012.

[35] K. Wendel, Hydrodynamic Masses and Hydrodynamic Moments of Inertia, Washington, DC: Navy Department, 1956.

[36] J. R. Morison, M. P. O'Brien, J. W. Johnson and S. A. Shaaf, "The forces exerted by surface waves on piles," *Petroleum Transactions, AIME*, vol. 189, pp. 149-157, 1950.

[37] M. J. Tait, "Modelling and preliminary design of a structure-TLD system," *Engineering Structures*, vol. 30, no. 10, pp. 2644-2655, 2008.

Table 6.1: TMD-TLD System Configurations

System	f_{TMD} (Hz)	ζ_{TMD} (%)	TLD Depth (mm)	Damping Element Width (mm)	Test #	X_0 (mm)
1	0.60	0.43	113	34	1-4	1.0, 2.5, 5.0, 10.0
2	0.60	0.43	113	65	5-8	1.0, 2.5, 5.0, 7.0
3	0.50	0.33	79	18	9-12	1.0, 2.5, 5.0, 7.0
4	0.66	0.50	144	65	13-16	1.0, 2.5, 5.0, 7.0

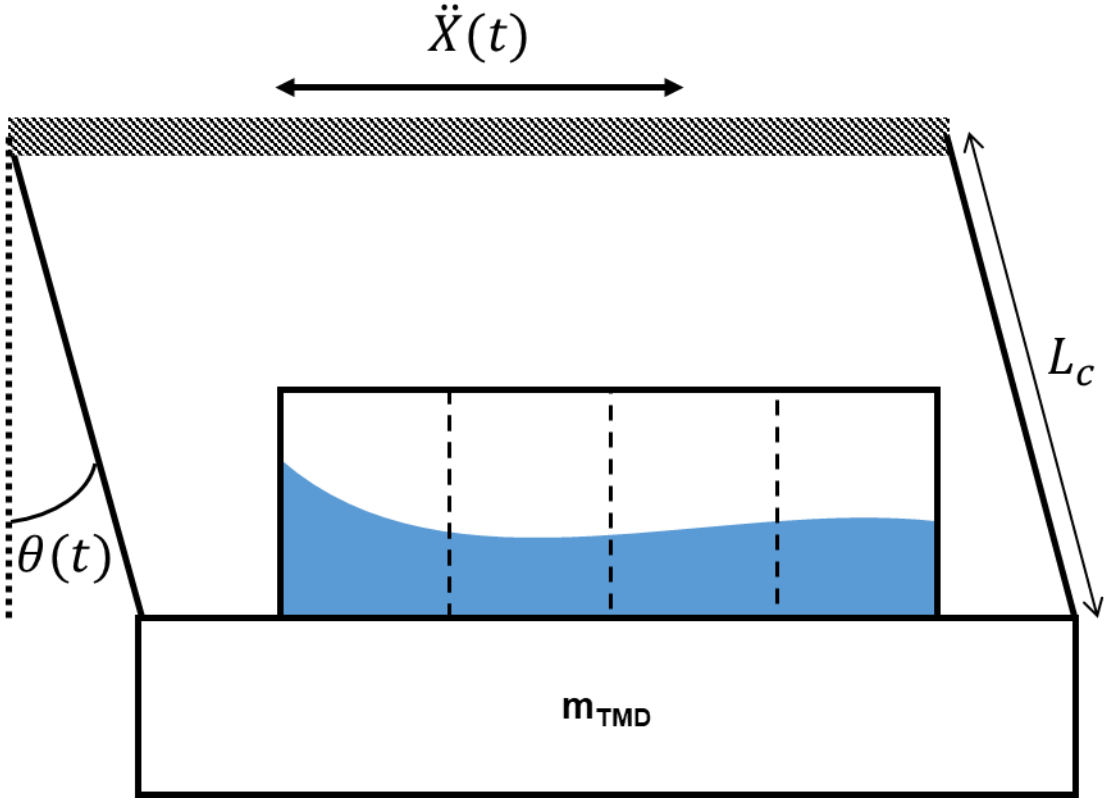

Figure 6.1: Pendulum TMD-TLD system schematic

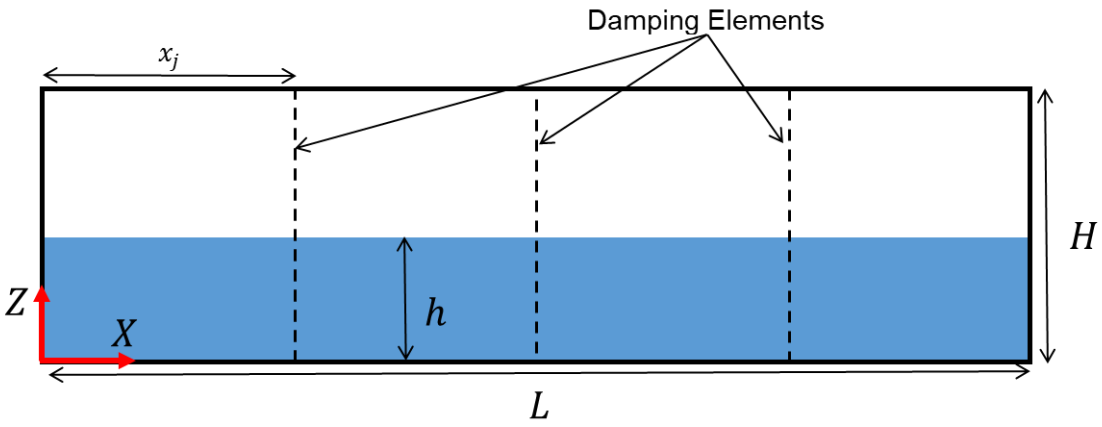

Figure 6.2: TLD domain schematic

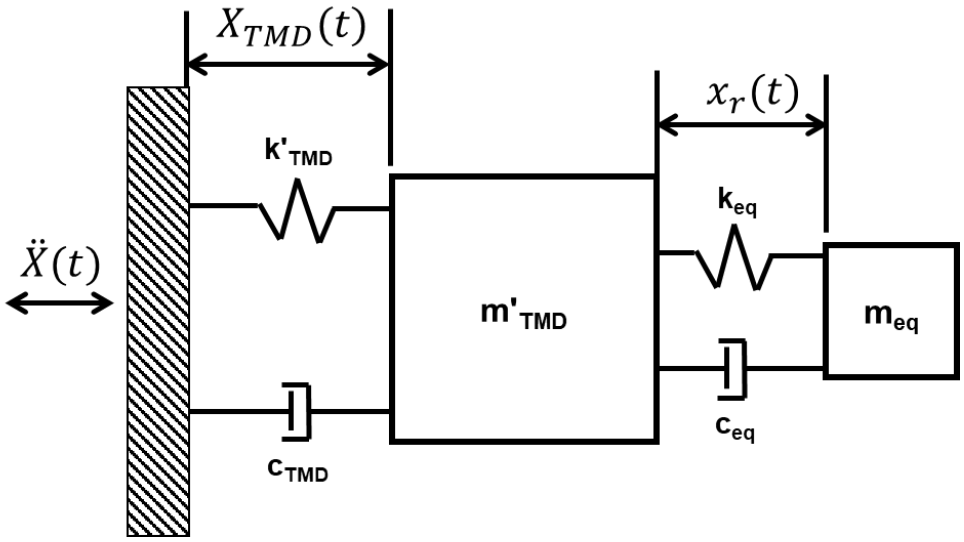

Figure 6.3: TMD-TLD linear equivalent mechanical model

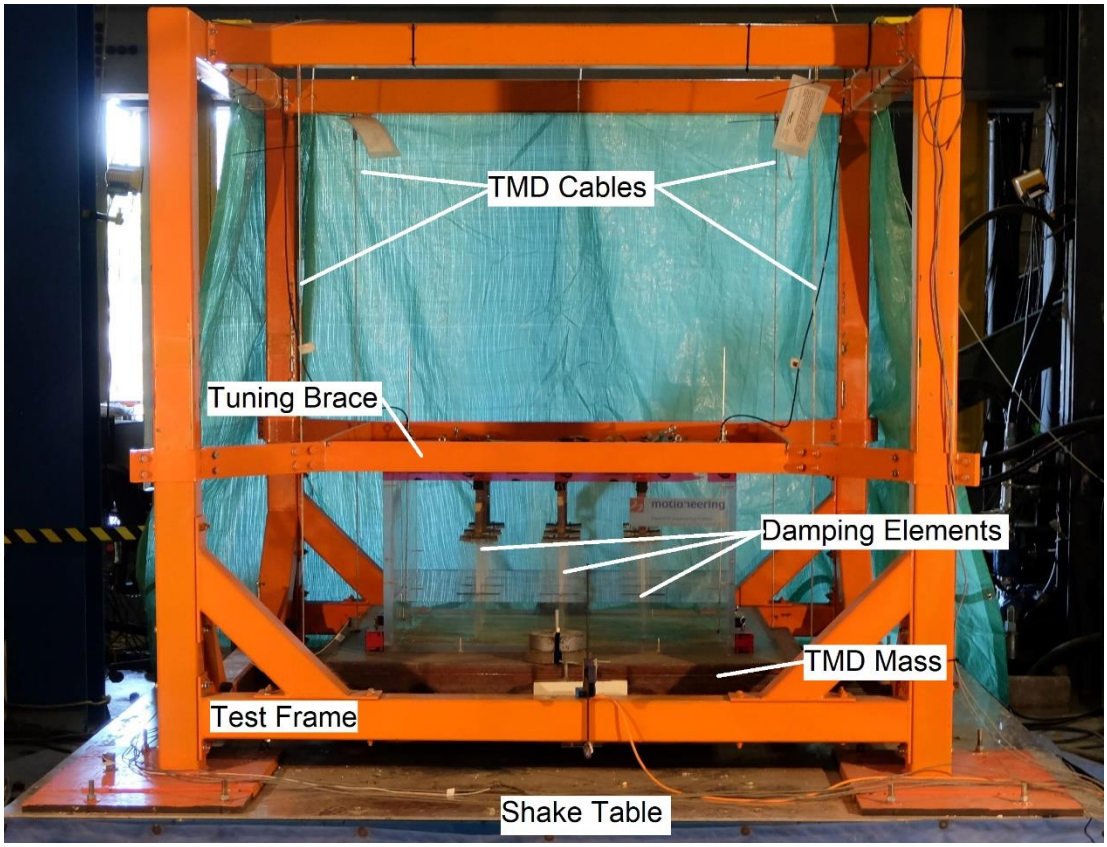

Figure 6.4: TMD-TLD experimental test setup

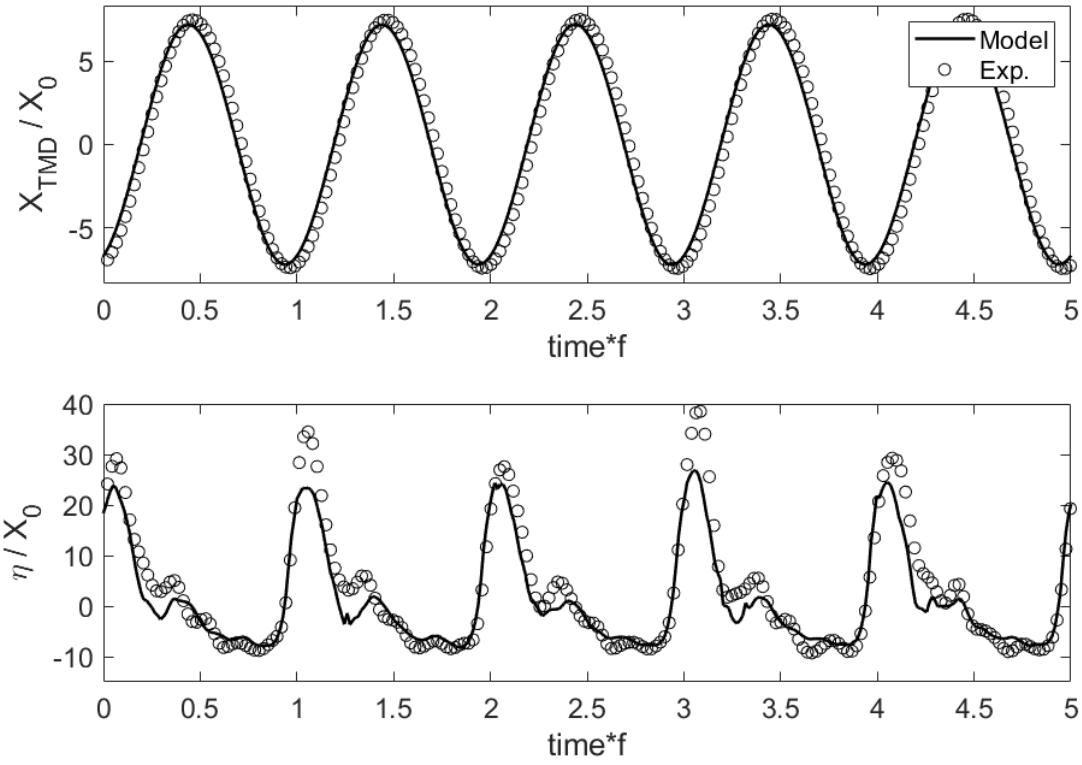

Figure 6.5: Test #3 time response for $\beta = 0.96$ and $X_0 = 5.0$ mm

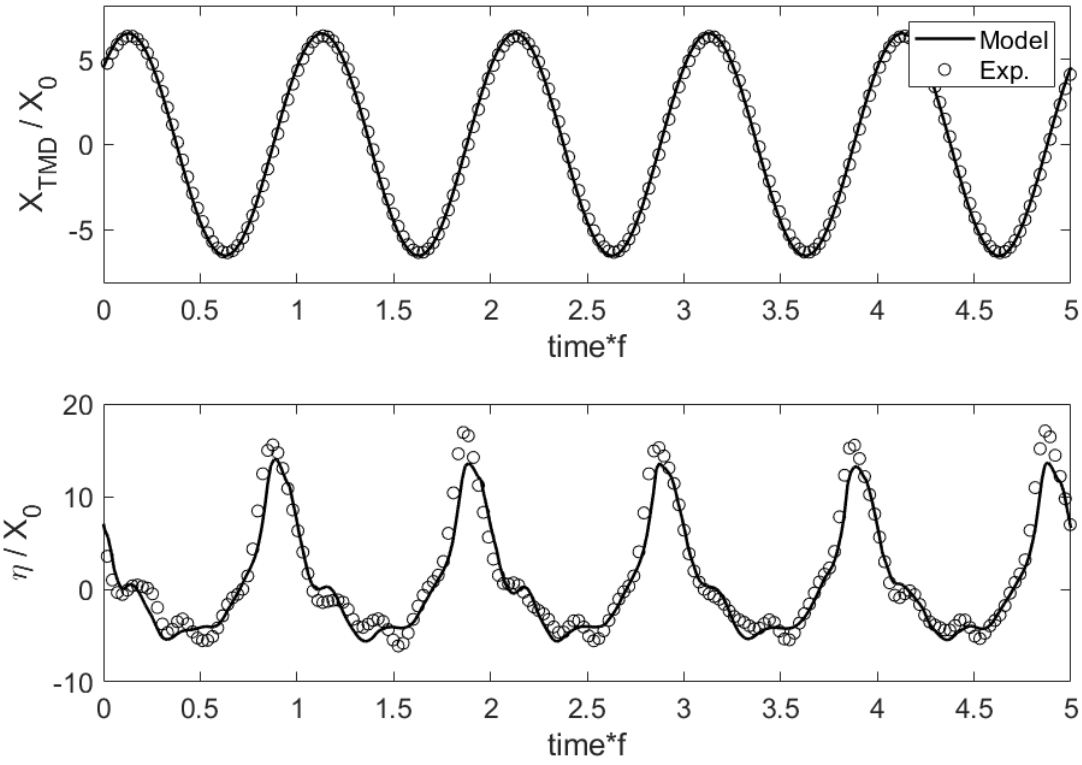

Figure 6.6: Test #8 time response for $\beta = 1.08$ and $X_0 = 7.0$ mm

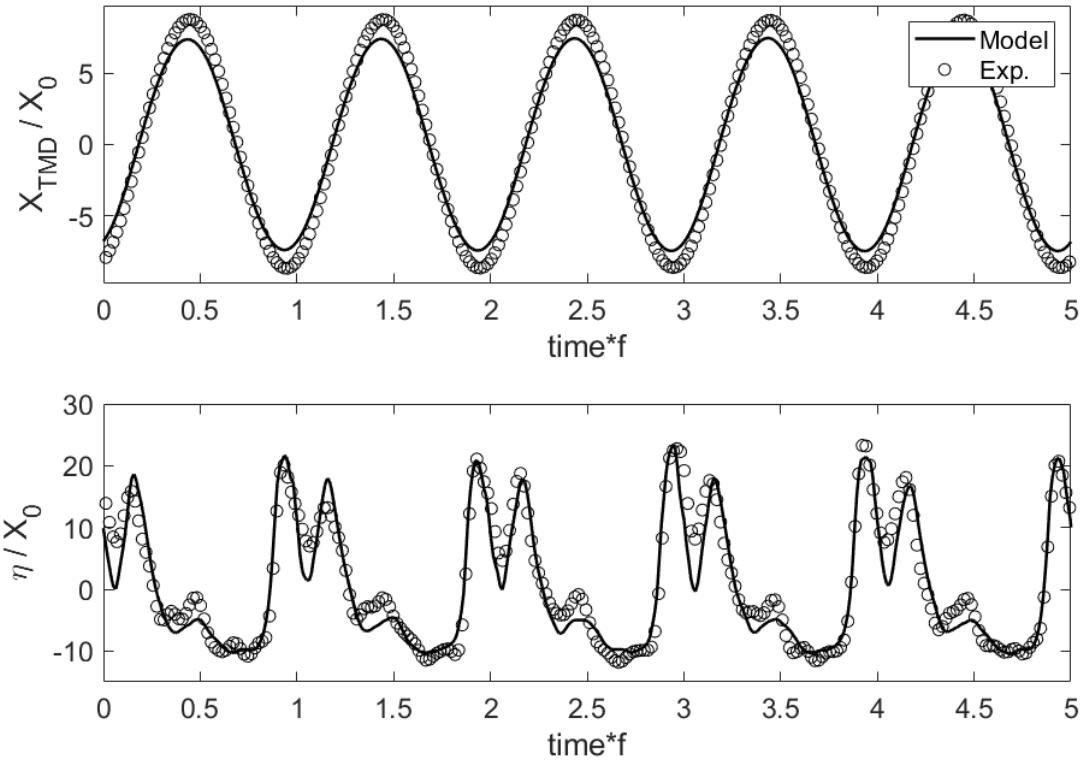

Figure 6.7: Test #10 time response for $\beta = 0.94$ and $X_0 = 2.5$ mm

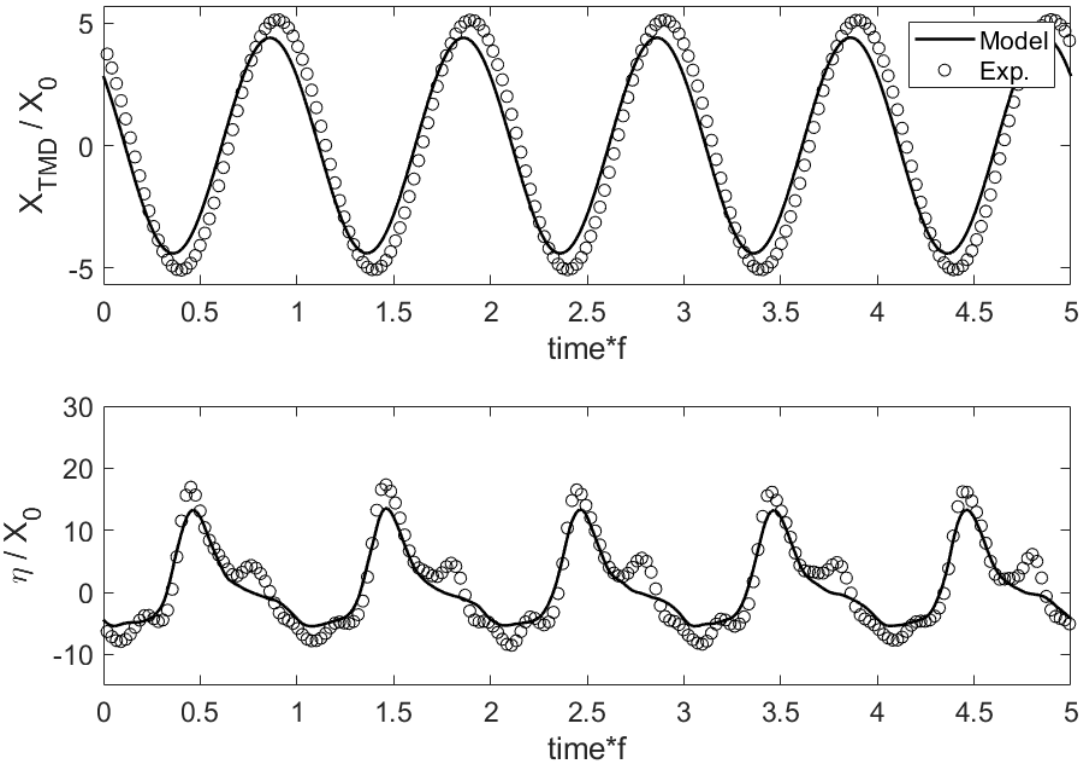

Figure 6.8: Test #16 time response for $\beta = 0.91$ and $X_0 = 7.0$ mm

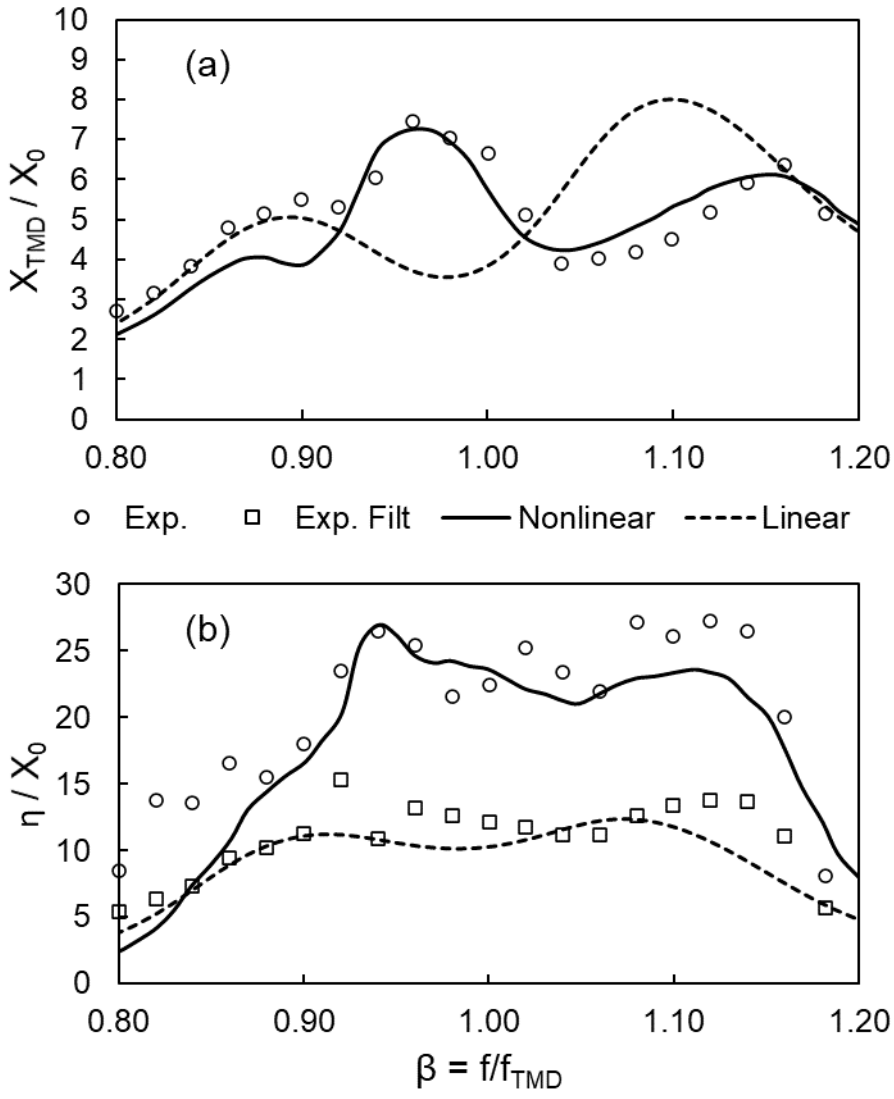

Figure 6.9: Test #3 frequency response (a) TMD displacement, (b) TLD wave height

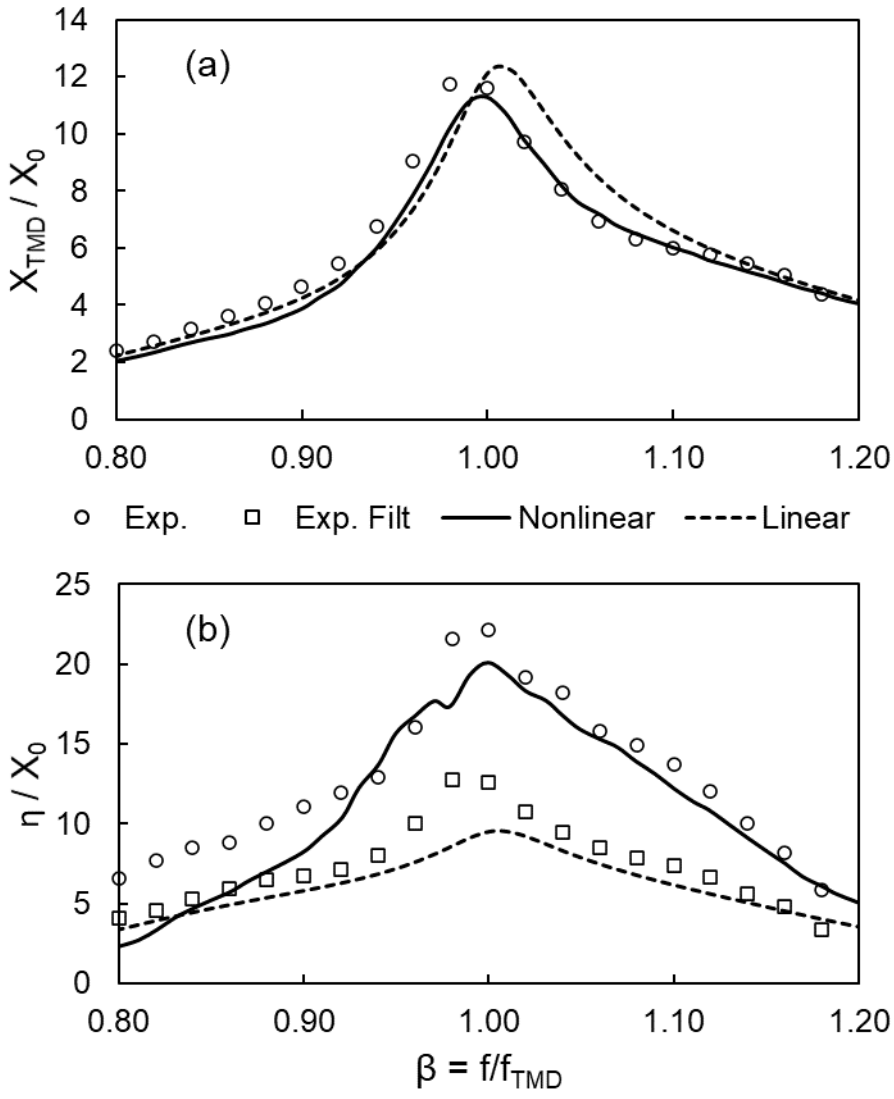

Figure 6.10: Test #8 frequency response (a) TMD displacement, (b) TLD wave height

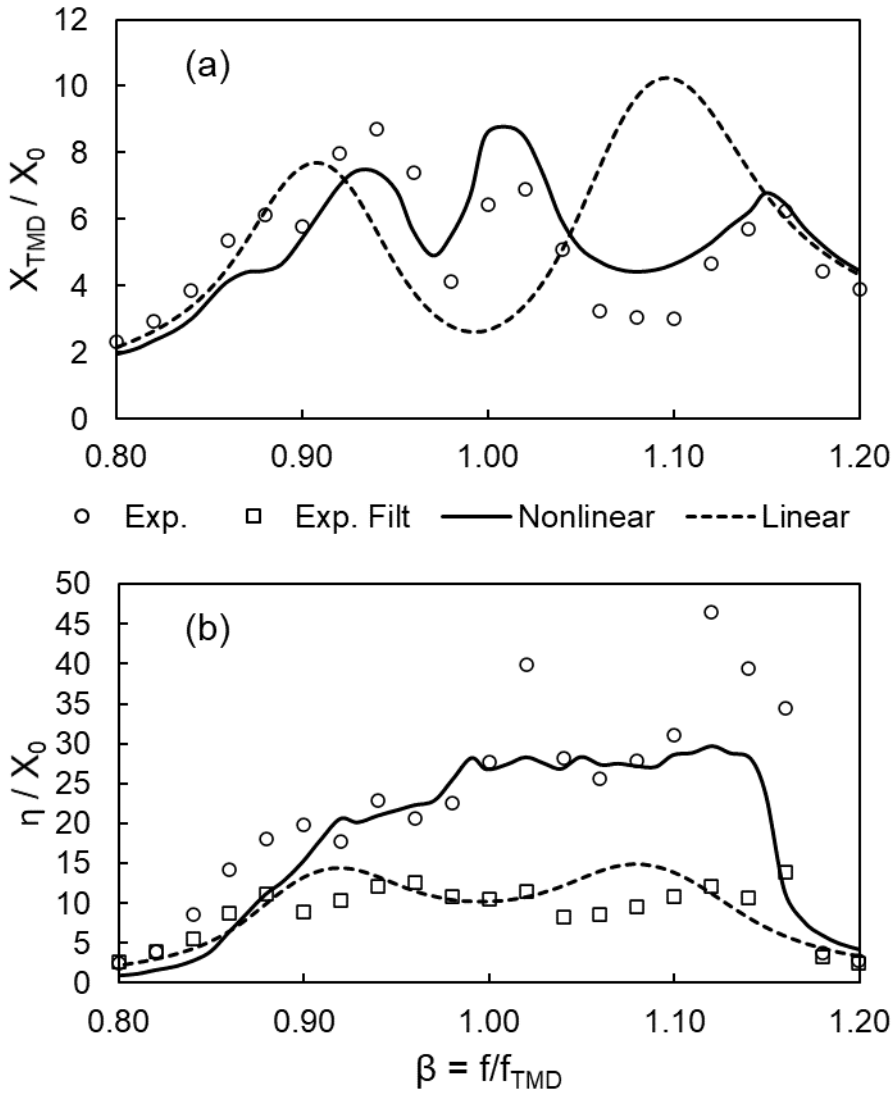

Figure 6.11: Test #10 frequency response (a) TMD displacement, (b) TLD wave height

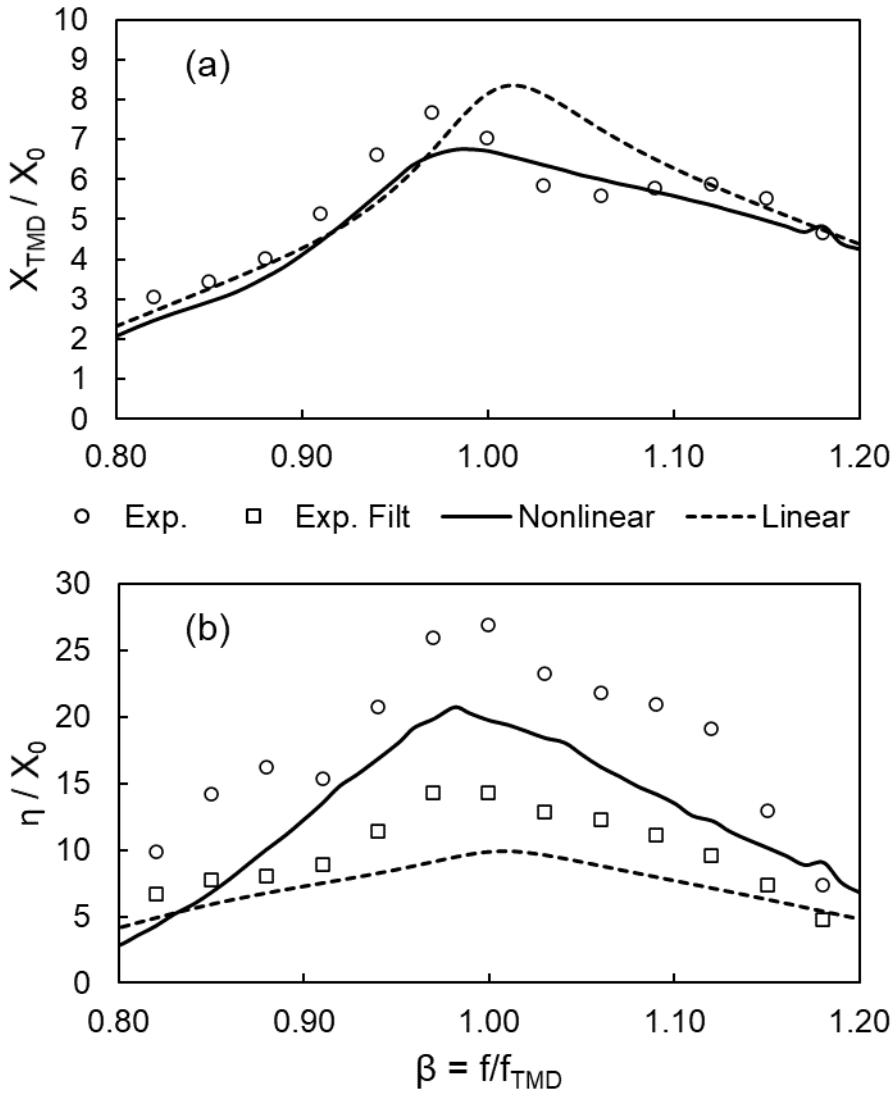

Figure 6.12: Test #16 frequency response (a) TMD displacement, (b) TLD wave height

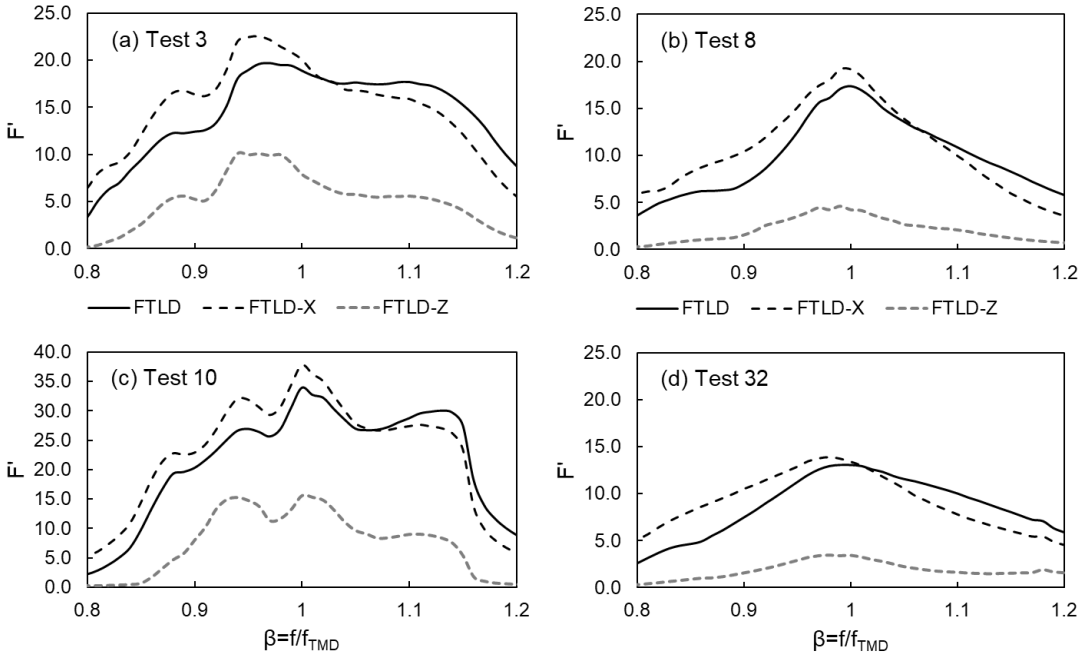

Figure 6.13: Normalized TLD force frequency response from nonlinear model: (a) Test #3, (b) Test #8, (c) Test #10, (d) Test #32

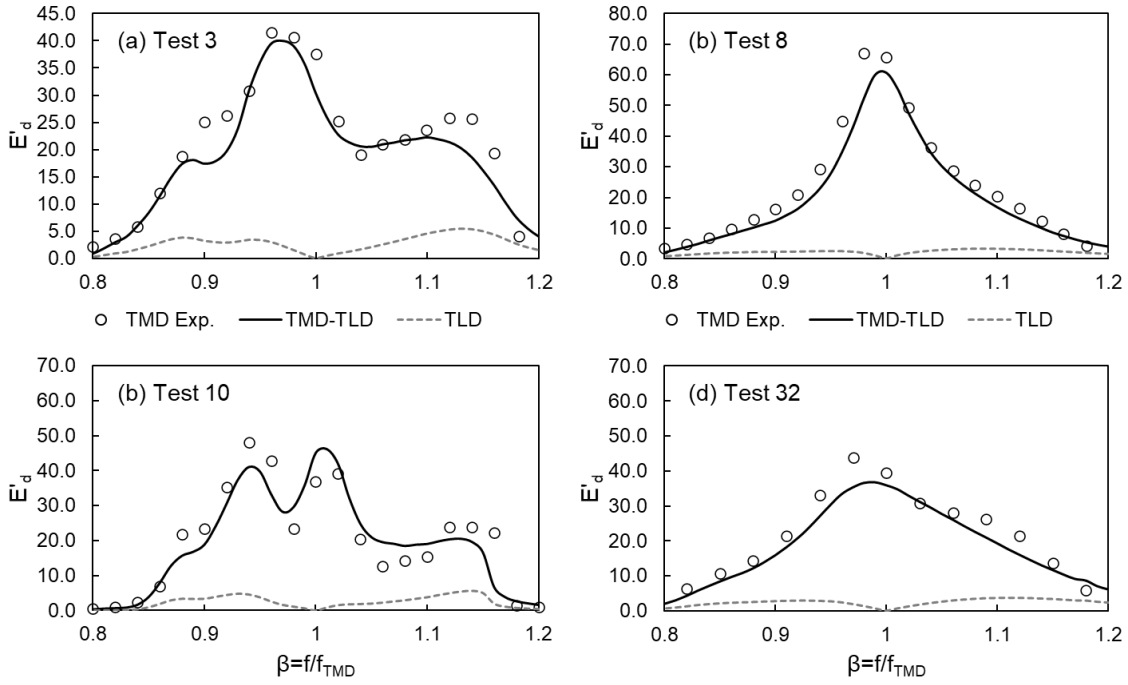

Figure 6.14: Normalized energy dissipated per cycle: (a) Test #3, (b) Test #8, (c) Test #10, (d) Test #32

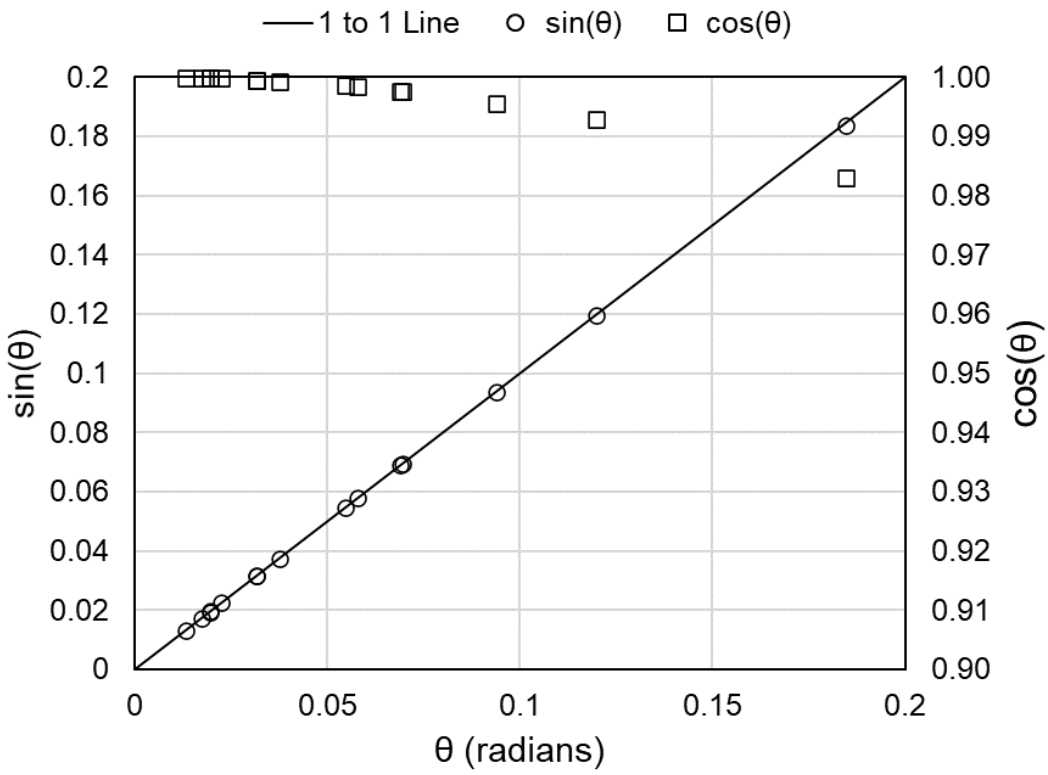

Figure 6.15: Maximum TMD angle θ vs sin(θ) and cos(θ) from experimental data

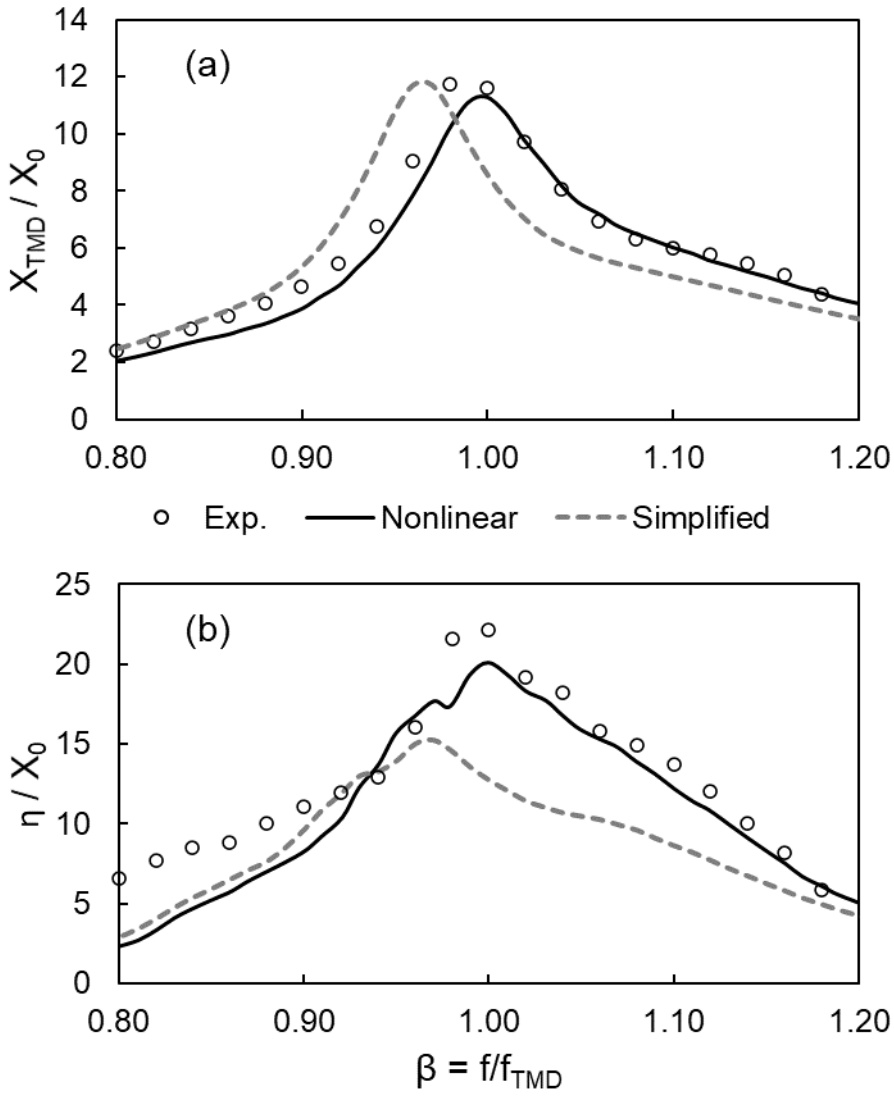

Figure 6.16: Test #8 frequency response (a) TMD displacement, (b) TLD wave height for nonlinear and simplified pendulum equation

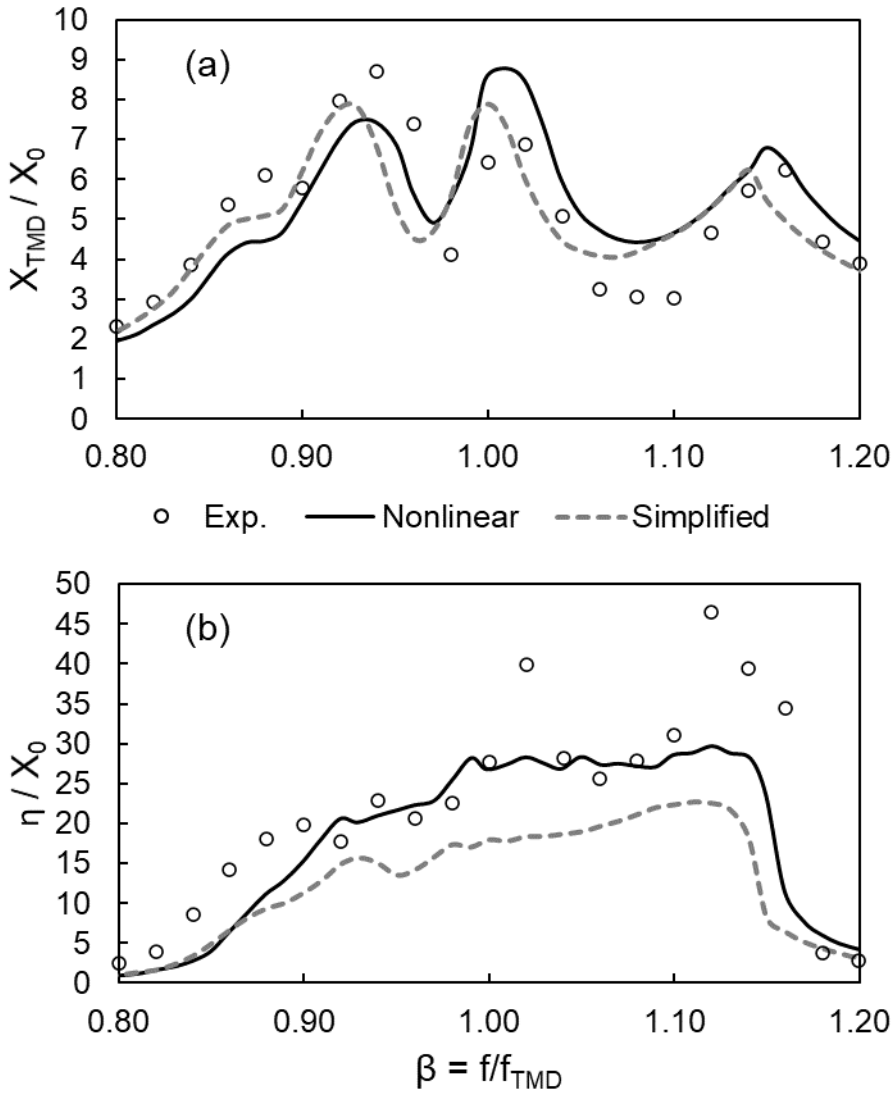

Figure 6.17: Test #10 frequency response (a) TMD displacement, (b) TLD wave height for nonlinear and simplified pendulum equation

Chapter 7: Conclusions and Recommendations

7.1 Summary and Conclusions

This research developed and validated an efficient explicit incompressible SPH model for tuned liquid dampers. This model addresses an important gap in existing numerical methods for TLDs, which have difficulty capturing shallow liquid depths, large amplitude sloshing, and impact with the tank ceiling. Additionally, the efficiency of the model allows for large particle resolutions enabling longer duration simulations than previously feasible with SPH. In Chapter 2, the SPH model was introduced and validated for a hydrostatic and dam break simulation. A novel method for modelling TLD damping screens on a macroscopic level was proposed and validated with experimental data for a wide range of TLD parameters. In Chapter 3, the SPH model was coupled to a structure to investigate the structure-TLD system response under large amplitude excitations. The large sloshing response led to the loss of some fluid particles through the solid boundaries, which compounded over the length of the four-hour simulations. In Chapter 4, simple modifications to the SPH boundary conditions were investigated to mitigate loss of fluid particles. These modifications were found to greatly improve the performance of the model for long duration simulations. In Chapter 5, the response of a structure equipped with a limited freeboard TLD was investigated to determine the impact on TLD performance. A simplified linear equivalent mechanical model was introduced to account for the additional damping from impact with the tank ceiling. Finally, in Chapter 6, the SPH model was used to study the nonlinear response of a series-type pendulum TMD-TLD system. The SPH model results were compared to experimental data and a linear model for the system.

The SPH model developed in this research was shown to be applicable to a wide range of TLD applications, including large amplitudes and limited freeboard. The code forms a basis for SPH simulations which can be adapted to various applications in future research. The major conclusions of each chapter are discussed in the following sections.

7.1.1 SPH Model for TLD with Screens

An explicit incompressible SPH model was developed. The model was validated using the theoretical pressure profile for a hydrostatic tank of water and experimental data for a dam break scenario represented by the collapse of a column of water. A novel implementation for TLD damping screens was proposed. The screens were represented macroscopically using ghost particles, which interact with the surrounding fluid based on the Morison equation for force on a submerged object. This method is much more computationally efficient compared to explicitly modelling the screen geometry using solid particles since it allows for a large SPH particle spacing. The major conclusions of this chapter are:

- The damping screen implementation reduces the SPH model computational time by a factor of approximately 700 compared to explicitly modelling the screen geometry.
- The model of a TLD with screens can accurately capture the TLD response (wave height, sloshing forces, screen forces) for a range of liquid depths, excitation amplitudes, and screen arrangements.
- The proposed novel damping screen implementation is an efficient and accurate method to represent the TLD damping screens in SPH.

The SPH model developed in this chapter can be applied to simulate various TLD configurations with internal damping elements. The results demonstrated that SPH can capture the behavior of TLDs over a wide range of parameters. In general, the performance of the model was best at larger amplitude excitations. This is a positive result, as the SPH model is unlikely to be used for small excitations where other less complicated numerical models can be applied.

7.1.2 Modelling of Large Amplitude Structure-TLD Response

The SPH model developed in Chapter 2 was coupled to a linear single degree of freedom structure to study the response of the structure-TLD system. Traditional TLD models often encounter convergence issues when the base motion of the TLD is large; however, the SPH model does not experience this. The system response was studied when

subject to four-hour duration random white noise excitation and a shorter transient signal scaled to different large amplitudes. The model results were compared to experimental data for the structure-TLD system. The following conclusions can be made:

- The SPH model captured the structure-TLD response (peak and RMS structure displacement, frequency response plots, and time domain response histories) when subject to white noise excitation for two of the three excitation amplitudes considered. For the largest amplitude studied the performance of the model was degraded over the length of the simulations.
- A portion of the SPH fluid particles were lost through solid boundaries during the four-hour simulations which led to reduced model performance. The impact of this became more prominent as the excitation amplitude was increased.
- The response of the structure-TLD system subject to shorter transient excitation was captured well by the SPH model. At the largest amplitudes, some discrepancies between the model and experimental wave heights were observed.

The structure-TLD model presented in this chapter can be used to study large amplitude structure-TLD excitation cases without convergence issues typically observed with large sloshing wave responses in other numerical models. Despite the good performance of the model, care must be taken when considering the loss of fluid particles through solid boundaries. Additionally, cases where three-dimensional sloshing effects may become important to the wave height response should be treated carefully.

7.1.3 SPH Boundary Conditions for Long Duration Simulations

From Chapter 3, the loss of fluid particles through the solid boundaries was observed for long duration simulations at large amplitudes. This chapter further investigated the cause of this behavior. It was determined that when splashing of the liquid in the TLD occurred at the tank walls some fluid particles would become attracted to the boundaries and eventually forced out of the tank. Four methods consisting of simple modifications to the boundary conditions were investigated to mitigate the loss of fluid particles. The

response of the structure-TLD system subject to a 3.75-hour white noise force excitation was considered. The major conclusions of this chapter are:

- Increasing the number of layers of solid boundary particles improves the effectiveness of containing the fluid particles within the tank; however, a significant percentage of fluid particles still penetrated the boundaries.
- Reducing the kernel support radius for boundary velocity calculations was very effective at containing the fluid particles within the tank, though < 1% of the fluid particles still penetrated the boundaries.
- Introducing a buffer zone where certain fluid-boundary particle interactions are neglected, and a conditional check which returns lost particles to inside the TLD were both found to completely contain the fluid particles within the solid boundaries.
- Compared to the base simulations with no boundary modifications, the results from reducing the kernel support radius and conditional methods showed significantly improved agreement with experimental data. The buffer zone method led to degraded pressure fields within the TLD.

The boundary condition modifications presented in this chapter should be considered for application in cases where long duration and large amplitude sloshing simulations are being completed. While these modifications may not be necessary for other situations, they do not require significant additional computational cost, and therefore may be a good addition to any SPH boundary implementation.

7.1.4 Response of Structure-Limited Freeboard TLD System

The response of a structure-TLD system where the freeboard in the TLD is limited was investigated using the SPH model. Typically, TLDs are designed such that the sloshing waves do not impact the tank ceiling. However, allowing this to occur could significantly reduce the height requirements for the TLD. The SPH model was validated using experimental data for a limited freeboard tank with ceiling impacts. The structure-TLD system was subject to a random white noise excitation signal scaled to seven intensities and nine freeboard levels. A simplified mechanical model was introduced including an

additional damping term due to ceiling impacts. The model can be used to capture the structure-limited freeboard TLD response during preliminary design stages. The major conclusions are:

- The limited freeboard TLD was less effective at reducing structural motion than an unlimited freeboard TLD. The structure response with a limited freeboard TLD was up to three times greater than the response with an unlimited freeboard TLD.
- Limiting the TLD freeboard led to a decrease in the effective damping and reduction in the TLD effectiveness.
- The damping ratio of the TLD was found to increase when freeboard was limited due to the additional energy dissipation arising from impact with the tank ceiling.
- The influence of limiting TLD freeboard was most significant when the fundamental sloshing mode was constrained by the presence of the tank ceiling. When the fundamental sloshing mode was not constrained, the limited freeboard TLD performed comparably to the unlimited freeboard TLD.

The SPH model described in this chapter can be applied to study structure-limited freeboard TLD scenarios. This chapter presented an initial investigation into the performance of a limited freeboard TLD and found that the TLD damping ratio can be significantly increased by allowing for sloshing wave impact with the tank ceiling. This is an important consideration for the design of limited freeboard TLDs to ensure the overall effectiveness of the TLD is not significantly reduced by the additional damping.

7.1.5 Nonlinear Modelling of Series-Type Pendulum TMD-TLD

The nonlinear response of a series-type pendulum TMD-TLD system was investigated. In this system, the TLD is installed on the TMD in series, providing energy dissipation to the TMD. The fully nonlinear pendulum TMD equation of motion was developed, and the TLD was simulated using SPH considering both the horizontal and vertical motion of the TMD. Since the TMD response is amplified compared to the structure, the TLD experiences a larger base excitation compared to a traditional TLD system. Shake table

testing was completed considering a range of TMD-TLD system parameters. The major findings of this chapter are:

- The nonlinear model captures the system response well in both the time and frequency domains covering a range of parameters.
- The nonlinear model provides improved agreement with experimental data compared to the linear model.
- Simplifying the pendulum TMD equation of motion by assuming small angles does not accurately capture the TMD natural frequency and can lead to significantly under-predicted TLD wave heights.

The TMD-TLD model presented in this chapter demonstrated the importance of capturing the complex behavior of all components in the system. Though the SPH model is very robust at capturing the behavior of a TLD, the results for the TMD-TLD system when using the linearized pendulum equation did not provide good agreement with experimental data, despite meeting the typical small angle requirements for linearization. It was necessary to consider the fully nonlinear pendulum equation of motion to capture the behavior of the overall TMD-TLD system. This chapter demonstrated the adaptability of the numerical code developed in this research, where the structure in a structure-TLD simulation could be easily modified to be represented as a nonlinear pendulum or multiple degree of freedom system.

7.2 SPH Model Implementation

This section provides a discussion on the implementation of the SPH code used in this research and the selection of appropriate simulation parameters. The goal is to summarize the model parameters and enable other researchers to successfully implement the SPH model for tuned liquid dampers.

7.2.1 Code Development and Computing Requirements

The code developed for this research was written entirely in Fortran due to its proven performance for scientific computing, though any high-performance computing language could be used. All post processing was done using MATLAB.

The SPH model is based on an explicit incompressible scheme. The incompressible method ensures smooth pressure fields without additional numerical treatment, and the explicit scheme greatly simplifies solving for pressure without the need for iteration. The incompressible SPH method was first described by Cummins and Rudman [1]. Explicit implementations have been presented by Yeylaghi et al. [2] and Nomeritae et al. [3], and these are excellent references for the explicit incompressible SPH method.

The SPH model code is made up of a series of subroutines which are called to execute the calculations according to the following steps:

1) **Pre-processing**: Simulation parameters are loaded from the input files. Fluid, boundary, and damping element particles are created. Each particle is initialized with zero velocity. The fluid particle pressures are initialized with a hydrostatic profile, and the boundary particle pressures are calculated based on Adami et al. [4].
2) **Time loop:** The code loops through each time step. For each loop:
    a) **Save previous state:** The particle properties (position, velocity, pressure) from the previous time step are preserved.
    b) **Structure response/base excitation:** If there is a structure-TLD simulation, calculate the structure response using the prescribed excitation force and the TLD force from the previous timestep. Otherwise, determine the base excitation of the TLD based on the prescribed input values.
    c) **Boundary velocity:** The numerical velocity of the boundary particles is calculated corresponding to either a no-slip or free-slip condition based on Adami et al. [4].
    d) **Half step:** the half step velocity and position are determined including only the viscous, gravity, external excitation, and damping element forces. The intermediate

density is then calculated based on the half step positions and velocities based on Nomeritae et al. [3].

e) **Neighbour search:** The neighbouring particles of each particle are determined only once per time step. The neighbours are stored in a list which is referred to when calculating all particle interactions.

f) **Boundary velocity:** The numerical velocity of the boundary particles is calculated corresponding to either a no-slip or free-slip condition based on Adami et al. [4].

g) **Free surface determination:** Free surface particles are identified based on calculating a numerical density from Yeylaghi et al. [2]. The pressure of free surface particles is set to zero.

h) **Fluid pressure:** The pressure of the fluid particles is calculated using the explicit method from Yeylaghi et al. [2]. Free surface particles are ignored since their pressure has already been set to zero. To improve the calculations, a blended method which includes both the divergence free and density invariant conditions of incompressibility was implemented based on Jiang et al. [5].

i) **Boundary pressure:** The pressure of the boundary particles is calculated based on Adami et al. [4].

j) **Full step:** The particle velocities and positions are corrected to include the pressure term from the governing equations.

k) **Save particle state:** After a prescribed number of time steps, the particle properties are output to a text file. To reduce space requirements, this should only be done when necessary.

l) **Save response values:** After a prescribed number of time steps, the TLD response values such as free surface height, sloshing force, and pressure are calculated and output to a text file.

The current version of the code is a serial implementation that can be run on a single CPU core. In general, the code took approximately one hour of computational time to simulate one second of model time for the TLDs studied in this research. This allows the code to be executed on a personal computer. Computing resources from Compute Canada

and Compute Ontario were utilized for several the simulations in this research. For frequency sweep simulations, multiple frequencies were run in parallel on individual CPU cores. For long duration excitations the simulations were run on the cluster to avoid keeping a personal computer dedicated to the run for multiple weeks. The serial code could be adapted to parallel computing in the future, which would require the use of high-performance computing resources.

7.2.2 Parameter Selection and Boundary Condition Modifiers

This section provides guidance for selection of parameters and boundary condition modifications for implementation of the SPH model:

- **Simulation time step (*dt*):** For an incompressible SPH model the time step should be limited based on the particle spacing, maximum fluid velocity, and fluid viscosity as described by Shao and Lo [6]. In general, the TLD simulations were not overly sensitive to the selected timestep. Based on the model results presented in this research, a timestep ranging from 10^{-3} to 10^{-4} seconds adequately described the TLD response.
- **Particle spacing (*dp*):** The selection of particle spacing has the most direct impact on efficiency of the simulations, since using smaller particle spacing results in many additional neighbour calculations. The SPH model performs best when the selected particle spacing provides integer divisions of the domain (i.e., the ratios of liquid depth/dp and tank length/dp should be integer numbers). Additionally, providing a minimum of ten layers of particles over the fluid depth is recommended to ensure sufficient resolution and accurate calculation of the screen forces.
- **Kernel function:** In this research the fifth order Wendland kernel function was used in all SPH simulations [7]. This kernel function was found to perform well, and requires less calculations compared to other kernel functions. Depending on the application, other kernel functions may be more appropriate and could be investigated.

- **Kernel radius multiplier (h_{ker}):** The SPH kernel radius multiplier should be slightly larger than the initial particle spacing. The SPH model was found to provide similar results for h_{ker} between 1.2 and 1.6 times the initial particle spacing. For 3D simulations this parameter would need to be revised.
- **Free surface particle density:** It is necessary to define a limit on free surface particle density to identify the free surface particles and enforce the constant pressure boundary condition. A value ranging from 85% to 95% of the fluid density was found to adequately capture the free surface in TLD simulations.
- **Damping element coefficients (C_l/C_m):** The drag/loss and added mass coefficients of the damping elements must be known to apply the method presented in this research. These coefficients are often determined empirically or theoretically. For the damping elements used in this research the coefficients were determined based on experimental data. For damping elements where the loss characteristics are unknown, it may be necessary to undertake an experimental study to determine the appropriate values. Additionally, it may be necessary to incorporate an adaptive loss coefficient in scenarios where the Keulegan-Carpenter number is small [8]. To better capture the liquid velocity at the damping elements in TLD simulations, it is recommended that a kernel radius multiplier of $3h_{ker}$ is used for the damping element calculations. This value was appropriate for the damping elements in this research but may require refinement for different types or geometries of damping elements.
- **Boundary condition modifications:** For long duration simulations where splashing is expected in the TLD, it may be necessary to modify the boundary condition calculations based on the results of Chapter 4. It is recommended to reduce the kernel radius by half for calculation of the boundary particle velocities, which was referred to as the qb = 1 method in Chapter 4. Additionally, it is recommended to periodically check the number of fluid particles outside of the boundaries throughout a long simulation and stop execution of the code if the loss of particles is found to be significant.

7.3 Recommendations for Further Study

Several recommendations for further study can be made based on this research:

- **Extension to a 3D SPH Model:** The SPH model developed in this research is limited to simulating a 2D flow. Extension of the model to 3D would allow for simulating more complex sloshing flows in rectangular tanks, and a wide variety of TLD tank shapes such as circular, annular, or other irregular geometries. The base SPH methodology can easily be extended to 3D by solving the governing equations including the third-dimension terms. The boundary condition implementation would need to be revisited for complex tank shapes involving curved or angled boundary walls. Further investigation into the computational efficiency of the code would be necessary to efficiently simulate 3D flows.
- **Parallelization of SPH Code:** Though the developed SPH code is efficient, it is based on a serial implementation. Introduction of a suitable parallelization scheme could improve the existing runtime significantly and allow for scaling of the code to larger numbers of particles and complex 3D flows. With significant improvement to the computational runtime, it would become feasible to simulate even longer durations, or finer particle spacings leading to the ability to directly model the geometry of damping screens in the TLD. This could allow for numerical investigation of novel screen shapes and geometries, rather than requiring the loss and added mass coefficients to be known. Additionally, it would be feasible to simulate multiple unique TLDs attached to a single structure, which is increasingly common in real-world TLD applications.
- **Other Applications of SPH:** Though TLDs are the specific application of the model developed in this research, the SPH code has the capability to be modified to simulate other applications. The explicit incompressible SPH method is particularly well suited for sloshing liquids in tanks. The macroscopic damping screen application could be applied to open channel flow problems with porous elements, such as breakwater structures located near shorelines. Extension of the tank geometry to complex shapes would allow for simulating tsunami wave impacts on shorelines or

structures. The governing equations could be modified for other physical phenomena, such as mudslides, viscous flows, incompressible solids, and crowd behavior.

- **Shallow Water SPH Implementation:** The SPH method can be applied to solve the depth averaged shallow water wave theory equations. Extension of shallow water SPH to simulate forced sloshing problems and TLD damping screens would provide an intermediary model between traditional finite difference based SWWT solvers and the full SPH method. Using the particle based shallow water SPH method would likely improve convergence of the SWWT equations at large amplitudes compared to the finite difference solver. Additionally, since only the free surface is modelled, shallow water SPH would have significantly improved computational runtime compared to the full SPH method. This method would also likely be attractive for TLDs with interior obstructions, such as an annular tank with inner and outer tank walls.
- **Experimental Study of Limited Freeboard TLD:** Few experimental studies have been completed on tanks with limited freeboard, and even less have been specifically for TLD applications. Completion of an experimental program on the response of limited freeboard TLDs would further advance the knowledge of the system performance. Direct measurement of pressures and forces on the tank walls and roof would allow for further validation of the SPH model, and quantification of parameters such as the energy dissipated by sloshing impact with the tank ceiling. Additionally, to confirm the results of Chapter 5 for a range of systems, it would be beneficial to complete tests on TLDs and structure-TLD systems considering different parameters such as TLD depth ratio and structure-TLD mass ratio.
- **Design Procedure for Limited Freeboard TLD:** Chapter 5 investigated the response of a structure-limited freeboard TLD system, which demonstrated increased TLD damping when the sloshing liquid impacts the tank ceiling. While this may increase the damping beyond its optimal value, it could also be used to the designer's advantage if there is difficulty achieving optimal TLD damping from the liquid or damping elements alone. Development of a prescriptive design procedure for limited

freeboard TLDs using simplified models would allow for simpler implementation of the system in practice. Additionally, development of simplified methods to quantify forces and pressures for conceptual structural tank design would be beneficial.

- **Performance of Structure-TMD-TLD System:** The model developed in Chapter 6 can be coupled to a structure to investigate the structure-TMD-TLD system response. Research referenced in Chapter 6 has demonstrated that the TMD-TLD system provides improved performance compared to a traditional TMD or TLD of equivalent mass; however, this has not been investigated using a suitable nonlinear model. Improving the understanding of the overall performance of the system will allow for increased potential adoption of this new technology.

7.4 References

[1] S. J. Cummins and M. Rudman, "An SPH Projection Method," *Journal of Computational Physics,* vol. 152, pp. 584-607, 1999.

[2] S. Yeylaghi, B. Moa, P. Oshkai, B. Buckham and C. Crawford, "ISPH modelling of an oscillating wave surge converter using an OpenMP-based parallel approach," *Journal of Ocean Engineering and Marine Energy,* vol. 2, pp. 301-312, 2016.

[3] Nomeritae, E. Daly, S. Grimaldi and H. H. Bui, "Explicit incompressible SPH algorithm for free-surface flow modelling: A comparison with weakly compressible schemes," *Advances in Water Resources,* vol. 97, pp. 156-167, 2016.

[4] S. Adami, X. Y. Hu and N. A. Adams, "A generalized wall boundary condition for smoothed particle hydrodynamics," *Journal of Computational Physics,* vol. 231, no. 21, pp. 7057-7075, 2012.

[5] H. Jiang, Y. You, Z. Hu, X. Zheng and A. Ma, "Comparative study on violent sloshing withwater jet flows by using the ISPH method," *Water (Switzerland),* vol. 11, p. 2590, 2019.

[6] S. Shao and E. Y. Lo, "Incompressible SPH method for simulating Newtonian and non-Newtonian flows with a free surface," *Advances in Water Resources,* vol. 26, pp. 787-800, 2003.

[7] H. Wendland, "Piecewise polynomial, positive definite and compactly supported radial functions of minimal degree," *Advances in Computational Mathematics,* vol. 4, pp. 389-396, 1995.

[8] J. A. Hamelin, J. S. Love, M. J. Tait and J. C. Wilson, "Tuned liquid dampers with a Keulegan-Carpenter number-dependent screen drag coefficient," *Journal of Fluids and Structures,* vol. 43, pp. 271-286, 2013.